

Generalized $T_e(\text{[O III]}) - T_e(\text{He I})$ Discrepancies in Ionized Nebulae: Possible Evidence of Case B Deviations and Temperature Inhomogeneities

J. E. MÉNDEZ-DELGADO ,^{1,2} E. D. SKILLMAN ,³ E. AVER,⁴ C. MORISSET ,^{5,6} C. ESTEBAN ,^{7,8}

J. GARCÍA-ROJAS ,^{7,8} K. KRECKEL ,² N. S. J. ROGERS ,^{9,10} F. F. ROSALES-ORTEGA ,¹¹

K. Z. ARELLANO-CÓRDOVA ,¹² S. R. FLURY ,¹² E. REYES-RODRÍGUEZ ,^{8,13} AND M. ORTE-GARCÍA ,^{7,8}

¹ Instituto de Astronomía, Universidad Nacional Autónoma de México, Ap. 70-264, 04510 CDMX, México

² Astronomisches Rechen-Institut, Zentrum für Astronomie der Universität Heidelberg, Mönchhofstraße 12-14, D-69120 Heidelberg, Germany

³ Minnesota Institute for Astrophysics, University of Minnesota, 116 Church Street South East, Minneapolis, MN 55455, USA

⁴ Department of Physics, Gonzaga University, 502 E Boone Ave., Spokane, WA 99258, USA

⁵ Instituto de Astronomía, Universidad Nacional Autónoma de México, Ap. 106, 22800 Ensenada, Baja California, México

⁶ Instituto de Ciencias Físicas, Universidad Nacional Autónoma de México, Av. Universidad s/n, 62210 Cuernavaca, Mor., México

⁷ Instituto de Astrofísica de Canarias, E-38205 La Laguna, Tenerife, Spain

⁸ Departamento de Astrofísica, Universidad de La Laguna, E-38206 La Laguna, Tenerife, Spain

⁹ Department of Physics and Astronomy, Northwestern University, 2145 Sheridan Road, Evanston, IL 60208, USA

¹⁰ Center for Interdisciplinary Exploration and Research in Astrophysics (CIERA), Northwestern University, 1800 Sherman Avenue, Evanston, IL 60201, USA

¹¹ Instituto Nacional de Astrofísica, Óptica y Electrónica (INAOE-CONAHCyT), Luis E. Erro 1, 72840, Tonantzintla, Puebla, México

¹² Institute for Astronomy, University of Edinburgh, Royal Observatory, Edinburgh, EH9 3HJ, United Kingdom

¹³ Isaac Newton Group of Telescopes, Apt 321, E-38700 Santa Cruz de La Palma, Canary Islands, Spain

ABSTRACT

The physics of recombination lines (RLs) in the He I singlet system is expected to be relatively simple, supported by accurate atomic models. We examine the intensities of He I singlets $\lambda\lambda 3614, 3965, 5016, 6678, 7281$ and the triplet He I $\lambda 5876$ in various types of ionized nebulae and compare them with theoretical predictions to test the validity of the “Case B” recombination scenario and the assumption of thermal homogeneity. Our analysis includes 85 spectra from Galactic and extra-galactic H II regions, 90 from star-forming galaxies, and 218 planetary nebulae, all compiled by the DEep Spectra of Ionized REgions Database Extended (DESIRED-E) project. By evaluating the ratios He I $\lambda 7281/\lambda 6678$ and He I $\lambda 7281/\lambda 5876$, we determine $T_e(\text{He I})$ and compare it with direct measurements of $T_e(\text{[O III]}) \lambda 4363/\lambda 5007$. We find that $T_e(\text{He I})$ is systematically lower than $T_e(\text{[O III]})$ across most objects and nebula types. Additionally, we identify a correlation between the abundance discrepancy factor ($\text{ADF}(\text{O}^{2+})$) and the difference $T_e(\text{[O III]}) - T_e(\text{He I})$ for planetary nebulae. We explore two potential explanations: photon loss from $n^1P \rightarrow 1^1S$ transitions and temperature inhomogeneities. Deviations from “Case B” may indicate photon absorption by H I rather than He I and/or generalized ionizing photon escape, highlighting the need for detailed consideration of radiative transfer effects. If temperature inhomogeneities are widespread, identifying a common physical phenomenon affecting all ionized nebulae is crucial. Our results suggest that both scenarios can contribute to the observed discrepancies.

Keywords: Galaxy abundances; Interstellar abundances; H II regions; Planetary nebulae

1. INTRODUCTION

Corresponding author: J. Eduardo Méndez-Delgado
 jmendez@astro.unam.mx

Helium is the second most abundant element in the universe, and the precise determination of its abundance is of profound importance for cosmology, as it was created in large quantities during the Big Bang (Alpher et al. 1948; Peebles 1966a,b; Peimbert & Spinrad 1970;

(Peimbert & Torres-Peimbert 1974). In star-forming regions, He I lines are frequently detected in a large number of spectra. These are recombination lines (RLs), produced after the capture of free electrons by ionized helium atoms. Since He I is an atomic system with two electrons, this atom has two level states depending on its total spin quantum number: singlets, and triplets (Heisenberg 1926).

Approximately three-quarters of the recombinations will occur in the triplet system (Burgess & Seaton 1960), giving rise to the brightest He I lines, such as $\lambda\lambda 4471, 5875, 7065$. However, in the triplet configuration, the 2^3S level is metastable, making it susceptible to the effects of self-absorption and collisional excitation and de-excitation. Consequently, the fluxes of the triplet He I lines can significantly diverge from pure recombination predictions. For instance, lines such as He I $\lambda 7065$ increase their flux at the expense of lines such as He I $\lambda 3889$, although the total flux of the triplet system lines must be conserved (Porter et al. 2007). These effects are well known and are considered in great detail in many works dedicated to the precise determination of the fraction of primordial mass in helium Y_p (Izotov & Thuan 1998a; Peimbert et al. 2002; Aver et al. 2015; Valerdi et al. 2019).

In contrast to the triplet system, the physics involved in the emission of singlet lines is relatively simple. The effects of self-absorption and collisional excitation are expected to be very small, and the fluxes of these lines should be well described in terms of pure recombination (Porter et al. 2007, 2009). Additionally, the recombination probabilities and atomic data for He I are extremely precise (Benjamin et al. 1999; Porter et al. 2005, 2012, 2013; Del Zanna & Storey 2022), with potential errors on the order of $\sim 1\%$. Therefore, the study of these lines is extremely relevant for testing our most basic (and general) physical assumptions adopted for determining chemical abundances in ionized nebulae, such as the thermal homogeneity (see the discussion in Ferland et al. 2016) and the assumption that the nebula is optically thick to Lyman transitions also referred as “Case B” (Baker & Menzel 1938).

Intensity ratios of He I singlet lines originating from $n^1S \rightarrow n^1P$ and $n^1P \rightarrow n^1S$ transitions (such as He I $\lambda 7281$ and He I $\lambda 5016$, respectively) compared to those originating from $n^1D \rightarrow n^1P$ transitions (such as He I $\lambda 6678$) are sensitive to the electron temperature of the gas (T_e), with a small dependence on the density (n_e) (Zhang et al. 2005). Additionally, these same ratios are very sensitive to deviations from “Case B” since the transitions between the n^1P levels and the ground

level 1^1S are permitted by the electric-dipole rules (See Fig. 6).

When comparing $T_e(\text{He I } \lambda 7281/\lambda 6678)$ with classical nebular diagnostics based on collisionally excited lines (CELs) of high ionization degree, such as $T_e([\text{O III}] \lambda 4363/\lambda 5007)$, one would expect relatively good consistency, as assumed in multiple studies (Izotov et al. 2014; Valerdi et al. 2021a; Dors et al. 2024). However, in the presence of small-scale temperature variations, $T_e([\text{O III}])$ would have a systematic bias toward higher temperatures, while $T_e(\text{He I})$ would remain relatively unaffected (Peimbert 1967). Under these conditions, one would observe that $T_e(\text{He I}) < T_e([\text{O III}])$. The presence of these temperature inhomogeneities would imply that most nebular chemical abundance determinations based on CELs would be systematically underestimated and are part of the academic debate due to their profound implications (García-Rojas & Esteban 2007; Esteban et al. 2009; Cameron et al. 2023; Méndez-Delgado et al. 2023a, 2024a; Chen et al. 2023).

If deviations from “Case B” such as photon loss originating from He I $n^1P \rightarrow 1^1S$ transitions exist, one would see a decrease in the overall flux of He I singlets, primarily affecting the lines originating from n^1P levels, followed by those from n^1S and n^1D levels, in that order, due to the permitted interconnection transitions. In that case, one would observe that $T_e(\text{He I } \lambda 7281/\lambda 6678) < T_e([\text{O III}] \lambda 4363/\lambda 5007)$. If fluorescent excitations He I $1^1S \rightarrow n^1P$ in an optically thick nebula exist (known as “Case D”-recombination see Luridiana et al. 2009), one would observe the opposite effect, obtaining $T_e(\text{He I}) > T_e([\text{O III}])$. If significant deviations from “Case B” are observed in the singlet He I atom, this may indicate the widespread presence of fluorescent effects in the radiative transfer of different ions and/or the escape of these ionizing photons into the interstellar medium (ISM).

The main drawback of studying He I singlet lines is that they are relatively faint, with the exception of He I $\lambda 6678$. Through the DESIRED project (Méndez-Delgado et al. 2023b), and its extension (DESIRED-E, Méndez-Delgado et al. 2024b), we have collected an extensive set of deep spectroscopic data from numerous ionized nebulae. This has enabled us to study the physical and chemical properties of nebulae through a homogeneous analysis of very weak emission lines. As a result, we are opening a new frontier in astrophysics by facilitating a comprehensive study of the physical phenomena associated with these faint lines. In this work, we consistently and homogeneously analyze direct determinations of $T_e(\text{He I})$ in 175 deep spectra of Galactic and extragalactic star-forming regions. Additionally,

we adopt 218 deep spectra of Galactic and extragalactic planetary nebulae with the same criteria as for the star-forming regions to contrast the results under different photoionization conditions. This is the largest sample of ionized nebulae used for this purpose in the literature. In each case, we have compared $T_e(\text{He I})$ with $T_e([\text{O III}])$.

In Sec. 2, we present the observations adopted in this work, as well as the methodology used to determine the physical conditions and ionic abundances of the gas. In Sec. 3, we present the observed trend between $T_e(\text{He I})$ and $T_e([\text{O III}])$ determined for the observational sample. In Sec. 4, we discuss the results in several subsections, considering various phenomena and models that could explain the unexpected trend observed in Sec. 3. Finally, in Sec. 5, we summarize our conclusions and final thoughts. In Appendix A, we present the relevant data, calculations, and observational values for this study, as well as additional figures that complement our findings.

2. OBSERVATIONS AND METHODOLOGY

The observational sample used for this study comes from the deepest optical spectra published to date, collected and treated homogeneously as part of the DESIRED and DESIRED-E projects (Méndez-Delgado et al. 2023b, 2024b). In these projects, the reddening-corrected fluxes of all emission lines reported by the referenced authors have been compiled, surpassing previous works that generally only include a limited number of lines of interest. By default, all spectra considered in DESIRED-E have at least one of the following available temperature diagnostics: [N II] $\lambda 5755/\lambda 6584$, [O III] $\lambda 4363/\lambda 5007$, or [S III] $\lambda 6312/\lambda 9069$, with uncertainties in the auroral lines of less than 40%. For this study, we required the direct detection of the [O III] $\lambda 4363/\lambda 5007$ diagnostic, as well as the detection of He I $\lambda 7281$ and [O III] $\lambda 4363$, with uncertainties of 20% or less. Additionally, we required the detection of one or both of the following lines: He I $\lambda 6678$ and He I $\lambda 5876$, which are essential for determining $T_e(\text{He I})$. In addition to the aforementioned He I RLs, a large portion of the selected observational sample has multiple detections of He I singlets with errors of 20% or less. As part of our study, we also analyzed the fluxes of the He I $\lambda 5016$ line in those objects where it is reported.

Our sample of star-forming regions covers the metallicity range from $12+\log(\text{O/H}) \approx 7.05$ to $12+\log(\text{O/H}) \approx 8.60$, while the PNe cover from $12+\log(\text{O/H}) \approx 7.50$ to $12+\log(\text{O/H}) \approx 9.10$ (derived via

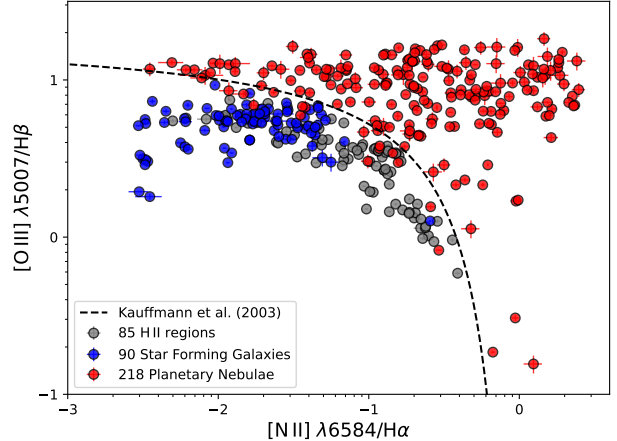


Figure 1. BPT diagram of the selected nebular spectra. The dashed line represents the empirical relation by Kauffmann et al. (2003) that distinguishes regions ionized by sources with effective temperatures typical of O and early B type stars (such as star-forming regions) from regions with harder ionizing sources (such as active galactic nuclei or some planetary nebulae).

the direct method, i.e., $t^2 = 0$; Peimbert 1967)¹. The references to the analyzed spectra are presented in Tables A2, A3, and A4. The Baldwin-Phillips-Terlevich (BPT) diagram (Baldwin et al. 1981) of the studied sample is shown in Fig. 1.

In this work, we determine n_e and T_e considering various CEL-diagnostics following the so-called “direct method” (Dinerstein 1990; Peimbert et al. 2017), with the methodology described in detail in Sec. 2 of Méndez-Delgado et al. (2023b) and Méndez-Delgado et al. (2024b). In short, we determine n_e considering different diagnostics such as [S II] $\lambda 6731/\lambda 6716$, [O II] $\lambda 3726/\lambda 3729$, [Cl III] $\lambda 5538/\lambda 5518$, [Fe III] $\lambda 4658/\lambda 4702$, and [Ar IV] $\lambda 4740/\lambda 4711$. Then, we adopt an average value considering the following criteria that take into account the different sensitivity ranges of each diagnostic: if $n_e([\text{S II}] \lambda 6731/\lambda 6716) < 100 \text{ cm}^{-3}$, we adopt $n_e = 100 \pm 100 \text{ cm}^{-3}$. If $100 \text{ cm}^{-3} \leq n_e([\text{S II}] \lambda 6731/\lambda 6716) < 1000 \text{ cm}^{-3}$, we adopt the average between $n_e([\text{S II}] \lambda 6731/\lambda 6716)$ and $n_e([\text{O II}] \lambda 3726/\lambda 3729)$. If $n_e([\text{S II}] \lambda 6731/\lambda 6716) \geq 1000 \text{ cm}^{-3}$, we adopt the averages of $n_e([\text{S II}] \lambda 6731/\lambda 6716)$, $n_e([\text{O II}] \lambda 3726/\lambda 3729)$, $n_e([\text{Cl III}] \lambda 5538/\lambda 5518)$, $n_e([\text{Fe III}] \lambda 4658/\lambda 4702)$, and

¹ The “ t^2 ” parameter is the root mean square deviation from the averaged nebular temperature. It is a quantitative measure of the internal temperature variations of the gas, according to the formalism proposed by M. Peimbert. $t^2 = 0$ implies a homogeneous temperature structure.

n_e ([Ar IV] $\lambda 4740/\lambda 4711$). In some star-forming regions, it was not possible to determine the density; in such cases, we adopted $n_e = 100 \pm 100 \text{ cm}^{-3}$. With the average n_e , we then calculated T_e ([O III] $\lambda 4363/\lambda 5007$). In all cases, we used PyNeb 3.11 (Luridiana et al. 2015), adopting the atomic data from Table A1.

The determination of $T_e(\text{He I})$ was carried out by comparing the observed intensity ratios of He I RLs $\lambda 7281/6678$ and $\lambda 7281/5876$ with theoretical recombination predictions, adopting the average density of each region. As established by Zhang et al. (2005) and Méndez-Delgado et al. (2021a), the dependence of these line intensity ratios on n_e is small, and potential errors in this parameter introduced by internal density variations (Rubin 1989) will not influence our results. Although He I $\lambda 5876$ is a line from the triplet system, it is minimally affected by the metastability of the 2^3S level. As shown in Fig. 4 of Zhang et al. (2005) and our Figs A1, A2, there is excellent consistency between $T_e(\text{He I } \lambda 7281/\lambda 6678)$ and $T_e(\text{He I } \lambda 7281/\lambda 5876)$. The determination of $T_e(\text{He I})$ was made using effective recombination coefficients under the assumption of “Case B” from both Porter et al. (2012, 2013) and the most recent values from Del Zanna & Storey (2022) to detect possible errors or anomalies in the atomic data. The first set of atomic data has been widely adopted in the scientific literature for the determination of Y_p (Izotov et al. 2014; Valerdi et al. 2019; Aver et al. 2022) and other studies of He^+ abundances, and is used by default in the latest version of the Cloudy photoionization model (Ferland et al. 2017). The second set of data has undergone a careful revision of the He I model and is expected to be a substantial improvement over previous data.

Unlike the case with CEL-ratios, PyNeb does not have a routine like *getTemDen* to directly determine T_e using RL-ratios. For these cases, we define the emissivity of each line using the *getEmissivity* routine from PyNeb over a wide range of temperatures. For the atomic data from Porter et al. (2012, 2013), the temperature range considered is from 5,000K to 25,000K in steps of 10K. The atomic data were not calculated by these authors outside the mentioned temperature range. For the data from Del Zanna & Storey (2022), we considered a range from 500K to 32,000K, also using steps of 10K. We then used the *interp1d* function from the SciPy package (Virtanen et al. 2020) to interpolate these emissivities and transform the RL-ratios into T_e values. In each case, we considered the observational errors of the lines and propagated their effects using Monte Carlo calculations with 1,000 points. The final $T_e(\text{He I})$ adopted in this work is the average of $T_e(\text{He I } \lambda 7281/\lambda 6678)$ and

$T_e(\text{He I } \lambda 7281/\lambda 5876)$, using the atomic data from Del Zanna & Storey (2022).

In the case of PNe, we analyze the relationship between the temperature structure, $T_e(\text{[O III]})-T_e(\text{He I})$, and the abundance discrepancy of O^{2+} obtained from RLs and CELs. For the determination of these ionic abundances, $T_e(\text{[O III]})$ and the averaged density for each region are used in all cases, as well as the reported intensities of [O III] $\lambda\lambda 4959, 5007$ and the observed RLs from the O II V1 multiplet ($\lambda\lambda 4638.86, 4641.81, 4649.13, 4650.84, 4661.63, 4673.73, 4676.23, 4696.35$), following the methodology described in detail by Méndez-Delgado et al. (2023a). For this purpose, we adopt the O II effective recombination coefficients from Storey et al. (2014).

The densities, temperatures, He I line intensities, theoretical He I fluxes, and ionic abundances of the analyzed nebulae are presented in Tables from A5 to A23.

3. RESULTS

In Fig. 2, we show the resulting distribution of $T_e(\text{He I})$ and $T_e(\text{[O III]})$ for the sample of ionized nebulae analyzed in this work, considering the atomic data from Del Zanna & Storey (2022). We have drawn the PNe with smaller symbols than the star-forming regions to avoid overlapping. There is a clear and pronounced trend of $T_e(\text{He I}) < T_e(\text{[O III]})$. Interestingly, qualitatively, the trend observed in star-forming regions does not differ from what is obtained in PNe. In the same figure, we have performed a linear fit between $T_e(\text{He I})$ and $T_e(\text{[O III]})$ considering only the star-forming regions, presented in Eq. (1):

$$T_e(\text{He I}) = (0.48 \pm 0.05) \times T_e(\text{[O III]}) + (2500 \pm 600) \text{ [K].} \quad (1)$$

The fit was conducted using the Orthogonal Distance Regression (ODR) method, considering uncertainties in both $T_e(\text{He I})$ and $T_e(\text{[O III]})$. The Pearson correlation coefficient $r = 0.46$ is moderate due to the observational scatter. However, it is statistically significant ($p < 0.01$) for a sample size of 175 H II regions and star-forming galaxies. The histogram of the differences is presented in Fig. 3, which shows that the largest deviations occur in planetary nebulae, followed by star-forming galaxies, with H II regions being the least discrepant.

We highlight that the observed trend in Fig. 2 does not depend on the choice of He I atomic data. In Fig. A3, we show that $T_e(\text{He I})$ determined using both the atomic

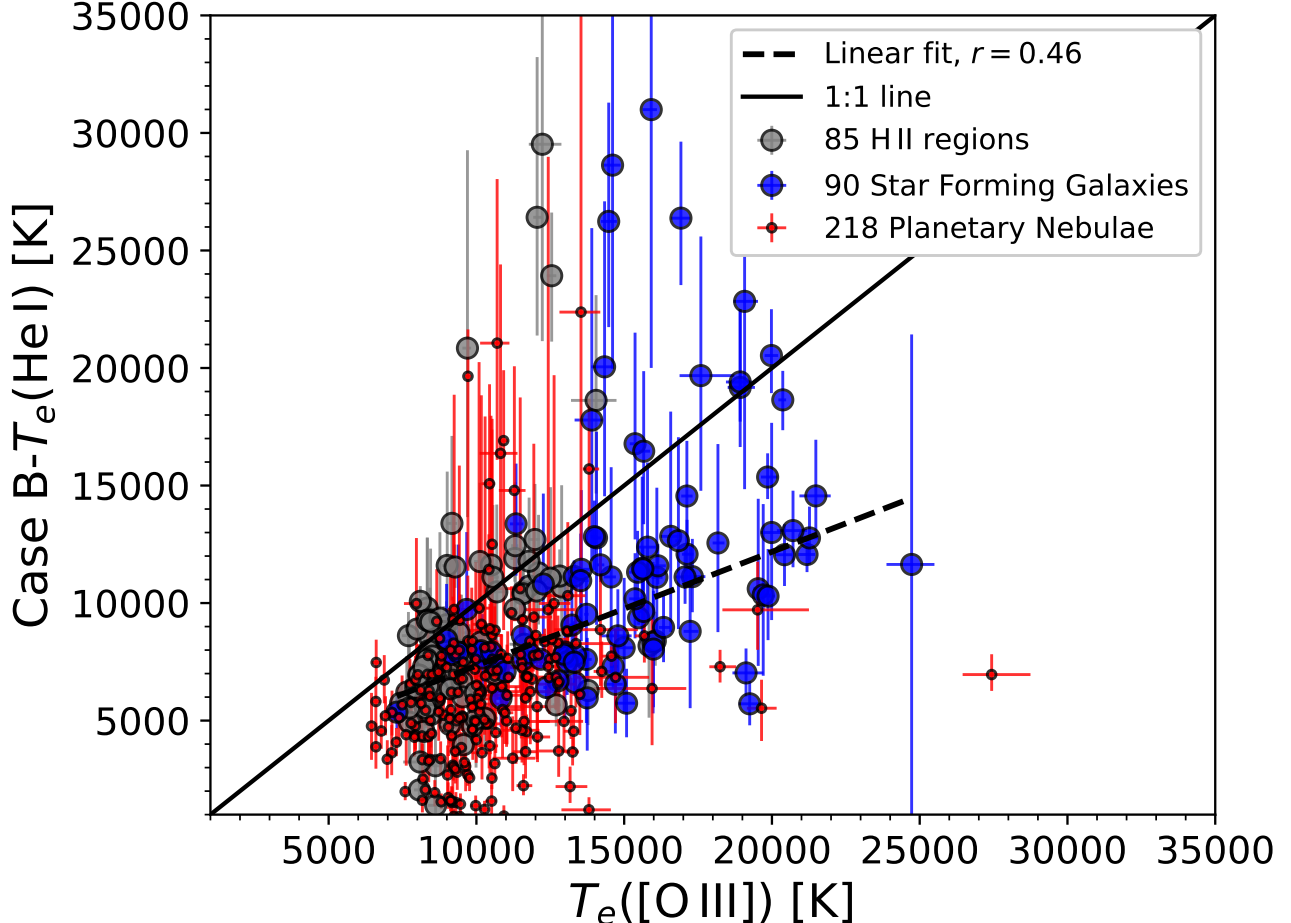


Figure 2. Comparison of direct determinations of high-ionization gas temperature diagnostics, $T_e(\text{He I})$ and $T_e(\text{[O III]})$, in several types of photoionized nebulae. $T_e(\text{He I})$ was derived by using He I $\lambda 7281/\lambda 5876$ and/or He I $\lambda 7281/\lambda 6678$ assuming the “Case B” recombination conditions. The linear fit shown considers only H II regions and star-forming Galaxies and is presented in Eq. (1). Note the overall trend of lower values of $T_e(\text{He I})$ compared to $T_e(\text{[O III]})$.

data from Porter et al. (2012, 2013) and Del Zanna & Storey (2022) are reasonably consistent².

4. DISCUSSION

Under ideal conditions of thermal and chemical homogeneity and dominance of the “Case B” recombinations, as is generally assumed in the determination of chemical abundances in ionized nebulae, one would expect relatively good consistency between $T_e(\text{He I})$ and $T_e(\text{[O III]})$, given that both are high-ionization ions. In Fig. 2, we demonstrate that statistically, there is a gen-

eral trend of $T_e(\text{He I}) < T_e(\text{[O III]})$ across all ionized nebulae, including star-forming regions and planetary nebulae, both Galactic and extragalactic. This result is very important because it indicates a serious issue in one of the basic physical principles assumed to infer $T_e(\text{He I})$ and/or $T_e(\text{[O III]})$.

4.1. Are There Potential Systematic Errors in $T_e(\text{He I})$?

$T_e(\text{He I})$ was determined from the line ratios of He I $\lambda 7281/\lambda 6678$ and He I $\lambda 7281/\lambda 5876$. If $T_e(\text{He I})$ is “too low” it could be because the flux of He I $\lambda 7281$ is fainter or the flux of He I $\lambda 6678, 5876$ is brighter than expected. Quantitatively, in star-forming regions, the flux of He I $\lambda 7281$ should be systematically about $\sim 15\%$ more intense than what we observe to achieve good consistency between $T_e(\text{He I})$ and $T_e(\text{[O III]})$, as shown in Fig. 4. For PNe, the difference is approximately $\sim 30\%$.

² Note, however, that there is a slight overestimate of $T_e(\text{He I})$ when using the data from Porter et al. (2012, 2013) in high-temperature regions ($T_e > 15,000\text{K}$). This is due to the overestimate of the emissivity of He I $\lambda 6678$ by the atomic data from Porter et al. (2012, 2013), which has been widely discussed and corrected by Del Zanna & Storey (2022).

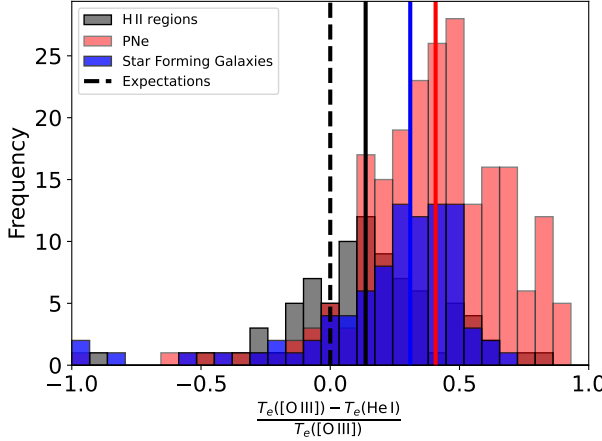


Figure 3. Histogram of the differences between $T_e([O\text{ III}])$ and $T_e(\text{He I})$ observed in Fig. 2. The colored vertical lines represent the median values of each distribution. The vast majority of all targets show a positive difference with $T_e([O\text{ III}])$ significantly larger than $T_e(\text{He I})$.

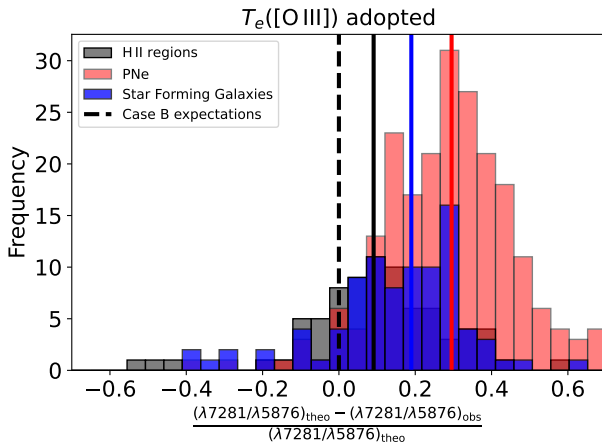


Figure 4. Distribution of the differences between the theoretical and observed values of the intensities of the He I $\lambda 7281$ line, using the flux of the He I $\lambda 5876$ line as normalization in the sample of analyzed regions. $T_e([O\text{ III}])$ was adopted to model the line emissivities under “Case B” using the recombination coefficients from Del Zanna & Storey (2022). The colored vertical lines represent the median values of each distribution.

One might wonder if this is simply an error in the effective recombination coefficients for this line. This hypothesis seems unlikely considering that almost all available atomic calculations in the literature, using various approaches and independently, converge on very similar emissivities for this line (Smits 1996; Benjamin et al. 1999; Porter et al. 2005, 2012, 2013; Del Zanna & Storey 2022).

Alternatively, there could be errors in the emissivities of He I $\lambda 6678$ and He I $\lambda 5876$. This hypothesis would call into question most determinations of He⁺ abundance in the literature, which are generally based on the intensity of the brighter optical He I lines, particularly He I $\lambda 5876$. Nevertheless, the good consistency shown between observational and theoretical values of the relative fluxes of He I $\lambda 5876/\lambda 6678$ (see Fig. A2), despite coming from systems with different spin multiplicity, seems to rule out this idea.

The fact that the observed flux of He I $\lambda 7281$ is significantly fainter than expected from recombination theory was noted by Porter et al. (2007) in the observations of the Orion Nebula reported by Esteban et al. (2004). In the face of the mismatch between the model and observations for this line, those authors suggested that the error must come from the observations, particularly from the reddening correction adopted by Esteban et al. (2004), which was based on the work of Costero & Peimbert (1970). Certainly, extinction plays an important role when comparing the relative fluxes to H β of the different He I lines, and in this sense, the use of the extinction curve by Blagrave et al. (2007) in the Orion Nebula induces a notable improvement³. However, the role that optical extinction plays in the He I $\lambda 7281/\lambda 6678$ and He I $\lambda 7281/\lambda 5876$ ratios is very small. More importantly, to explain the general trend observed in Fig. 2 in terms of errors in the extinction correction, there would need to be a widespread error in all the reddening curves used in the spectral range around $\sim \lambda 7281$, regardless of the geometric, dust, and metallicity conditions of the ionized regions studied here, which is highly unlikely.

Other errors in He I $\lambda 7281$, such as contamination by sky lines, which are abundant in this spectral region, may still be present, even though the DESIRED project carefully noted observational defects to avoid introducing spurious noise. This contamination could artificially increase the measured flux of He I $\lambda 7281$, thus raising $T_e(\text{He I})$, which might explain why a small subset of regions show $T_e(\text{He I}) > T_e([O\text{ III}])$ in Fig. 2 despite visual checks. Hypothetically speaking, the presence of telluric absorptions in He I $\lambda 7281$ could induce the observed effect of $T_e(\text{He I}) < T_e([O\text{ III}])$. However, our sample includes both Galactic and extragalactic objects with dif-

³ In this work, we use the fluxes of the Orion Nebula from Esteban et al. (2004), corrected for reddening using the curve from Blagrave et al. (2007) instead of that from Costero & Peimbert (1970) and the HI Balmer and Paschen lines (Méndez-Delgado et al. 2023b). As shown in Table A8, the “problem” with He I $\lambda 7281$ is not eliminated; it is only reduced by 6% with respect to the use of the reddening curve from Costero & Peimbert (1970).

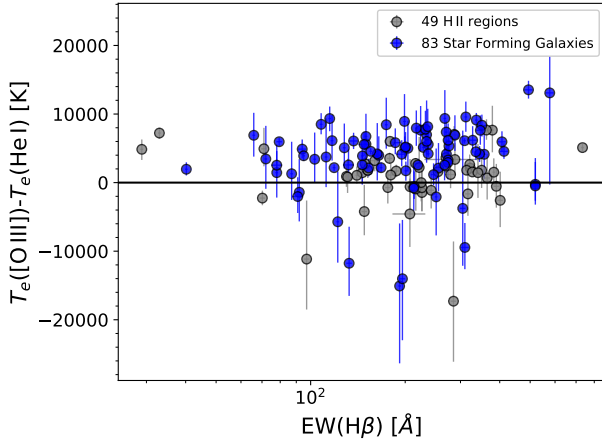


Figure 5. Comparison between the temperature difference $T_e(\text{[O III]}) - T_e(\text{He I})$ and the reported equivalent width of $\text{H}\beta$ ($\text{EW}(\text{H}\beta)$). If the temperature differences were due to uncorrected stellar absorption in the He I lines, a trend with $\text{EW}(\text{H}\beta)$ would be expected. The effects of stellar absorption should be more pronounced in regions with lower $\text{EW}(\text{H}\beta)$.

ferent radial velocities and spectral resolutions, making it unlikely that a systematic effect, such as sky contamination or telluric absorptions, would affect all objects in the same way. This effect alone cannot explain the general trend that, statistically, $T_e(\text{He I}) < T_e(\text{[O III]})$.

Underlying stellar absorption can significantly affect He I emission lines, reducing their observed flux, as demonstrated in studies on primordial helium abundance (Skillman et al. 1998; Olive & Skillman 2001; Peimbert et al. 2007; Aver et al. 2015). If absorption is more significant in He I $\lambda 7281$ than in He I $\lambda 5876$ or He I $\lambda 6678$, it could artificially lower $T_e(\text{He I})$. To test this in our extragalactic H II regions and star-forming galaxies, we compared the $T_e(\text{[O III]}) - T_e(\text{He I})$ difference with the equivalent width of $\text{H}\beta$ ($\text{EW}(\text{H}\beta)$), as stellar absorption is expected to be more important in regions with low $\text{EW}(\text{H}\beta)$ (Izotov & Thuan 2004). Fig. 5 shows no clear correlation between $T_e(\text{[O III]}) - T_e(\text{He I})$ and $\text{EW}(\text{H}\beta)$, suggesting that stellar absorption does not cause the trend in Fig. 2. Additionally, Galactic H II regions and PNe, where stellar absorption is absent, also show the same pattern of $T_e(\text{He I}) < T_e(\text{[O III]})$ found in the extragalactic star-forming regions.

Finally, it is important to note that a hypothetical metastability of the 2^1S level, analogous to the 2^3S level in the triplet system, would cause lines such as He I $\lambda 5016$ to be less intense than their theoretical recombination predictions, while He I $\lambda 7281$ would show the opposite effect, being more intense than predicted. This scenario is not observed and is therefore ruled out.

4.2. Assessing the Validity of the “Case B” Assumption for the Singlet He I Atom

The fact that He I $\lambda 7281$ is fainter than predicted by recombination theory could indicate that some process is reducing the population of the 3^1S level. In addition to direct recombination to this level, it is substantially populated through transitions from the n^1P levels, as shown in Fig. 6.

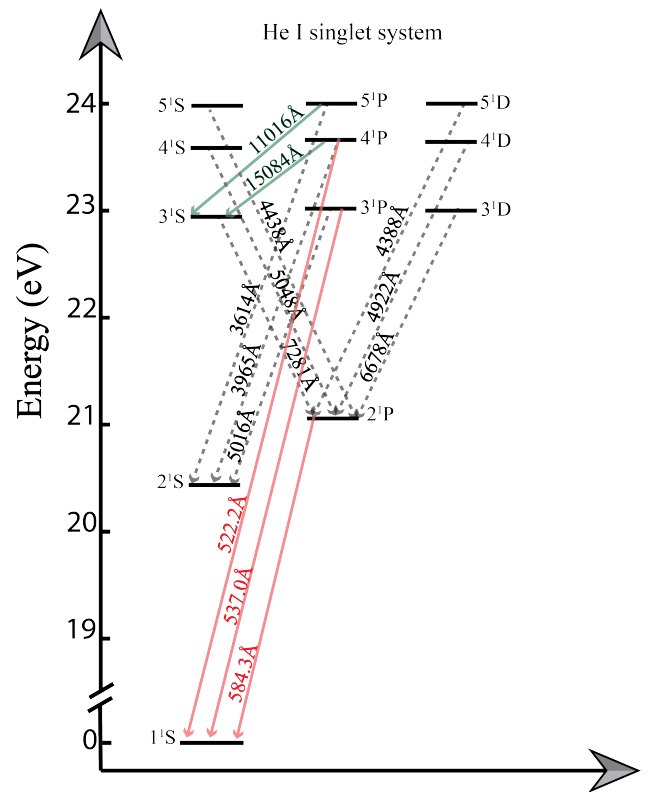


Figure 6. Grotrian diagram (Grotrian et al. 1928) for the singlet system of He I. Adapted and extended from Fig. D4 of Méndez-Delgado et al. (2021a). Some permitted transitions from the levels $n^1P \rightarrow 1^1S$ are marked in red. The transitions $4^1P \rightarrow 3^1S$ and $5^1P \rightarrow 3^1S$, which give rise to He I $\lambda\lambda 15084, 11016$ lines, respectively, are the most important for increasing the population of the 3^1S level after direct recombination and are highlighted in green.

Among all $n^1P \rightarrow 3^1S$ transitions, the most important are those from the 4^1P and 5^1P levels, which give rise to the infrared lines He I $\lambda 15084\text{\AA}$ and $\lambda 11016\text{\AA}$, re-

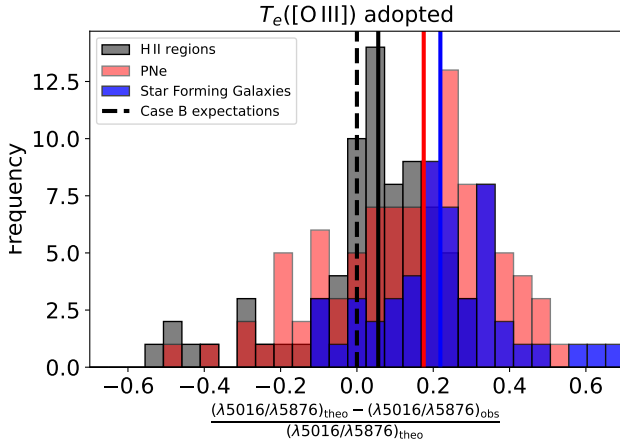


Figure 7. The distribution of the differences between the theoretical and observed values of the intensities of the He I $\lambda 5016$ line, using the flux of the He I $\lambda 5876$ line as normalization in the sample of analyzed regions. This is the same plot as in Fig. 4 but considering the He I $\lambda 5016$ line instead of the He I $\lambda 7281$ line.

spectively⁴. These transitions contribute approximately 30% and 20% of the flux from all lines emitted by transitions from various P levels to the 3^1S level (Del Zanna & Storey 2022). If the rate of $n^1P \rightarrow 3^1S$ transitions decreases for some reason, the population of the 3^1S level will also decrease significantly, and consequently, the flux of He I $\lambda 7281$ will be lower than expected.

A phenomenon that could cause a decrease in the rate of $n^1P \rightarrow 3^1S$ transitions is a general reduction in the electron population of the n^1P levels. This could occur if, on average, photons originating from the transitions $n^1P \rightarrow 1^1S$, such as those marked in red in Fig. 6, “escape” or are absorbed by other ions or compounds rather than being reabsorbed by HeI. This would violate the “Case B” recombination assumption, and in the extreme case where all photons from $n^1P \rightarrow 1^1S$ are lost, the conditions would resemble those of “Case A”⁵. Obviously, “Case A” generally does not apply for HeI because it would imply that the emissivity of the HeI singlets arising from the n^1P levels should be

⁴ Note that these lines have been scarcely studied in the literature, but they fall within the spectral range covered by instruments like NIRSPEC on the James Webb Space Telescope (JWST). In the presence of temperature variations and/or deviations from Case B recombination, these lines should also be affected in a manner analogous to the rest of the HeI singlets studied in the present article.

⁵ Note that the fact that photons from $n^1P \rightarrow 1^1S$ could be escaping on average does not imply the absence of potential fluorescent excitations $1^1S \rightarrow n^1P$ coexisting with the aforementioned photon escaping. This is known as “Case C” (Baker & Menzel 1938; Ferland 1999).

up to two orders of magnitude smaller than in “Case B” (Brocklehurst 1972; Smits 1996), and therefore lines such as He I $\lambda\lambda 5016, 3614, 3965$ should not be widely detected. In reality, these lines are observed, although with a flux lower than expected, as shown in Figs 7, A4, and A5. An interesting hypothetical case to explore would be an intermediate situation in which a fraction of the singlet He I is in conditions close to “Case A” while the rest is in “Case B”.

4.3. A toy model with a mixed Case A+Case B scenario

Now, let us explore the case where the differences between the observed fluxes and the theoretical predictions presented in Figs. 4, 7, A4, and A5 are assumed to be due to deviations from “Case B” as some authors have suggested (Liu et al. 2006; Izotov et al. 2007). For this purpose, let us assume the following toy model:

$$I(\lambda)_{\text{obs}} = \gamma \times I(\lambda)_{\text{Case B}} + (1 - \gamma) \times I(\lambda)_{\text{Case A}}, \quad (2)$$

where $I(\lambda)_{\text{obs}}$ represents the total observed intensity of a HeI singlet line, $I(\lambda)_{\text{Case B}}$ is the intensity that would be emitted under “Case B” and γ is the fraction of the gas that is in “Case B” conditions. To determine γ in each case is relatively straightforward. One can use the fact that the “Case B” and “Case A” emissivities of He I $\lambda 5016$ differ substantially and to a greater extent than He I $\lambda 7281$, as do the other transitions originating from the n^1P levels. We can use the intensity of the He I $\lambda 5876$ line to normalize the emissivities, as it is a triplet case-independent line with very small effects from self-absorption. Considering Eq. 2 for the specific case of He I $\lambda 5016$, we derive Eq. 3:

$$\frac{I(5016)_{\text{obs}}}{I(5876)_{\text{obs}}} \times \frac{j(5876)_{\text{Case B}}}{j(5016)_{\text{Case B}}} = \gamma + \epsilon \times (1 - \gamma), \quad (3)$$

where $j(\lambda)$ represents the emissivity of the line at λ , and $\epsilon = j(5016)_{\text{Case A}}/j(5016)_{\text{Case B}}$. The precise value of ϵ depends very little on the physical conditions of the gas and is approximately $\epsilon \approx 2.30 \times 10^{-2}$ (Smits 1996).

Using the observational values of He I $\lambda 5016$ from our sample of ionized nebulae and adopting $T_e([O III])$ by default, we determine γ following Eq. 3. Subsequently, we use this value of γ to model the emissivities of He I $\lambda 7281$ and He I $\lambda 6678$, considering Eq. 2, although for the latter line, the difference between “Case A” and “Case B” is around 1%. Note that for this, we need to use the “Case A” recombination coefficients from Smits (1996), as the calculations by Porter et al. (2012, 2013) and Del Zanna & Storey (2022) are limited to “Case B”.

This may introduce some additional uncertainties. To mitigate them, instead of directly combining the predictions of $j(\lambda)_{\text{Case A}}$ from Smits (1996) along with the predictions of $j(\lambda)_{\text{Case B}}$ from Del Zanna & Storey (2022), we use $j(\lambda)_{\text{Case B, DZ22}} \times j(\lambda)_{\text{Case A, S96}} / j(\lambda)_{\text{Case B, S96}}$. Although the emissivities for He I $\lambda 5016$, He I $\lambda 7281$, and He I $\lambda 6678$ may differ slightly between Smits (1996) and Del Zanna & Storey (2022), the relative ratios of the emissivities between the two recombination cases are in excellent agreement. This can be seen in Table A1 of Del Zanna & Storey (2022), which shows the comparison of the emissivities between “Case A” and “Case B” for the strongest He I lines at $T_e = 20,000$ K and $n_e = 10^6$ cm $^{-3}$.

The median γ values obtained for each type of object are 0.75, 0.88, and 0.75 for PNe, HII regions, and SFGs, respectively. Using the toy model described above, we can re-determine $T_e(\text{He I } \lambda 7281/\lambda 6678)$ and $T_e(\text{He I } \lambda 7281/\lambda 5876)$ using the same procedure described in Sec 2, now adding the subscript TM . In Fig. 8, we show the resulting distribution from this toy model, where $T_e(\text{He I})_{TM} < T_e([\text{O III}])$, although the difference is substantially smaller than that shown in Fig. 1. The linear fit considering only the star-forming regions is shown in Eq. (4):

$$T_e(\text{He I})_{TM} = (0.77 \pm 0.08) \times T_e([\text{O III}]) + (540 \pm 940) \text{ [K].} \quad (4)$$

The slope in Eq. (4) is closer to one than in Eq. (1) and the offset is significantly smaller. However, a discrepancy still exists.

The comparison between $T_e(\text{He I})$ and $T_e(\text{He I})_{TM}$ is shown in Fig. 9, and the fitted relationship is presented in Eq. (5):

$$T_e(\text{He I})_{TM} = (1.19 \pm 0.03) \times T_e(\text{He I})_{\text{Case B}} + (70 \pm 170) \text{ [K].} \quad (5)$$

Here, the slope is actually greater than one but the offset has diminished considerably.

The fact that $T_e(\text{He I})_{TM} < T_e([\text{O III}])$ implies a failure of the initial hypothesis that the differences between the theoretical and observed values of He I singlets were due to deviations from “Case B” to “Case A.” This demonstrates that this toy model cannot completely explain Fig. 2. Even if there are deviations from “Case B” to “Case A”, one would need to invoke temperature variations or another additional phenomenon to achieve simultaneous consistency between the observed and predicted intensities of He I $\lambda 5016$ and He I $\lambda 7281$. Possibly, a complete radiative treatment, such as in “Case C” where there is a fluorescent excitation component, could be useful for exploring this. In principle, the photoionization code Cloudy (Ferland et al. 2017) in-

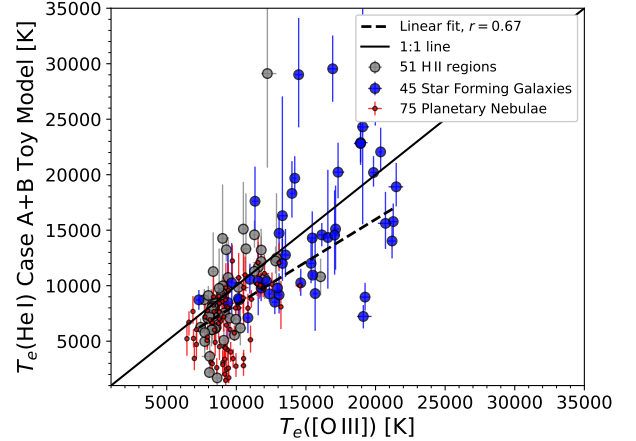


Figure 8. The same as Fig. 2, but considering a combination of “Case B” and “Case A” conditions in a toy model described by Eq. (2). The linear fit shown considers only H II regions and star-forming Galaxies and is presented in Eq. (4).

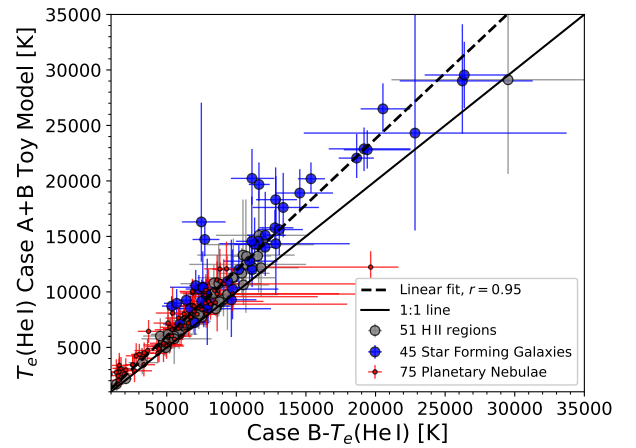


Figure 9. Comparison between $T_e(\text{He I})$ obtained assuming the “Case B” recombination versus $T_e(\text{He I})_{TM}$, calculated assuming a mixture between “Case A” and “Case B”, as described in Sec. 4.3. The linear fit considering all spectra is shown in Eq. (5).

cludes a complete radiative treatment and its models include predictions “with all processes included”. However, as demonstrated by Izotov et al. (2013), this treatment appears inconsistent with observational values for He I and remains as an open issue. A comprehensive radiative treatment requires studying each object individually, which is well beyond the scope of this work.

As a consequence of the previous discussion, we caution against using He I singlet lines for extinction corrections as is suggested by some authors (Zamora et al. 2022). Relying on their observed fluxes for such correc-

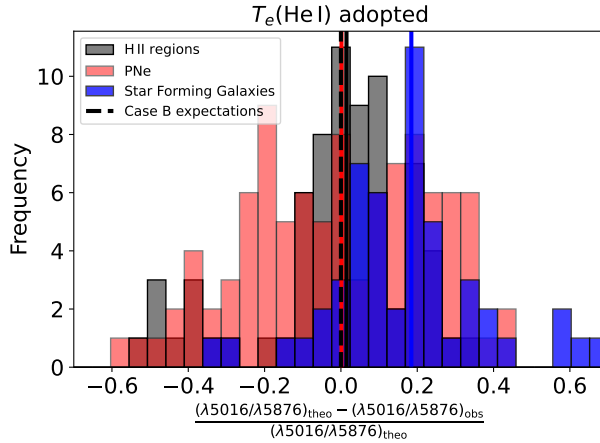


Figure 10. Same as in Fig. 4, but considering the He I $\lambda 5016$ line and $T_e(\text{He I})$. This temperature was derived from the He I $\lambda 7281/\lambda 5876$ and/or $\lambda 7281/\lambda 6678$ ratios under “Case B”, using the recombination coefficients from Del Zanna & Storey (2022).

tions while assuming a “Case B” scenario will lead to systematic errors.

4.4. Are the temperature variations sufficient to simultaneously explain He I $\lambda 5016$ and He I $\lambda 7281$?

In Sec. 4.3 we have demonstrated that “Case B” deviations alone are not sufficient to simultaneously explain, in a quantitatively way, the low observed fluxes of He I $\lambda 5016$ and He I $\lambda 7281$ compared to what is expected when adopting $T_e(\text{[O III]})$. Now it is time to explore if $T_e(\text{He I})$ derived assuming “Case B” and the ratios $\lambda 7281/\lambda 6678$ and/or $\lambda 7281/\lambda 5876$ could be representative of the He⁺ ion. Under this premise, one would expect the theoretical predictions of He I $\lambda 5016/\lambda 5876$, assuming $T_e(\text{He I})$, to be consistent with the observed values. If this premise holds true, it could be interpreted as suggesting that the temperature variations, caused by some physical phenomenon, are sufficient to explain the trend of $T_e(\text{He I}) < T_e(\text{[O III]})$ observed in Fig. 2.

In Fig. 10, we show that, statistically, there is good consistency between the predictions and observations of He I $\lambda 5016/5876$ in H II regions and PNe, but not in SFGs, when adopting $T_e(\text{He I})$ derived under “Case B” conditions. This suggests that, in the first two groups of objects, $T_e(\text{He I})$ might be representative of the He⁺ ion, and its discrepancy with $T_e(\text{[O III]})$ could reveal the presence of temperature inhomogeneities caused by gas heating or the presence of cold, high-metallicity clumps, with only a minor impact from potential deviations from “Case B”. However, the broad width in the distribution of observed values does not allow us to rule out

the possibility that deviations from “Case B” may still be generally relevant. In the case of SFGs, even when considering $T_e(\text{He I})$, the observed values of $\lambda 5016/5876$ are statistically too low. This indicates that, although temperature variations may be present, an additional phenomenon is required to achieve simultaneous consistency between the predictions and observations of the $\lambda 7281$ and $\lambda 5016$ singlets.

4.5. Potential Causes and Consequences of Partial Deviations from “Case B”

As discussed in Sec. 4.3, the deviations from the “Case B” recombination towards the “Case A” as modeled in Eq. 2 does not seem to explain, on its own, the observed trend of $T_e(\text{He I}) < T_e(\text{[O III]})$. However, it is likely to contribute substantially to the reduction in the flux of He I $\lambda 7281$. This phenomenon appears to be generally present in all the ionized regions analyzed here, including Galactic and extragalactic H II regions, star-forming galaxies, and planetary nebulae. In the sample analyzed, factors such as geometry, dust abundance, and velocity gradients—physical conditions that might induce deviations from the “Case B” recombination scenario towards “Case A” (Cota & Ferland 1988)—are expected to vary widely. It is difficult to identify a single physical mechanism that could account for this recombination case deviation, given that it must be present across all ionized nebulae.

Helium accounts for approximately $\sim 10\%$ of the total number of atoms in the gas of ionized nebulae. If around $\sim 25\%$ of He I atoms in the singlet system are losing $n^1P \rightarrow 1^1S$ photons, this number of atoms is comparable to the total number of all metals combined. This makes it unlikely that a specific heavy element ion could completely absorb these photons before they are reabsorbed by helium, although certainly many heavy elements could be excited or ionized by these photons, as they have energies between 21.2 and 24.6 eV. Given that dust abundance within photoionized environments changes with metallicity, dramatically decreasing in metal-poor regions (Roman-Duval et al. 2022a,b; Méndez-Delgado et al. 2024b), it is unlikely that dust alone accounts for all the missing photons. This is especially true in metal poor star-forming galaxies, which have lower dust-to-gas ratios, and yet exhibit significant discrepancies in He I $\lambda\lambda 5016, 7281$ (see Figs. 7 and 4). The only element that appears sufficiently abundant to absorb such photons is H I.

The photons from the $n^1P \rightarrow 1^1S$ transitions of the singlet system of He I are able to photoionize H I. This suggests that these photons could be lost by being absorbed through the photoionization process of

H I, rather than being reabsorbed by He I. The photoionization cross-section of H I is quite high around ~ 13.6 eV but decreases rapidly at higher energies (Bell & Kingston 1967; Brown 1971). The probability that H I is ionized by a photon of ~ 22 eV is approximately ~ 4 times less than being ionized by a photon near 13.6 eV, which makes this scenario seem plausible as the H I is around ~ 9 times more abundant than He I. If this mechanism is indeed operating, it would imply the need to include complete radiative treatments that consider these photoionizations of H I originating from He I, which current photoionization models do not naturally predict. Additionally, the possibility that $n^1P \rightarrow 1^1S$ photons could partially excite permitted transitions in a wide variety of ions should not be dismissed (Reyes-Rodríguez et al. 2024) and remains an open question for several elements.

Another possibility, though more speculative, is the escape of these ionizing photons into the ISM without being degraded into lower-energy photons. Since helium is the second most abundant element in the universe, the quantity of ionizing photons contributing to the ISM would be significant enough to play an important role in the presence of the Diffuse Ionized Gas (DIG). The DIG is observed in nearly all galaxies, and its origin is widely debated (Wood & Mathis 2004; Haffner et al. 2009; Belfiore et al. 2022; McClymont et al. 2024; González-Díaz et al. 2024b,a). The escape of relatively energetic photons, such as the He I $n^1P \rightarrow 1^1S$ photons, could contribute to the relatively hard ionization conditions of the DIG (Wood & Mathis 2004).

In the speculative case of a He I $n^1P \rightarrow 1^1S$ photon escaping from the ionized ISM, one might wonder if such escape could also occur for H I, an atom with similar configuration. The emissivity of some H I RLs, such as H α or H β , under “Case A” recombination is approximately 65% lower than the predictions under “Case B” (Storey & Hummer 1995). If there is a $\sim 25\%$ deviation from “Case B” to “Case A” for H I, the overall emissivity of these H I RLs would decrease by roughly $\sim 10\%$. This would imply a general systematic error in the chemical abundances derived from CELs or RLs that are independent of the recombination case with respect to H I, resulting in overestimations by the same fraction of about $\sim 10\%$. For example, the determinations of He/H abundances obtained from He I RLs of the triplet system, as is generally the case in the literature (Izotov et al. 2007; Aver et al. 2015; Valerdi et al. 2019), would be systematically overestimated by this effect, as the triplet system has no Case A-Case B distinction since the $2^3S \rightarrow 1^1S$ transition is highly forbidden. Galaxy masses, star formation rates, or other properties that directly depend on

the effective recombination coefficient of H α or H β under the assumption of “Case B” would also be affected. The extinction coefficient $c(H\beta)$, computed with the H α /H β ratio, would also be affected, but to a relatively small degree that would only become noticeable in cases of significant deviations and high observational precision (Scarlata et al. 2024).

4.6. $T_e(O\text{III}) - T_e(\text{HeI})$ and the Abundance Discrepancy Problem

The observation of $T_e(\text{HeI}) < T_e(\text{[O III]})$ in a large sample of ionized nebulae aligns qualitatively with the temperature variations paradigm proposed by Peimbert (1967). In this paradigm, the presence of internal temperature variations in the gas introduces systematic biases toward higher temperatures in CEL diagnostics, as the emissivities of these lines have an exponential dependence on T_e . This issue does not affect RL-based diagnostics, such as $T_e(\text{HeI})$, which have a linear dependence on T_e . An overestimation of T_e induced by CEL diagnostics will lead to a general underestimation of chemical abundances based on CEL ratios relative to H β or H α , which are RLs. Notably, in all nebular studies where heavy-element RLs have been detected, a systematic discrepancy has been found between determinations based on these lines and their collisionally excited counterparts (Peimbert 2003; Esteban et al. 2004; García-Rojas et al. 2007; Méndez-Delgado et al. 2022; Berg et al. 2024). This longstanding problem, where CELs systematically yield lower abundances and the difference is usually quantified by the abundance discrepancy factor (ADF), dates back to the pioneering works of Bowen & Wyse (1939) and Wyse (1942) and continues to be widely debated to this day.

Zhang et al. (2005) studied $T_e(\text{HeI})$ and $T_e(\text{[O III]})$ in a group of planetary nebulae using the same methodology as ours, described in Sec. 2, with the difference that they used the effective recombination coefficients for He I from Benjamin et al. (1999). These authors found that $T_e(\text{HeI}) < T_e(\text{H I})$, which had been determined in previous works using the Balmer jump (BJ) and/or Paschen jump (PJ) continua. Among these works, the study by Liu et al. (2001) is particularly important, as they found that $T_e(\text{H I}) < T_e(\text{[O III]})$ and established a tight correlation between the ADF(O $^{2+}$) and $T_e(\text{[O III]}) - T_e(\text{H I})$ (see their Fig. 8). Although the correlation between ADF(O $^{2+}$) and $T_e(\text{[O III]}) - T_e(\text{H I})$ is one of the predictions of the Peimbert (1967) formalism, the finding that $T_e(\text{HeI})$ was lower than $T_e(\text{H I})$ was interpreted by Zhang et al. (2005) as evidence of a failure in the temperature fluctuation paradigm, which predicts $T_e(\text{HeI}) \approx T_e(\text{H I})$.

In Fig. 11, we show a correlation between $T_e(\text{[O III]}) - T_e(\text{He I})$ and the ADF(O^{2+}) in planetary nebulae where $T_e(\text{He I}) < T_e(\text{[O III]})$. This is consistent with the idea that hydrogen-poor clumps may exist in these objects, where cooling is especially efficient due to the concentration of heavy elements, as proposed by Torres-Peimbert et al. (1980) and Liu et al. (2001). The linear fit of this relationship for PNe is shown in Eq. (6):

$$\begin{aligned} \text{ADF}(\text{O}^{2+}) &= (2.15 \pm 0.23) \times 10^{-4} \\ &\times [T_e(\text{[O III]}) - T_e(\text{He I})] - (5.13 \pm 1.34) \times 10^{-1} [\text{dex}] \end{aligned} \quad (6)$$

However, it is important to note that under this paradigm, temperatures based on CEL ratios like $T_e(\text{[O III]})$ may be overestimated due to auroral level population by recombination from high-metallicity clumps (Gómez-Llanos et al. 2020, 2024; García-Rojas et al. 2022). In this hypothetical scenario, both O^{2+} abundances based on CELs and those based on RLs using the direct method are conceptually incorrect, as this method assumes a homogeneous chemical composition. However, depending on the contrast between the different chemical components, sometimes the CELs and sometimes the RLs will be closer to the average abundances (Morisset et al. 2023; Méndez-Delgado & García-Rojas 2023).

Note, however, that Fig. 11 is not inconsistent with the idea of temperature variations as proposed by Peimbert (1967). In contrast to the interpretation of Zhang et al. (2005), the possibility that $T_e(\text{He I}) < T_e(\text{H I})$ in PNe could be due to photon loss from the $n^1P \rightarrow 1^1S$ transitions, an effect not considered by Zhang et al. (2005). The correlation between $T_e(\text{[O III]}) - T_e(\text{He I})$ and the ADF(O^{2+}) in PNe shown in this work would not be lost when considering such effects, assuming the toy model described in Sec. 4.3, as $T_e(\text{He I})$ and $T_e(\text{He I})_{TM}$ are linearly related, as shown in Fig. 9. In any case, it would modify the slope and intercept shown in Eq. (6), but the correlation would remain.

For the case of H II regions and star-forming galaxies, if we follow the formalism of Peimbert (1967), assuming that $T_e(\text{He I}) \approx T_0$ (see Eq. 11 in Zhang et al. 2005) and considering Eq. (4) with a typical temperature of $T_e(\text{[O III]}) \approx 10,000$ K and Eq. 10 from Peimbert & Peimbert (2013), we obtain a root mean square deviation parameter (t^2) of $t^2 \approx 0.05$, which is typically found in star-forming regions to explain the ADF(O^{2+}) (García-Rojas & Esteban 2007; Esteban et al. 2009; Peimbert et al. 2017; Méndez-Delgado et al. 2022; Chen et al. 2024).

The above discussion is consistent with the general finding that RLs seem to predict lower temperatures

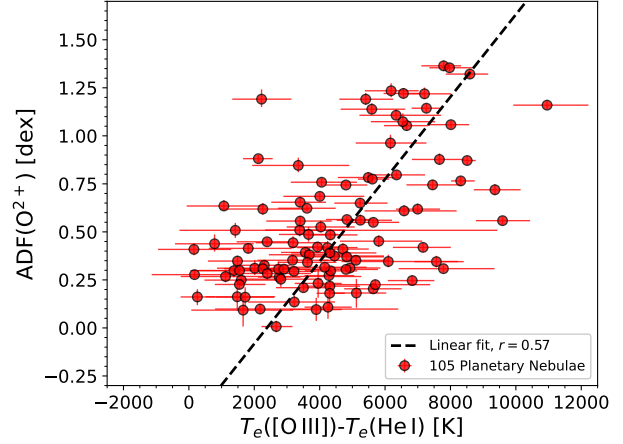


Figure 11. Relationship between the ADF(O^{2+}) and the temperature difference $T_e(\text{[O III]}) - T_e(\text{He I})$ for planetary nebulae, derived assuming the “Case B”, considering objects where $T_e(\text{He I}) < T_e(\text{[O III]})$. The ADF(O^{2+}) is the logarithmic difference between the O^{2+}/H^+ abundance determined using CELs ($\text{[O III]} \lambda\lambda 4959, 5007$) and RLs ($\text{O II } \lambda\lambda 4638.86, 4641.81, 4649.13, 4650.84, 4661.63, 4673.73, 4676.23, 4696.35$), using the direct method and adopting $T_e(\text{[O III]}) \lambda 4363/5007$. For consistency, only regions where the error in the flux of the O II-RLs is equal to or less than 20% were considered

than CELs. This is true for both O II (Méndez-Delgado et al. 2023a) and C II (Torres-Peimbert et al. 1980), and our work demonstrates that it could also be true for singlet-He I. Additionally, H I-RLs usually follow the same trend (although with some contradictory examples, see Guseva et al. 2007). Recently, Khan et al. (2024) determined $T_e(\text{H I})$ using H I radio RLs and the radio continuum in 496 Galactic H II regions. The resulting temperature distribution predicts notably lower temperatures than those provided by CELs. For example, the regions M42, Sh 2-83, and M20 (Esteban et al. 2004, 2017; García-Rojas et al. 2006), located at Galactic distances of 8.54, 13.2, and 4.88 kpc (Méndez-Delgado et al. 2022), have measured $T_e(\text{[O III]})$ temperatures of 8370 K, 10370 K, and 7800 K, respectively, while the $T_e(\text{H I})$ predicted by the radio RLs is 7780 K, 9160 K, and 7270 K, respectively.

Our results highlight the need to understand the nature of the discrepancies between the physical conditions derived from CELs and RLs. If anomalies such as the ADF were to stem from RLs, it would imply fundamental errors in our understanding of recombination processes, potentially involving atoms like He I and H I. To understand the ADF and nebular thermal structure, it is crucial to observe more faint and ultra-faint RLs, as these often reveal the most fundamental and important processes in our physical models. Relying solely on the

analysis of strong CELs from different transitions (in UV, optical, or infrared wavelengths) seems insufficient, as it may not detect inconsistencies in the photoionization equilibrium processes, dominated by H and He, which emit exclusively RLs.

Regarding the tensions between CELs and RLs, which sometimes exclusively focus on proving the absence or presence of temperature variations, it is important to address several points: (i) Potential shortcomings in the predictions of the t^2 -formalism proposed by Peimbert (1967) do not necessarily imply the absence of temperature variations; they may simply indicate that the modeling approach needs to be revised or it could indicate the existence of additional physical phenomena impacting the nebular abundances. Alternative paradigms also model temperature variations (see the excellent discussion by Stasińska 2002); (ii) The absence of temperature variations does not equate to the absence of problems. The existence of the ADF could have various causes. Depending on the source of this issue, the abundances derived from CELs might still be systematically incorrect (Méndez-Delgado & García-Rojas 2023).

5. SUMMARY AND FINAL THOUGHTS

In this manuscript, we report a systematic discrepancy between the observed fluxes of the singlet He I lines $\lambda\lambda 3614, 3965, 5016, 7281$ and the theoretical predictions under “Case B” in 393 optical spectra of Galactic and extragalactic H II regions, star-forming galaxies, and planetary nebulae. Of these spectra, 85 correspond to H II regions, 90 to star-forming galaxies, and the rest to planetary nebulae. In our analysis, we distinguish between star-forming regions and planetary nebulae. The observed He I-singlet lines are systematically weaker than expected, as shown in Figs. 4, 7, A4, and A5. These discrepancies persist regardless of whether the recombination coefficients from Porter et al. (2012, 2013) or Del Zanna & Storey (2022) are used. The latter dataset significantly improves the consistency between theoretical predictions and observations for the He I $\lambda 6678$ and He I $\lambda 5876$ lines.

When determining $T_e(\text{He I})$ observationally using the He I $\lambda 7281/\lambda 5876$ and He I $\lambda 7281/\lambda 6678$ ratios under the “Case B” recombination model, we systematically find that $T_e(\text{He I})$ is lower than $T_e([\text{O III}])$ across most spectra for all types of objects. Additionally, we find that for the case of planetary nebulae where $T_e(\text{He I}) < T_e([\text{O III}])$, there is a correlation between the discrepancy in abundances determined with [O III]-CELs and O II-RLs, quantified by the ADF(O^{2+}), and $T_e([\text{O III}]) - T_e(\text{He I})$. We have explored two potential explanations for the discrepancy between $T_e(\text{He I})$ and

$T_e([\text{O III}])$: deviations from the “Case B” for $n^1P \rightarrow 1^1S$ He I-transitions and the presence of temperature inhomogeneities, as proposed by Peimbert (1967).

In the scenario where photons from the $n^1P \rightarrow 1^1S$ transitions are lost rather than being reabsorbed by He I, we demonstrated that the toy model assuming a fraction of He I singlets are under “Case B” conditions while the rest are under “Case A” conditions fails to simultaneously explain the differences between the observations and the predictions for He I $\lambda\lambda 5016, 7281$. Even if this model is operating in reality, an additional phenomenon, such as temperature variations, must be invoked. It is necessary to explore a “Case C” that includes fluorescent excitations $1^1S \rightarrow n^1P$ to shed more light on what is happening with the He I singlets.

If we consider $T_e(\text{He I})_{TM}$ obtained from the toy model described earlier, this value remains systematically lower than $T_e([\text{O III}])$. The correlation between ADF(O^{2+}) and $T_e([\text{O III}]) - T_e(\text{He I})$ in planetary nebulae is maintained when considering this toy model. The linear fit between $T_e(\text{He I})_{TM}$ and $T_e([\text{O III}])$ for H II regions and star-forming galaxies, represented in Eq. (4), is roughly consistent with what is expected under the presence of temperature inhomogeneities as proposed by Peimbert (1967). This linear fit predicts $t^2 \approx 0.05$ with $T_e([\text{O III}]) \approx 10,000$ K, a commonly observed case in the literature. However, this model is not self-consistent, as it assumes $T_e([\text{O III}])$ to determine the fraction of He I in “Case B” conditions.

If significant deviations from “Case B” are observed in the singlet system of He I, it is important to understand why this issue is prevalent across a broad spectrum of objects. This phenomenon seems to affect a wide range of H II regions, star-forming galaxies, and planetary nebulae, which differ widely in their geometry, dust content, metallicity, and velocity gradients. We consider it possible that HI is absorbing some of the $n^1P \rightarrow 1^1S$ photons from the He I singlet system. However, this phenomenon does not seem to be naturally predicted by photoionization models, indicating radiative transfer effects that are generally not included. Such effects could also impact other elements with permitted transitions between different levels.

In a more speculative scenario, we also discuss the possibility that $n^1P \rightarrow 1^1S$ photons might be escaping into the ISM without being degraded into lower-energy photons. In that case, these photons could be contributing to the presence of the DIG, as they have energies around ~ 22 eV, capable of photoionizing a wide range of chemical elements. If this escape of ionizing photons occurs in the He I singlet system, it could also happen with HI due to their similar atomic configurations.

This speculative case would affect many properties dependent on the emissivity of optical lines like H α or H β , such as chemical abundances, star formation rates, galaxy masses, and other quantities. Although speculative, this possibility should be interesting enough to test observationally whether there is a correlation between the observed deviations in He I singlets and the escape fraction of ionizing photons determined by other means.

In the case of temperature variations, one would need to explain the scale at which they operate and the physical phenomena that seem to generate them in most objects. The existence of high-metallicity clumps has been invoked in several studies to explain the low temperatures $T_e(\text{He I } \lambda 7281/\lambda 6678)$ found in planetary nebulae. While the creation and maintenance of such clumps in these objects remain subjects of debate, it seems a plausible explanation given the origin of planetary nebulae from the ejection of material from intermediate-mass stars in their late stages of life, which may not be well-mixed, especially in binary systems. However, extending this scenario to star-forming regions in a generalized manner seems implausible, as there is no accepted physical mechanism capable of generating large chemical variations within these objects. While generalized overheating from stellar feedback has been proposed in various studies to explain the ADF through temperature variations, no widely accepted physical mechanism consistent with the observations has been identified.

Our findings suggest that a combination of ionizing photon escape and temperature inhomogeneities may provide a better explanation for the observed discrepancies in He I $\lambda\lambda 5016, 7281$. Although other singlet lines such as He I $\lambda\lambda 3614, 3965$ also exhibit discrepancies in a similar manner to He I $\lambda\lambda 5016, 7281$, (See Figs A4 and A5) their detections are considerably less frequent, and a deeper analysis of these lines is deferred to future work.

¹ JEMD and KK gratefully acknowledge funding from
² the Deutsche Forschungsgemeinschaft (DFG, German
³ Research Foundation) in the form of an Emmy
⁴ Noether Research Group (grant number KR4598/2-1, PI
⁵ Kreckel) and the European Research Council's starting
⁶ grant ERC StG-101077573 ("ISM-METALS"). CE and
⁷ JGR acknowledge financial support from the Agencia
⁸ Estatal de Investigación of the Ministerio de Ciencia e
⁹ Innovación (AEI- MCINN) under grant "Espectroscopía
¹⁰ de campo integral de regiones H II locales. Modelos para
¹¹ el estudio de regiones H II extragalácticas" with refer-
¹² ence DOI:10.13039/501100011033. JGR also acknowl-
¹³ edges financial support from the AEI-MCINN, under
¹⁴ Severo Ochoa Centres of Excellence Programme 2020-
¹⁵ 2023 (CEX2019-000920-S), and from grant "Planetary
¹⁶ nebulae as the key to understanding binary stel-
¹⁷ lar evolution" with reference PID-2022136653NA-I00
¹⁸ (DOI:10.13039/501100011033) funded by the Ministe-
¹⁹ rio de Ciencia, Innovación y Universidades (MCIU/AEI)
²⁰ and by ERDF "A way of making Europe" of the Euro-
²¹ pean Union.

APPENDIX

A. TABLES AND FIGURES

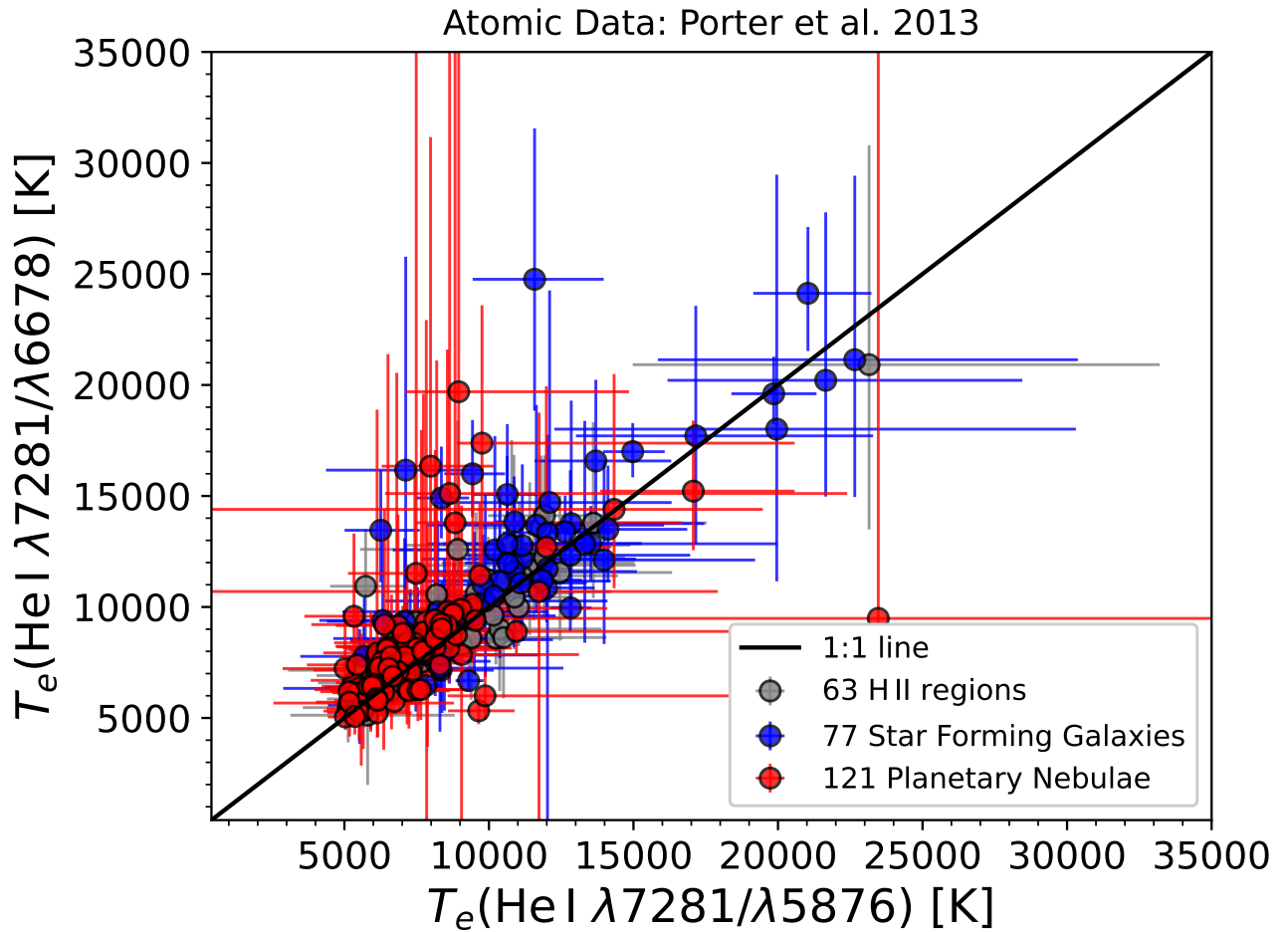


Figure A1. Comparison between $T_e(\text{He I } \lambda 7281/\lambda 5876)$ and $T_e(\text{He I } \lambda 7281/\lambda 6678)$ determined with the atomic data from Porter et al. (2012, 2013).

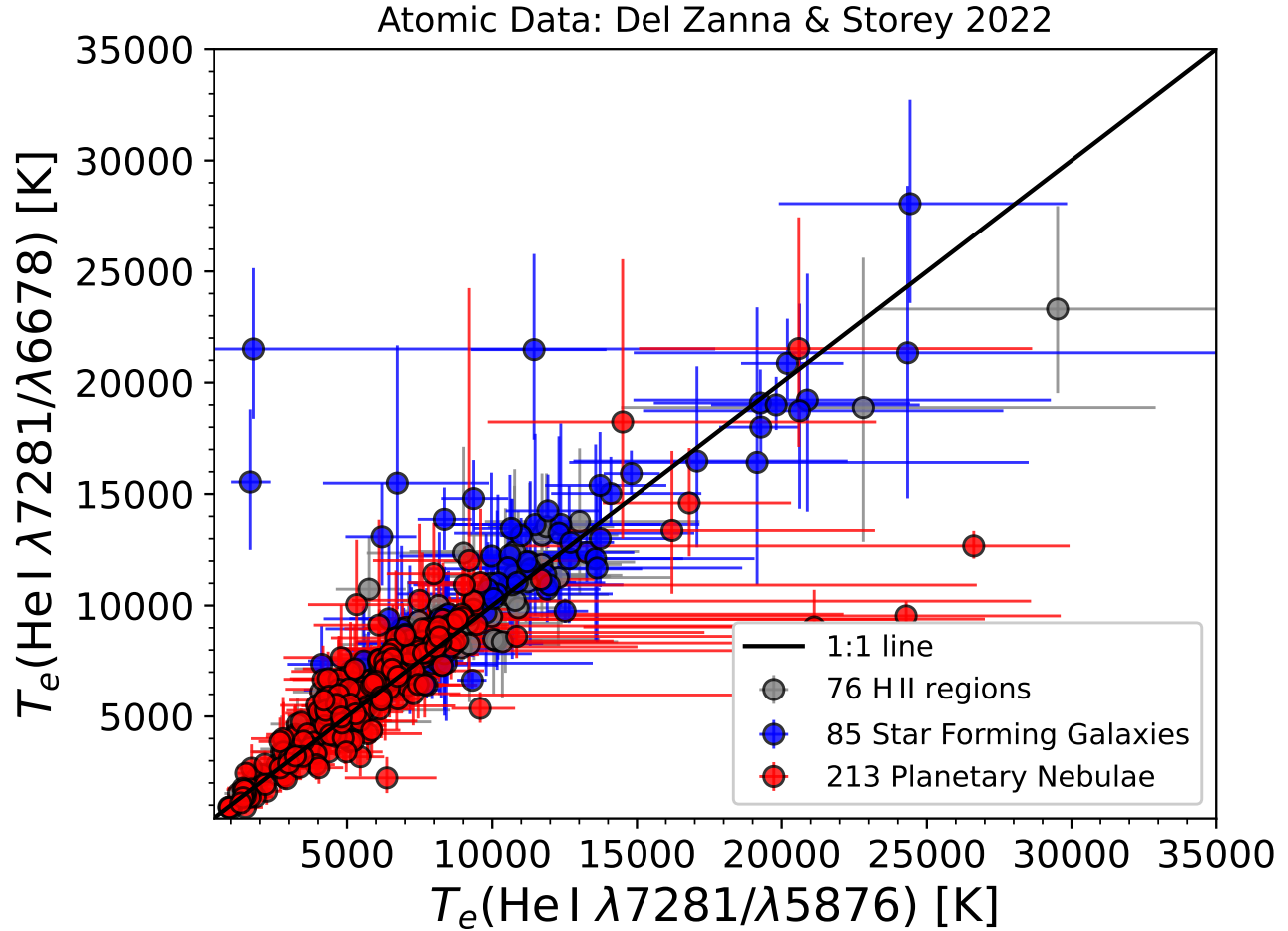


Figure A2. The same as in Fig. A1 but considering the atomic data estimated by [Del Zanna & Storey \(2022\)](#).

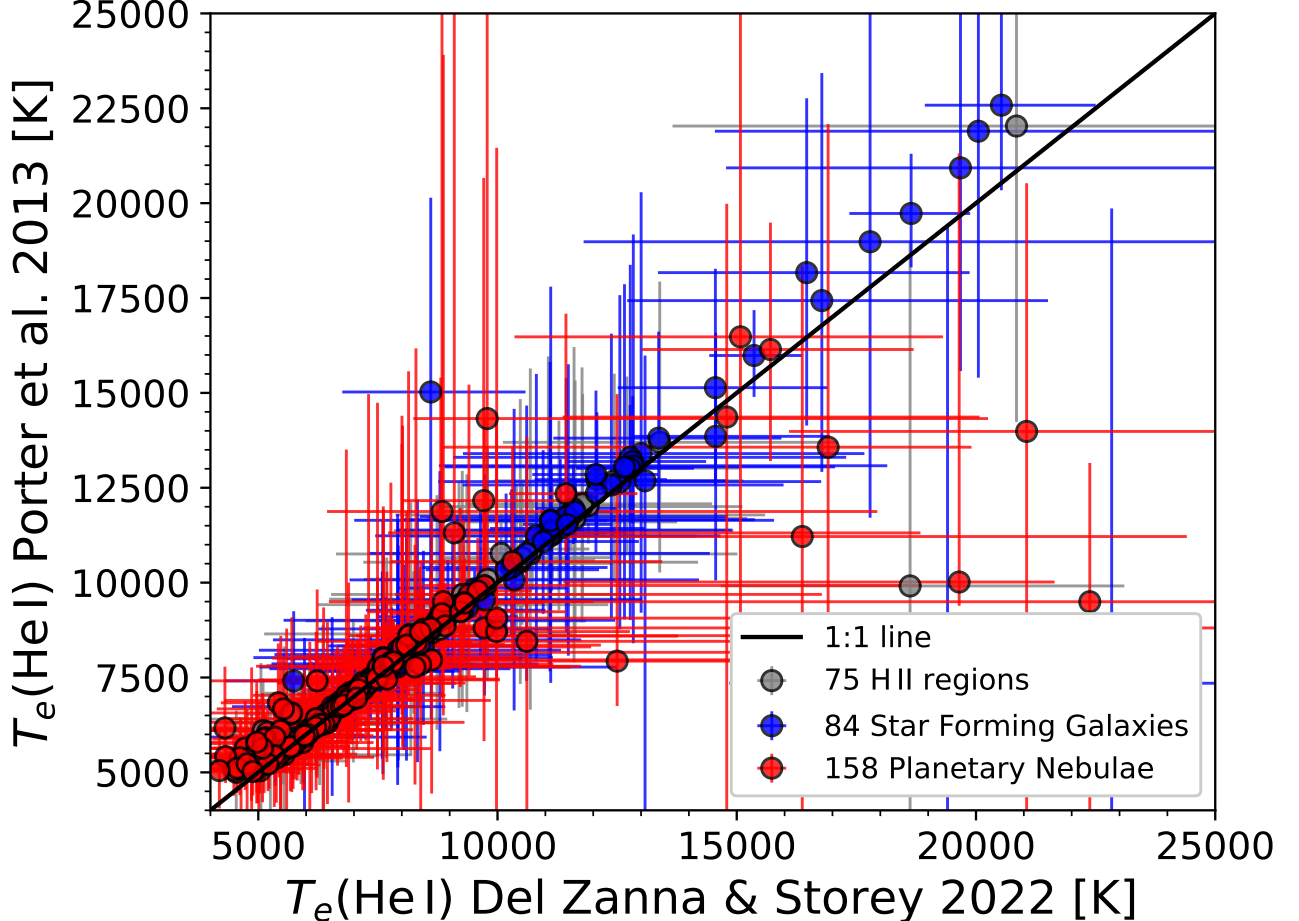


Figure A3. Comparison between the final $T_e(\text{HeI})$ values, resulting from averaging $T_e(\text{HeI} \lambda 7281/\lambda 5876)$ and $T_e(\text{HeI} \lambda 7281/\lambda 6678)$, obtained using the atomic data from Porter et al. (2012, 2013) and Del Zanna & Storey (2022). The first set of atomic data defines the effective recombination coefficients for a temperature range between 5,000 and 25,000 K, whereas the second set of calculations covers a broader range, from 500 to 32,000 K

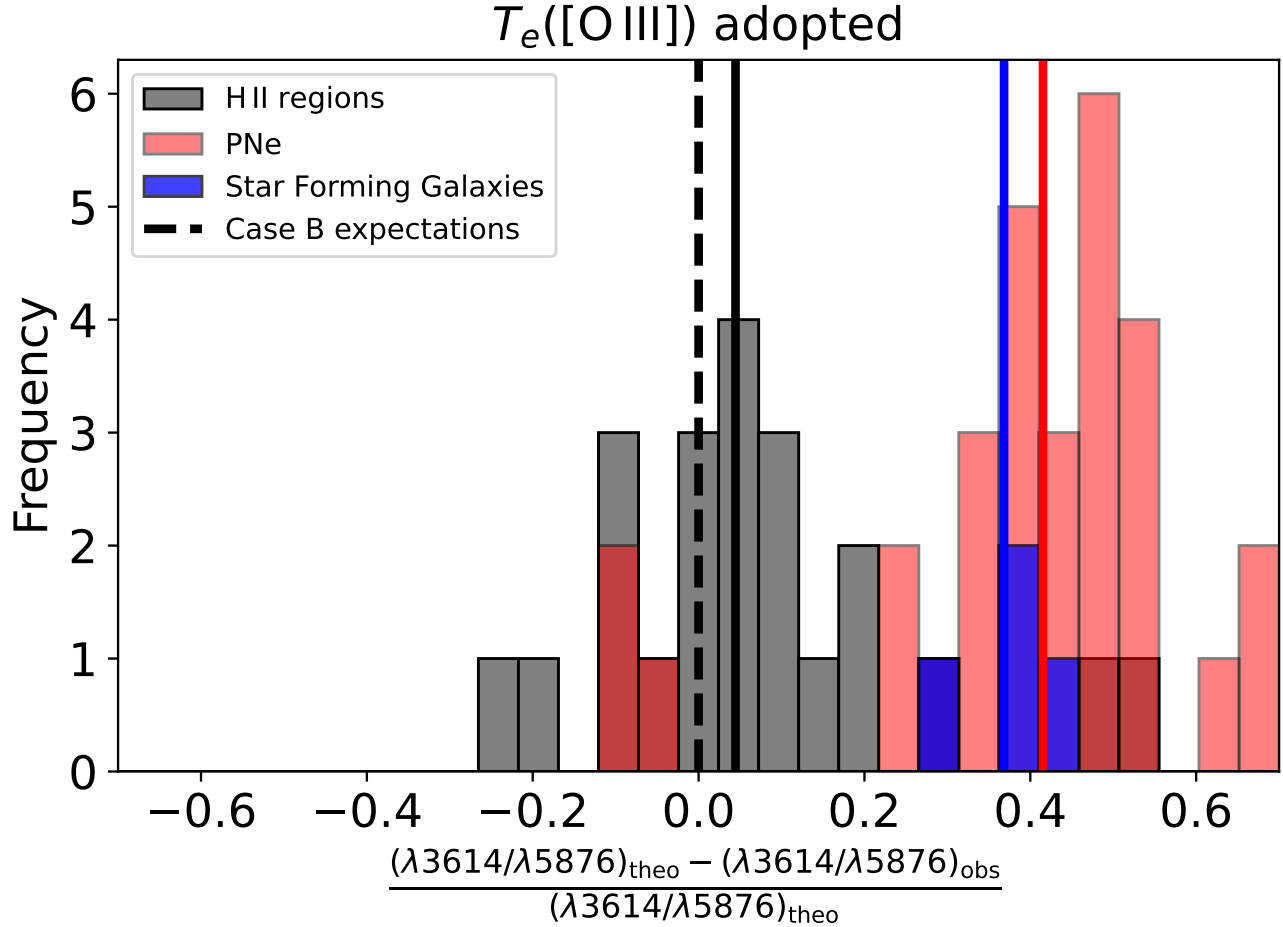


Figure A4. Same as in Fig. 4 but considering the He I $\lambda 3614$ line.

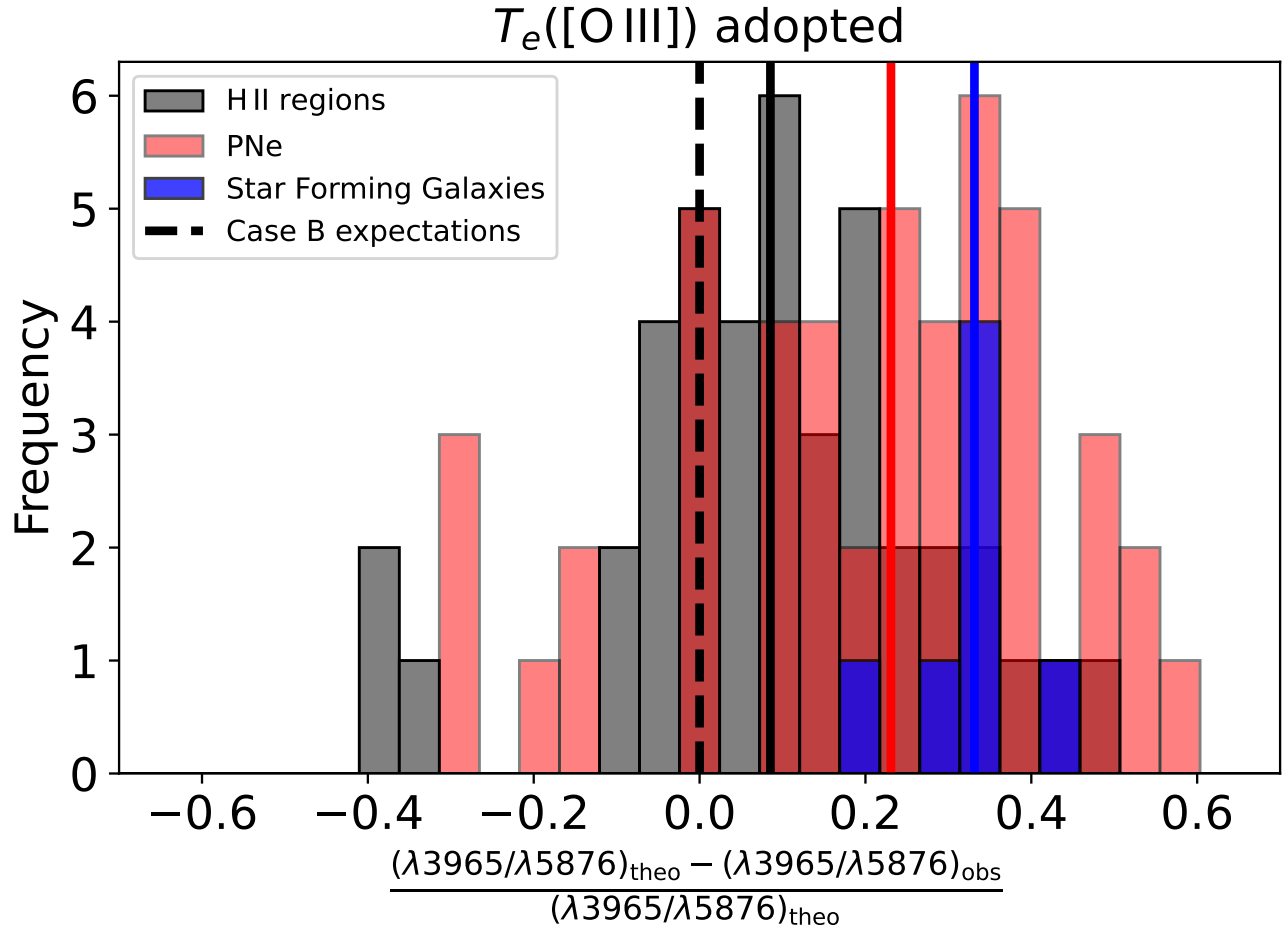


Figure A5. Same as in Fig. 4 but considering the He I $\lambda 3965$ line.

Table A1. Atomic data set used for collisionally excited lines

Ion	Transition probabilities	Collision strengths
O ⁺	Froese Fischer & Tachiev (2004)	Kisielius et al. (2009)
O ²⁺	Wiese et al. (1996), Storey & Zeippen (2000)	Aggarwal & Keenan (1999)
S ⁺	Irimia & Froese Fischer (2005)	Tayal & Zatsarinny (2010)
Cl ²⁺	Fritzsche et al. (1999)	Butler & Zeippen (1989)
Ar ³⁺	Mendoza & Zeippen (1982)	Ramsbottom & Bell (1997)
Fe ²⁺	Deb & Hibbert (2009), Mendoza et al. (2023)	Zhang (1996), Mendoza et al. (2023)

Table A2. Reference number, galaxy, region name and references to the sample of H II regions analyzed in this study

Reference number	Galaxy	Region	Reference
HII-1	LMC	30Doradus	Peimbert (2003)
HII-2	LMC	IC2111	Domínguez-Guzmán et al. (2022)
HII-3	LMC	N11B	Domínguez-Guzmán et al. (2022)
HII-4	LMC	N44C	Domínguez-Guzmán et al. (2022)
HII-5	LMC	NGC1714	Domínguez-Guzmán et al. (2022)
HII-6	M101	H1013	Bresolin (2007)
HII-7	M101	H1013	Croxall et al. (2016)
HII-8	M101	H1052	Croxall et al. (2016)
HII-9	M101	H1122	Croxall et al. (2016)
HII-10	M101	H1216	Croxall et al. (2016)
HII-11	M101	H1216	Esteban et al. (2020)
HII-12	M101	H143	Croxall et al. (2016)
HII-13	M101	H27	Croxall et al. (2016)
HII-14	M101	H71	Croxall et al. (2016)
HII-15	M101	NGC5447-1	Croxall et al. (2016)
HII-16	M101	NGC5447-2	Croxall et al. (2016)
HII-17	M101	NGC5447-3	Croxall et al. (2016)
HII-18	M101	NGC5449-1	Croxall et al. (2016)
HII-19	M101	NGC5455	Croxall et al. (2016)
HII-20	M101	NGC5455	Esteban et al. (2020)
HII-21	M101	NGC5461-2	Croxall et al. (2016)
HII-22	M101	NGC5461-3	Croxall et al. (2016)
HII-23	M101	NGC5461	Croxall et al. (2016)
HII-24	M101	NGC5461	Esteban et al. (2009)

Table A2 *continued*

Table A2 (*continued*)

Reference number	Galaxy	Region	Reference
HII-25	M101	NGC5462-1	Croxall et al. (2016)
HII-26	M101	NGC5471	Croxall et al. (2016)
HII-27	M101	NGC5471	Esteban et al. (2020)
HII-28	M31	BA310	Zurita & Bresolin (2012)
HII-29	M31	K932	Esteban et al. (2009)
HII-30	M33	BA379	Esteban et al. (2020)
HII-31	M33	NGC588	Toribio San Cipriano et al. (2016)
HII-32	M33	NGC604	Esteban et al. (2009)
HII-33	MilkyWay	M17	García-Rojas et al. (2007)
HII-34	MilkyWay	M20	García-Rojas et al. (2006)
HII-35	MilkyWay	M42-1	Méndez-Delgado et al. (2021a)
HII-36	MilkyWay	M42-1	Méndez-Delgado et al. (2021b)
HII-37	MilkyWay	M42-2	Méndez-Delgado et al. (2021a)
HII-38	MilkyWay	M42-2	Méndez-Delgado et al. (2021b)
HII-39	MilkyWay	M42-2	Méndez-Delgado et al. (2022)
HII-40	MilkyWay	M42-3	Méndez-Delgado et al. (2021a)
HII-41	MilkyWay	M42-3	Méndez-Delgado et al. (2022)
HII-42	MilkyWay	M42-4	Méndez-Delgado et al. (2021a)
HII-43	MilkyWay	M42-P1	Delgado-Inglada et al. (2016)
HII-44	MilkyWay	M42	Esteban et al. (2004)
HII-45	MilkyWay	M42	Mesa-Delgado et al. (2009)
HII-46	MilkyWay	M8	García-Rojas et al. (2007)
HII-47	MilkyWay	NGC2579	Esteban et al. (2013)
HII-48	MilkyWay	NGC3576	García-Rojas et al. (2004)
HII-49	MilkyWay	NGC3603	García-Rojas et al. (2006)
HII-50	MilkyWay	Sh2-100	Esteban et al. (2017)
HII-51	MilkyWay	Sh2-128	Esteban et al. (2017)
HII-52	MilkyWay	Sh2-156	Fernández-Martín et al. (2017)
HII-53	MilkyWay	Sh2-283	Esteban et al. (2017)
HII-54	MilkyWay	Sh2-288	Esteban et al. (2017)
HII-55	MilkyWay	Sh2-311	García-Rojas et al. (2005)
HII-56	NGC2363	A2	Gonzalez-Delgado et al. (1994)
HII-57	NGC2366	Mrk71	Esteban et al. (2009)
HII-58	NGC2403	VS24	Esteban et al. (2009)
HII-59	NGC2403	VS38	Esteban et al. (2009)
HII-60	NGC2403	VS44	Esteban et al. (2009)
HII-61	NGC300	R23	Toribio San Cipriano et al. (2016)
HII-62	NGC5398	Tol89-1	Guseva et al. (2011)
HII-63	NGC5398	Tol89-2	Guseva et al. (2011)
HII-64	NGC628	-184d7+83d4	Berg et al. (2015)
HII-65	NGC628	-42d8-158d2	Berg et al. (2015)

Table A2 *continued*

Table A2 (*continued*)

Reference number	Galaxy	Region	Reference
HII-66	NGC628	-44-159	Berg et al. (2013)
HII-67	NGC628	-90d1+190d2	Berg et al. (2015)
HII-68	NGC628	+289d9-17d4	Berg et al. (2015)
HII-69	NGC628	+298d4+12d3	Berg et al. (2015)
HII-70	NGC628	+31d6-191d1	Berg et al. (2015)
HII-71	NGC6822	HuV	Lee et al. (2006)
HII-72	NGC6822	HubbleV-1-l	Guseva et al. (2011)
HII-73	NGC6822	HubbleV-1-m	Guseva et al. (2011)
HII-74	NGC6822	HubbleV-2-L	Guseva et al. (2011)
HII-75	NGC6822	HubbleV-2-m	Guseva et al. (2011)
HII-76	NGC6822	HubbleV	Esteban et al. (2014)
HII-77	NGC6822	HubbleV	Guseva et al. (2011)
HII-78	NGC6822	HubbleV	Peimbert et al. (2005)
HII-79	NGC6822	Ka	Lee et al. (2006)
HII-80	SMC	N66A	Domínguez-Guzmán et al. (2022)
HII-81	SMC	N81	Domínguez-Guzmán et al. (2022)
HII-82	SMC	N90	Domínguez-Guzmán et al. (2022)
HII-83	SMC	NGC456-1	Peña-Guerrero et al. (2012)
HII-84	SMC	NGC456-2	Peña-Guerrero et al. (2012)
HII-85	SMC	NGC460	Peña-Guerrero et al. (2012)

Table A3. Reference number, galaxy, region name and references to the sample of Star Forming Galaxies analyzed in this study

Reference number	Galaxy	Region	Reference
SFG-1	0723+692A	-	Izotov et al. (1997)
SFG-2	0930+554N	-	Izotov et al. (1997)
SFG-3	1030+583	-	Izotov et al. (1997)
SFG-4	1054+365	-	Izotov et al. (1997)
SFG-5	1135+581	-	Izotov et al. (1994)
SFG-6	1152+579	-	Izotov et al. (1994)
SFG-7	1222+614	-	Izotov et al. (1997)
SFG-8	1223+487	-	Izotov et al. (1997)
SFG-9	1331+493N	-	Izotov et al. (1994)
SFG-10	1358+576	-	Izotov et al. (1997)
SFG-11	1415+437	-	Thuan et al. (1995)
SFG-12	1533+574B	-	Izotov et al. (1997)
SFG-13	CGCG007-025-1	-	Izotov & Thuan (2004)

Table A3 *continued*

Table A3 (*continued*)

Reference number	Galaxy	Region	Reference
SFG-14	DDO68	Reg-1	Annibali et al. (2019)
SFG-15	ESO338-IG004	-	Guseva et al. (2012)
SFG-16	HS1214+3801	-	Izotov & Thuan (2004)
SFG-17	HS1851+6933	-	Izotov et al. (2021a)
SFG-18	He2-10	E	Guseva et al. (2011)
SFG-19	J0014-0044	J0014-0044-1	Guseva et al. (2009)
SFG-20	J1253-0312	-	Thuan & Izotov (2005)
SFG-21	J1444+4840	-	Guseva et al. (2024)
SFG-22	J2302+0049	1	Guseva et al. (2009)
SFG-23	Mrk1271	-	Guseva et al. (2011)
SFG-24	Mrk1329	-	Izotov & Thuan (2004)
SFG-25	Mrk35	-	Izotov & Thuan (2004)
SFG-26	Mrk36	A2	Fernández et al. (2018)
SFG-27	Mrk450-1	-	Izotov & Thuan (2004)
SFG-28	Mrk475	-	Fernández et al. (2018)
SFG-29	Mrkn-59	1	Noeske et al. (2000)
SFG-30	NGC3125	-	Esteban et al. (2014)
SFG-31	NGC3125	-	Guseva et al. (2011)
SFG-32	NGC4449	HII-1	Annibali et al. (2017)
SFG-33	NGC4449	HII-2	Annibali et al. (2017)
SFG-34	NGC4449	HII-4	Annibali et al. (2017)
SFG-35	NGC4449	HII-5	Annibali et al. (2017)
SFG-36	NGC4861	-	Esteban et al. (2009)
SFG-37	NGC5253	NGC5253-C2	Guseva et al. (2011)
SFG-38	NGC5253	UV-1	López-Sánchez et al. (2007)
SFG-39	NGC5408	1	Guseva et al. (2011)
SFG-40	NGC5408	-	Esteban et al. (2014)
SFG-41	NGC7667	1-l	Guseva et al. (2011)
SFG-42	NGC7667	1-m	Guseva et al. (2011)
SFG-43	NGC7667	3	Guseva et al. (2011)
SFG-44	NGC7667	a	Valerdi et al. (2021b)
SFG-45	PHL-293B	-	Izotov et al. (2011)
SFG-46	POX4	-	Esteban et al. (2014)
SFG-47	POX4	-	Guseva et al. (2011)
SFG-48	SBS0335-052E	1+2_h	Izotov et al. (2009)
SFG-49	SBS0335-052E	1+2_l	Izotov et al. (2009)
SFG-50	SBS0335-052E	1+2a	Izotov et al. (2009)
SFG-51	SBS0335-052E	4+5c	Izotov et al. (2009)
SFG-52	SBS0335-052E	7_h	Izotov et al. (2009)
SFG-53	SBS1415+437	-	Izotov & Thuan (1998b)
SFG-54	SBS1420+540	-	Guseva et al. (2024)

Table A3 *continued*

Table A3 (*continued*)

Reference number	Galaxy	Region	Reference
SFG-55	J0159+0751	-	Izotov et al. (2017)
SFG-56	J0202-0047	-	Guseva et al. (2009)
SFG-57	J0813+3132	-	Fernández et al. (2018)
SFG-58	J0823+0313	-	Fernández et al. (2018)
SFG-59	J1011+1308	-	Fernández et al. (2022)
SFG-60	J1205+4551	-	Izotov et al. (2017)
SFG-61	J1205+4551	-	Izotov et al. (2021a)
SFG-62	J1219+1560	-	Fernández et al. (2022)
SFG-63	J1253-0312	-	Esteban et al. (2014)
SFG-64	J1355+4651	-	Izotov et al. (2017)
SFG-65	J1608+3528	-	Izotov et al. (2017)
SFG-66	J2104-0035	1	Guseva et al. (2009)
SFG-67	J2229+2725	-	Izotov et al. (2021b)
SFG-68	J2324-0006	-	Guseva et al. (2009)
SFG-69	SHOC133	-	Izotov et al. (2021a)
SFG-70	SHOC148	-	Fernández et al. (2022)
SFG-71	SHOC220	-	Fernández et al. (2018)
SFG-72	SHOC391	-	Guseva et al. (2011)
SFG-73	SHOC588	-	Fernández et al. (2018)
SFG-74	TOL1457-262	-	Esteban et al. (2014)
SFG-75	TOL1924-416	-	Esteban et al. (2014)
SFG-76	Tol-1214-277	-	Izotov et al. (2001)
SFG-77	Tol-1214-277	-	Izotov et al. (2004)
SFG-78	Tol-65	1+2	Izotov et al. (2004)
SFG-79	Tol-65	-	Izotov et al. (2001)
SFG-80	Tol0357-3915	C	Peimbert et al. (2012)
SFG-81	Tol0357-3915	E	Peimbert et al. (2012)
SFG-82	Tol1214-277	1	Guseva et al. (2011)
SFG-83	Tol1457-262	-	Guseva et al. (2011)
SFG-84	Tol1924-416	1	Guseva et al. (2011)
SFG-85	Tol1924-416	2	Guseva et al. (2011)
SFG-86	Tol2146-391	C	Peimbert et al. (2012)
SFG-87	Tol2146-391	E	Peimbert et al. (2012)
SFG-88	UGC993	-	Fernández et al. (2018)
SFG-89	UM133	H	Guseva et al. (2011)
SFG-90	W1702+18	-	Izotov et al. (2021a)

Table A4. Reference number, galaxy, region name and references to the sample of planetary nebulae analyzed in this

Reference number	Galaxy	Region	Reference
PNe-1	LMC	SMP38	Mampaso et al. (in prep)
PNe-2	LMC	SMP52	Mampaso et al. (in prep)
PNe-3	LMC	SMP73	Mampaso et al. (in prep)
PNe-4	LMC	SMP92	Mampaso et al. (in prep)
PNe-5	MilkyWay	A12	Henry et al. (2010)
PNe-6	MilkyWay	BB1	Kwitter et al. (2003)
PNe-7	MilkyWay	Cn1-5	García-Rojas et al. (2012)
PNe-8	MilkyWay	Cn2-1	Wang & Liu (2007)
PNe-9	MilkyWay	DdD-1	Kwitter & Henry (1998)
PNe-10	MilkyWay	H1-35	Wang & Liu (2007)
PNe-11	MilkyWay	H1-40	García-Rojas et al. (2018)
PNe-12	MilkyWay	H1-41	Wang & Liu (2007)
PNe-13	MilkyWay	H1-42	Wang & Liu (2007)
PNe-14	MilkyWay	H1-50	García-Rojas et al. (2018)
PNe-15	MilkyWay	H1-54	Wang & Liu (2007)
PNe-16	MilkyWay	H4-1	Otsuka & Tajitsu (2013)
PNe-17	MilkyWay	Hb12	Kwitter et al. (2003)
PNe-18	MilkyWay	He2-111	Milingo et al. (2010)
PNe-19	MilkyWay	He2-115	Milingo et al. (2002)
PNe-20	MilkyWay	He2-118	Wang & Liu (2007)
PNe-21	MilkyWay	He2-141	Milingo et al. (2002)
PNe-22	MilkyWay	He2-158	García-Rojas et al. (2018)
PNe-23	MilkyWay	He2-21	Milingo et al. (2002)
PNe-24	MilkyWay	He2-73	García-Rojas et al. (2018)
PNe-25	MilkyWay	He2-86	García-Rojas et al. (2012)
PNe-26	MilkyWay	He2-96	García-Rojas et al. (2018)
PNe-27	MilkyWay	Hu2-1	Kwitter et al. (2003)
PNe-28	MilkyWay	IC1257	Milingo et al. (2002)
PNe-29	MilkyWay	IC1747	Henry et al. (2010)
PNe-30	MilkyWay	IC2149	Henry et al. (2010)
PNe-31	MilkyWay	IC2165	Kwitter et al. (2003)
PNe-32	MilkyWay	IC2448	Milingo et al. (2002)
PNe-33	MilkyWay	IC2501	Sharpee et al. (2007)
PNe-34	MilkyWay	IC2621	Milingo et al. (2002)
PNe-35	MilkyWay	IC3568	Liu et al. (2004)
PNe-36	MilkyWay	IC418	Sharpee et al. (2003)
PNe-37	MilkyWay	IC4191	Sharpee et al. (2007)
PNe-38	MilkyWay	IC4406	Tsamis et al. (2003)
PNe-39	MilkyWay	IC4699	Wang & Liu (2007)
PNe-40	MilkyWay	IC4776	Sowicka et al. (2017)

Table A4 *continued*

Table A4 (*continued*)

Reference number	Galaxy	Region	Reference
PNe-41	MilkyWay	IC4846	Hyung et al. (2001)
PNe-42	MilkyWay	J900	Kwitter et al. (2003)
PNe-43	MilkyWay	K3-66	Henry et al. (2010)
PNe-44	MilkyWay	K3-67	Henry et al. (2010)
PNe-45	MilkyWay	K4-48	Henry et al. (2010)
PNe-46	MilkyWay	M1-11	Otsuka & Tajitsu (2013)
PNe-47	MilkyWay	M1-13	Milingo et al. (2010)
PNe-48	MilkyWay	M1-16	Henry et al. (2010)
PNe-49	MilkyWay	M1-20	Wang & Liu (2007)
PNe-50	MilkyWay	M1-25	García-Rojas et al. (2012)
PNe-51	MilkyWay	M1-30	García-Rojas et al. (2012)
PNe-52	MilkyWay	M1-31	García-Rojas et al. (2018)
PNe-53	MilkyWay	M1-32	García-Rojas et al. (2012)
PNe-54	MilkyWay	M1-33	García-Rojas et al. (2018)
PNe-55	MilkyWay	M1-40	Milingo et al. (2010)
PNe-56	MilkyWay	M1-4	Henry et al. (2010)
PNe-57	MilkyWay	M1-50	Milingo et al. (2002)
PNe-58	MilkyWay	M1-54	Milingo et al. (2002)
PNe-59	MilkyWay	M1-57	Milingo et al. (2002)
PNe-60	MilkyWay	M1-5	Milingo et al. (2002)
PNe-61	MilkyWay	M1-61	García-Rojas et al. (2012)
PNe-62	MilkyWay	M1-6	Henry et al. (2010)
PNe-63	MilkyWay	M1-7	Henry et al. (2010)
PNe-64	MilkyWay	M1-9	Henry et al. (2010)
PNe-65	MilkyWay	M2-23	Wang & Liu (2007)
PNe-66	MilkyWay	M2-27	Wang & Liu (2007)
PNe-67	MilkyWay	M2-2	Henry et al. (2010)
PNe-68	MilkyWay	M2-33	Wang & Liu (2007)
PNe-69	MilkyWay	M2-36	Espíritu & Peimbert (2021)
PNe-70	MilkyWay	M2-39	Wang & Liu (2007)
PNe-71	MilkyWay	M2-42	Wang & Liu (2007)
PNe-72	MilkyWay	M2-4	Wang & Liu (2007)
PNe-73	MilkyWay	M2-6	Wang & Liu (2007)
PNe-74	MilkyWay	M3-15	García-Rojas et al. (2012)
PNe-75	MilkyWay	M3-21	Wang & Liu (2007)
PNe-76	MilkyWay	M3-32	Wang & Liu (2007)
PNe-77	MilkyWay	M3-33	Wang & Liu (2007)
PNe-78	MilkyWay	M3-5	Milingo et al. (2010)
PNe-79	MilkyWay	M3-6	Milingo et al. (2002)
PNe-80	MilkyWay	M3-7	Wang & Liu (2007)
PNe-81	MilkyWay	Me2-2	Milingo et al. (2010)

Table A4 *continued*

Table A4 (*continued*)

Reference number	Galaxy	Region	Reference
PNe-82	MilkyWay	MyCn18	Tsamis et al. (2003)
PNe-83	MilkyWay	Mz3	Milingo et al. (2010)
PNe-84	MilkyWay	NGC1501	Ercolano et al. (2004)
PNe-85	MilkyWay	NGC1535	Milingo et al. (2010)
PNe-86	MilkyWay	NGC2440	Sharpee et al. (2007)
PNe-87	MilkyWay	NGC2867-1	García-Rojas et al. (2009)
PNe-88	MilkyWay	NGC2867-2	García-Rojas et al. (2009)
PNe-89	MilkyWay	NGC3132	Tsamis et al. (2003)
PNe-90	MilkyWay	NGC3211	Milingo et al. (2002)
PNe-91	MilkyWay	NGC3242A	Milingo et al. (2002)
PNe-92	MilkyWay	NGC3242B	Milingo et al. (2002)
PNe-93	MilkyWay	NGC3242	Tsamis et al. (2003)
PNe-94	MilkyWay	NGC3918	García-Rojas et al. (2015)
PNe-95	MilkyWay	NGC40	Liu et al. (2004)
PNe-96	MilkyWay	NGC5189	García-Rojas et al. (2012)
PNe-97	MilkyWay	NGC5307	Ruiz et al. (2003)
PNe-98	MilkyWay	NGC5315	Madonna et al. (2017)
PNe-99	MilkyWay	NGC5882	Tsamis et al. (2003)
PNe-100	MilkyWay	NGC6210	Liu et al. (2004)
PNe-101	MilkyWay	NGC6302	Tsamis et al. (2003)
PNe-102	MilkyWay	NGC6309	Milingo et al. (2002)
PNe-103	MilkyWay	NGC6369	García-Rojas et al. (2012)
PNe-104	MilkyWay	NGC6439	Milingo et al. (2002)
PNe-105	MilkyWay	NGC6439	Wang & Liu (2007)
PNe-106	MilkyWay	NGC650A	Kwitter et al. (2003)
PNe-107	MilkyWay	NGC650B	Kwitter et al. (2003)
PNe-108	MilkyWay	NGC6537	Milingo et al. (2010)
PNe-109	MilkyWay	NGC6543	Wesson & Liu (2004)
PNe-110	MilkyWay	NGC6563	Milingo et al. (2002)
PNe-111	MilkyWay	NGC6565	Milingo et al. (2002)
PNe-112	MilkyWay	NGC6567	Wang & Liu (2007)
PNe-113	MilkyWay	NGC6572	Hyung et al. (1994)
PNe-114	MilkyWay	NGC6620	Wang & Liu (2007)
PNe-115	MilkyWay	NGC6629	Milingo et al. (2002)
PNe-116	MilkyWay	NGC6720	Liu et al. (2004)
PNe-117	MilkyWay	NGC6741	Hyung & Aller (1997)
PNe-118	MilkyWay	NGC6790	Kwitter & Henry (2001)
PNe-119	MilkyWay	NGC6803	Milingo et al. (2010)
PNe-120	MilkyWay	NGC6818	Tsamis et al. (2003)
PNe-121	MilkyWay	NGC6826	Liu et al. (2004)
PNe-122	MilkyWay	NGC6853	Milingo et al. (2010)

Table A4 *continued*

Table A4 (*continued*)

Reference number	Galaxy	Region	Reference
PNe-123	MilkyWay	NGC6881	Milingo et al. (2010)
PNe-124	MilkyWay	NGC6884	Kwitter & Henry (2001)
PNe-125	MilkyWay	NGC7009	Fang & Liu (2011)
PNe-126	MilkyWay	NGC7354	Milingo et al. (2010)
PNe-127	MilkyWay	PB1	Henry et al. (2010)
PNe-128	MilkyWay	PB8	García-Rojas et al. (2009)
PNe-129	MilkyWay	PC14	García-Rojas et al. (2012)
PNe-130	MilkyWay	PNG_000.1+02.6	Tan et al. (2024)
PNe-131	MilkyWay	PNG_000.1+04.3	Tan et al. (2024)
PNe-132	MilkyWay	PNG_000.2-01.9	Tan et al. (2024)
PNe-133	MilkyWay	PNG_000.2-04.6	Tan et al. (2024)
PNe-134	MilkyWay	PNG_000.3-04.6	Tan et al. (2024)
PNe-135	MilkyWay	PNG_000.4-01.9	Tan et al. (2024)
PNe-136	MilkyWay	PNG_000.4-02.9	Tan et al. (2024)
PNe-137	MilkyWay	PNG_000.7+03.2	Tan et al. (2024)
PNe-138	MilkyWay	PNG_000.7-02.7	Tan et al. (2024)
PNe-139	MilkyWay	PNG_000.7-07.4	Tan et al. (2024)
PNe-140	MilkyWay	PNG_000.9-02.0	Tan et al. (2024)
PNe-141	MilkyWay	PNG_001.1-01.6	Tan et al. (2024)
PNe-142	MilkyWay	PNG_001.2+02.1	Tan et al. (2024)
PNe-143	MilkyWay	PNG_001.4+05.3	Tan et al. (2024)
PNe-144	MilkyWay	PNG_001.6-01.3	Tan et al. (2024)
PNe-145	MilkyWay	PNG_001.7+05.7	Tan et al. (2024)
PNe-146	MilkyWay	PNG_002.0-06.2	Tan et al. (2024)
PNe-147	MilkyWay	PNG_002.1-02.2	Tan et al. (2024)
PNe-148	MilkyWay	PNG_002.1-04.2	Tan et al. (2024)
PNe-149	MilkyWay	PNG_002.2-09.4	Tan et al. (2024)
PNe-150	MilkyWay	PNG_002.7-04.8	Tan et al. (2024)
PNe-151	MilkyWay	PNG_002.9-03.9	Tan et al. (2024)
PNe-152	MilkyWay	PNG_003.2-06.2	Tan et al. (2024)
PNe-153	MilkyWay	PNG_003.6-02.3	Tan et al. (2024)
PNe-154	MilkyWay	PNG_003.8-04.3	Tan et al. (2024)
PNe-155	MilkyWay	PNG_003.9-02.3	Tan et al. (2024)
PNe-156	MilkyWay	PNG_003.9-03.1	Tan et al. (2024)
PNe-157	MilkyWay	PNG_004.1-03.8	Tan et al. (2024)
PNe-158	MilkyWay	PNG_004.2-03.2	Tan et al. (2024)
PNe-159	MilkyWay	PNG_004.2-04.3	Tan et al. (2024)
PNe-160	MilkyWay	PNG_004.6+06.0	Tan et al. (2024)
PNe-161	MilkyWay	PNG_004.8+02.0	Tan et al. (2024)
PNe-162	MilkyWay	PNG_005.2+05.6	Tan et al. (2024)
PNe-163	MilkyWay	PNG_005.8-06.1	Tan et al. (2024)

Table A4 *continued*

Table A4 (*continued*)

Reference number	Galaxy	Region	Reference
PNe-164	MilkyWay	PNG_006.1+08.3	Tan et al. (2024)
PNe-165	MilkyWay	PNG_006.4+02.0	Tan et al. (2024)
PNe-166	MilkyWay	PNG_006.8+02.3	Tan et al. (2024)
PNe-167	MilkyWay	PNG_006.8-03.4	Tan et al. (2024)
PNe-168	MilkyWay	PNG_007.0+06.3	Tan et al. (2024)
PNe-169	MilkyWay	PNG_007.0-06.8	Tan et al. (2024)
PNe-170	MilkyWay	PNG_007.5+07.4	Tan et al. (2024)
PNe-171	MilkyWay	PNG_007.6+06.9	Tan et al. (2024)
PNe-172	MilkyWay	PNG_007.8-03.7	Tan et al. (2024)
PNe-173	MilkyWay	PNG_008.2+06.8	Tan et al. (2024)
PNe-174	MilkyWay	PNG_008.6-02.6	Tan et al. (2024)
PNe-175	MilkyWay	PNG_009.4-09.8	Tan et al. (2024)
PNe-176	MilkyWay	PNG_009.8-04.6	Tan et al. (2024)
PNe-177	MilkyWay	PNG_351.1+04.8	Tan et al. (2024)
PNe-178	MilkyWay	PNG_351.2+05.2	Tan et al. (2024)
PNe-179	MilkyWay	PNG_351.6-06.2	Tan et al. (2024)
PNe-180	MilkyWay	PNG_351.9-01.9	Tan et al. (2024)
PNe-181	MilkyWay	PNG_352.0-04.6	Tan et al. (2024)
PNe-182	MilkyWay	PNG_352.1+05.1	Tan et al. (2024)
PNe-183	MilkyWay	PNG_352.6+03.0	Tan et al. (2024)
PNe-184	MilkyWay	PNG_353.3+06.3	Tan et al. (2024)
PNe-185	MilkyWay	PNG_353.7+06.3	Tan et al. (2024)
PNe-186	MilkyWay	PNG_354.5+03.3	Tan et al. (2024)
PNe-187	MilkyWay	PNG_355.4-02.4	Tan et al. (2024)
PNe-188	MilkyWay	PNG_355.9+03.6	Tan et al. (2024)
PNe-189	MilkyWay	PNG_355.9-04.2	Tan et al. (2024)
PNe-190	MilkyWay	PNG_356.1-03.3	Tan et al. (2024)
PNe-191	MilkyWay	PNG_356.3-06.2	Tan et al. (2024)
PNe-192	MilkyWay	PNG_356.5-03.6	Tan et al. (2024)
PNe-193	MilkyWay	PNG_356.8-05.4	Tan et al. (2024)
PNe-194	MilkyWay	PNG_357.0+02.4	Tan et al. (2024)
PNe-195	MilkyWay	PNG_357.1+03.6	Tan et al. (2024)
PNe-196	MilkyWay	PNG_357.2+02.0	Tan et al. (2024)
PNe-197	MilkyWay	PNG_357.3+04.0	Tan et al. (2024)
PNe-198	MilkyWay	PNG_357.9-05.1	Tan et al. (2024)
PNe-199	MilkyWay	PNG_358.0+09.3	Tan et al. (2024)
PNe-200	MilkyWay	PNG_358.2+03.5	Tan et al. (2024)
PNe-201	MilkyWay	PNG_358.2+04.2	Tan et al. (2024)
PNe-202	MilkyWay	PNG_358.5+02.9	Tan et al. (2024)
PNe-203	MilkyWay	PNG_358.5-04.2	Tan et al. (2024)
PNe-204	MilkyWay	PNG_358.6+07.8	Tan et al. (2024)

Table A4 *continued*

Table A4 (*continued*)

Reference number	Galaxy	Region	Reference
PNe-205	MilkyWay	PNG_358.6-05.5	Tan et al. (2024)
PNe-206	MilkyWay	PNG_358.8+03.0	Tan et al. (2024)
PNe-207	MilkyWay	PNG_358.9+03.4	Tan et al. (2024)
PNe-208	MilkyWay	PNG_359.0-04.1	Tan et al. (2024)
PNe-209	MilkyWay	PNG_359.7-01.8	Tan et al. (2024)
PNe-210	MilkyWay	PNG_359.8+03.7	Tan et al. (2024)
PNe-211	MilkyWay	PNG_359.8+06.9	Tan et al. (2024)
PNe-212	MilkyWay	PNG_359.8-07.2	Tan et al. (2024)
PNe-213	MilkyWay	PNG_359.9-04.5	Tan et al. (2024)
PNe-214	MilkyWay	Pe1-18	Milingo et al. (2002)
PNe-215	MilkyWay	Pe1-1	García-Rojas et al. (2012)
PNe-216	MilkyWay	Vy1-1	Milingo et al. (2010)
PNe-217	MilkyWay	Vy2-1	Wang & Liu (2007)
PNe-218	SgrdS+h	BoBn1	Kniazev et al. (2008)

Table A5. Electron densities derived from the sample of H II regions.

Reference number	$n_e(\text{[S II]})$ [cm $^{-3}$]	$n_e(\text{[O II]})$ [cm $^{-3}$]	$n_e(\text{[Fe III]})$ [cm $^{-3}$]	$n_e(\text{[Cl III]})$ [cm $^{-3}$]	$n_e(\text{[Ar IV]})$ [cm $^{-3}$]	Adopted n_e [cm $^{-3}$]
HII-1	340 ± 20	440 ± 20	1730^{+1840}_{-1670}	330^{+260}_{-200}	550^{+590}_{-300}	390 ± 20
HII-2	230^{+130}_{-110}	250^{+120}_{-100}	4600^{+9360}_{-3530}	640^{+450}_{-440}	2270^{+2270}_{-1390}	240^{+130}_{-110}
HII-3	270^{+70}_{-60}	270^{+120}_{-100}	2860^{+2170}_{-2080}	340^{+160}_{-150}	680^{+610}_{-440}	270^{+90}_{-80}
HII-4	110 ± 50	200^{+100}_{-90}	2130^{+1870}_{-960}	600 ± 320	580 ± 370	150^{+80}_{-70}
HII-5	360^{+140}_{-130}	450^{+180}_{-140}	4230^{+9660}_{-3160}	620^{+500}_{-400}	1580^{+1280}_{-1060}	410^{+160}_{-130}
HII-6	30^{+50}_{-20}	-	-	210^{+210}_{-130}	-	100 ± 100
HII-7	60 ± 40	220^{+40}_{-60}	-	-	-	100 ± 100
HII-8	140 ± 60	270^{+60}_{-50}	-	-	-	210 ± 60
HII-9	30^{+40}_{-20}	320 ± 40	-	-	-	100 ± 100
HII-10	40^{+40}_{-30}	10^{+20}_{-10}	-	-	-	100 ± 100
HII-11	50 ± 30	40^{+40}_{-30}	-	340^{+330}_{-240}	-	100 ± 100
HII-12	70 ± 50	60^{+40}_{-30}	-	-	-	100 ± 100
HII-13	70^{+90}_{-50}	150^{+70}_{-50}	-	-	-	100 ± 100
HII-14	50^{+50}_{-30}	110^{+60}_{-50}	-	-	-	100 ± 100
HII-15	60 ± 40	50 ± 30	-	-	-	100 ± 100
HII-16	90^{+60}_{-50}	50^{+50}_{-30}	-	-	-	100 ± 100
HII-17	100 ± 50	150^{+60}_{-50}	-	-	-	130^{+60}_{-50}
HII-18	50^{+50}_{-30}	70 ± 40	-	-	-	100 ± 100
HII-19	170^{+100}_{-80}	370^{+90}_{-70}	-	-	-	270^{+90}_{-80}

Table A5 *continued*

Table A5 (*continued*)

Reference number	$n_e(\text{[S II]})$ [cm $^{-3}$]	$n_e(\text{[O II]})$ [cm $^{-3}$]	$n_e(\text{[Fe III]})$ [cm $^{-3}$]	$n_e(\text{[Cl III]})$ [cm $^{-3}$]	$n_e(\text{[Ar IV]})$ [cm $^{-3}$]	Adopted n_e [cm $^{-3}$]
HII-20	150^{+60}_{-50}	240 ± 60	-	70^{+250}_{-50}	-	200^{+60}_{-50}
HII-21	30 ± 20	200^{+50}_{-40}	-	-	-	100 ± 100
HII-22	50^{+40}_{-30}	260^{+50}_{-60}	-	-	-	100 ± 100
HII-23	190^{+110}_{-100}	310^{+110}_{-90}	-	-	-	250^{+110}_{-90}
HII-24	210^{+140}_{-100}	310^{+100}_{-90}	-	390^{+520}_{-250}	-	260^{+120}_{-90}
HII-25	60^{+50}_{-30}	70^{+50}_{-40}	-	-	-	100 ± 100
HII-26	200 ± 90	260^{+90}_{-80}	-	-	-	230 ± 90
HII-27	170 ± 60	210^{+70}_{-50}	-	270^{+340}_{-180}	-	190 ± 60
HII-28	130^{+140}_{-80}	-	-	590^{+710}_{-360}	-	130^{+140}_{-80}
HII-29	110^{+60}_{-40}	250 ± 30	4850^{+7840}_{-3390}	770^{+370}_{-390}	2170^{+2450}_{-1240}	180^{+50}_{-40}
HII-30	50 ± 30	30 ± 20	-	350^{+330}_{-250}	-	100 ± 100
HII-31	120^{+150}_{-80}	80^{+80}_{-50}	-	690^{+720}_{-420}	-	100 ± 100
HII-32	40^{+40}_{-30}	60 ± 20	-	480^{+370}_{-350}	-	100 ± 100
HII-33	390^{+140}_{-110}	500^{+110}_{-100}	-	390^{+290}_{-260}	-	440^{+130}_{-110}
HII-34	280^{+70}_{-80}	260^{+50}_{-60}	-	470^{+310}_{-290}	-	270^{+60}_{-70}
HII-35	4080^{+990}_{-670}	5260^{+710}_{-630}	9840^{+3120}_{-2580}	6830^{+690}_{-580}	4120^{+1340}_{-1250}	5560 ± 1260
HII-36	1320^{+240}_{-190}	1090^{+120}_{-90}	-	1570^{+280}_{-270}	-	1180 ± 160
HII-37	4030^{+1150}_{-680}	5130^{+780}_{-600}	10520^{+2280}_{-2070}	6500^{+720}_{-650}	5800^{+740}_{-700}	5660 ± 1170
HII-38	1210^{+170}_{-180}	1470 ± 120	-	2100 ± 530	-	1410 ± 170
HII-39	3840^{+1340}_{-830}	5810^{+800}_{-660}	10150^{+2400}_{-1920}	7620^{+740}_{-780}	6630^{+530}_{-540}	6450 ± 1210
HII-40	4170^{+1300}_{-1010}	5340^{+720}_{-640}	12040^{+3360}_{-2720}	7370^{+920}_{-890}	6100 ± 1270	5910 ± 1410
HII-41	4200^{+840}_{-800}	5360^{+800}_{-620}	7940^{+2180}_{-1960}	7630^{+750}_{-650}	4580^{+430}_{-390}	5260 ± 1220
HII-42	3880^{+1000}_{-670}	4870^{+700}_{-530}	10900^{+3110}_{-2760}	6810^{+730}_{-650}	5150^{+780}_{-710}	5340 ± 1210
HII-43	2880^{+820}_{-650}	4650^{+860}_{-760}	6820^{+2800}_{-2290}	6010^{+1480}_{-1250}	6040^{+4130}_{-3440}	4140 ± 1260
HII-44	4820^{+2840}_{-1650}	6780^{+2570}_{-1590}	9190^{+3530}_{-2960}	6980^{+590}_{-570}	4760^{+1130}_{-940}	6460 ± 1030
HII-45	1720^{+580}_{-450}	2690^{+760}_{-560}	-	1920^{+960}_{-900}	-	2060 ± 440
HII-46	1240^{+220}_{-170}	1630^{+710}_{-490}	2260^{+1950}_{-1050}	1810^{+340}_{-300}	4110^{+3710}_{-2600}	1420 ± 300
HII-47	900 ± 210	1250^{+300}_{-220}	3420^{+4350}_{-2370}	1660^{+540}_{-500}	4200^{+4720}_{-2970}	1070^{+250}_{-210}
HII-48	1060^{+330}_{-240}	1680^{+290}_{-260}	1790^{+1260}_{-1700}	2940^{+610}_{-560}	3020^{+1500}_{-1340}	1570 ± 580
HII-49	2850^{+1030}_{-640}	2500^{+600}_{-500}	8600^{+43060}_{-3180}	4510^{+1560}_{-1280}	1730^{+1360}_{-1200}	2680 ± 650
HII-50	390^{+190}_{-180}	-	-	720^{+390}_{-380}	-	390^{+190}_{-180}
HII-51	470^{+100}_{-60}	-	-	870^{+520}_{-530}	-	470^{+100}_{-60}
HII-52	880^{+50}_{-40}	-	-	2750^{+760}_{-870}	-	880^{+50}_{-40}
HII-53	270^{+90}_{-70}	-	-	320^{+370}_{-180}	-	270^{+90}_{-70}
HII-54	460^{+200}_{-240}	-	-	420^{+350}_{-290}	-	460^{+200}_{-240}
HII-55	300^{+90}_{-80}	280 ± 80	-	590^{+500}_{-380}	-	290^{+90}_{-80}
HII-56	100^{+50}_{-60}	-	-	-	-	100^{+50}_{-60}
HII-57	170^{+120}_{-100}	290 ± 100	9800^{+31740}_{-6920}	340^{+290}_{-210}	500^{+380}_{-320}	230^{+110}_{-100}
HII-58	90^{+50}_{-40}	240 ± 30	-	840^{+920}_{-570}	-	100 ± 100
HII-59	50^{+40}_{-30}	120 ± 30	-	290^{+460}_{-150}	-	100 ± 100

Table A5 *continued*

Table A5 (*continued*)

Reference number	$n_e(\text{[S II]})$ [cm $^{-3}$]	$n_e(\text{[O II]})$ [cm $^{-3}$]	$n_e(\text{[Fe III]})$ [cm $^{-3}$]	$n_e(\text{[Cl III]})$ [cm $^{-3}$]	$n_e(\text{[Ar IV]})$ [cm $^{-3}$]	Adopted n_e [cm $^{-3}$]
HII-60	90 ± 40	150 ± 30	-	510_{-330}^{+510}	-	100 ± 100
HII-61	60_{-40}^{+60}	50_{-30}^{+80}	-	-	-	100 ± 100
HII-62	120 ± 30	-	-	270_{-170}^{+200}	-	120 ± 30
HII-63	80_{-20}^{+30}	-	-	-	-	100 ± 100
HII-64	60 ± 20	100 ± 30	-	-	-	100 ± 100
HII-65	50_{-20}^{+30}	70_{-50}^{+60}	-	-	-	100 ± 100
HII-66	90_{-60}^{+70}	-	-	-	-	100 ± 100
HII-67	70_{-30}^{+20}	370 ± 50	-	-	-	100 ± 100
HII-68	40_{-20}^{+30}	20 ± 20	-	-	-	100 ± 100
HII-69	70_{-20}^{+30}	70_{-30}^{+40}	-	-	-	100 ± 100
HII-70	50_{-20}^{+30}	240_{-40}^{+30}	-	-	-	100 ± 100
HII-71	130_{-90}^{+110}	-	-	-	-	130_{-90}^{+110}
HII-72	70 ± 30	-	-	1900_{-1140}^{+1920}	-	100 ± 100
HII-73	70_{-40}^{+30}	-	-	870_{-680}^{+710}	-	100 ± 100
HII-74	70_{-40}^{+30}	-	-	-	-	100 ± 100
HII-75	20 ± 20	-	-	3260_{-2430}^{+3140}	-	100 ± 100
HII-76	130_{-80}^{+100}	150_{-80}^{+110}	6150_{-4300}^{+13300}	750_{-510}^{+600}	560_{-350}^{+510}	140_{-80}^{+110}
HII-77	100 ± 30	-	-	110_{-80}^{+130}	-	100 ± 30
HII-78	100_{-50}^{+60}	70_{-30}^{+40}	-	1500_{-1000}^{+1050}	-	100 ± 100
HII-79	290_{-150}^{+120}	-	-	-	-	290_{-150}^{+120}
HII-80	180_{-70}^{+80}	200_{-110}^{+80}	2490_{-2360}^{+2630}	420_{-260}^{+250}	300_{-200}^{+410}	190_{-90}^{+80}
HII-81	330_{-90}^{+110}	460_{-130}^{+140}	2710_{-2130}^{+1730}	460_{-150}^{+160}	900_{-460}^{+530}	390_{-110}^{+130}
HII-82	130_{-70}^{+80}	310_{-160}^{+340}	-	-	-	220_{-120}^{+210}
HII-83	70_{-40}^{+60}	130_{-30}^{+40}	-	1850_{-1140}^{+1590}	-	100 ± 100
HII-84	210 ± 50	210 ± 20	-	660_{-490}^{+750}	-	210_{-30}^{+40}
HII-85	40_{-30}^{+40}	300_{-30}^{+50}	-	-	-	100 ± 100

Table A6. Electron densities derived from the sample of Star Forming Galaxies.

Reference number	$n_e(\text{[S II]})$ [cm $^{-3}$]	$n_e(\text{[O II]})$ [cm $^{-3}$]	$n_e(\text{[Fe III]})$ [cm $^{-3}$]	$n_e(\text{[Cl III]})$ [cm $^{-3}$]	$n_e(\text{[Ar IV]})$ [cm $^{-3}$]	Adopted n_e [cm $^{-3}$]
SFG-1	80_{-40}^{+60}	-	-	-	-	100 ± 100
SFG-2	210_{-120}^{+150}	-	-	-	-	210_{-120}^{+150}
SFG-3	20 ± 10	-	-	-	-	100 ± 100
SFG-4	30 ± 30	-	-	-	-	100 ± 100
SFG-5	30 ± 20	-	-	-	-	100 ± 100
SFG-6	170_{-80}^{+70}	-	-	-	-	170_{-80}^{+70}

Table A6 *continued*

Table A6 (*continued*)

Reference number	$n_e(\text{[S II]})$ [cm $^{-3}$]	$n_e(\text{[O II]})$ [cm $^{-3}$]	$n_e(\text{[Fe III]})$ [cm $^{-3}$]	$n_e(\text{[Cl III]})$ [cm $^{-3}$]	$n_e(\text{[Ar IV]})$ [cm $^{-3}$]	Adopted n_e [cm $^{-3}$]
SFG-7	40^{+30}_{-20}	-	-	-	-	100 ± 100
SFG-8	70^{+30}_{-40}	-	-	-	-	100 ± 100
SFG-9	150 ± 60	-	-	-	-	150 ± 60
SFG-10	50^{+30}_{-20}	-	-	-	-	100 ± 100
SFG-11	80 ± 50	-	-	-	-	100 ± 100
SFG-12	30 ± 20	-	-	-	-	100 ± 100
SFG-13	120^{+40}_{-30}	-	-	90 ± 50	-	120^{+40}_{-30}
SFG-14	60^{+100}_{-50}	-	-	-	-	100 ± 100
SFG-15	130^{+30}_{-40}	100 ± 30	-	-	-	120^{+30}_{-40}
SFG-16	50 ± 30	-	-	350^{+710}_{-290}	-	100 ± 100
SFG-17	460 ± 90	-	-	360^{+320}_{-260}	-	460 ± 90
SFG-18	700 ± 70	-	-	5320^{+1350}_{-1260}	-	700 ± 70
SFG-19	40^{+20}_{-30}	-	-	7740^{+5480}_{-3290}	-	100 ± 100
SFG-20	430 ± 50	-	-	-	-	430 ± 50
SFG-21	950^{+260}_{-220}	-	-	-	-	950^{+260}_{-220}
SFG-22	140 ± 40	-	-	-	-	140 ± 40
SFG-23	80 ± 30	-	-	180^{+320}_{-130}	-	100 ± 100
SFG-24	30 ± 20	-	-	330^{+480}_{-200}	-	100 ± 100
SFG-25	170^{+40}_{-30}	-	-	490^{+430}_{-330}	-	170^{+40}_{-30}
SFG-26	90^{+20}_{-10}	-	-	360^{+610}_{-220}	-	100 ± 100
SFG-27	120 ± 30	-	-	6110^{+3620}_{-3100}	-	120 ± 30
SFG-28	20^{+20}_{-10}	-	-	810^{+810}_{-510}	-	100 ± 100
SFG-29	80 ± 20	-	-	460^{+610}_{-390}	-	100 ± 100
SFG-30	120^{+80}_{-90}	170^{+100}_{-80}	5970^{+13640}_{-4220}	1130^{+1390}_{-770}	800^{+1130}_{-470}	150^{+90}_{-80}
SFG-31	200 ± 40	-	-	350^{+280}_{-240}	-	200 ± 40
SFG-32	50 ± 30	-	-	-	-	100 ± 100
SFG-33	170^{+150}_{-110}	-	-	-	-	170^{+150}_{-110}
SFG-34	200^{+220}_{-120}	-	-	-	-	200^{+220}_{-120}
SFG-35	150^{+140}_{-90}	-	-	-	-	150^{+140}_{-90}
SFG-36	90^{+70}_{-60}	140 ± 60	19690^{+46160}_{-14540}	490^{+450}_{-340}	900^{+710}_{-590}	100 ± 100
SFG-37	190^{+40}_{-30}	-	-	900^{+430}_{-410}	-	190^{+40}_{-30}
SFG-38	290^{+80}_{-90}	190 ± 70	5340^{+17410}_{-4090}	770^{+860}_{-510}	2550^{+2590}_{-1730}	240 ± 80
SFG-39	280^{+40}_{-50}	-	-	1100^{+790}_{-720}	-	280^{+40}_{-50}
SFG-40	200^{+110}_{-100}	220 ± 90	2970^{+3280}_{-2460}	370^{+320}_{-230}	880^{+560}_{-470}	210^{+100}_{-90}
SFG-41	90^{+40}_{-60}	-	-	-	-	100 ± 100
SFG-42	130 ± 40	-	-	2070^{+2080}_{-1020}	-	130 ± 40
SFG-43	30^{+30}_{-20}	-	-	-	-	100 ± 100
SFG-44	130^{+100}_{-70}	20^{+20}_{-10}	-	-	-	100 ± 100
SFG-45	100^{+130}_{-60}	90^{+50}_{-40}	-	-	1960 ± 1360	100 ± 100
SFG-46	60^{+80}_{-50}	150^{+90}_{-80}	$59750^{+234300}_{-36370}$	1050^{+1800}_{-690}	1600^{+1100}_{-870}	100 ± 100

Table A6 *continued*

Table A6 (*continued*)

Reference number	$n_e(\text{[S II]})$ [cm $^{-3}$]	$n_e(\text{[O II]})$ [cm $^{-3}$]	$n_e(\text{[Fe III]})$ [cm $^{-3}$]	$n_e(\text{[Cl III]})$ [cm $^{-3}$]	$n_e(\text{[Ar IV]})$ [cm $^{-3}$]	Adopted n_e [cm $^{-3}$]
SFG-47	130 $^{+40}_{-30}$	-	-	140 $^{+190}_{-90}$	-	130 $^{+40}_{-30}$
SFG-48	310 $^{+60}_{-50}$	-	-	2280 $^{+2310}_{-1450}$	-	310 $^{+60}_{-50}$
SFG-49	520 $^{+80}_{-90}$	-	-	1190 $^{+1960}_{-690}$	-	520 $^{+80}_{-90}$
SFG-50	50 $^{+50}_{-30}$	-	-	-	-	100 \pm 100
SFG-51	220 $^{+50}_{-60}$	-	-	-	-	220 $^{+50}_{-60}$
SFG-52	140 $^{+100}_{-90}$	-	-	-	-	140 $^{+100}_{-90}$
SFG-53	80 \pm 20	-	-	-	-	100 \pm 100
SFG-54	20 $^{+30}_{-10}$	-	-	3340 $^{+2810}_{-2350}$	-	100 \pm 100
SFG-55	620 \pm 140	-	-	-	-	620 \pm 140
SFG-56	70 $^{+40}_{-20}$	-	-	-	-	100 \pm 100
SFG-57	60 \pm 20	-	-	-	-	100 \pm 100
SFG-58	130 \pm 20	-	-	-	-	130 \pm 20
SFG-59	220 \pm 30	-	-	2840 $^{+1870}_{-2250}$	-	220 \pm 30
SFG-60	600 $^{+120}_{-150}$	-	-	-	-	600 $^{+120}_{-150}$
SFG-61	600 $^{+170}_{-140}$	-	-	-	-	600 $^{+170}_{-140}$
SFG-62	500 $^{+60}_{-50}$	-	-	-	-	500 $^{+60}_{-50}$
SFG-63	1240 \pm 60	290 $^{+130}_{-100}$	4800 $^{+15370}_{-3920}$	2560 $^{+2970}_{-1700}$	-	1040 \pm 390
SFG-64	260 $^{+120}_{-100}$	-	-	-	-	260 $^{+120}_{-100}$
SFG-65	190 $^{+90}_{-110}$	-	-	-	-	190 $^{+90}_{-110}$
SFG-66	80 \pm 50	-	-	-	-	100 \pm 100
SFG-67	980 $^{+700}_{-520}$	-	-	-	-	980 $^{+700}_{-520}$
SFG-68	80 $^{+40}_{-30}$	-	-	1730 $^{+1660}_{-1100}$	-	100 \pm 100
SFG-69	440 $^{+90}_{-80}$	-	-	-	-	440 $^{+90}_{-80}$
SFG-70	-	-	-	-	-	100 \pm 100
SFG-71	110 \pm 80	-	-	-	-	110 \pm 80
SFG-72	1290 \pm 120	-	-	-	-	1290 \pm 120
SFG-73	10 \pm 10	-	-	-	-	100 \pm 100
SFG-74	100 $^{+70}_{-60}$	210 $^{+120}_{-100}$	10400 $^{+40660}_{-7920}$	3130 $^{+2760}_{-1960}$	280 $^{+1040}_{-160}$	100 \pm 100
SFG-75	120 $^{+80}_{-70}$	150 \pm 80	6030 $^{+15330}_{-4470}$	2310 $^{+1860}_{-1640}$	700 $^{+640}_{-400}$	140 \pm 80
SFG-76	310 $^{+110}_{-80}$	-	-	-	-	310 $^{+110}_{-80}$
SFG-77	240 \pm 90	-	-	-	-	240 \pm 90
SFG-78	170 \pm 40	-	-	2520 $^{+2230}_{-2000}$	-	170 \pm 40
SFG-79	50 $^{+40}_{-30}$	-	-	-	-	100 \pm 100
SFG-80	140 $^{+70}_{-80}$	130 $^{+30}_{-40}$	-	1420 $^{+1720}_{-990}$	-	130 $^{+50}_{-60}$
SFG-81	150 \pm 100	170 \pm 60	-	-	-	160 \pm 80
SFG-82	-	-	-	-	-	100 \pm 100
SFG-83	90 \pm 30	-	-	800 $^{+600}_{-500}$	-	100 \pm 100
SFG-84	100 $^{+40}_{-30}$	-	-	220 $^{+220}_{-180}$	-	100 $^{+40}_{-30}$
SFG-85	140 \pm 40	-	-	50 $^{+120}_{-20}$	-	140 \pm 40
SFG-86	160 \pm 60	40 \pm 30	-	-	-	100 \pm 100

Table A6 *continued*

Table A6 (*continued*)

Reference number	$n_e(\text{[S II]})$ [cm $^{-3}$]	$n_e(\text{[O II]})$ [cm $^{-3}$]	$n_e(\text{[Fe III]})$ [cm $^{-3}$]	$n_e(\text{[Cl III]})$ [cm $^{-3}$]	$n_e(\text{[Ar IV]})$ [cm $^{-3}$]	Adopted n_e [cm $^{-3}$]
SFG-87	130 ± 70	50 ± 30	-	660^{+70}_{-360}	-	100 ± 100
SFG-88	40^{+40}_{-30}	-	-	-	-	100 ± 100
SFG-89	70^{+30}_{-40}	-	-	-	-	100 ± 100
SFG-90	280^{+80}_{-60}	-	-	-	-	280^{+80}_{-60}

Table A7. Electron densities derived from the sample of Planetary Nebulae.

Reference number	$n_e(\text{[S II]})$ [cm $^{-3}$]	$n_e(\text{[O II]})$ [cm $^{-3}$]	$n_e(\text{[Fe III]})$ [cm $^{-3}$]	$n_e(\text{[Cl III]})$ [cm $^{-3}$]	$n_e(\text{[Ar IV]})$ [cm $^{-3}$]	Adopted n_e [cm $^{-3}$]
PNe-1	7890^{+4620}_{-2680}	26330^{+38100}_{-10780}	18260^{+68580}_{-10950}	16350^{+6100}_{-4620}	18850^{+1940}_{-1750}	16640 ± 4250
PNe-2	3780^{+1180}_{-770}	5310^{+1400}_{-1030}	-	4550^{+860}_{-760}	-	4460 ± 550
PNe-3	6770^{+3050}_{-1910}	11930^{+6650}_{-3820}	-	10960^{+1560}_{-1350}	10920^{+970}_{-990}	10560 ± 1240
PNe-4	5690^{+1370}_{-1030}	9360^{+4420}_{-2490}	-	11940^{+1750}_{-1650}	9390^{+930}_{-830}	8690 ± 2100
PNe-5	330^{+370}_{-210}	-	-	-	-	330^{+370}_{-210}
PNe-6	-	-	-	-	-	100 ± 100
PNe-7	3760^{+1890}_{-1070}	5300^{+2530}_{-1530}	12860^{+24750}_{-7860}	4010^{+870}_{-900}	10670^{+5410}_{-5820}	4230 ± 1010
PNe-8	4730^{+2440}_{-1410}	7160^{+2880}_{-2110}	-	9000^{+1840}_{-1270}	19600^{+2610}_{-2480}	9190 ± 4780
PNe-9	3320^{+2970}_{-1540}	-	-	6660^{+7760}_{-4190}	-	4990^{+5360}_{-2870}
PNe-10	14650^{+12560}_{-6310}	40360^{+53520}_{-18840}	58990^{+32760}_{-21470}	48070^{+16810}_{-10540}	1770^{+1770}_{-1130}	2770 ± 6090
PNe-11	8810^{+10290}_{-3830}	7320^{+13750}_{-3950}	-	6550^{+7140}_{-4460}	-	7430 ± 990
PNe-12	1030^{+300}_{-250}	-	-	1430^{+390}_{-420}	710^{+450}_{-470}	1070 ± 240
PNe-13	5520^{+2920}_{-1690}	-	-	6680^{+1260}_{-930}	7670^{+1250}_{-1290}	6920 ± 680
PNe-14	6890^{+4000}_{-2370}	11100^{+9030}_{-3720}	-	13180^{+4170}_{-3380}	-	9710 ± 2940
PNe-15	7850^{+6170}_{-2480}	-	21280^{+17100}_{-7460}	16160^{+2810}_{-2540}	2220^{+2030}_{-1330}	6510 ± 6170
PNe-16	890^{+220}_{-180}	770 ± 120	-	2180^{+1370}_{-990}	1960^{+1340}_{-1020}	830^{+170}_{-150}
PNe-17	2430^{+5140}_{-1740}	-	-	-	-	2430^{+5140}_{-1740}
PNe-18	670^{+520}_{-450}	-	-	16730^{+57120}_{-11810}	-	670^{+520}_{-450}
PNe-19	6950^{+8920}_{-3490}	-	-	30410^{+7920}_{-21340}	-	18680^{+44060}_{-12410}
PNe-20	7230^{+5080}_{-2420}	14040^{+12010}_{-5360}	22490^{+24940}_{-12370}	13640^{+2850}_{-2110}	25940^{+3740}_{-3200}	15430 ± 6630
PNe-21	1200^{+720}_{-530}	-	-	980^{+860}_{-620}	-	1090^{+790}_{-570}
PNe-22	2750^{+1100}_{-720}	3820^{+1330}_{-810}	19040^{+72420}_{-16360}	5960^{+4510}_{-3050}	32300^{+64930}_{-21220}	3300 ± 880
PNe-23	1160^{+720}_{-440}	-	-	9190^{+8010}_{-5770}	-	5180^{+4360}_{-3110}
PNe-24	6850^{+4970}_{-2120}	8710^{+5760}_{-2930}	-	13000^{+4680}_{-3700}	-	9220 ± 2590
PNe-25	9610^{+13490}_{-5570}	13360^{+23810}_{-6690}	40690^{+35180}_{-16970}	21840^{+6080}_{-4620}	36690^{+6170}_{-5930}	25160 ± 9830
PNe-26	8760^{+8820}_{-3050}	15150^{+33500}_{-7400}	-	24030^{+32510}_{-12050}	42020^{+31590}_{-23190}	11410 ± 7260
PNe-27	12250^{+12740}_{-6430}	-	-	-	-	12250^{+12740}_{-6430}
PNe-28	2070^{+1580}_{-830}	-	-	2130^{+1090}_{-1050}	-	2100^{+1340}_{-940}

Table A7 *continued*

Table A7 (*continued*)

Reference number	$n_e(\text{[S II]})$ [cm $^{-3}$]	$n_e(\text{[O II]})$ [cm $^{-3}$]	$n_e(\text{[Fe III]})$ [cm $^{-3}$]	$n_e(\text{[Cl III]})$ [cm $^{-3}$]	$n_e(\text{[Ar IV]})$ [cm $^{-3}$]	Adopted n_e [cm $^{-3}$]
PNe-29	1730^{+2100}_{-940}	-	-	3390^{+1590}_{-1580}	-	2560^{+1840}_{-1260}
PNe-30	3270^{+5450}_{-1910}	-	-	-	-	3270^{+5450}_{-1910}
PNe-31	3030^{+2560}_{-1400}	-	-	-	-	3030^{+2560}_{-1400}
PNe-32	550^{+430}_{-260}	-	-	2720^{+1080}_{-1430}	-	550^{+430}_{-260}
PNe-33	8510^{+3420}_{-2000}	17020^{+10520}_{-4760}	605280 ± 48980	10120^{+1100}_{-890}	8690^{+800}_{-730}	9320 ± 7230
PNe-34	6230^{+6740}_{-2720}	-	-	18750^{+8410}_{-6240}	-	12490^{+7570}_{-4480}
PNe-35	1350^{+580}_{-410}	2550^{+690}_{-460}	-	270^{+340}_{-170}	1590^{+680}_{-730}	840 ± 810
PNe-36	14720^{+11600}_{-4820}	16150^{+9440}_{-5130}	-	12340^{+1350}_{-1140}	5430^{+3910}_{-3010}	11720 ± 2300
PNe-37	7540^{+2450}_{-1620}	14050^{+7020}_{-3370}	-	14340^{+1400}_{-1370}	11410^{+930}_{-970}	11770 ± 2060
PNe-38	800^{+230}_{-180}	-	-	4050^{+830}_{-730}	840^{+620}_{-520}	800^{+230}_{-180}
PNe-39	2440^{+750}_{-450}	-	-	120^{+140}_{-110}	-	1280^{+450}_{-280}
PNe-40	11030^{+10110}_{-4080}	13830^{+23670}_{-6280}	20390^{+28010}_{-11530}	22750^{+7190}_{-5290}	37380^{+3950}_{-3450}	29040 ± 10470
PNe-41	3230^{+6340}_{-2200}	13390^{+20050}_{-8060}	-	20220^{+59350}_{-16130}	8310^{+5690}_{-5180}	5720 ± 3270
PNe-42	3020^{+2720}_{-1260}	-	-	-	-	3020^{+2720}_{-1260}
PNe-43	4710^{+6810}_{-3120}	-	-	-	-	4710^{+6810}_{-3120}
PNe-44	4940^{+7410}_{-2760}	-	-	2070^{+1590}_{-1240}	-	3510^{+4500}_{-2000}
PNe-45	2260^{+3070}_{-1150}	-	-	$29390^{+133520}_{-20300}$	-	15820^{+68290}_{-10730}
PNe-46	$35600^{+1026260}_{-10690}$	-	-	22920^{+26670}_{-12300}	-	$29260^{+526470}_{-11490}$
PNe-47	830^{+790}_{-470}	-	-	-	-	830^{+790}_{-470}
PNe-48	1980^{+2230}_{-1160}	-	-	6300^{+11600}_{-4160}	-	4140^{+6910}_{-2660}
PNe-49	6970^{+4220}_{-2280}	17520^{+18850}_{-6880}	-	10590^{+1830}_{-1740}	10400^{+1470}_{-1300}	10160 ± 1210
PNe-50	5960^{+10790}_{-2820}	12020^{+18700}_{-5010}	-	14130^{+2990}_{-2660}	-	12890 ± 2830
PNe-51	4610^{+6170}_{-2040}	4520^{+3030}_{-1430}	-	7090^{+1550}_{-1290}	-	6210 ± 1210
PNe-52	9420^{+7720}_{-3480}	15270^{+27190}_{-8300}	-	20240^{+19040}_{-8890}	-	11260 ± 3770
PNe-53	5870^{+11430}_{-2980}	9440^{+13800}_{-4550}	-	13890^{+4420}_{-3350}	-	11770 ± 3260
PNe-54	4130^{+1710}_{-1030}	5710^{+3570}_{-1640}	-	7080^{+2510}_{-1810}	-	5100 ± 1250
PNe-55	4030^{+6450}_{-2350}	-	-	-	-	4030^{+6450}_{-2350}
PNe-56	3180^{+3980}_{-1800}	-	-	-	-	3180^{+3980}_{-1800}
PNe-57	3990^{+3400}_{-1850}	-	-	7920^{+9060}_{-5060}	-	5960^{+6230}_{-3460}
PNe-58	1350^{+870}_{-540}	-	-	1980^{+1160}_{-1030}	-	1660^{+1010}_{-790}
PNe-59	3300^{+3120}_{-1580}	-	-	6380^{+5030}_{-3940}	-	4840^{+4080}_{-2760}
PNe-60	4390^{+5790}_{-2010}	-	-	13700^{+23590}_{-9800}	-	9040^{+14690}_{-5900}
PNe-61	10070^{+11660}_{-4660}	22550^{+34750}_{-12050}	15780^{+44160}_{-10930}	19730^{+5560}_{-4300}	33560^{+8570}_{-7940}	20510 ± 7530
PNe-62	5540^{+7320}_{-3900}	-	-	-	-	5540^{+7320}_{-3900}
PNe-63	840^{+820}_{-540}	-	-	670^{+780}_{-400}	-	840^{+820}_{-540}
PNe-64	4200^{+7430}_{-2280}	-	-	15760^{+10600}_{-5580}	-	9980^{+9010}_{-3930}
PNe-65	11350^{+7820}_{-4030}	-	$85060^{+247240}_{-33770}$	15500^{+2540}_{-2030}	53410^{+10620}_{-8650}	16770 ± 8280
PNe-66	5130^{+2990}_{-1500}	-	-	14830^{+2540}_{-1800}	10960^{+1700}_{-1420}	10550 ± 3450
PNe-67	1510^{+1700}_{-790}	-	-	-	-	1510^{+1700}_{-790}
PNe-68	1220^{+350}_{-250}	-	1700^{+5980}_{-1650}	-	1160^{+720}_{-650}	1210 ± 40

Table A7 *continued*

Table A7 (*continued*)

Reference number	n_e ([S II]) [cm $^{-3}$]	n_e ([O II]) [cm $^{-3}$]	n_e ([Fe III]) [cm $^{-3}$]	n_e ([Cl III]) [cm $^{-3}$]	n_e ([Ar IV]) [cm $^{-3}$]	Adopted n_e [cm $^{-3}$]
PNe-69	2630 $^{+320}_{-290}$	3940 $^{+580}_{-540}$	-	5050 $^{+1260}_{-930}$	3990 $^{+1000}_{-980}$	3100 \pm 730
PNe-70	4210 $^{+2030}_{-1040}$	-	-	1780 $^{+500}_{-510}$	1420 $^{+630}_{-840}$	1840 \pm 660
PNe-71	2610 $^{+850}_{-690}$	-	-	3510 $^{+720}_{-700}$	3940 $^{+960}_{-850}$	3310 \pm 540
PNe-72	4550 $^{+2490}_{-1160}$	7010 $^{+3490}_{-1920}$	17990 $^{+14160}_{-7450}$	7780 $^{+1450}_{-1190}$	9030 $^{+1520}_{-1350}$	7520 \pm 1780
PNe-73	5990 $^{+3100}_{-1710}$	-	13640 $^{+11060}_{-6870}$	7680 $^{+1250}_{-1140}$	7940 $^{+2020}_{-2040}$	7550 \pm 910
PNe-74	4810 $^{+6920}_{-2380}$	9060 $^{+20870}_{-4780}$	-	9120 $^{+2730}_{-2450}$	8310 $^{+4670}_{-4110}$	8160 \pm 1620
PNe-75	8190 $^{+7070}_{-2670}$	8890 $^{+5410}_{-2750}$	39340 $^{+43670}_{-19170}$	12700 $^{+2420}_{-1830}$	22890 $^{+3380}_{-2810}$	14270 \pm 5340
PNe-76	2130 $^{+680}_{-380}$	4970 $^{+1730}_{-1190}$	-	1050 $^{+460}_{-360}$	1210 $^{+460}_{-620}$	1520 \pm 800
PNe-77	870 $^{+250}_{-240}$	-	-	1760 $^{+650}_{-450}$	3060 $^{+660}_{-920}$	870 $^{+250}_{-240}$
PNe-78	730 $^{+820}_{-450}$	-	-	1690 $^{+1060}_{-1030}$	-	730 $^{+820}_{-450}$
PNe-79	3160 $^{+2820}_{-1500}$	-	-	2090 $^{+1160}_{-1040}$	-	2630 $^{+1990}_{-1270}$
PNe-80	3860 $^{+2160}_{-1030}$	-	-	2940 $^{+610}_{-560}$	-	3400 $^{+1380}_{-800}$
PNe-81	4460 $^{+7170}_{-2900}$	-	-	-	-	4460 $^{+7170}_{-2900}$
PNe-82	4120 $^{+1670}_{-1190}$	-	-	11260 $^{+1820}_{-1590}$	-	7690 $^{+1750}_{-1390}$
PNe-83	3120 $^{+5550}_{-1880}$	-	-	9200 $^{+3660}_{-3380}$	-	6160 $^{+4600}_{-2630}$
PNe-84	780 $^{+180}_{-190}$	1180 $^{+230}_{-240}$	-	2000 $^{+720}_{-860}$	480 $^{+530}_{-370}$	980 $^{+210}_{-220}$
PNe-85	1970 $^{+13110}_{-1570}$	-	-	840 $^{+1020}_{-540}$	-	1410 $^{+7070}_{-1060}$
PNe-86	2700 $^{+410}_{-370}$	4240 $^{+730}_{-560}$	-	5620 $^{+580}_{-530}$	5090 $^{+670}_{-600}$	4000 \pm 1240
PNe-87	3020 $^{+1450}_{-790}$	4400 $^{+1480}_{-970}$	-	4250 $^{+970}_{-850}$	-	3920 \pm 590
PNe-88	2220 $^{+720}_{-620}$	3120 $^{+1160}_{-820}$	-	4360 $^{+950}_{-1090}$	-	2930 \pm 860
PNe-89	470 $^{+150}_{-120}$	-	-	830 \pm 430	440 $^{+470}_{-310}$	470 $^{+150}_{-120}$
PNe-90	1120 $^{+660}_{-450}$	-	-	1490 $^{+1020}_{-760}$	-	1300 $^{+840}_{-600}$
PNe-91	1330 $^{+800}_{-420}$	-	-	2410 $^{+1090}_{-1160}$	-	1870 $^{+950}_{-790}$
PNe-92	1200 $^{+690}_{-540}$	-	-	2150 $^{+1280}_{-990}$	-	1670 $^{+980}_{-770}$
PNe-93	1840 $^{+530}_{-360}$	-	-	1360 $^{+500}_{-490}$	2150 $^{+810}_{-750}$	1710 \pm 290
PNe-94	4800 $^{+3650}_{-1700}$	-	-	7050 $^{+1240}_{-1010}$	5960 $^{+1090}_{-1020}$	6340 \pm 690
PNe-95	1480 $^{+420}_{-320}$	1460 $^{+220}_{-210}$	-	980 $^{+430}_{-370}$	-	1380 \pm 180
PNe-96	1070 $^{+490}_{-370}$	1260 $^{+410}_{-360}$	-	1310 $^{+510}_{-550}$	1380 $^{+510}_{-700}$	1230 \pm 110
PNe-97	4260 $^{+3470}_{-1670}$	5060 $^{+1200}_{-900}$	-	1830 $^{+1340}_{-950}$	1760 $^{+660}_{-560}$	2520 \pm 1350
PNe-98	5950 $^{+9270}_{-2770}$	13220 $^{+28480}_{-6700}$	12410 $^{+28040}_{-8370}$	34100 $^{+14430}_{-9300}$	39470 $^{+13010}_{-11440}$	15760 \pm 13640
PNe-99	3220 $^{+1370}_{-930}$	5440 $^{+2630}_{-1290}$	-	3620 $^{+690}_{-640}$	3920 $^{+870}_{-760}$	3750 \pm 470
PNe-100	3070 $^{+1090}_{-850}$	5640 $^{+2450}_{-1480}$	15310 $^{+30780}_{-11020}$	3630 $^{+760}_{-750}$	6240 $^{+990}_{-1100}$	4220 \pm 1280
PNe-101	9760 $^{+5120}_{-2990}$	10070 $^{+5470}_{-2720}$	-	29350 $^{+4740}_{-4620}$	13970 $^{+2120}_{-2010}$	14500 \pm 5620
PNe-102	3060 $^{+2290}_{-1470}$	-	-	2880 $^{+2300}_{-1770}$	-	2970 $^{+2300}_{-1620}$
PNe-103	3020 $^{+1970}_{-950}$	4080 $^{+1600}_{-1150}$	-	4060 $^{+1110}_{-950}$	5030 $^{+1390}_{-1270}$	4090 \pm 640
PNe-104	2740 $^{+2490}_{-1160}$	-	-	5920 $^{+2400}_{-1690}$	-	4330 $^{+2440}_{-1430}$
PNe-105	3930 $^{+1530}_{-1090}$	4780 $^{+1570}_{-1040}$	-	5880 $^{+980}_{-930}$	6070 $^{+970}_{-1070}$	5380 \pm 820
PNe-106	200 $^{+170}_{-150}$	-	-	-	-	200 $^{+170}_{-150}$
PNe-107	230 $^{+220}_{-130}$	-	-	-	-	230 $^{+220}_{-130}$
PNe-108	3750 $^{+5520}_{-2230}$	-	-	29380 $^{+96570}_{-22810}$	-	16560 $^{+51040}_{-12520}$

Table A7 *continued*

Table A7 (*continued*)

Reference number	n_e ([S II]) [cm $^{-3}$]	n_e ([O II]) [cm $^{-3}$]	n_e ([Fe III]) [cm $^{-3}$]	n_e ([Cl III]) [cm $^{-3}$]	n_e ([Ar IV]) [cm $^{-3}$]	Adopted n_e [cm $^{-3}$]
PNe-109	4670 $^{+2800}_{-1400}$	5990 $^{+2270}_{-1760}$	11250 $^{+23050}_{-8780}$	5610 $^{+2760}_{-2100}$	3010 $^{+1610}_{-1280}$	4410 \pm 1330
PNe-110	160 $^{+140}_{-100}$	-	-	-	-	160 $^{+140}_{-100}$
PNe-111	1110 $^{+780}_{-470}$	-	-	2430 $^{+1200}_{-1210}$	-	1770 $^{+990}_{-840}$
PNe-112	5200 $^{+2690}_{-1420}$	14070 $^{+13080}_{-5920}$	-	9200 $^{+1460}_{-1370}$	8490 $^{+1400}_{-1390}$	8200 \pm 1560
PNe-113	16120 $^{+13560}_{-9370}$	15990 $^{+25340}_{-8630}$	-	19920 $^{+27800}_{-12140}$	28990 $^{+7780}_{-7140}$	23740 \pm 6120
PNe-114	2040 $^{+600}_{-470}$	2730 $^{+770}_{-510}$	-	3120 $^{+750}_{-690}$	2350 $^{+570}_{-700}$	2480 \pm 400
PNe-115	820 $^{+520}_{-370}$	-	-	2180 $^{+1050}_{-1060}$	-	820 $^{+520}_{-370}$
PNe-116	490 $^{+190}_{-120}$	560 $^{+130}_{-120}$	11530 $^{+54120}_{-8660}$	620 $^{+350}_{-340}$	710 $^{+570}_{-440}$	520 $^{+160}_{-120}$
PNe-117	5090 $^{+1500}_{-1100}$	7390 $^{+13590}_{-3820}$	-	8440 $^{+1310}_{-1210}$	5350 $^{+2760}_{-2800}$	6690 \pm 1640
PNe-118	11310 $^{+16920}_{-5180}$	-	-	-	-	11310 $^{+16920}_{-5180}$
PNe-119	3200 $^{+4280}_{-1660}$	-	-	19160 $^{+30200}_{-11100}$	-	11180 $^{+17240}_{-6380}$
PNe-120	1550 $^{+380}_{-340}$	2130 $^{+450}_{-410}$	-	2810 $^{+550}_{-670}$	1760 $^{+820}_{-710}$	1940 \pm 440
PNe-121	1430 $^{+440}_{-320}$	1880 $^{+390}_{-360}$	6160 $^{+25670}_{-4130}$	1440 $^{+520}_{-430}$	2120 $^{+680}_{-660}$	1660 \pm 270
PNe-122	250 $^{+230}_{-170}$	-	-	360 $^{+460}_{-260}$	-	250 $^{+230}_{-170}$
PNe-123	5160 $^{+8570}_{-3300}$	-	-	22560 $^{+53050}_{-18200}$	-	13860 $^{+30810}_{-10750}$
PNe-124	6500 $^{+11760}_{-3490}$	-	-	7770 $^{+10070}_{-5040}$	-	7140 $^{+10920}_{-4270}$
PNe-125	-	-	-	3940 \pm 140	4290 $^{+290}_{-260}$	100 \pm 100
PNe-126	1690 $^{+2100}_{-850}$	-	-	5030 $^{+2240}_{-2080}$	-	3360 $^{+2170}_{-1460}$
PNe-127	-	-	-	-	-	100 \pm 100
PNe-128	1840 $^{+870}_{-500}$	3510 $^{+1500}_{-840}$	-	2330 $^{+1540}_{-1370}$	-	2280 \pm 670
PNe-129	3020 $^{+1790}_{-1020}$	4450 $^{+2090}_{-1210}$	-	3470 $^{+960}_{-780}$	4620 $^{+1230}_{-1040}$	3820 \pm 620
PNe-130	660 $^{+340}_{-250}$	-	-	-	1740 $^{+1250}_{-940}$	660 $^{+340}_{-250}$
PNe-131	9860 $^{+11310}_{-4140}$	-	-	15550 $^{+3250}_{-2670}$	13870 $^{+1320}_{-1280}$	14050 \pm 890
PNe-132	1060 $^{+380}_{-310}$	-	-	-	-	1060 $^{+380}_{-310}$
PNe-133	450 $^{+130}_{-110}$	-	-	250 \pm 20	-	450 $^{+130}_{-110}$
PNe-134	1070 $^{+420}_{-270}$	-	-	1920 $^{+450}_{-560}$	1400 $^{+500}_{-490}$	1360 \pm 340
PNe-135	3760 $^{+1530}_{-1110}$	-	-	7610 $^{+1200}_{-1050}$	-	5680 $^{+1370}_{-1080}$
PNe-136	1970 $^{+2480}_{-840}$	-	-	-	200 $^{+210}_{-90}$	1090 $^{+1350}_{-460}$
PNe-137	1970 $^{+1370}_{-750}$	-	-	3830 $^{+480}_{-670}$	2260 $^{+760}_{-640}$	3010 \pm 840
PNe-138	320 $^{+190}_{-160}$	-	-	8850 $^{+2600}_{-2540}$	6190 $^{+810}_{-880}$	320 $^{+190}_{-160}$
PNe-139	330 $^{+340}_{-210}$	-	-	640 $^{+500}_{-310}$	460 $^{+610}_{-280}$	330 $^{+340}_{-210}$
PNe-140	2570 $^{+3860}_{-1450}$	-	-	2410 $^{+1000}_{-980}$	3100 $^{+640}_{-570}$	2900 \pm 310
PNe-141	810 $^{+330}_{-320}$	-	-	3790 $^{+630}_{-550}$	-	810 $^{+330}_{-320}$
PNe-142	2430 $^{+1120}_{-650}$	-	-	4330 $^{+1760}_{-1310}$	680 $^{+480}_{-360}$	1190 \pm 1020
PNe-143	2410 $^{+880}_{-710}$	-	-	1410 $^{+1030}_{-710}$	-	1910 $^{+950}_{-710}$
PNe-144	6220 $^{+7340}_{-3800}$	-	-	2480 $^{+1210}_{-1160}$	7150 $^{+1320}_{-1250}$	4670 \pm 2310
PNe-145	840 $^{+170}_{-210}$	-	-	-	1600 \pm 420	840 $^{+170}_{-210}$
PNe-146	2080 $^{+430}_{-350}$	2660 $^{+500}_{-440}$	-	1500 $^{+690}_{-720}$	-	2190 \pm 390
PNe-147	4820 $^{+3740}_{-1860}$	-	-	4280 $^{+640}_{-630}$	6810 $^{+650}_{-580}$	5560 \pm 1250
PNe-148	8490 $^{+6870}_{-3520}$	-	-	30900 $^{+33190}_{-12810}$	-	19700 $^{+20030}_{-8160}$

Table A7 *continued*

Table A7 (*continued*)

Reference number	$n_e(\text{[S II]})$ [cm $^{-3}$]	$n_e(\text{[O II]})$ [cm $^{-3}$]	$n_e(\text{[Fe III]})$ [cm $^{-3}$]	$n_e(\text{[Cl III]})$ [cm $^{-3}$]	$n_e(\text{[Ar IV]})$ [cm $^{-3}$]	Adopted n_e [cm $^{-3}$]
PNe-149	2700 $^{+840}_{-600}$	-	-	4830 $^{+1500}_{-1270}$	-	3770 $^{+1170}_{-940}$
PNe-150	750 $^{+250}_{-220}$	-	-	1420 $^{+450}_{-470}$	240 $^{+150}_{-170}$	750 $^{+250}_{-220}$
PNe-151	9260 $^{+5600}_{-3930}$	1810 $^{+410}_{-400}$	-	-	1080 $^{+420}_{-620}$	1570 \pm 630
PNe-152	2430 $^{+960}_{-830}$	7000 $^{+4860}_{-2460}$	-	5170 $^{+780}_{-850}$	3880 $^{+740}_{-700}$	3960 \pm 1110
PNe-153	660 $^{+220}_{-150}$	1050 \pm 260	-	-	210 $^{+180}_{-100}$	860 $^{+240}_{-200}$
PNe-154	1480 $^{+340}_{-270}$	-	-	1580 \pm 240	1390 $^{+290}_{-330}$	1500 \pm 80
PNe-155	3340 $^{+1210}_{-830}$	-	-	6910 $^{+1140}_{-950}$	4430 $^{+700}_{-550}$	4710 \pm 1210
PNe-156	2600 $^{+1310}_{-910}$	-	-	3230 $^{+2320}_{-1390}$	1220 $^{+540}_{-380}$	1510 \pm 620
PNe-157	1330 $^{+510}_{-450}$	-	-	1620 $^{+510}_{-490}$	870 $^{+480}_{-410}$	1240 \pm 310
PNe-158	990 $^{+1030}_{-520}$	-	-	-	630 $^{+500}_{-380}$	990 $^{+1030}_{-520}$
PNe-159	3120 $^{+2340}_{-1680}$	-	-	4910 $^{+1830}_{-2110}$	1480 $^{+600}_{-510}$	1820 \pm 930
PNe-160	2970 $^{+1100}_{-560}$	-	-	2820 $^{+860}_{-660}$	-	2900 $^{+980}_{-610}$
PNe-161	5630 $^{+5560}_{-2320}$	-	-	-	-	5630 $^{+5560}_{-2320}$
PNe-162	3330 $^{+830}_{-680}$	-	-	1100 $^{+290}_{-360}$	1160 $^{+570}_{-460}$	1380 \pm 710
PNe-163	2420 $^{+740}_{-630}$	3370 $^{+1110}_{-750}$	-	3540 $^{+580}_{-620}$	2380 $^{+480}_{-440}$	2790 \pm 530
PNe-164	6040 $^{+3210}_{-2190}$	-	-	13320 $^{+1480}_{-1670}$	15220 $^{+1110}_{-1020}$	13800 \pm 2670
PNe-165	7110 $^{+10330}_{-3630}$	-	-	14480 $^{+2580}_{-2080}$	9040 $^{+1080}_{-990}$	9890 \pm 2030
PNe-166	2570 $^{+990}_{-650}$	-	-	1600 $^{+570}_{-500}$	4510 $^{+750}_{-850}$	2520 \pm 1190
PNe-167	7780 $^{+1280}_{-890}$	5470 $^{+3160}_{-1940}$	-	-	3790 $^{+430}_{-340}$	4250 \pm 1250
PNe-168	3290 $^{+4090}_{-1500}$	-	-	2770 $^{+850}_{-810}$	2990 $^{+2700}_{-1780}$	2830 \pm 150
PNe-169	1630 $^{+830}_{-560}$	3970 $^{+2430}_{-1340}$	-	2680 $^{+1080}_{-930}$	6210 $^{+930}_{-1000}$	3120 \pm 1850
PNe-170	560 $^{+210}_{-200}$	-	-	240 $^{+200}_{-150}$	240 $^{+430}_{-100}$	560 $^{+210}_{-200}$
PNe-171	1010 $^{+180}_{-200}$	-	-	1030 $^{+390}_{-410}$	1010 $^{+510}_{-410}$	1010 \pm 10
PNe-172	580 $^{+180}_{-200}$	-	-	9130 $^{+4460}_{-2790}$	1040 $^{+160}_{-200}$	580 $^{+180}_{-200}$
PNe-173	10090 $^{+6830}_{-3430}$	-	-	3070 $^{+510}_{-540}$	-	6580 $^{+3670}_{-1980}$
PNe-174	6660 $^{+12640}_{-3120}$	-	-	1410 $^{+700}_{-600}$	6600 $^{+1410}_{-1150}$	2500 \pm 2120
PNe-175	2210 $^{+2040}_{-1000}$	-	-	2440 $^{+550}_{-570}$	1440 $^{+510}_{-440}$	1870 \pm 490
PNe-176	1060 $^{+380}_{-260}$	-	-	-	1430 $^{+660}_{-540}$	1240 $^{+520}_{-400}$
PNe-177	4630 $^{+3080}_{-1730}$	-	-	6750 $^{+1200}_{-940}$	-	5690 $^{+2140}_{-1340}$
PNe-178	1080 $^{+270}_{-190}$	-	-	2630 $^{+340}_{-390}$	-	1860 $^{+300}_{-290}$
PNe-179	1240 $^{+310}_{-300}$	-	-	1590 $^{+410}_{-370}$	1120 $^{+380}_{-340}$	1300 \pm 180
PNe-180	4370 $^{+1890}_{-880}$	11800 $^{+13900}_{-4590}$	14040 $^{+5160}_{-3980}$	4370 $^{+460}_{-340}$	20110 $^{+1770}_{-1540}$	5240 \pm 3540
PNe-181	3450 $^{+1480}_{-1100}$	-	-	7300 $^{+1210}_{-1120}$	4200 $^{+780}_{-710}$	4780 \pm 1420
PNe-182	2620 $^{+270}_{-200}$	5090 $^{+1050}_{-1070}$	-	5720 $^{+380}_{-350}$	4650 $^{+370}_{-340}$	3820 \pm 1320
PNe-183	3470 $^{+1540}_{-900}$	4330 $^{+3420}_{-1740}$	-	10920 $^{+2290}_{-1880}$	13040 $^{+830}_{-600}$	10290 \pm 4140
PNe-184	4480 $^{+2060}_{-1280}$	-	13730 $^{+10710}_{-5940}$	4380 $^{+2220}_{-2130}$	7540 $^{+1430}_{-1410}$	5990 \pm 1780
PNe-185	380 $^{+290}_{-200}$	940 $^{+420}_{-320}$	-	170 $^{+130}_{-80}$	-	660 $^{+350}_{-260}$
PNe-186	9760 $^{+15380}_{-4620}$	-	-	15260 $^{+1980}_{-1790}$	10010 $^{+1040}_{-770}$	10980 \pm 2040
PNe-187	3170 $^{+1320}_{-970}$	4680 $^{+1840}_{-1210}$	-	8080 $^{+1100}_{-1150}$	9870 $^{+990}_{-1060}$	6890 \pm 2750
PNe-188	15670 $^{+19440}_{-8550}$	-	-	-	-	15670 $^{+19440}_{-8550}$

Table A7 *continued*

Table A7 (*continued*)

Reference number	$n_e(\text{[S II]})$ [cm $^{-3}$]	$n_e(\text{[O II]})$ [cm $^{-3}$]	$n_e(\text{[Fe III]})$ [cm $^{-3}$]	$n_e(\text{[Cl III]})$ [cm $^{-3}$]	$n_e(\text{[Ar IV]})$ [cm $^{-3}$]	Adopted n_e [cm $^{-3}$]
PNe-189	5940 $^{+1240}_{-990}$	-	-	5420 $^{+1430}_{-1600}$	-	5680 $^{+1340}_{-1290}$
PNe-190	240 $^{+100}_{-90}$	-	-	880 $^{+200}_{-270}$	3500 $^{+700}_{-750}$	240 $^{+100}_{-90}$
PNe-191	190 \pm 100	-	-	-	1280 $^{+780}_{-600}$	190 \pm 100
PNe-192	3030 $^{+2750}_{-1320}$	-	-	3760 $^{+890}_{-830}$	3320 $^{+570}_{-590}$	3440 \pm 220
PNe-193	280 $^{+120}_{-100}$	-	-	230 $^{+250}_{-130}$	-	280 $^{+120}_{-100}$
PNe-194	1470 $^{+510}_{-340}$	-	-	1960 $^{+560}_{-390}$	130 $^{+80}_{-70}$	200 \pm 340
PNe-195	3190 $^{+1190}_{-760}$	-	-	1880 $^{+1240}_{-980}$	-	2540 $^{+1210}_{-870}$
PNe-196	2460 $^{+1240}_{-790}$	-	-	1340 $^{+600}_{-510}$	2670 $^{+660}_{-710}$	1960 \pm 640
PNe-197	6210 $^{+4360}_{-2230}$	-	-	24560 $^{+10600}_{-5890}$	2110 $^{+700}_{-640}$	2420 \pm 1940
PNe-198	650 $^{+220}_{-190}$	-	-	750 $^{+370}_{-380}$	880 $^{+620}_{-440}$	650 $^{+220}_{-190}$
PNe-199	360 $^{+410}_{-220}$	-	-	1190 $^{+1410}_{-710}$	390 $^{+300}_{-180}$	360 $^{+410}_{-220}$
PNe-200	5260 $^{+6730}_{-2270}$	2050 $^{+1860}_{-1140}$	-	6690 $^{+1240}_{-1470}$	8910 $^{+870}_{-1060}$	6810 \pm 2660
PNe-201	9600 $^{+10550}_{-3830}$	2340 $^{+570}_{-490}$	-	4480 $^{+770}_{-700}$	5940 $^{+2910}_{-2810}$	3160 \pm 1150
PNe-202	2000 $^{+740}_{-570}$	-	-	-	1630 $^{+610}_{-450}$	1820 $^{+670}_{-510}$
PNe-203	7270 $^{+4100}_{-2090}$	10130 $^{+8230}_{-4720}$	-	16120 $^{+3090}_{-3680}$	-	11180 \pm 4170
PNe-204	1810 $^{+520}_{-470}$	3610 $^{+990}_{-910}$	7570 $^{+24680}_{-4950}$	1310 $^{+380}_{-420}$	1510 $^{+410}_{-450}$	1650 \pm 560
PNe-205	100 $^{+70}_{-60}$	590 $^{+190}_{-150}$	-	-	2040 $^{+1010}_{-1150}$	350 $^{+130}_{-100}$
PNe-206	1660 $^{+420}_{-380}$	-	-	3360 \pm 1130	1180 $^{+510}_{-400}$	1580 \pm 520
PNe-207	11600 $^{+13350}_{-4160}$	-	-	14680 $^{+1840}_{-1640}$	-	13140 $^{+7590}_{-2900}$
PNe-208	760 $^{+230}_{-210}$	-	-	130 $^{+140}_{-50}$	1050 $^{+530}_{-550}$	760 $^{+230}_{-210}$
PNe-209	1380 $^{+1190}_{-770}$	2170 $^{+1980}_{-1020}$	-	320 $^{+340}_{-180}$	1430 $^{+540}_{-600}$	590 \pm 510
PNe-210	4770 $^{+4020}_{-1770}$	-	-	2890 $^{+1620}_{-1180}$	-	3830 $^{+2820}_{-1480}$
PNe-211	620 $^{+200}_{-190}$	1200 $^{+480}_{-430}$	-	5150 $^{+2000}_{-1640}$	-	910 $^{+340}_{-310}$
PNe-212	9360 $^{+10600}_{-4840}$	-	-	1730 $^{+1080}_{-1030}$	3690 $^{+640}_{-600}$	3220 \pm 950
PNe-213	4170 $^{+3460}_{-1750}$	7880 $^{+5060}_{-2970}$	-	12010 $^{+2340}_{-1920}$	15550 $^{+2190}_{-1580}$	11430 \pm 4340
PNe-214	8980 $^{+14300}_{-5130}$	-	-	-	-	8980 $^{+14300}_{-5130}$
PNe-215	9640 $^{+9700}_{-4710}$	22290 $^{+29750}_{-12010}$	-	31080 $^{+11730}_{-8410}$	-	17290 \pm 9870
PNe-216	-	-	-	-	-	100 \pm 100
PNe-217	2440 $^{+910}_{-530}$	-	-	5800 $^{+930}_{-980}$	3110 $^{+880}_{-730}$	3470 \pm 1340
PNe-218	-	-	-	-	-	100 \pm 100

Table A8. Electron temperatures derived from the sample of H II regions, considering recombination under “Case B” conditions.

Reference number	$T_e(\text{[O III]} \lambda 4363/\lambda 5007)$ [K]	$T_e(\text{He I } \lambda 7281/\lambda 5876)$ [K]	$T_e(\text{He I } \lambda 7281/\lambda 6678)$ [K]	Adopted $T_e(\text{He I})$ [K]
HII-1	9870 \pm 70	4630 $^{+400}_{-410}$	4890 $^{+490}_{-440}$	4760 $^{+450}_{-420}$

Table A8 *continued*

Table A8 (*continued*)

Reference number	T_e ([O III] $\lambda 4363/\lambda 5007$)	T_e (He I $\lambda 7281/\lambda 5876$)	T_e (He I $\lambda 7281/\lambda 6678$)	Adopted T_e (He I)
	[K]	[K]	[K]	[K]
HII-2	9100 $^{+150}_{-170}$	4740 $^{+1000}_{-850}$	4920 $^{+1060}_{-820}$	4830 $^{+1030}_{-830}$
HII-3	9150 $^{+90}_{-80}$	6880 $^{+580}_{-630}$	6740 $^{+640}_{-650}$	6810 $^{+610}_{-640}$
HII-4	11300 $^{+160}_{-150}$	11900 $^{+1000}_{-990}$	-	11900 $^{+1000}_{-990}$
HII-5	9520 $^{+210}_{-150}$	6790 $^{+1360}_{-1180}$	6510 $^{+1280}_{-1270}$	6650 $^{+1320}_{-1230}$
HII-6	7640 $^{+210}_{-180}$	6060 $^{+1590}_{-1460}$	6370 $^{+1480}_{-1400}$	6210 $^{+1530}_{-1430}$
HII-7	7440 $^{+170}_{-180}$	5720 $^{+680}_{-660}$	5760 $^{+830}_{-760}$	5740 $^{+750}_{-710}$
HII-8	7730 $^{+90}_{-70}$	4320 $^{+580}_{-520}$	5540 $^{+810}_{-710}$	4930 $^{+700}_{-610}$
HII-9	9010 $^{+190}_{-170}$	10770 $^{+4300}_{-3620}$	12430 $^{+3690}_{-3840}$	11600 $^{+3990}_{-3730}$
HII-10	10630 $^{+90}_{-70}$	6920 $^{+1830}_{-1850}$	7050 $^{+1950}_{-1870}$	6990 $^{+1890}_{-1860}$
HII-11	10500 $^{+140}_{-110}$	11290 $^{+3640}_{-2970}$	11950 $^{+3550}_{-3210}$	11620 $^{+3600}_{-3090}$
HII-12	9750 $^{+70}_{-80}$	8020 $^{+1110}_{-1000}$	7880 $^{+1170}_{-1020}$	7950 $^{+1140}_{-1010}$
HII-13	12880 $^{+130}_{-100}$	9010 $^{+3890}_{-3340}$	12360 $^{+4760}_{-4780}$	10690 $^{+4330}_{-4060}$
HII-14	11320 $^{+100}_{-140}$	11720 $^{+2640}_{-2570}$	13160 $^{+2760}_{-2450}$	12440 $^{+2700}_{-2510}$
HII-15	9740 \pm 70	8060 $^{+1120}_{-970}$	7840 $^{+1150}_{-990}$	7950 $^{+1130}_{-980}$
HII-16	9250 $^{+80}_{-50}$	7010 $^{+710}_{-740}$	7260 $^{+790}_{-850}$	7130 $^{+750}_{-790}$
HII-17	9540 $^{+70}_{-60}$	5710 $^{+700}_{-740}$	6310 $^{+850}_{-800}$	6010 $^{+780}_{-770}$
HII-18	9700 $^{+120}_{-170}$	22810 $^{+10100}_{-8360}$	18880 $^{+6740}_{-6020}$	20850 $^{+8420}_{-7190}$
HII-19	9410 $^{+60}_{-90}$	7170 $^{+810}_{-740}$	8480 $^{+1040}_{-970}$	7820 $^{+930}_{-850}$
HII-20	9560 $^{+90}_{-110}$	3290 \pm 930	4650 $^{+1180}_{-1250}$	3970 $^{+1060}_{-1090}$
HII-21	8540 $^{+140}_{-110}$	5190 $^{+1320}_{-1100}$	6590 $^{+1300}_{-1390}$	5890 $^{+1310}_{-1240}$
HII-22	9170 $^{+170}_{-180}$	13020 $^{+4150}_{-3270}$	13760 $^{+3290}_{-3280}$	13390 $^{+3720}_{-3280}$
HII-23	8700 $^{+70}_{-50}$	6020 $^{+850}_{-880}$	6560 $^{+1080}_{-960}$	6290 $^{+970}_{-920}$
HII-24	8460 $^{+190}_{-160}$	4930 $^{+1550}_{-1300}$	5570 $^{+1620}_{-1480}$	5250 $^{+1580}_{-1390}$
HII-25	9490 $^{+90}_{-80}$	7120 $^{+2490}_{-2430}$	8250 $^{+2860}_{-2600}$	7680 $^{+2670}_{-2510}$
HII-26	12700 $^{+150}_{-120}$	4890 $^{+980}_{-770}$	6450 $^{+1120}_{-1060}$	5670 $^{+1050}_{-910}$
HII-27	13780 $^{+150}_{-130}$	5640 $^{+1520}_{-1370}$	6930 $^{+1810}_{-1580}$	6280 $^{+1660}_{-1470}$
HII-28	8340 $^{+220}_{-160}$	9370 $^{+3020}_{-2500}$	10210 $^{+2970}_{-2660}$	9790 $^{+3000}_{-2580}$
HII-29	8280 $^{+150}_{-100}$	5250 $^{+860}_{-800}$	5810 $^{+950}_{-900}$	5530 $^{+910}_{-850}$
HII-30	8610 $^{+250}_{-320}$	2750 $^{+1440}_{-1080}$	3410 $^{+1630}_{-1450}$	3080 $^{+1530}_{-1260}$
HII-31	10690 $^{+330}_{-310}$	10450 $^{+3570}_{-3040}$	10500 $^{+3860}_{-3530}$	10480 $^{+3720}_{-3280}$
HII-32	8070 $^{+160}_{-180}$	1890 \pm 410	2210 $^{+480}_{-430}$	2050 $^{+450}_{-420}$
HII-33	7950 $^{+100}_{-80}$	6540 $^{+740}_{-750}$	6220 $^{+680}_{-870}$	6380 $^{+710}_{-810}$
HII-34	7700 $^{+260}_{-220}$	8770 $^{+1000}_{-960}$	8450 $^{+1010}_{-990}$	8610 $^{+1010}_{-980}$
HII-35	8430 $^{+50}_{-60}$	8930 $^{+670}_{-630}$	8090 \pm 510	8510 $^{+590}_{-570}$
HII-36	7990 \pm 50	8220 \pm 510	9560 $^{+450}_{-560}$	8890 $^{+480}_{-540}$
HII-37	8390 \pm 50	-	7970 $^{+400}_{-490}$	7970 $^{+400}_{-490}$
HII-38	8100 \pm 60	-	10070 $^{+650}_{-560}$	10070 $^{+650}_{-560}$
HII-39	8500 \pm 50	7090 $^{+480}_{-450}$	7650 $^{+430}_{-440}$	7370 $^{+450}_{-440}$
HII-40	8510 $^{+40}_{-70}$	-	7750 $^{+480}_{-500}$	7750 $^{+480}_{-500}$
HII-41	8400 \pm 50	6680 $^{+490}_{-480}$	7460 $^{+470}_{-450}$	7070 $^{+480}_{-460}$

Table A8 *continued*

Table A8 (*continued*)

Reference number	T_e ([O III] $\lambda\lambda 4363/\lambda 5007$)	T_e (He I $\lambda 7281/\lambda 5876$)	T_e (He I $\lambda 7281/\lambda 6678$)	Adopted T_e (He I)
	[K]	[K]	[K]	[K]
HII-42	8320^{+50}_{-40}	7640^{+510}_{-500}	7430^{+470}_{-450}	7540^{+490}_{-470}
HII-43	8320^{+80}_{-90}	6830 ± 780	8400^{+890}_{-790}	7610^{+830}_{-790}
HII-44	8380^{+40}_{-50}	6430^{+780}_{-900}	6530^{+810}_{-920}	6480^{+800}_{-910}
HII-45	8080^{+190}_{-200}	6570^{+1130}_{-1000}	7280^{+1360}_{-1060}	6920^{+1250}_{-1030}
HII-46	8050^{+90}_{-100}	7080^{+520}_{-500}	6810^{+510}_{-400}	6940^{+510}_{-450}
HII-47	9300^{+150}_{-130}	7030^{+760}_{-610}	9020^{+800}_{-770}	8030^{+780}_{-690}
HII-48	8430 ± 40	10140^{+1590}_{-1110}	8430^{+1150}_{-1180}	9280^{+1370}_{-1150}
HII-49	9010^{+150}_{-120}	8240^{+870}_{-920}	8680^{+860}_{-870}	8460^{+860}_{-890}
HII-50	8230^{+130}_{-110}	4070^{+1240}_{-1110}	5010^{+1580}_{-1340}	4540^{+1410}_{-1220}
HII-51	9960^{+280}_{-270}	5770^{+940}_{-950}	6630^{+980}_{-940}	6200^{+960}_{-950}
HII-52	8990^{+330}_{-320}	8150^{+1030}_{-920}	10000^{+960}_{-860}	9080^{+1000}_{-890}
HII-53	10290^{+430}_{-370}	4100^{+1120}_{-960}	6100^{+1450}_{-1430}	5100^{+1280}_{-1190}
HII-54	9120^{+470}_{-630}	5550^{+2410}_{-2360}	7150^{+2790}_{-2600}	6350^{+2600}_{-2480}
HII-55	8900^{+130}_{-100}	8910^{+1180}_{-1080}	8670^{+970}_{-1000}	8790^{+1080}_{-1040}
HII-56	15840 ± 170	-	8190^{+3380}_{-3060}	8190^{+3380}_{-3060}
HII-57	16050^{+330}_{-360}	7470^{+1100}_{-990}	9300^{+1390}_{-1110}	8390^{+1240}_{-1050}
HII-58	8090^{+290}_{-570}	2950^{+1100}_{-940}	3530^{+1190}_{-1030}	3240^{+1150}_{-980}
HII-59	8620^{+290}_{-270}	1260^{+400}_{-490}	1530^{+550}_{-610}	1400^{+470}_{-550}
HII-60	8210 ± 190	7090^{+1230}_{-1350}	7510^{+1490}_{-1320}	7300^{+1360}_{-1340}
HII-61	7730^{+410}_{-300}	5790^{+2760}_{-2540}	5280^{+2600}_{-2170}	5540^{+2680}_{-2360}
HII-62	10150 ± 60	8350^{+650}_{-600}	8340^{+590}_{-570}	8340^{+620}_{-590}
HII-63	9280^{+130}_{-160}	-	11530^{+960}_{-890}	11530^{+960}_{-890}
HII-64	9410^{+380}_{-400}	9210^{+3130}_{-2880}	8260^{+3100}_{-2610}	8730^{+3110}_{-2750}
HII-65	8340^{+370}_{-430}	10050^{+3670}_{-3030}	8480^{+3360}_{-2450}	9260^{+3510}_{-2740}
HII-66	9990^{+640}_{-500}	5360^{+2540}_{-2190}	4750^{+2290}_{-1920}	5060^{+2420}_{-2060}
HII-67	8760^{+370}_{-420}	10350^{+4000}_{-3220}	8370^{+3310}_{-2530}	9360^{+3650}_{-2880}
HII-68	10120^{+250}_{-200}	12280^{+3890}_{-2940}	11260^{+2810}_{-3050}	11770^{+3350}_{-3000}
HII-69	10560^{+200}_{-140}	10890^{+3200}_{-3010}	11300 ± 2940	11100^{+3070}_{-2970}
HII-70	8450^{+420}_{-460}	9180^{+3240}_{-2910}	9210^{+3000}_{-2980}	9190^{+3120}_{-2950}
HII-71	11620^{+610}_{-500}	5760^{+1270}_{-1150}	10740^{+2340}_{-2050}	8250^{+1800}_{-1600}
HII-72	11590 ± 160	9970^{+1570}_{-1650}	11000^{+1550}_{-1570}	10480^{+1560}_{-1610}
HII-73	11790^{+100}_{-90}	10560^{+1120}_{-1140}	10890^{+1270}_{-1060}	10730^{+1190}_{-1100}
HII-74	11980^{+170}_{-240}	11870^{+2340}_{-2020}	13540^{+2390}_{-2150}	12700^{+2360}_{-2090}
HII-75	12100^{+190}_{-130}	11170^{+2580}_{-2240}	11400^{+2360}_{-2150}	11280^{+2470}_{-2200}
HII-76	11580^{+200}_{-220}	10890^{+1940}_{-1790}	9900^{+2050}_{-1760}	10400^{+2000}_{-1770}
HII-77	11300^{+100}_{-90}	9980^{+450}_{-440}	9510^{+490}_{-480}	9750^{+470}_{-460}
HII-78	11780 ± 280	11710^{+2760}_{-2530}	11850^{+2660}_{-2400}	11780^{+2710}_{-2460}
HII-79	14050^{+690}_{-850}	-	18620^{+4480}_{-3960}	18620^{+4480}_{-3960}
HII-80	12550^{+160}_{-170}	-	23930^{+2690}_{-2800}	23930^{+2690}_{-2800}
HII-81	12820^{+230}_{-200}	11230^{+1030}_{-1090}	11070^{+1230}_{-1080}	11150^{+1130}_{-1080}

Table A8 *continued*

Table A8 (*continued*)

Reference number	$T_e(\text{[O III]} \lambda 4363/\lambda 5007)$	$T_e(\text{He I } \lambda 7281/\lambda 5876)$	$T_e(\text{He I } \lambda 7281/\lambda 6678)$	Adopted $T_e(\text{He I})$
	[K]	[K]	[K]	[K]
HII-82	12050^{+180}_{-130}	29520^{+9000}_{-6280}	23310^{+4640}_{-3780}	26410^{+6820}_{-5030}
HII-83	12510^{+310}_{-450}	10770^{+3730}_{-3220}	11360^{+4010}_{-3230}	11060^{+3870}_{-3230}
HII-84	12040 ± 170	10790^{+1870}_{-1750}	10230^{+1820}_{-1470}	10510^{+1840}_{-1610}
HII-85	12230^{+650}_{-460}	-	29520^{+8060}_{-8380}	29520^{+8060}_{-8380}

Table A9. Electron temperatures derived from the sample of Star Forming Galaxies, considering recombination under “Case B” conditions.

Reference number	$T_e(\text{[O III]} \lambda 4363/\lambda 5007)$	$T_e(\text{He I } \lambda 7281/\lambda 5876)$	$T_e(\text{He I } \lambda 7281/\lambda 6678)$	Adopted $T_e(\text{He I})$
	[K]	[K]	[K]	[K]
SFG-1	15610^{+100}_{-90}	11310^{+3870}_{-3490}	11650^{+3930}_{-3460}	11480^{+3900}_{-3470}
SFG-2	19990^{+330}_{-360}	12360^{+4800}_{-3760}	13640^{+4530}_{-3690}	13000^{+4670}_{-3720}
SFG-3	15370^{+110}_{-180}	17080^{+5200}_{-4270}	16480^{+4250}_{-3860}	16780^{+4730}_{-4070}
SFG-4	13720^{+180}_{-200}	7170^{+3340}_{-2480}	8040^{+3760}_{-2940}	7600^{+3550}_{-2710}
SFG-5	13000^{+130}_{-120}	6880^{+3090}_{-2630}	8950^{+3730}_{-3180}	7920^{+3410}_{-2900}
SFG-6	16110^{+190}_{-180}	9970^{+3880}_{-3170}	12220^{+3740}_{-3270}	11100^{+3810}_{-3220}
SFG-7	14060^{+160}_{-110}	12300^{+4680}_{-3610}	13250^{+4340}_{-3790}	12770^{+4510}_{-3700}
SFG-8	15980^{+100}_{-70}	8360^{+3400}_{-3020}	8290^{+3450}_{-3020}	8330^{+3420}_{-3020}
SFG-9	15920^{+190}_{-290}	-	30990^{+8930}_{-10990}	30990^{+8930}_{-10990}
SFG-10	14560^{+160}_{-240}	6730^{+3160}_{-2560}	15490^{+6180}_{-5650}	11110^{+4670}_{-4110}
SFG-11	18170^{+220}_{-180}	11480^{+4340}_{-3500}	13630^{+4070}_{-4090}	12560^{+4210}_{-3790}
SFG-12	12260^{+290}_{-270}	10690^{+3840}_{-3400}	10930^{+3850}_{-3330}	10810^{+3850}_{-3370}
SFG-13	16330^{+220}_{-150}	8380^{+1470}_{-1380}	9550^{+1440}_{-1580}	8960^{+1460}_{-1480}
SFG-14	19120^{+590}_{-460}	7100^{+810}_{-840}	6960^{+1270}_{-1170}	7030^{+1040}_{-1000}
SFG-15	14630^{+150}_{-100}	6890^{+870}_{-950}	7730^{+900}_{-950}	7310^{+880}_{-950}
SFG-16	13230^{+140}_{-100}	8500^{+1940}_{-1650}	9630^{+1940}_{-1970}	9060^{+1940}_{-1810}
SFG-17	16140^{+270}_{-290}	11190^{+910}_{-840}	11980^{+930}_{-750}	11590^{+920}_{-790}
SFG-18	7310^{+320}_{-220}	5090^{+680}_{-640}	5620^{+700}_{-750}	5360^{+690}_{-700}
SFG-19	13070 ± 120	7600^{+1070}_{-910}	7870^{+1030}_{-860}	7730^{+1050}_{-880}
SFG-20	13360^{+140}_{-110}	8250^{+1960}_{-1510}	7320^{+1380}_{-1480}	7780^{+1670}_{-1500}
SFG-21	21490^{+500}_{-560}	14100^{+3130}_{-2060}	15020^{+1650}_{-1440}	14560^{+2390}_{-1750}
SFG-22	17130^{+220}_{-170}	9360^{+1200}_{-1110}	14800^{+1730}_{-1490}	12080^{+1460}_{-1300}
SFG-23	13310^{+80}_{-70}	12520^{+800}_{-610}	9740^{+570}_{-520}	11130^{+680}_{-560}
SFG-24	10650^{+80}_{-60}	6910^{+1110}_{-1060}	7780^{+1130}_{-1070}	7350^{+1120}_{-1070}
SFG-25	10070^{+100}_{-120}	8110^{+1280}_{-1110}	7750^{+1220}_{-1090}	7930^{+1250}_{-1100}
SFG-26	15790^{+290}_{-320}	12650^{+3940}_{-3320}	12110^{+3250}_{-2900}	12380^{+3600}_{-3110}
SFG-27	11550^{+120}_{-100}	8460^{+2500}_{-2370}	8770^{+2510}_{-2350}	8610^{+2500}_{-2360}

Table A9 *continued*

Table A9 (*continued*)

Reference number	T_e ([O III] $\lambda\lambda 4363/\lambda 5007$)	T_e (He I $\lambda\lambda 7281/\lambda 5876$)	T_e (He I $\lambda\lambda 7281/\lambda 6678$)	Adopted T_e (He I)
	[K]	[K]	[K]	[K]
SFG-28	14340 $^{+300}_{-450}$	20880 $^{+8400}_{-6010}$	19210 $^{+5680}_{-5000}$	20050 $^{+7040}_{-5510}$
SFG-29	13350 $^{+50}_{-60}$	6320 $^{+570}_{-540}$	6900 $^{+550}_{-540}$	6610 $^{+560}_{-540}$
SFG-30	10200 $^{+190}_{-140}$	7930 $^{+1910}_{-1670}$	7390 $^{+1830}_{-1610}$	7660 $^{+1870}_{-1640}$
SFG-31	10970 $^{+60}_{-70}$	7760 $^{+520}_{-450}$	6410 $^{+450}_{-470}$	7080 $^{+480}_{-460}$
SFG-32	9180 $^{+140}_{-100}$	8130 $^{+880}_{-780}$	7500 $^{+800}_{-700}$	7810 $^{+840}_{-740}$
SFG-33	8990 \pm 290	8370 $^{+2480}_{-1970}$	8530 $^{+2240}_{-2030}$	8450 $^{+2360}_{-2000}$
SFG-34	9390 $^{+340}_{-420}$	8420 $^{+5050}_{-3170}$	7410 $^{+4100}_{-2610}$	7910 $^{+4580}_{-2890}$
SFG-35	9670 $^{+500}_{-440}$	9790 $^{+3050}_{-2720}$	9670 $^{+3540}_{-2830}$	9730 $^{+3290}_{-2780}$
SFG-36	12770 $^{+240}_{-220}$	6410 $^{+980}_{-950}$	6980 $^{+930}_{-960}$	6690 $^{+950}_{-960}$
SFG-37	10150 $^{+60}_{-70}$	9310 $^{+490}_{-520}$	6630 $^{+350}_{-370}$	7970 $^{+420}_{-440}$
SFG-38	10830 $^{+140}_{-150}$	5640 $^{+1190}_{-1150}$	6250 $^{+1340}_{-1280}$	5950 $^{+1270}_{-1210}$
SFG-39	15490 $^{+50}_{-110}$	9190 $^{+370}_{-380}$	9560 $^{+240}_{-220}$	9370 \pm 300
SFG-40	15450 $^{+280}_{-290}$	11900 $^{+1840}_{-1460}$	10730 $^{+1680}_{-1480}$	11310 $^{+1760}_{-1470}$
SFG-41	13550 $^{+290}_{-340}$	10610 $^{+3140}_{-2990}$	12260 $^{+3600}_{-3130}$	11440 $^{+3370}_{-3060}$
SFG-42	13990 $^{+100}_{-130}$	13260 $^{+1640}_{-1510}$	12380 $^{+1430}_{-1320}$	12820 $^{+1540}_{-1410}$
SFG-43	11570 \pm 90	7220 $^{+2500}_{-2270}$	7960 $^{+2860}_{-2450}$	7590 $^{+2680}_{-2360}$
SFG-44	13900 $^{+370}_{-580}$	19150 $^{+9360}_{-6500}$	16420 $^{+6970}_{-5480}$	17790 $^{+8160}_{-5990}$
SFG-45	16570 \pm 330	13570 $^{+5500}_{-4440}$	12110 $^{+5120}_{-3680}$	12840 $^{+5310}_{-4060}$
SFG-46	13070 $^{+240}_{-260}$	6950 $^{+1340}_{-1300}$	8050 $^{+1850}_{-1520}$	7500 $^{+1600}_{-1410}$
SFG-47	12960 $^{+70}_{-60}$	7840 $^{+370}_{-390}$	7810 $^{+440}_{-430}$	7830 \pm 410
SFG-48	21190 $^{+270}_{-290}$	10990 $^{+740}_{-720}$	13140 $^{+790}_{-780}$	12070 $^{+770}_{-750}$
SFG-49	20430 $^{+250}_{-310}$	10650 $^{+1270}_{-1300}$	13460 $^{+1330}_{-1370}$	12060 $^{+1300}_{-1330}$
SFG-50	20370 $^{+110}_{-150}$	19280 $^{+1320}_{-1440}$	18010 \pm 1140	18640 $^{+1230}_{-1290}$
SFG-51	21270 $^{+290}_{-330}$	12710 $^{+1500}_{-1170}$	12840 $^{+1160}_{-1080}$	12770 $^{+1330}_{-1130}$
SFG-52	19080 $^{+450}_{-370}$	24330 $^{+14260}_{-9450}$	21340 $^{+7520}_{-6530}$	22840 $^{+10890}_{-7990}$
SFG-53	16840 \pm 100	13620 $^{+5020}_{-4190}$	11690 $^{+3780}_{-3330}$	12650 $^{+4400}_{-3760}$
SFG-54	17310 $^{+440}_{-330}$	10540 $^{+1560}_{-1540}$	11700 $^{+1650}_{-1490}$	11120 $^{+1610}_{-1510}$
SFG-55	20710 $^{+470}_{-550}$	11920 $^{+1770}_{-1460}$	14250 $^{+1630}_{-1660}$	13080 $^{+1700}_{-1560}$
SFG-56	14480 $^{+280}_{-260}$	24420 $^{+5430}_{-4520}$	28060 $^{+4680}_{-4480}$	26240 $^{+5050}_{-4500}$
SFG-57	15000 $^{+300}_{-350}$	8360 $^{+3010}_{-2720}$	7840 $^{+2940}_{-2800}$	8100 $^{+2970}_{-2760}$
SFG-58	13750 $^{+140}_{-190}$	5740 $^{+2490}_{-2230}$	6190 $^{+2620}_{-2260}$	5970 $^{+2550}_{-2240}$
SFG-59	14790 $^{+470}_{-600}$	1670 $^{+700}_{-660}$	15540 $^{+3260}_{-3040}$	8600 $^{+1980}_{-1850}$
SFG-60	18930 $^{+500}_{-420}$	19270 $^{+5150}_{-3680}$	19080 $^{+1510}_{-1390}$	19170 $^{+3330}_{-2540}$
SFG-61	18930 $^{+390}_{-480}$	19810 $^{+4940}_{-2250}$	19000 $^{+1260}_{-1130}$	19410 $^{+3100}_{-1690}$
SFG-62	15990 $^{+90}_{-110}$	7740 $^{+2520}_{-2450}$	8340 $^{+2440}_{-2500}$	8040 $^{+2480}_{-2470}$
SFG-63	13310 $^{+340}_{-290}$	7490 $^{+1740}_{-1400}$	-	7490 $^{+1740}_{-1400}$
SFG-64	19250 $^{+340}_{-370}$	5750 $^{+960}_{-930}$	5680 $^{+990}_{-900}$	5710 $^{+970}_{-910}$
SFG-65	17060 $^{+350}_{-320}$	8350 $^{+940}_{-920}$	13870 $^{+1430}_{-1370}$	11110 $^{+1180}_{-1140}$
SFG-66	19980 \pm 230	20200 $^{+1930}_{-1600}$	20860 $^{+2010}_{-1600}$	20530 $^{+1970}_{-1600}$
SFG-67	24730 $^{+770}_{-850}$	1780 $^{+15930}_{-21880}$	21510 $^{+3640}_{-3130}$	11640 $^{+9790}_{-12510}$

Table A9 *continued*

Table A9 (*continued*)

Reference number	T_e ([O III] $\lambda 4363/\lambda 5007$)	T_e (He I $\lambda 7281/\lambda 5876$)	T_e (He I $\lambda 7281/\lambda 6678$)	Adopted T_e (He I)
	[K]	[K]	[K]	[K]
SFG-68	14200^{+130}_{-120}	11850^{+800}_{-740}	11400^{+750}_{-730}	11630^{+770}_{-730}
SFG-69	15630^{+190}_{-250}	11970^{+1050}_{-1060}	10930^{+850}_{-770}	11450^{+950}_{-920}
SFG-70	15080^{+290}_{-400}	4130^{+1200}_{-1180}	7350^{+1730}_{-1720}	5740^{+1460}_{-1450}
SFG-71	19540^{+150}_{-170}	10200^{+3700}_{-3110}	11020^{+3950}_{-3450}	10610^{+3830}_{-3280}
SFG-72	13730^{+60}_{-80}	-	9520^{+340}_{-360}	9520^{+340}_{-360}
SFG-73	10500^{+170}_{-220}	6440^{+2540}_{-2250}	9400^{+3320}_{-3040}	7920^{+2930}_{-2650}
SFG-74	11340^{+240}_{-210}	13730^{+2540}_{-2240}	13010^{+2590}_{-2170}	13370^{+2570}_{-2200}
SFG-75	13530^{+270}_{-280}	10860^{+2030}_{-1750}	11040^{+1980}_{-1990}	10950^{+2000}_{-1870}
SFG-76	19700^{+270}_{-250}	10170^{+3990}_{-3460}	10520^{+3740}_{-3420}	10350^{+3860}_{-3440}
SFG-77	19870^{+240}_{-290}	9860^{+1900}_{-1840}	10730^{+2120}_{-1900}	10290^{+2010}_{-1870}
SFG-78	17120 ± 190	13720^{+2300}_{-1900}	15390^{+2400}_{-2180}	14550^{+2350}_{-2040}
SFG-79	17230^{+280}_{-220}	8180^{+3450}_{-3100}	9410^{+3880}_{-3430}	8800^{+3660}_{-3270}
SFG-80	14700^{+250}_{-300}	5580^{+2150}_{-1930}	7510^{+2570}_{-2260}	6540^{+2360}_{-2090}
SFG-81	14610^{+270}_{-300}	-	28630^{+8310}_{-8660}	28630^{+8310}_{-8660}
SFG-82	19850^{+330}_{-220}	14810^{+990}_{-960}	15920^{+1030}_{-920}	15360^{+1010}_{-940}
SFG-83	11780^{+50}_{-60}	7020^{+600}_{-560}	8710^{+760}_{-780}	7870^{+680}_{-670}
SFG-84	12370^{+100}_{-110}	6050^{+500}_{-480}	6770^{+480}_{-490}	6410 ± 490
SFG-85	12170 ± 50	7310^{+330}_{-350}	7900^{+450}_{-430}	7610 ± 390
SFG-86	15660^{+160}_{-170}	6210^{+1190}_{-1260}	13080^{+2410}_{-2180}	9640^{+1800}_{-1720}
SFG-87	15660^{+220}_{-170}	11440^{+2500}_{-2170}	21480^{+4310}_{-4040}	16460^{+3400}_{-3110}
SFG-88	17600^{+1140}_{-720}	20620^{+7030}_{-5410}	18730^{+4810}_{-4390}	19680^{+5920}_{-4900}
SFG-89	15370^{+240}_{-200}	10040^{+1980}_{-1710}	10310^{+1900}_{-1650}	10180^{+1940}_{-1680}
SFG-90	16920^{+310}_{-330}	-	26380^{+3250}_{-2850}	26380^{+3250}_{-2850}

Table A10. Electron temperatures derived from the sample of Planetary Nebulae, considering recombination under “Case B” conditions.

Reference number	T_e ([O III] $\lambda 4363/\lambda 5007$)	T_e (He I $\lambda 7281/\lambda 5876$)	T_e (He I $\lambda 7281/\lambda 6678$)	Adopted T_e (He I)
	[K]	[K]	[K]	[K]
PNe-1	10920^{+140}_{-130}	24290^{+5340}_{-15530}	9530^{+650}_{-590}	16910^{+3000}_{-8060}
PNe-2	13090^{+230}_{-180}	8490^{+740}_{-650}	9070^{+650}_{-680}	8780^{+700}_{-670}
PNe-3	12310^{+170}_{-190}	8070^{+580}_{-530}	8650^{+530}_{-520}	8360^{+550}_{-530}
PNe-4	13070^{+160}_{-180}	8500^{+660}_{-580}	9130^{+470}_{-490}	8810^{+560}_{-540}
PNe-5	11480^{+640}_{-840}	9200^{+4040}_{-3310}	12020^{+12230}_{-5420}	10610^{+8130}_{-4370}
PNe-6	13090^{+600}_{-860}	9600^{+2950}_{-2480}	11030^{+3310}_{-2590}	10310^{+3130}_{-2540}
PNe-7	8770^{+140}_{-130}	5310^{+1080}_{-880}	6380^{+830}_{-980}	5840^{+950}_{-930}
PNe-8	10100^{+200}_{-170}	4840^{+590}_{-610}	5940^{+590}_{-650}	5390^{+590}_{-630}

Table A10 *continued*

Table A10 (*continued*)

Reference number	T_e ([O III] $\lambda\lambda 4363/\lambda 5007$)	T_e (He I $\lambda\lambda 7281/\lambda 5876$)	T_e (He I $\lambda\lambda 7281/\lambda 6678$)	Adopted T_e (He I)
	[K]	[K]	[K]	[K]
PNe-9	11940 $^{+620}_{-560}$	9190 $^{+12940}_{-1730}$	9610 $^{+1810}_{-1370}$	9400 $^{+7380}_{-1550}$
PNe-10	9300 $^{+140}_{-130}$	7170 $^{+780}_{-800}$	8460 $^{+770}_{-750}$	7810 \pm 770
PNe-11	10150 $^{+280}_{-380}$	5820 $^{+960}_{-920}$	6660 $^{+780}_{-960}$	6240 $^{+870}_{-940}$
PNe-12	9700 $^{+130}_{-180}$	2590 $^{+520}_{-480}$	2820 $^{+580}_{-480}$	2710 $^{+550}_{-480}$
PNe-13	10090 $^{+140}_{-170}$	5930 $^{+710}_{-690}$	6380 $^{+610}_{-710}$	6150 $^{+660}_{-700}$
PNe-14	11080 $^{+240}_{-250}$	6540 $^{+710}_{-730}$	7140 $^{+650}_{-640}$	6840 \pm 680
PNe-15	9520 $^{+170}_{-160}$	4340 $^{+650}_{-640}$	6050 $^{+670}_{-630}$	5190 $^{+660}_{-630}$
PNe-16	13200 $^{+160}_{-170}$	4170 $^{+1270}_{-1050}$	6660 $^{+1530}_{-1360}$	5420 $^{+1400}_{-1200}$
PNe-17	19510 $^{+1740}_{-1190}$	7990 $^{+1810}_{-1620}$	11430 $^{+2280}_{-1780}$	9710 $^{+2050}_{-1700}$
PNe-18	15940 $^{+1160}_{-1980}$	6310 $^{+3170}_{-2310}$	6420 $^{+2720}_{-2510}$	6370 $^{+2940}_{-2410}$
PNe-19	9060 \pm 300	3960 \pm 1260	5500 $^{+1190}_{-1210}$	4730 $^{+1220}_{-1230}$
PNe-20	12470 \pm 260	6090 $^{+630}_{-650}$	7570 \pm 600	6830 $^{+610}_{-630}$
PNe-21	12780 $^{+660}_{-670}$	3230 $^{+1380}_{-1010}$	4190 $^{+1340}_{-1190}$	3710 $^{+1360}_{-1100}$
PNe-22	9250 $^{+230}_{-220}$	10840 $^{+17070}_{-1580}$	8610 $^{+1200}_{-970}$	9730 $^{+9140}_{-1280}$
PNe-23	12700 $^{+520}_{-690}$	6740 $^{+1430}_{-1380}$	6960 $^{+1280}_{-1400}$	6850 $^{+1350}_{-1390}$
PNe-24	11930 $^{+280}_{-340}$	7570 $^{+820}_{-730}$	7960 $^{+600}_{-620}$	7770 $^{+710}_{-680}$
PNe-25	8350 $^{+190}_{-170}$	6520 $^{+1160}_{-1230}$	7420 $^{+1220}_{-1090}$	6970 $^{+1190}_{-1160}$
PNe-26	8990 $^{+230}_{-130}$	7040 $^{+690}_{-620}$	7500 $^{+610}_{-590}$	7270 $^{+650}_{-600}$
PNe-27	9230 $^{+210}_{-190}$	7800 $^{+9540}_{-1390}$	8790 $^{+1420}_{-1120}$	8300 $^{+5480}_{-1260}$
PNe-28	10030 $^{+440}_{-350}$	6060 $^{+1540}_{-1610}$	5800 $^{+1430}_{-1330}$	5930 $^{+1480}_{-1470}$
PNe-29	10860 $^{+670}_{-740}$	6090 $^{+2110}_{-2200}$	6800 $^{+2330}_{-2120}$	6450 $^{+2220}_{-2160}$
PNe-30	9840 $^{+550}_{-800}$	7630 $^{+2760}_{-2310}$	8400 $^{+2510}_{-2330}$	8020 $^{+2640}_{-2320}$
PNe-31	13540 $^{+650}_{-730}$	22380 $^{+46800}_{-12380}$	-	22380 $^{+46800}_{-12380}$
PNe-32	12960 $^{+650}_{-860}$	5710 $^{+1870}_{-1480}$	4220 $^{+1500}_{-1190}$	4970 $^{+1680}_{-1330}$
PNe-33	9400 $^{+110}_{-80}$	6350 $^{+410}_{-420}$	7110 $^{+370}_{-320}$	6730 $^{+390}_{-370}$
PNe-34	12760 $^{+610}_{-740}$	6110 $^{+1350}_{-1270}$	6980 $^{+1310}_{-1270}$	6550 $^{+1330}_{-1270}$
PNe-35	11190 $^{+220}_{-150}$	9340 $^{+1200}_{-1000}$	9830 $^{+1050}_{-950}$	9590 $^{+1130}_{-970}$
PNe-36	8760 $^{+90}_{-80}$	8700 $^{+520}_{-510}$	8290 $^{+410}_{-350}$	8500 $^{+470}_{-430}$
PNe-37	9710 $^{+120}_{-110}$	26620 $^{+3310}_{-15980}$	12680 $^{+670}_{-570}$	19650 $^{+1990}_{-8270}$
PNe-38	9920 $^{+120}_{-190}$	4610 $^{+770}_{-700}$	5380 $^{+850}_{-780}$	5000 $^{+810}_{-740}$
PNe-39	11590 $^{+300}_{-240}$	2090 $^{+490}_{-390}$	2370 $^{+480}_{-430}$	2230 $^{+490}_{-410}$
PNe-40	9950 $^{+190}_{-220}$	7200 $^{+460}_{-440}$	7170 $^{+470}_{-400}$	7190 $^{+460}_{-420}$
PNe-41	10520 $^{+360}_{-420}$	8160 $^{+14620}_{-2400}$	9080 $^{+2900}_{-2510}$	8620 $^{+8760}_{-2460}$
PNe-42	11810 $^{+700}_{-430}$	8590 $^{+2120}_{-1600}$	8160 $^{+1440}_{-1480}$	8370 $^{+1780}_{-1540}$
PNe-43	9710 $^{+630}_{-640}$	7800 $^{+2800}_{-2220}$	8990 $^{+2750}_{-2040}$	8390 $^{+2770}_{-2130}$
PNe-44	14200 $^{+1270}_{-1570}$	7500 $^{+2840}_{-2320}$	10240 $^{+3430}_{-2460}$	8870 $^{+3140}_{-2390}$
PNe-45	11530 $^{+1070}_{-990}$	6910 $^{+2080}_{-2070}$	8070 $^{+2030}_{-1890}$	7490 $^{+2060}_{-1980}$
PNe-46	8790 $^{+1070}_{-870}$	7210 $^{+390}_{-340}$	7800 $^{+380}_{-370}$	7510 $^{+380}_{-360}$
PNe-47	10430 $^{+410}_{-830}$	4930 $^{+2490}_{-1850}$	4790 $^{+2620}_{-1930}$	4860 $^{+2560}_{-1890}$
PNe-48	12430 $^{+900}_{-780}$	9720 $^{+19270}_{-2530}$	-	9720 $^{+19270}_{-2530}$

Table A10 *continued*

Table A10 (*continued*)

Reference number	T_e ([O III] $\lambda 4363/\lambda 5007$)	T_e (He I $\lambda 7281/\lambda 5876$)	T_e (He I $\lambda 7281/\lambda 6678$)	Adopted T_e (He I)
	[K]	[K]	[K]	[K]
PNe-49	9800^{+120}_{-180}	5260^{+720}_{-650}	6540 ± 600	5900^{+660}_{-620}
PNe-50	7750 ± 130	6170^{+1020}_{-1180}	6950 ± 1100	6560^{+1060}_{-1140}
PNe-51	6600^{+150}_{-130}	5490^{+1030}_{-1020}	6140^{+1070}_{-1140}	5810^{+1050}_{-1080}
PNe-52	8280^{+220}_{-250}	5180^{+750}_{-690}	5690^{+650}_{-620}	5440^{+700}_{-650}
PNe-53	9420^{+170}_{-230}	8030^{+14030}_{-1480}	7970^{+1670}_{-1480}	8000^{+7850}_{-1480}
PNe-54	8880^{+180}_{-200}	5110^{+690}_{-700}	5350^{+770}_{-700}	5230^{+730}_{-700}
PNe-55	11040^{+650}_{-850}	5120^{+2080}_{-2040}	7030^{+2230}_{-2130}	6080^{+2160}_{-2090}
PNe-56	11820^{+850}_{-1150}	4800 ± 1990	7660^{+2360}_{-2480}	6230^{+2180}_{-2240}
PNe-57	10540^{+390}_{-510}	7420^{+1530}_{-1470}	7810^{+1310}_{-1230}	7610^{+1420}_{-1350}
PNe-58	10190^{+330}_{-360}	3200^{+1340}_{-990}	4070^{+1390}_{-1290}	3630^{+1360}_{-1140}
PNe-59	13170^{+580}_{-490}	1720^{+620}_{-500}	2670^{+1070}_{-890}	2190^{+850}_{-700}
PNe-60	10090^{+450}_{-360}	9370^{+19230}_{-1680}	10200^{+1700}_{-1410}	9780^{+10470}_{-1540}
PNe-61	9120^{+200}_{-160}	7600^{+6590}_{-1280}	8410^{+1320}_{-1140}	8000^{+3950}_{-1210}
PNe-62	7970^{+330}_{-420}	-	9980^{+2790}_{-2420}	9980^{+2790}_{-2420}
PNe-63	10620^{+590}_{-720}	6720^{+3000}_{-2540}	7060^{+2940}_{-2660}	6890^{+2970}_{-2600}
PNe-64	10290^{+470}_{-610}	8300^{+15640}_{-2560}	9370^{+2550}_{-2250}	8840^{+9100}_{-2400}
PNe-65	11890^{+290}_{-260}	6100^{+650}_{-630}	7430^{+590}_{-520}	6760^{+620}_{-580}
PNe-66	8190 ± 100	2170^{+450}_{-430}	2850^{+600}_{-530}	2510^{+530}_{-480}
PNe-67	12480^{+1130}_{-810}	6690^{+2620}_{-2240}	8540^{+3030}_{-2410}	7620^{+2830}_{-2330}
PNe-68	7940^{+100}_{-80}	4050^{+710}_{-640}	4710^{+720}_{-700}	4380^{+710}_{-670}
PNe-69	8400^{+70}_{-120}	6750^{+380}_{-350}	5790^{+360}_{-350}	6270^{+370}_{-350}
PNe-70	27440^{+1310}_{-980}	6930^{+920}_{-710}	6980^{+810}_{-680}	6960^{+870}_{-690}
PNe-71	8430 ± 100	3190^{+670}_{-510}	3500^{+630}_{-610}	3350^{+650}_{-560}
PNe-72	8500^{+120}_{-110}	6990^{+780}_{-640}	6920^{+570}_{-630}	6960^{+670}_{-640}
PNe-73	10010^{+190}_{-120}	6340^{+630}_{-720}	6670^{+580}_{-720}	6510^{+600}_{-720}
PNe-74	8360^{+210}_{-230}	7420^{+1640}_{-1540}	8120^{+1520}_{-1590}	7770^{+1580}_{-1560}
PNe-75	9850^{+140}_{-170}	5380^{+640}_{-600}	5760^{+620}_{-560}	5570^{+630}_{-580}
PNe-76	8810^{+100}_{-140}	1460^{+340}_{-300}	1630^{+360}_{-340}	1550^{+350}_{-320}
PNe-77	10350^{+170}_{-200}	4620^{+740}_{-730}	5100^{+820}_{-730}	4860^{+780}_{-730}
PNe-78	13370^{+1250}_{-840}	7590^{+3080}_{-2680}	8960^{+3430}_{-2750}	8270^{+3260}_{-2720}
PNe-79	8160^{+170}_{-220}	4150^{+1340}_{-1260}	4540^{+1480}_{-1200}	4350^{+1410}_{-1230}
PNe-80	7590^{+100}_{-70}	1520^{+350}_{-300}	2440^{+470}_{-440}	1980^{+410}_{-370}
PNe-81	10150^{+620}_{-830}	4720^{+1940}_{-1910}	6680^{+1960}_{-2180}	5700^{+1950}_{-2040}
PNe-82	7290^{+70}_{-90}	3420^{+600}_{-550}	4740^{+610}_{-630}	4080^{+600}_{-590}
PNe-83	11230^{+770}_{-680}	2800^{+1680}_{-1100}	4000^{+1880}_{-1690}	3400^{+1780}_{-1400}
PNe-84	11060^{+210}_{-230}	7620^{+1230}_{-1170}	7670^{+1070}_{-1020}	7650^{+1150}_{-1090}
PNe-85	11610^{+870}_{-560}	4960^{+2260}_{-1860}	-	4960^{+2260}_{-1860}
PNe-86	14570^{+270}_{-320}	7500^{+440}_{-500}	7980^{+380}_{-350}	7740^{+410}_{-430}
PNe-87	12010^{+340}_{-220}	8820^{+1140}_{-880}	8430^{+970}_{-790}	8620^{+1050}_{-840}
PNe-88	11490^{+230}_{-260}	7740^{+1060}_{-950}	7880^{+970}_{-1000}	7810^{+1020}_{-980}

Table A10 *continued*

Table A10 (*continued*)

Reference number	T_e ([O III] $\lambda 4363/\lambda 5007$)	T_e (He I $\lambda 7281/\lambda 5876$)	T_e (He I $\lambda 7281/\lambda 6678$)	Adopted T_e (He I)
	[K]	[K]	[K]	[K]
PNe-89	9440 $^{+110}_{-150}$	9010 $^{+1160}_{-1210}$	9520 $^{+1040}_{-1110}$	9270 $^{+1100}_{-1160}$
PNe-90	13810 $^{+740}_{-930}$	1500 \pm 600	900 $^{+470}_{-290}$	1200 $^{+540}_{-440}$
PNe-91	11660 $^{+400}_{-450}$	3940 $^{+1370}_{-1190}$	3410 $^{+1190}_{-1090}$	3680 $^{+1280}_{-1140}$
PNe-92	11540 $^{+620}_{-420}$	7090 $^{+2030}_{-1620}$	7410 $^{+1730}_{-1540}$	7250 $^{+1880}_{-1580}$
PNe-93	11700 $^{+130}_{-270}$	4330 $^{+680}_{-650}$	4740 $^{+770}_{-650}$	4540 $^{+720}_{-650}$
PNe-94	12760 $^{+350}_{-370}$	8240 $^{+1250}_{-1040}$	8370 $^{+1080}_{-910}$	8300 $^{+1160}_{-970}$
PNe-95	10420 $^{+190}_{-220}$	11680 $^{+1850}_{-1380}$	11180 $^{+1140}_{-1000}$	11430 $^{+1490}_{-1190}$
PNe-96	11560 $^{+300}_{-330}$	8960 $^{+1690}_{-1610}$	9620 $^{+1680}_{-1590}$	9290 $^{+1680}_{-1600}$
PNe-97	11680 $^{+80}_{-100}$	6680 $^{+810}_{-920}$	7060 $^{+990}_{-890}$	6870 $^{+900}_{-910}$
PNe-98	8770 $^{+230}_{-180}$	5590 $^{+1080}_{-1140}$	6340 $^{+950}_{-1060}$	5960 $^{+1020}_{-1100}$
PNe-99	9330 $^{+90}_{-160}$	4700 $^{+690}_{-660}$	5280 $^{+740}_{-610}$	4990 $^{+720}_{-630}$
PNe-100	9500 $^{+130}_{-160}$	7310 $^{+690}_{-760}$	7080 $^{+640}_{-700}$	7190 $^{+670}_{-730}$
PNe-101	18240 $^{+540}_{-360}$	7290 $^{+720}_{-670}$	-	7290 $^{+720}_{-670}$
PNe-102	12070 $^{+430}_{-600}$	6380 $^{+1710}_{-1450}$	2230 $^{+940}_{-690}$	4300 $^{+1330}_{-1070}$
PNe-103	10630 $^{+170}_{-240}$	8540 $^{+1320}_{-1170}$	9140 $^{+1270}_{-1020}$	8840 $^{+1290}_{-1090}$
PNe-104	9880 $^{+290}_{-340}$	4140 $^{+1220}_{-1270}$	5140 $^{+1330}_{-1350}$	4640 $^{+1270}_{-1310}$
PNe-105	10270 $^{+180}_{-150}$	5000 $^{+680}_{-660}$	5070 $^{+650}_{-620}$	5040 $^{+660}_{-640}$
PNe-106	11280 $^{+380}_{-520}$	16210 $^{+7000}_{-4020}$	13370 $^{+3570}_{-2840}$	14790 $^{+5280}_{-3430}$
PNe-107	11540 $^{+590}_{-660}$	4590 $^{+1770}_{-1390}$	4580 $^{+1660}_{-1350}$	4590 $^{+1710}_{-1370}$
PNe-108	14710 $^{+1140}_{-1420}$	6110 $^{+1890}_{-2030}$	7570 $^{+2260}_{-1870}$	6840 $^{+2070}_{-1950}$
PNe-109	7790 $^{+120}_{-160}$	5400 $^{+1070}_{-960}$	6140 $^{+950}_{-1030}$	5770 $^{+1010}_{-990}$
PNe-110	10700 $^{+420}_{-580}$	20590 $^{+8050}_{-5520}$	21530 $^{+5910}_{-4410}$	21060 $^{+6980}_{-4970}$
PNe-111	10460 $^{+280}_{-420}$	3640 $^{+1340}_{-1030}$	4210 $^{+1390}_{-1280}$	3920 $^{+1370}_{-1150}$
PNe-112	10530 $^{+180}_{-200}$	6550 $^{+640}_{-710}$	7700 $^{+580}_{-650}$	7120 $^{+610}_{-680}$
PNe-113	10490 $^{+350}_{-330}$	7970 $^{+18250}_{-1260}$	8320 $^{+1410}_{-1260}$	8140 $^{+9830}_{-1260}$
PNe-114	9490 $^{+140}_{-130}$	3870 $^{+650}_{-670}$	3840 $^{+660}_{-590}$	3850 $^{+650}_{-630}$
PNe-115	8660 $^{+330}_{-300}$	8980 $^{+2300}_{-2020}$	9460 $^{+2140}_{-1850}$	9220 $^{+2220}_{-1930}$
PNe-116	10460 $^{+220}_{-200}$	8650 $^{+1160}_{-1050}$	9160 $^{+950}_{-1090}$	8910 $^{+1050}_{-1070}$
PNe-117	12560 $^{+500}_{-660}$	8080 $^{+840}_{-640}$	8830 $^{+790}_{-690}$	8450 $^{+810}_{-660}$
PNe-118	12630 $^{+560}_{-520}$	9040 $^{+17680}_{-1620}$	10920 $^{+1740}_{-1500}$	9980 $^{+9710}_{-1560}$
PNe-119	9160 $^{+360}_{-530}$	5270 $^{+2050}_{-1790}$	7150 $^{+2000}_{-1900}$	6210 $^{+2020}_{-1850}$
PNe-120	13260 $^{+210}_{-240}$	3730 $^{+670}_{-620}$	3590 $^{+590}_{-520}$	3660 $^{+630}_{-570}$
PNe-121	9210 $^{+150}_{-130}$	9470 $^{+1100}_{-1050}$	9150 $^{+820}_{-890}$	9310 $^{+960}_{-970}$
PNe-122	10820 $^{+570}_{-710}$	14500 $^{+8760}_{-4660}$	18230 $^{+7320}_{-5230}$	16370 $^{+8040}_{-4940}$
PNe-123	12430 $^{+840}_{-1310}$	6580 $^{+2030}_{-1880}$	8030 $^{+2010}_{-1950}$	7310 $^{+2020}_{-1910}$
PNe-124	10700 $^{+310}_{-280}$	6460 \pm 1330	7830 $^{+1190}_{-1180}$	7140 $^{+1260}_{-1250}$
PNe-125	9860 $^{+210}_{-120}$	4020 $^{+300}_{-320}$	5210 $^{+1220}_{-880}$	4620 $^{+760}_{-600}$
PNe-126	10880 $^{+740}_{-840}$	4710 $^{+2110}_{-1840}$	6230 $^{+2240}_{-2300}$	5470 $^{+2170}_{-2070}$
PNe-127	12050 $^{+680}_{-1170}$	5710 $^{+3020}_{-2280}$	5480 $^{+3000}_{-2200}$	5590 $^{+3010}_{-2240}$
PNe-128	6880 $^{+80}_{-100}$	7080 $^{+1200}_{-1020}$	6380 $^{+910}_{-970}$	6730 $^{+1060}_{-990}$

Table A10 *continued*

Table A10 (*continued*)

Reference number	T_e ([O III] $\lambda 4363/\lambda 5007$)	T_e (He I $\lambda 7281/\lambda 5876$)	T_e (He I $\lambda 7281/\lambda 6678$)	Adopted T_e (He I)
	[K]	[K]	[K]	[K]
PNe-129	9220 $^{+180}_{-140}$	6650 $^{+980}_{-1080}$	7270 $^{+940}_{-1010}$	6960 $^{+960}_{-1050}$
PNe-130	9550 $^{+280}_{-300}$	7180 $^{+2360}_{-2500}$	7800 $^{+2760}_{-2470}$	7490 $^{+2560}_{-2490}$
PNe-131	11710 $^{+210}_{-250}$	6300 $^{+900}_{-1080}$	7470 $^{+970}_{-1020}$	6880 $^{+940}_{-1050}$
PNe-132	6600 $^{+100}_{-150}$	4370 $^{+980}_{-1010}$	3400 $^{+1070}_{-850}$	3880 $^{+1020}_{-930}$
PNe-133	8590 \pm 120	2240 $^{+530}_{-540}$	1620 $^{+540}_{-610}$	1930 $^{+540}_{-570}$
PNe-134	9350 $^{+200}_{-220}$	2950 $^{+790}_{-760}$	2660 $^{+790}_{-750}$	2810 $^{+790}_{-760}$
PNe-135	7130 $^{+140}_{-120}$	3940 $^{+910}_{-850}$	3320 $^{+1450}_{-1050}$	3630 $^{+1180}_{-950}$
PNe-136	8170 $^{+130}_{-90}$	1840 $^{+610}_{-440}$	1380 $^{+460}_{-600}$	1610 $^{+540}_{-520}$
PNe-137	9040 $^{+120}_{-130}$	1710 $^{+660}_{-450}$	1730 $^{+640}_{-490}$	1720 $^{+650}_{-470}$
PNe-138	12790 $^{+240}_{-230}$	7280 $^{+1620}_{-1400}$	6030 $^{+1780}_{-1440}$	6660 $^{+1700}_{-1420}$
PNe-139	9180 $^{+110}_{-190}$	1570 $^{+650}_{-690}$	1450 $^{+660}_{-610}$	1510 $^{+660}_{-650}$
PNe-140	9200 \pm 180	2810 $^{+1630}_{-1080}$	3400 $^{+2250}_{-1440}$	3100 $^{+1940}_{-1260}$
PNe-141	8270 $^{+90}_{-70}$	2180 $^{+840}_{-660}$	1930 $^{+730}_{-600}$	2060 $^{+780}_{-630}$
PNe-142	8440 $^{+130}_{-150}$	4700 $^{+980}_{-880}$	5320 $^{+1600}_{-1420}$	5010 $^{+1290}_{-1150}$
PNe-143	7930 $^{+170}_{-200}$	6310 $^{+950}_{-990}$	7160 $^{+1100}_{-890}$	6730 $^{+1020}_{-940}$
PNe-144	9140 $^{+170}_{-250}$	5580 $^{+1530}_{-1430}$	5350 $^{+1680}_{-1380}$	5460 $^{+1610}_{-1410}$
PNe-145	15680 $^{+510}_{-320}$	8160 $^{+1270}_{-1020}$	9050 $^{+1380}_{-1250}$	8600 $^{+1320}_{-1130}$
PNe-146	8020 $^{+100}_{-120}$	7450 $^{+900}_{-740}$	6450 $^{+1690}_{-1540}$	6950 $^{+1300}_{-1140}$
PNe-147	10530 $^{+120}_{-140}$	6470 $^{+1090}_{-1260}$	6280 $^{+1210}_{-1330}$	6380 $^{+1150}_{-1300}$
PNe-148	10310 $^{+180}_{-170}$	6830 $^{+690}_{-770}$	6970 $^{+870}_{-950}$	6900 $^{+780}_{-860}$
PNe-149	8820 $^{+110}_{-130}$	7630 $^{+1160}_{-960}$	7870 $^{+1100}_{-1050}$	7750 $^{+1130}_{-1000}$
PNe-150	9310 $^{+90}_{-200}$	1670 $^{+440}_{-410}$	1360 $^{+450}_{-540}$	1520 $^{+440}_{-480}$
PNe-151	13290 $^{+190}_{-330}$	4840 $^{+840}_{-800}$	4250 $^{+1000}_{-880}$	4550 $^{+920}_{-840}$
PNe-152	8720 \pm 170	5560 $^{+1370}_{-1210}$	5200 $^{+1400}_{-1260}$	5380 $^{+1390}_{-1240}$
PNe-153	9290 $^{+150}_{-180}$	3500 $^{+850}_{-730}$	3890 $^{+890}_{-820}$	3700 $^{+870}_{-770}$
PNe-154	10650 $^{+190}_{-200}$	5130 $^{+810}_{-790}$	3850 $^{+1000}_{-950}$	4490 $^{+910}_{-870}$
PNe-155	8380 $^{+70}_{-110}$	5460 $^{+830}_{-770}$	3180 $^{+1190}_{-890}$	4320 $^{+1010}_{-830}$
PNe-156	13500 $^{+230}_{-260}$	5840 $^{+1540}_{-1650}$	6390 $^{+1840}_{-1820}$	6120 $^{+1690}_{-1730}$
PNe-157	11020 $^{+180}_{-220}$	5140 $^{+1170}_{-1050}$	4840 $^{+1350}_{-1160}$	4990 $^{+1260}_{-1110}$
PNe-158	11340 $^{+180}_{-240}$	4300 $^{+1540}_{-1350}$	5050 $^{+2020}_{-1680}$	4680 $^{+1780}_{-1520}$
PNe-159	9640 $^{+130}_{-150}$	3010 $^{+1220}_{-1020}$	3100 $^{+1740}_{-1100}$	3050 $^{+1480}_{-1060}$
PNe-160	6610 $^{+160}_{-140}$	9580 $^{+1210}_{-980}$	5360 $^{+730}_{-650}$	7470 $^{+970}_{-820}$
PNe-161	8110 $^{+250}_{-280}$	5990 $^{+1020}_{-910}$	6590 $^{+910}_{-1070}$	6290 $^{+960}_{-990}$
PNe-162	8790 $^{+110}_{-130}$	3940 $^{+640}_{-680}$	2820 $^{+830}_{-680}$	3380 $^{+740}_{-680}$
PNe-163	9380 $^{+150}_{-180}$	5900 $^{+930}_{-920}$	6500 $^{+890}_{-1000}$	6200 $^{+910}_{-960}$
PNe-164	10280 $^{+160}_{-180}$	8060 $^{+6960}_{-1250}$	8140 $^{+1160}_{-1140}$	8100 $^{+4060}_{-1200}$
PNe-165	7620 \pm 100	4230 $^{+1120}_{-1250}$	4570 $^{+1160}_{-1390}$	4400 $^{+1140}_{-1320}$
PNe-166	14240 $^{+310}_{-280}$	6560 $^{+1140}_{-1020}$	7630 $^{+1400}_{-1230}$	7090 $^{+1270}_{-1130}$
PNe-167	12100 $^{+140}_{-100}$	8290 $^{+360}_{-310}$	7300 $^{+280}_{-290}$	7790 $^{+320}_{-300}$
PNe-168	7380 $^{+110}_{-100}$	5450 $^{+1100}_{-1140}$	4790 $^{+1520}_{-1250}$	5120 $^{+1310}_{-1200}$

Table A10 *continued*

Table A10 (*continued*)

Reference number	T_e ([O III] $\lambda 4363/\lambda 5007$)	T_e (He I $\lambda 7281/\lambda 5876$)	T_e (He I $\lambda 7281/\lambda 6678$)	Adopted T_e (He I)
	[K]	[K]	[K]	[K]
PNe-169	8130^{+150}_{-140}	6120^{+1180}_{-1210}	5330^{+1200}_{-1220}	5730^{+1190}_{-1220}
PNe-170	9770^{+140}_{-180}	2840^{+630}_{-540}	2290^{+710}_{-580}	2560^{+670}_{-560}
PNe-171	10520^{+120}_{-150}	2910^{+540}_{-450}	2190^{+630}_{-480}	2550^{+580}_{-470}
PNe-172	9460^{+110}_{-140}	1490^{+470}_{-560}	1400^{+430}_{-580}	1450^{+450}_{-570}
PNe-173	19650^{+510}_{-500}	4350^{+1200}_{-1320}	6700^{+1220}_{-1470}	5530^{+1210}_{-1390}
PNe-174	10830^{+190}_{-160}	7000^{+830}_{-860}	8650^{+860}_{-1060}	7830^{+840}_{-960}
PNe-175	9020^{+120}_{-130}	2700^{+1170}_{-950}	2680^{+1340}_{-1040}	2690^{+1260}_{-1000}
PNe-176	10930^{+180}_{-190}	1020^{+390}_{-290}	860^{+520}_{-220}	940^{+460}_{-250}
PNe-177	7490^{+80}_{-90}	5080^{+1110}_{-890}	6260^{+1390}_{-1350}	5670^{+1250}_{-1120}
PNe-178	6780^{+160}_{-140}	5230^{+780}_{-820}	3890^{+740}_{-700}	4560 ± 760
PNe-179	10620^{+130}_{-160}	3190^{+720}_{-580}	3150^{+800}_{-700}	3170^{+760}_{-640}
PNe-180	9540^{+60}_{-80}	4380^{+450}_{-520}	5920 ± 680	5150^{+570}_{-600}
PNe-181	9420^{+130}_{-110}	5850^{+990}_{-910}	4370^{+1590}_{-1230}	5110^{+1290}_{-1070}
PNe-182	9160^{+40}_{-50}	4620^{+300}_{-270}	4100^{+920}_{-880}	4360^{+610}_{-580}
PNe-183	7900^{+70}_{-60}	4420^{+640}_{-770}	4160^{+980}_{-890}	4290^{+810}_{-830}
PNe-184	9870^{+140}_{-90}	8180^{+1030}_{-860}	8590^{+1010}_{-880}	8390^{+1020}_{-870}
PNe-185	6980^{+80}_{-90}	4030^{+840}_{-920}	2690^{+780}_{-720}	3360^{+810}_{-820}
PNe-186	10530^{+90}_{-120}	19030^{+9740}_{-10510}	5970^{+930}_{-1090}	12500^{+5340}_{-5800}
PNe-187	8480 ± 130	4870^{+750}_{-780}	4020^{+1060}_{-1040}	4450 ± 910
PNe-188	10440^{+180}_{-280}	21120^{+6790}_{-7980}	9030^{+1680}_{-1470}	15080^{+4230}_{-4720}
PNe-189	6450^{+40}_{-50}	4260^{+1360}_{-1350}	5270^{+1460}_{-1520}	4770^{+1410}_{-1440}
PNe-190	9220^{+170}_{-220}	3360^{+780}_{-640}	2700^{+560}_{-530}	3030^{+670}_{-590}
PNe-191	9430^{+140}_{-100}	930^{+250}_{-120}	910 ± 0	920^{+120}_{-60}
PNe-192	9160^{+220}_{-140}	1420^{+530}_{-540}	1760^{+710}_{-510}	1590^{+620}_{-530}
PNe-193	9230^{+90}_{-110}	950^{+310}_{-160}	890^{+360}_{-200}	920^{+340}_{-180}
PNe-194	9120^{+130}_{-180}	1530^{+390}_{-550}	1650^{+450}_{-370}	1590^{+420}_{-460}
PNe-195	7140^{+130}_{-160}	4710^{+850}_{-860}	5990^{+1000}_{-1100}	5350^{+930}_{-980}
PNe-196	9990^{+160}_{-210}	4970^{+1260}_{-1060}	3400^{+1090}_{-910}	4190^{+1170}_{-980}
PNe-197	8170^{+90}_{-70}	3480^{+630}_{-570}	3200^{+710}_{-560}	3340^{+670}_{-570}
PNe-198	9290^{+140}_{-90}	2990^{+680}_{-550}	2880^{+790}_{-680}	2940^{+730}_{-610}
PNe-199	10520^{+170}_{-210}	1460^{+530}_{-600}	1700^{+860}_{-690}	1580^{+690}_{-650}
PNe-200	10960^{+290}_{-230}	5120^{+1230}_{-1130}	5550^{+1690}_{-1520}	5330^{+1460}_{-1330}
PNe-201	7930^{+50}_{-100}	4820^{+780}_{-720}	4700^{+1310}_{-1220}	4760^{+1050}_{-970}
PNe-202	11730^{+220}_{-210}	6550^{+970}_{-940}	7130^{+1040}_{-910}	6840^{+1000}_{-920}
PNe-203	9520^{+240}_{-190}	6750^{+1430}_{-1360}	6810 ± 1270	6780^{+1350}_{-1310}
PNe-204	8430^{+90}_{-70}	6180^{+710}_{-840}	5890^{+810}_{-880}	6030^{+760}_{-860}
PNe-205	9980^{+130}_{-160}	1420^{+430}_{-610}	1340^{+430}_{-540}	1380^{+430}_{-570}
PNe-206	10280^{+130}_{-150}	1340^{+360}_{-560}	1100^{+370}_{-440}	1220^{+370}_{-500}
PNe-207	6920^{+50}_{-60}	5300^{+780}_{-710}	5110^{+890}_{-950}	5200 ± 830
PNe-208	9090^{+130}_{-80}	4630^{+1040}_{-830}	5550^{+1420}_{-1230}	5090^{+1230}_{-1030}

Table A10 *continued*

Table A10 (*continued*)

Reference number	$T_e(\text{[O III]} \lambda 4363/\lambda 5007)$	$T_e(\text{He I } \lambda 7281/\lambda 5876)$	$T_e(\text{He I } \lambda 7281/\lambda 6678)$	Adopted $T_e(\text{He I})$
	[K]	[K]	[K]	[K]
PNe-209	12680^{+310}_{-280}	5330^{+1810}_{-1680}	10040^{+2910}_{-2720}	7690^{+2360}_{-2200}
PNe-210	8720^{+160}_{-200}	7680^{+1230}_{-1280}	6440^{+1500}_{-1490}	7060^{+1370}_{-1380}
PNe-211	9590 ± 90	3220^{+770}_{-660}	3210^{+800}_{-700}	3220^{+790}_{-680}
PNe-212	11660^{+230}_{-170}	6180^{+1080}_{-1290}	5740^{+1810}_{-1720}	5960^{+1440}_{-1510}
PNe-213	8390^{+90}_{-110}	2690^{+800}_{-740}	3870^{+1080}_{-1060}	3280^{+940}_{-900}
PNe-214	9970^{+320}_{-430}	4210^{+1190}_{-1200}	5730^{+1210}_{-1270}	4970^{+1200}_{-1240}
PNe-215	10170^{+210}_{-290}	8800^{+18200}_{-1360}	9390^{+1280}_{-1410}	9100^{+9740}_{-1380}
PNe-216	9980^{+620}_{-730}	6100^{+3540}_{-2260}	9120^{+4730}_{-3060}	7610^{+4140}_{-2660}
PNe-217	7790 ± 90	4800^{+790}_{-710}	4970^{+680}_{-650}	4890^{+740}_{-680}
PNe-218	13810^{+340}_{-210}	16810^{+3520}_{-2990}	14600^{+2470}_{-2390}	15700^{+2990}_{-2690}

Table A11. Abundances of O^{2+}/H^+ determined in the planetary nebulae sample and the ADF(O^{2+}). The abundances were determined using both [O III]-CELS and O II-RLs, as well as the “direct method”, assuming $T_e(\text{[O III]})$ and adopted n_e , as presented in Tables A10 and A7, respectively. The abundances are presented in units of $12 + \log(\text{X/H})$. Only regions with a 20% error or less in the flux of the O II RLs were considered.

Reference number	O^{2+}	O^{2+}	ADF(O^{2+})
	[O III]-CELS, $t^2 = 0$	O II-RLs	
PNe-2	8.27 ± 0.02	8.49 ± 0.04	0.22 ± 0.02
PNe-3	8.40 ± 0.02	$8.63^{+0.08}_{-0.07}$	$0.23^{+0.08}_{-0.07}$
PNe-4	8.32 ± 0.02	8.43 ± 0.06	$0.11^{+0.07}_{-0.06}$
PNe-8	$8.71^{+0.03}_{-0.02}$	9.11 ± 0.03	0.41 ± 0.03
PNe-10	$8.38^{+0.02}_{-0.03}$	$8.73^{+0.06}_{-0.05}$	0.35 ± 0.02
PNe-12	$8.54^{+0.03}_{-0.02}$	9.16 ± 0.03	$0.62^{+0.03}_{-0.02}$
PNe-13	8.54 ± 0.02	8.96 ± 0.03	0.42 ± 0.02
PNe-14	$8.61^{+0.04}_{-0.03}$	9.03 ± 0.07	$0.42^{+0.04}_{-0.03}$
PNe-15	8.28 ± 0.03	$8.76^{+0.05}_{-0.04}$	0.48 ± 0.03
PNe-16	8.01 ± 0.02	8.31 ± 0.05	0.31 ± 0.02
PNe-20	8.32 ± 0.03	8.53 ± 0.06	0.20 ± 0.03
PNe-25	8.77 ± 0.04	$9.07^{+0.04}_{-0.03}$	0.30 ± 0.04
PNe-33	8.59 ± 0.02	8.60 ± 0.03	0.01 ± 0.03
PNe-35	8.42 ± 0.02	8.67 ± 0.06	0.25 ± 0.02
PNe-36	8.10 ± 0.02	$8.26^{+0.04}_{-0.05}$	$0.16^{+0.05}_{-0.04}$
PNe-38	$8.59^{+0.03}_{-0.02}$	8.90 ± 0.03	$0.31^{+0.03}_{-0.02}$
PNe-39	8.44 ± 0.03	9.16 ± 0.03	0.72 ± 0.03
PNe-40	8.54 ± 0.03	8.81 ± 0.02	$0.26^{+0.04}_{-0.03}$

Table A11 *continued*

Table A11 (*continued*)

Reference number	O ²⁺	O ²⁺	ADF(O ²⁺)
	[O III]-CELS, $t^2 = 0$	O II-RLs	
PNe-49	8.57 ^{+0.03} _{-0.02}	8.66 ^{+0.06} _{-0.07}	0.10 ± 0.06
PNe-51	8.51 ^{+0.05} _{-0.04}	8.95 ^{+0.05} _{-0.04}	0.43 ^{+0.05} _{-0.04}
PNe-53	8.27 ± 0.04	8.78 ± 0.06	0.51 ± 0.04
PNe-54	8.73 ± 0.04	9.22 ± 0.06	0.49 ± 0.04
PNe-61	8.65 ^{+0.03} _{-0.04}	8.92 ^{+0.07} _{-0.06}	0.27 ± 0.03
PNe-65	8.34 ± 0.03	8.51 ± 0.07	0.18 ± 0.07
PNe-68	8.70 ± 0.02	9.10 ^{+0.02} _{-0.03}	0.39 ± 0.02
PNe-69	8.73 ± 0.02	9.61 ± 0.03	0.88 ± 0.02
PNe-72	8.70 ^{+0.03} _{-0.02}	8.93 ± 0.04	0.23 ^{+0.03} _{-0.02}
PNe-73	8.39 ± 0.02	8.60 ± 0.04	0.21 ± 0.02
PNe-75	8.79 ± 0.02	9.06 ± 0.03	0.27 ± 0.02
PNe-76	8.59 ^{+0.03} _{-0.02}	9.74 ± 0.02	1.14 ^{+0.03} _{-0.02}
PNe-77	8.55 ± 0.03	9.34 ± 0.03	0.78 ^{+0.03} _{-0.02}
PNe-80	8.66 ^{+0.03} _{-0.02}	9.43 ± 0.02	0.77 ± 0.02
PNe-82	8.54 ± 0.02	8.84 ^{+0.03} _{-0.04}	0.29 ± 0.02
PNe-86	8.26 ^{+0.03} _{-0.02}	8.51 ^{+0.04} _{-0.03}	0.25 ^{+0.03} _{-0.02}
PNe-87	8.38 ^{+0.04} _{-0.03}	8.90 ± 0.05	0.51 ^{+0.04} _{-0.03}
PNe-88	8.47 ^{+0.04} _{-0.03}	8.85 ^{+0.08} _{-0.09}	0.38 ± 0.03
PNe-89	8.54 ± 0.02	8.82 ^{+0.05} _{-0.04}	0.28 ^{+0.03} _{-0.02}
PNe-93	8.44 ± 0.02	8.86 ± 0.03	0.42 ± 0.02
PNe-94	8.42 ± 0.04	8.80 ^{+0.02} _{-0.03}	0.38 ^{+0.04} _{-0.03}
PNe-97	8.50 ± 0.01	8.80 ± 0.09	0.30 ± 0.01
PNe-98	8.69 ^{+0.05} _{-0.04}	8.95 ^{+0.05} _{-0.04}	0.25 ^{+0.05} _{-0.04}
PNe-99	8.68 ± 0.02	8.98 ± 0.03	0.30 ± 0.02
PNe-100	8.66 ^{+0.03} _{-0.02}	8.99 ^{+0.04} _{-0.03}	0.33 ^{+0.03} _{-0.02}
PNe-101	7.95 ^{+0.03} _{-0.02}	9.11 ± 0.03	1.16 ^{+0.03} _{-0.02}
PNe-105	8.61 ± 0.02	9.26 ± 0.03	0.65 ^{+0.03} _{-0.02}
PNe-109	8.79 ^{+0.04} _{-0.03}	9.10 ± 0.07	0.31 ± 0.04
PNe-112	8.45 ± 0.03	9.10 ± 0.03	0.65 ^{+0.03} _{-0.02}
PNe-114	8.73 ± 0.02	9.28 ± 0.02	0.55 ± 0.02
PNe-116	8.51 ^{+0.04} _{-0.03}	8.81 ± 0.05	0.30 ^{+0.04} _{-0.03}
PNe-120	8.37 ± 0.02	8.93 ± 0.03	0.56 ± 0.02
PNe-125	8.64 ^{+0.03} _{-0.02}	9.20 ± 0.03	0.56 ± 0.03
PNe-128	8.75 ± 0.03	9.15 ^{+0.05} _{-0.04}	0.41 ^{+0.04} _{-0.03}
PNe-129	8.75 ± 0.03	9.06 ^{+0.08} _{-0.09}	0.31 ± 0.03
PNe-131	8.49 ± 0.03	8.86 ± 0.04	0.37 ^{+0.03} _{-0.02}
PNe-133	8.57 ^{+0.03} _{-0.02}	9.62 ± 0.04	1.05 ^{+0.03} _{-0.02}
PNe-134	8.48 ± 0.04	9.55 ± 0.04	1.08 ± 0.04
PNe-136	8.62 ± 0.03	9.85 ± 0.03	1.22 ^{+0.03} _{-0.02}
PNe-139	8.51 ± 0.03	9.39 ± 0.05	0.88 ± 0.03

Table A11 *continued*

Table A11 (*continued*)

Reference number	O ²⁺	O ²⁺	ADF(O ²⁺)
	[O III]-CELS, $t^2 = 0$	O II-RLs	
PNe-140	8.60 ± 0.03	8.94 ± 0.07	0.35 ± 0.03
PNe-147	8.57 ± 0.02	8.88 ± 0.04	0.32 ± 0.02
PNe-148	8.10 ^{+0.03} _{-0.02}	8.66 ± 0.06	0.56 ^{+0.03} _{-0.02}
PNe-149	8.68 ± 0.03	9.32 ± 0.03	0.64 ^{+0.03} _{-0.02}
PNe-150	8.38 ± 0.03	9.75 ± 0.03	1.36 ^{+0.03} _{-0.02}
PNe-152	8.67 ± 0.04	9.51 ± 0.03	0.85 ^{+0.04} _{-0.03}
PNe-153	8.46 ± 0.03	9.61 ± 0.05	1.14 ± 0.03
PNe-154	8.53 ^{+0.04} _{-0.03}	9.50 ± 0.03	0.96 ± 0.04
PNe-155	8.63 ± 0.02	9.39 ± 0.04	0.76 ± 0.02
PNe-159	8.62 ± 0.03	9.23 ^{+0.07} _{-0.08}	0.61 ^{+0.03} _{-0.02}
PNe-162	8.53 ± 0.03	9.72 ± 0.03	1.19 ± 0.03
PNe-163	8.84 ^{+0.04} _{-0.03}	9.28 ^{+0.04} _{-0.05}	0.45 ± 0.03
PNe-164	8.49 ^{+0.03} _{-0.02}	8.59 ± 0.03	0.10 ^{+0.03} _{-0.02}
PNe-165	8.95 ± 0.03	9.08 ^{+0.05} _{-0.04}	0.14 ± 0.03
PNe-167	8.29 ± 0.02	8.47 ± 0.07	0.18 ^{+0.06} _{-0.07}
PNe-168	8.74 ± 0.03	9.36 ± 0.08	0.62 ± 0.03
PNe-169	8.74 ^{+0.03} _{-0.04}	9.03 ± 0.06	0.28 ^{+0.04} _{-0.03}
PNe-170	8.40 ± 0.03	9.62 ± 0.03	1.22 ± 0.03
PNe-171	8.35 ± 0.02	9.71 ± 0.03	1.35 ± 0.02
PNe-172	8.42 ± 0.02	9.48 ± 0.05	1.06 ± 0.02
PNe-175	8.57 ± 0.03	9.68 ^{+0.02} _{-0.03}	1.11 ± 0.03
PNe-177	8.76 ± 0.03	9.18 ^{+0.07} _{-0.08}	0.41 ± 0.03
PNe-178	7.72 ^{+0.05} _{-0.04}	8.91 ± 0.04	1.19 ^{+0.06} _{-0.04}
PNe-179	8.44 ^{+0.03} _{-0.02}	9.19 ^{+0.08} _{-0.07}	0.74 ^{+0.03} _{-0.02}
PNe-181	8.78 ^{+0.03} _{-0.02}	9.17 ± 0.04	0.39 ^{+0.03} _{-0.02}
PNe-182	8.61 ± 0.01	9.36 ± 0.04	0.74 ± 0.01
PNe-183	8.80 ± 0.02	9.43 ± 0.03	0.62 ± 0.02
PNe-184	8.42 ± 0.02	8.59 ± 0.07	0.17 ± 0.07
PNe-185	8.50 ^{+0.03} _{-0.02}	8.84 ± 0.04	0.34 ^{+0.03} _{-0.02}
PNe-187	8.71 ± 0.03	9.23 ± 0.06	0.52 ± 0.03
PNe-190	8.52 ^{+0.04} _{-0.03}	9.75 ± 0.05	1.24 ^{+0.04} _{-0.03}
PNe-191	8.41 ^{+0.03} _{-0.02}	9.29 ± 0.02	0.87 ± 0.02
PNe-192	8.55 ± 0.03	8.90 ^{+0.09} _{-0.08}	0.34 ^{+0.04} _{-0.03}
PNe-193	8.58 ± 0.02	9.34 ^{+0.05} _{-0.06}	0.77 ± 0.02
PNe-196	8.74 ± 0.03	9.19 ± 0.08	0.45 ± 0.03
PNe-197	8.81 ± 0.02	9.37 ± 0.05	0.56 ± 0.02
PNe-198	8.53 ± 0.02	9.32 ± 0.03	0.80 ± 0.02
PNe-201	8.74 ± 0.02	9.10 ± 0.05	0.35 ± 0.02
PNe-203	8.34 ± 0.04	8.64 ^{+0.06} _{-0.05}	0.30 ^{+0.04} _{-0.03}
PNe-204	8.75 ± 0.02	9.20 ^{+0.07} _{-0.06}	0.45 ± 0.02

Table A11 *continued*

Table A11 (*continued*)

Reference number	O ²⁺	O ²⁺	ADF(O ²⁺)
	[O III]-CELS, $t^2 = 0$	O II-RLs	
PNe-205	8.27 ± 0.02	$9.60_{-0.02}^{+0.03}$	1.32 ± 0.02
PNe-207	8.92 ± 0.02	9.09 ± 0.05	0.16 ± 0.05
PNe-208	8.53 ± 0.02	9.21 ± 0.04	0.68 ± 0.02
PNe-210	8.49 ± 0.04	$8.58_{-0.08}^{+0.09}$	$0.10_{-0.09}^{+0.08}$
PNe-212	8.45 ± 0.03	8.67 ± 0.07	$0.22_{-0.02}^{+0.03}$
PNe-213	8.79 ± 0.02	$9.14_{-0.05}^{+0.06}$	0.35 ± 0.02
PNe-217	8.76 ± 0.02	9.06 ± 0.03	0.31 ± 0.02

Table A12. Reddening-corrected He I fluxes in the sample of H II regions are reported by the reference authors. Intensities are given relative to H $\beta = 100$. The equivalent width of H β (EW(H β)) is also reported.

Reference number	He I $\lambda 3614$ [H $\beta=100$]	He I $\lambda 3965$ [H $\beta=100$]	He I $\lambda 5016$ [H $\beta=100$]	He I $\lambda 5876$ [H $\beta=100$]	He I $\lambda 6678$ [H $\beta=100$]	He I $\lambda 7281$ [H $\beta=100$]	EW(H β) [Å]
HII-1	0.40 ± 0.02	0.86 ± 0.03	2.20 ± 0.04	12.1 ± 0.1	3.38 ± 0.07	0.45 ± 0.02	734 ± 7
HII-2	-	0.89 ± 0.05	2.28 ± 0.09	11.8 ± 0.6	3.3 ± 0.2	0.44 ± 0.03	-
HII-3	0.49 ± 0.03	0.78 ± 0.05	2.11 ± 0.06	11.5 ± 0.2	3.3 ± 0.1	0.52 ± 0.02	-
HII-4	0.30 ± 0.03	0.60 ± 0.04	1.69 ± 0.07	9.8 ± 0.2	-	0.58 ± 0.02	-
HII-5	0.51 ± 0.08	0.71 ± 0.04	2.22 ± 0.09	11.6 ± 0.6	3.4 ± 0.2	0.52 ± 0.04	-
HII-6	-	-	2.4 ± 0.1	12.1 ± 0.6	3.4 ± 0.2	0.51 ± 0.05	146 ± 6
HII-7	-	-	2.07 ± 0.04	11.6 ± 0.2	3.3 ± 0.1	0.47 ± 0.02	187 ± 4
HII-8	-	1.1 ± 0.1	2.65 ± 0.05	14.0 ± 0.3	3.6 ± 0.1	0.51 ± 0.03	216 ± 4
HII-9	-	-	1.9 ± 0.3	12.0 ± 0.2	3.2 ± 0.1	0.7 ± 0.1	401 ± 8
HII-10	-	-	3.4 ± 0.1	10.7 ± 0.2	3.00 ± 0.09	0.47 ± 0.06	270 ± 5
HII-11	-	-	1.6 ± 0.2	10.9 ± 0.3	3.0 ± 0.1	0.62 ± 0.09	-
HII-12	-	0.9 ± 0.1	2.99 ± 0.06	11.1 ± 0.2	3.2 ± 0.1	0.54 ± 0.03	152 ± 3
HII-13	-	-	1.6 ± 0.2	9.1 ± 0.3	2.2 ± 0.1	0.46 ± 0.09	222 ± 4
HII-14	-	-	2.5 ± 0.1	10.3 ± 0.2	2.7 ± 0.1	0.59 ± 0.07	242 ± 5
HII-15	-	0.9 ± 0.1	2.99 ± 0.06	11.1 ± 0.2	3.2 ± 0.1	0.54 ± 0.03	152 ± 3
HII-16	-	1.4 ± 0.1	3.30 ± 0.07	11.8 ± 0.2	3.3 ± 0.1	0.53 ± 0.03	322 ± 6
HII-17	-	1.3 ± 0.1	3.61 ± 0.07	11.7 ± 0.2	3.2 ± 0.1	0.48 ± 0.02	178 ± 4
HII-18	-	-	2.6 ± 0.2	9.6 ± 0.3	2.9 ± 0.1	0.8 ± 0.1	97 ± 2
HII-19	-	-	3.65 ± 0.07	12.5 ± 0.2	3.2 ± 0.1	0.57 ± 0.03	254 ± 5
HII-20	-	0.67 ± 0.07	2.95 ± 0.06	12.8 ± 0.4	3.2 ± 0.1	0.41 ± 0.05	-
HII-21	-	-	2.21 ± 0.07	11.8 ± 0.2	3.06 ± 0.09	0.46 ± 0.05	321 ± 6
HII-22	-	-	2.4 ± 0.2	10.0 ± 0.2	2.8 ± 0.1	0.62 ± 0.09	148 ± 3
HII-23	-	-	2.41 ± 0.05	14.4 ± 0.4	3.9 ± 0.2	0.60 ± 0.04	269 ± 5
HII-24	-	0.7 ± 0.1	2.00 ± 0.08	11.6 ± 0.6	3.2 ± 0.2	0.45 ± 0.05	160 ± 5

Table A12 *continued*

Table A12 (*continued*)

Reference number	He I $\lambda 3614$ [H β =100]	He I $\lambda 3965$ [H β =100]	He I $\lambda 5016$ [H β =100]	He I $\lambda 5876$ [H β =100]	He I $\lambda 6678$ [H β =100]	He I $\lambda 7281$ [H β =100]	EW(H β) [Å]
HII-25	-	-	2.9 ± 0.2	11.3 ± 0.2	3.0 ± 0.1	0.51 ± 0.09	350 ± 7
HII-26	-	-	3.75 ± 0.07	11.0 ± 0.3	2.8 ± 0.1	0.42 ± 0.03	286 ± 6
HII-27	-	0.56 ± 0.03	2.30 ± 0.09	9.7 ± 0.2	2.51 ± 0.08	0.39 ± 0.05	-
HII-28	-	-	2.2 ± 0.2	13 ± 1	3.5 ± 0.3	0.68 ± 0.09	(2.3 ± 0.2) × 10 ²
HII-29	0.46 ± 0.09	0.86 ± 0.08	2.13 ± 0.04	11.7 ± 0.2	3.2 ± 0.1	0.46 ± 0.03	149 ± 1
HII-30	-	-	2.4 ± 0.1	12.0 ± 0.2	3.2 ± 0.1	0.36 ± 0.06	-
HII-31	-	0.59 ± 0.08	1.9 ± 0.2	12 ± 1	3.4 ± 0.4	0.7 ± 0.1	-
HII-32	-	0.72 ± 0.06	2.02 ± 0.04	10.7 ± 0.2	2.90 ± 0.09	0.28 ± 0.02	179 ± 2
HII-33	-	0.96 ± 0.05	2.37 ± 0.07	13.4 ± 0.4	3.9 ± 0.2	0.59 ± 0.03	-
HII-34	0.40 ± 0.05	0.80 ± 0.03	1.98 ± 0.06	10.3 ± 0.3	3.0 ± 0.1	0.52 ± 0.03	-
HII-35	0.48 ± 0.02	0.88 ± 0.02	2.16 ± 0.04	11.1 ± 0.3	3.3 ± 0.1	0.64 ± 0.03	-
HII-36	0.49 ± 0.02	0.89 ± 0.02	1.99 ± 0.04	10.6 ± 0.2	2.69 ± 0.08	0.54 ± 0.02	-
HII-37	0.43 ± 0.01	0.89 ± 0.02	2.22 ± 0.04	-	3.4 ± 0.1	0.65 ± 0.03	-
HII-38	0.64 ± 0.03	1.15 ± 0.03	2.47 ± 0.05	-	2.77 ± 0.08	0.58 ± 0.02	-
HII-39	0.44 ± 0.01	0.90 ± 0.02	2.06 ± 0.04	13.1 ± 0.4	3.5 ± 0.1	0.64 ± 0.03	-
HII-40	0.41 ± 0.02	0.85 ± 0.02	2.22 ± 0.04	-	3.5 ± 0.1	0.66 ± 0.03	-
HII-41	0.47 ± 0.01	0.90 ± 0.02	2.14 ± 0.04	13.4 ± 0.4	3.5 ± 0.1	0.62 ± 0.03	-
HII-42	0.39 ± 0.02	0.86 ± 0.02	2.19 ± 0.04	11.8 ± 0.4	3.4 ± 0.1	0.60 ± 0.02	-
HII-43	0.49 ± 0.03	0.98 ± 0.03	2.43 ± 0.07	13.8 ± 0.4	3.3 ± 0.2	0.65 ± 0.05	-
HII-44	0.49 ± 0.03	0.99 ± 0.03	2.27 ± 0.02	13.9 ± 0.4	3.9 ± 0.2	0.63 ± 0.05	-
HII-45	0.43 ± 0.04	0.91 ± 0.08	2.4 ± 0.1	13.0 ± 0.6	3.5 ± 0.2	0.59 ± 0.05	-
HII-46	0.38 ± 0.05	0.79 ± 0.06	1.82 ± 0.05	9.9 ± 0.3	2.86 ± 0.09	0.46 ± 0.01	-
HII-47	0.30 ± 0.04	0.91 ± 0.05	2.28 ± 0.09	14.4 ± 0.6	3.5 ± 0.1	0.67 ± 0.03	-
HII-48	0.47 ± 0.04	0.94 ± 0.03	2.27 ± 0.05	11.4 ± 0.5	3.6 ± 0.2	0.67 ± 0.05	-
HII-49	-	0.9 ± 0.1	2.2 ± 0.1	14.4 ± 0.6	3.9 ± 0.2	0.75 ± 0.05	-
HII-50	-	-	2.3 ± 0.3	15.7 ± 0.8	4.1 ± 0.3	0.55 ± 0.06	-
HII-51	-	-	2.39 ± 0.07	13.0 ± 0.4	3.5 ± 0.1	0.54 ± 0.04	-
HII-52	-	-	2.5 ± 0.1	12.4 ± 0.4	3.04 ± 0.03	0.62 ± 0.04	-
HII-53	-	-	2.2 ± 0.2	12.9 ± 0.4	3.1 ± 0.2	0.46 ± 0.05	-
HII-54	-	-	1.79 ± 0.05	8.8 ± 0.5	2.2 ± 0.2	0.35 ± 0.07	-
HII-55	0.42 ± 0.06	0.90 ± 0.04	2.21 ± 0.07	11.3 ± 0.5	3.3 ± 0.1	0.58 ± 0.03	-
HII-56	-	-	-	-	2.90 ± 0.09	0.5 ± 0.1	379 ± 4
HII-57	0.22 ± 0.03	0.67 ± 0.04	1.77 ± 0.05	10.3 ± 0.4	2.6 ± 0.1	0.48 ± 0.03	(3.6 ± 0.1) × 10 ²
HII-58	-	-	1.79 ± 0.05	10.0 ± 0.2	2.7 ± 0.1	0.31 ± 0.04	29.0 ± 0.3
HII-59	-	0.48 ± 0.08	1.98 ± 0.08	11.2 ± 0.2	2.85 ± 0.09	0.23 ± 0.03	33.0 ± 0.3
HII-60	-	0.58 ± 0.07	1.85 ± 0.04	10.5 ± 0.2	2.90 ± 0.09	0.47 ± 0.04	130 ± 1
HII-61	-	0.7 ± 0.1	2.2 ± 0.2	12 ± 1	3.6 ± 0.3	0.5 ± 0.1	-
HII-62	-	-	2.19 ± 0.04	12.4 ± 0.2	3.54 ± 0.07	0.61 ± 0.02	314 ± 3
HII-63	-	-	1.97 ± 0.08	11.6 ± 0.2	7.0 ± 0.1	1.42 ± 0.06	70 ± 1
HII-64	-	1.9 ± 0.1	1.9 ± 0.1	11.7 ± 0.2	3.5 ± 0.1	0.6 ± 0.1	365 ± 7

Table A12 *continued*

Table A12 (*continued*)

Reference number	He I $\lambda 3614$ [H β =100]	He I $\lambda 3965$ [H β =100]	He I $\lambda 5016$ [H β =100]	He I $\lambda 5876$ [H β =100]	He I $\lambda 6678$ [H β =100]	He I $\lambda 7281$ [H β =100]	EW(H β) [Å]
HII-65	-	1.2 \pm 0.1	2.30 \pm 0.09	11.1 \pm 0.2	3.4 \pm 0.1	0.6 \pm 0.1	216 \pm 4
HII-66	-	-	-	12.6 \pm 0.3	3.8 \pm 0.1	0.5 \pm 0.1	71 \pm 1
HII-67	-	0.7 \pm 0.1	2.1 \pm 0.1	11.0 \pm 0.2	3.5 \pm 0.1	0.6 \pm 0.1	207 \pm 4
HII-68	-	-	2.5 \pm 0.3	11.7 \pm 0.2	3.5 \pm 0.1	0.7 \pm 0.1	317 \pm 6
HII-69	-	-	-	12.5 \pm 0.2	3.5 \pm 0.1	0.7 \pm 0.1	390 \pm 8
HII-70	-	-	-	11.7 \pm 0.2	3.3 \pm 0.1	0.6 \pm 0.1	226 \pm 5
HII-71	-	-	-	16.1 \pm 0.6	3.4 \pm 0.3	0.66 \pm 0.06	(2.9 \pm 0.6) $\times 10^2$
HII-72	-	-	-	11.8 \pm 0.2	3.18 \pm 0.06	0.63 \pm 0.05	180 \pm 4
HII-73	-	-	1.95 \pm 0.08	11.5 \pm 0.2	3.2 \pm 0.1	0.63 \pm 0.03	140 \pm 1
HII-74	-	-	-	11.5 \pm 0.2	2.99 \pm 0.09	0.67 \pm 0.06	176 \pm 4
HII-75	-	-	2.5 \pm 0.1	11.1 \pm 0.2	3.10 \pm 0.09	0.63 \pm 0.07	131 \pm 3
HII-76	0.41 \pm 0.05	0.84 \pm 0.05	2.21 \pm 0.09	11.7 \pm 0.6	3.5 \pm 0.2	0.66 \pm 0.05	(2.8 \pm 0.1) $\times 10^2$
HII-77	-	-	2.27 \pm 0.02	12.3 \pm 0.1	3.59 \pm 0.07	0.66 \pm 0.01	327 \pm 3
HII-78	-	-	2.4 \pm 0.2	11.4 \pm 0.5	3.2 \pm 0.2	0.66 \pm 0.07	225 \pm 2
HII-79	-	-	-	-	3.4 \pm 0.2	0.9 \pm 0.1	(2.1 \pm 0.2) $\times 10^2$
HII-80	0.40 \pm 0.03	1.06 \pm 0.08	2.7 \pm 0.5	10.7 \pm 0.2	3.03 \pm 0.09	0.97 \pm 0.06	-
HII-81	0.47 \pm 0.03	0.87 \pm 0.04	2.15 \pm 0.06	10.9 \pm 0.2	3.1 \pm 0.1	0.64 \pm 0.03	-
HII-82	-	1.01 \pm 0.08	2.7 \pm 0.5	11.1 \pm 0.4	3.0 \pm 0.2	0.96 \pm 0.07	-
HII-83	1.1 \pm 0.2	-	2.5 \pm 0.2	10.6 \pm 0.4	2.9 \pm 0.2	0.59 \pm 0.09	341 \pm 7
HII-84	1.22 \pm 0.09	-	2.5 \pm 0.1	11.2 \pm 0.2	3.2 \pm 0.1	0.63 \pm 0.06	383 \pm 4
HII-85	-	-	2.3 \pm 0.3	10.4 \pm 0.6	3.3 \pm 0.3	1.1 \pm 0.2	285 \pm 6

Table A13. Reddening-corrected He I fluxes in the sample of Star Forming Galaxies are reported by the reference authors. Intensities are given relative to H β = 100. The equivalent width of H β (EW(H β)) is also reported.

Reference number	He I $\lambda 3614$ [H β =100]	He I $\lambda 3965$ [H β =100]	He I $\lambda 5016$ [H β =100]	He I $\lambda 5876$ [H β =100]	He I $\lambda 6678$ [H β =100]	He I $\lambda 7281$ [H β =100]	EW(H β) [Å]
SFG-1	-	-	-	10.6 \pm 0.1	2.90 \pm 0.09	0.6 \pm 0.1	357 \pm 4
SFG-2	-	-	-	9.9 \pm 0.3	2.6 \pm 0.1	0.6 \pm 0.1	234 \pm 2
SFG-3	-	-	-	9.9 \pm 0.2	2.8 \pm 0.1	0.7 \pm 0.1	92.0 \pm 0.9
SFG-4	-	-	-	10.9 \pm 0.3	2.9 \pm 0.2	0.5 \pm 0.1	117 \pm 1
SFG-5	-	-	-	11.2 \pm 0.2	2.8 \pm 0.1	0.5 \pm 0.1	128 \pm 1
SFG-6	-	-	-	11.1 \pm 0.2	2.8 \pm 0.1	0.6 \pm 0.1	204 \pm 2
SFG-7	-	-	-	10.0 \pm 0.2	2.7 \pm 0.1	0.6 \pm 0.1	87.0 \pm 0.9
SFG-8	-	-	-	10.2 \pm 0.1	2.90 \pm 0.09	0.5 \pm 0.1	224 \pm 2
SFG-9	-	-	-	10.5 \pm 0.3	2.7 \pm 0.2	1.0 \pm 0.2	192 \pm 2
SFG-10	-	-	-	11.2 \pm 0.2	2.1 \pm 0.2	0.5 \pm 0.1	72.0 \pm 0.7

Table A13 *continued*

Table A13 (*continued*)

Reference number	He I $\lambda 3614$ [H β =100]	He I $\lambda 3965$ [H β =100]	He I $\lambda 5016$ [H β =100]	He I $\lambda 5876$ [H β =100]	He I $\lambda 6678$ [H β =100]	He I $\lambda 7281$ [H β =100]	EW(H β) [Å]
SFG-11	-	-	-	10.4 ± 0.2	2.7 ± 0.1	0.6 ± 0.1	150 ± 2
SFG-12	-	-	-	10.8 ± 0.3	3.0 ± 0.2	0.6 ± 0.1	78.0 ± 0.8
SFG-13	-	-	-	10.6 ± 0.2	2.83 ± 0.06	0.52 ± 0.04	270 ± 3
SFG-14	-	-	2.30 ± 0.09	9.3 ± 0.3	2.7 ± 0.2	0.42 ± 0.02	-
SFG-15	-	-	1.73 ± 0.05	11.3 ± 0.2	3.03 ± 0.06	0.50 ± 0.03	-
SFG-16	-	-	-	10.9 ± 0.2	2.93 ± 0.06	0.54 ± 0.06	271 ± 3
SFG-17	0.38 ± 0.05	-	1.91 ± 0.06	11.6 ± 0.3	3.07 ± 0.09	0.68 ± 0.02	(4.1 ± 0.1) × 10 ²
SFG-18	-	-	0.87 ± 0.03	8.7 ± 0.2	2.38 ± 0.05	0.34 ± 0.02	40.2 ± 0.4
SFG-19	-	-	0.90 ± 0.03	10.9 ± 0.2	3.05 ± 0.06	0.51 ± 0.03	276 ± 3
SFG-20	-	-	-	12.2 ± 0.2	3.8 ± 0.1	0.61 ± 0.07	237 ± 5
SFG-21	-	-	1.57 ± 0.09	11.5 ± 0.3	2.9 ± 0.1	0.78 ± 0.05	288 ± 9
SFG-22	-	-	1.78 ± 0.05	10.0 ± 0.2	2.18 ± 0.04	0.52 ± 0.03	199 ± 2
SFG-23	-	-	1.57 ± 0.03	7.6 ± 0.2	2.47 ± 0.05	0.460 ± 0.009	168 ± 2
SFG-24	-	-	-	12.1 ± 0.2	3.25 ± 0.07	0.54 ± 0.04	274 ± 3
SFG-25	-	-	-	11.6 ± 0.2	3.38 ± 0.07	0.56 ± 0.04	153 ± 2
SFG-26	-	-	-	9.5 ± 0.1	2.76 ± 0.06	0.58 ± 0.09	103 ± 1
SFG-27	-	-	-	11.4 ± 0.2	3.15 ± 0.09	0.56 ± 0.08	274 ± 3
SFG-28	-	-	-	10.9 ± 0.1	3.12 ± 0.09	0.9 ± 0.1	122 ± 1
SFG-29	-	-	-	10.8 ± 0.1	2.95 ± 0.03	0.46 ± 0.02	150 ± 2
SFG-30	-	0.60 ± 0.06	2.0 ± 0.1	10.8 ± 0.6	3.2 ± 0.2	0.52 ± 0.05	78 ± 3
SFG-31	-	-	2.01 ± 0.04	15.6 ± 0.2	4.9 ± 0.1	0.74 ± 0.02	146 ± 1
SFG-32	-	-	2.46 ± 0.07	11.8 ± 0.4	3.5 ± 0.1	0.57 ± 0.02	-
SFG-33	-	-	2.7 ± 0.2	12 ± 1	3.4 ± 0.3	0.59 ± 0.06	-
SFG-34	-	-	2.3 ± 0.3	12 ± 2	3.7 ± 0.6	0.6 ± 0.1	-
SFG-35	-	-	2.2 ± 0.2	12 ± 1	3.4 ± 0.4	0.63 ± 0.08	-
SFG-36	0.31 ± 0.06	0.79 ± 0.07	1.92 ± 0.08	10.9 ± 0.4	3.00 ± 0.09	0.47 ± 0.03	137 ± 4
SFG-37	-	-	2.05 ± 0.04	11.2 ± 0.2	3.78 ± 0.08	0.58 ± 0.01	119 ± 1
SFG-38	-	0.64 ± 0.06	2.0 ± 0.1	11.1 ± 0.4	3.0 ± 0.1	0.45 ± 0.04	94 ± 3
SFG-39	-	-	2.82 ± 0.06	14.6 ± 0.3	4.05 ± 0.04	0.760 ± 0.008	309 ± 3
SFG-40	0.33 ± 0.05	0.72 ± 0.04	1.98 ± 0.08	11.4 ± 0.5	3.4 ± 0.2	0.68 ± 0.04	195 ± 8
SFG-41	-	-	-	11.6 ± 0.3	3.0 ± 0.2	0.64 ± 0.09	255 ± 5
SFG-42	-	-	1.38 ± 0.07	10.1 ± 0.2	2.94 ± 0.09	0.63 ± 0.04	246 ± 5
SFG-43	-	-	1.6 ± 0.2	10.8 ± 0.3	2.9 ± 0.1	0.49 ± 0.08	165 ± 3
SFG-44	-	-	2.6 ± 0.4	10.1 ± 0.6	3.0 ± 0.3	0.8 ± 0.1	-
SFG-45	-	0.6 ± 0.1	1.8 ± 0.2	8.7 ± 0.4	2.6 ± 0.2	0.5 ± 0.1	112 ± 1
SFG-46	-	0.55 ± 0.06	2.0 ± 0.1	10.9 ± 0.5	2.9 ± 0.2	0.49 ± 0.04	148 ± 6
SFG-47	-	-	1.77 ± 0.04	10.1 ± 0.1	2.89 ± 0.06	0.48 ± 0.01	228 ± 2
SFG-48	-	-	2.09 ± 0.02	10.5 ± 0.2	2.63 ± 0.05	0.60 ± 0.02	337 ± 3
SFG-49	-	-	-	10.8 ± 0.2	2.57 ± 0.05	0.62 ± 0.04	351 ± 4
SFG-50	-	-	1.86 ± 0.04	9.2 ± 0.2	2.62 ± 0.05	0.69 ± 0.02	201 ± 2

Table A13 *continued*

Table A13 (*continued*)

Reference number	He I $\lambda 3614$ [H β =100]	He I $\lambda 3965$ [H β =100]	He I $\lambda 5016$ [H β =100]	He I $\lambda 5876$ [H β =100]	He I $\lambda 6678$ [H β =100]	He I $\lambda 7281$ [H β =100]	EW(H β) [Å]
SFG-51	-	-	1.71 ± 0.07	9.3 ± 0.2	2.56 ± 0.05	0.57 ± 0.03	108 ± 1
SFG-52	-	-	2.1 ± 0.1	9.1 ± 0.2	2.5 ± 0.2	0.8 ± 0.1	305 ± 6
SFG-53	-	-	-	9.5 ± 0.1	2.90 ± 0.09	0.6 ± 0.1	163 ± 2
SFG-54	-	-	0.91 ± 0.04	10.9 ± 0.3	2.92 ± 0.09	0.60 ± 0.04	(3.3 ± 0.1) × 10 ²
SFG-55	-	-	2.0 ± 0.1	11.2 ± 0.3	2.7 ± 0.1	0.69 ± 0.05	(3.5 ± 0.1) × 10 ²
SFG-56	-	-	2.2 ± 0.2	11.0 ± 0.2	2.7 ± 0.1	0.92 ± 0.08	133 ± 3
SFG-57	-	-	-	11.1 ± 0.1	3.3 ± 0.2	0.5 ± 0.1	65.9 ± 0.7
SFG-58	-	-	-	11.4 ± 0.1	3.08 ± 0.06	0.46 ± 0.09	232 ± 2
SFG-59	-	-	-	16 ± 1	1.60 ± 0.05	0.40 ± 0.05	274 ± 3
SFG-60	-	-	1.98 ± 0.08	11.8 ± 0.4	2.91 ± 0.09	0.89 ± 0.04	(5.2 ± 0.2) × 10 ²
SFG-61	-	-	1.98 ± 0.08	11.8 ± 0.4	2.91 ± 0.09	0.89 ± 0.03	(5.2 ± 0.2) × 10 ²
SFG-62	-	-	-	12.6 ± 0.1	3.40 ± 0.03	0.6 ± 0.1	217 ± 2
SFG-63	-	-	0.70 ± 0.09	11.6 ± 0.6	-	0.56 ± 0.06	186 ± 7
SFG-64	-	-	1.48 ± 0.07	10.5 ± 0.3	3.0 ± 0.1	0.43 ± 0.03	(4.9 ± 0.1) × 10 ²
SFG-65	-	-	1.91 ± 0.06	11.8 ± 0.4	2.49 ± 0.07	0.58 ± 0.03	(4.1 ± 0.1) × 10 ²
SFG-66	-	-	1.6 ± 0.2	9.4 ± 0.2	2.50 ± 0.07	0.72 ± 0.03	214 ± 4
SFG-67	-	-	-	9.5 ± 0.3	2.3 ± 0.1	0.79 ± 0.06	(5.8 ± 0.2) × 10 ²
SFG-68	-	-	0.96 ± 0.05	10.1 ± 0.2	2.91 ± 0.06	0.59 ± 0.02	220 ± 2
SFG-69	-	-	-	11.9 ± 0.4	3.5 ± 0.1	0.72 ± 0.03	(3.5 ± 0.1) × 10 ²
SFG-70	-	-	-	22.6 ± 0.9	5.0 ± 0.1	0.8 ± 0.1	115 ± 1
SFG-71	-	-	-	12.9 ± 0.1	3.5 ± 0.2	0.7 ± 0.1	199 ± 2
SFG-72	-	-	3.15 ± 0.06	5.52 ± 0.06	2.40 ± 0.05	0.48 ± 0.01	237 ± 2
SFG-73	-	-	-	13.3 ± 0.1	3.1 ± 0.2	0.6 ± 0.1	146 ± 1
SFG-74	-	-	1.7 ± 0.2	11.4 ± 0.5	3.3 ± 0.2	0.72 ± 0.06	91 ± 4
SFG-75	-	0.63 ± 0.06	2.0 ± 0.1	10.6 ± 0.5	3.0 ± 0.2	0.60 ± 0.05	132 ± 5
SFG-76	-	-	-	9.1 ± 0.2	2.5 ± 0.1	0.5 ± 0.1	268 ± 3
SFG-77	-	-	-	9.3 ± 0.2	2.49 ± 0.07	0.50 ± 0.05	312 ± 3
SFG-78	-	-	-	10.4 ± 0.2	2.69 ± 0.08	0.66 ± 0.05	267 ± 3
SFG-79	-	-	-	10.3 ± 0.2	2.7 ± 0.1	0.5 ± 0.1	174 ± 2
SFG-80	-	-	2.6 ± 0.2	11.2 ± 0.3	2.8 ± 0.2	0.45 ± 0.07	236 ± 5
SFG-81	-	-	2.7 ± 0.3	10.8 ± 0.5	2.8 ± 0.3	1.0 ± 0.2	196 ± 4
SFG-82	-	-	1.54 ± 0.03	9.0 ± 0.2	2.40 ± 0.05	0.59 ± 0.02	336 ± 3
SFG-83	-	-	1.94 ± 0.04	11.4 ± 0.1	2.91 ± 0.06	0.51 ± 0.02	95.0 ± 0.9
SFG-84	-	-	1.34 ± 0.03	9.1 ± 0.2	2.46 ± 0.05	0.38 ± 0.01	79 ± 2
SFG-85	-	-	1.63 ± 0.03	10.7 ± 0.1	2.92 ± 0.06	0.49 ± 0.01	155 ± 2
SFG-86	-	-	2.4 ± 0.1	10.9 ± 0.2	2.11 ± 0.08	0.46 ± 0.04	234 ± 2
SFG-87	-	-	2.6 ± 0.2	10.6 ± 0.3	2.1 ± 0.1	0.61 ± 0.06	213 ± 4
SFG-88	-	-	-	12.3 ± 0.2	3.6 ± 0.1	1.0 ± 0.1	251 ± 3
SFG-89	-	-	1.93 ± 0.08	10.0 ± 0.2	2.81 ± 0.08	0.54 ± 0.05	200 ± 4
SFG-90	0.27 ± 0.05	-	2.03 ± 0.06	10.5 ± 0.3	2.88 ± 0.09	1.00 ± 0.06	310 ± 9

Table A14. Reddening-corrected He I fluxes in the sample of Planetary Nebulae are reported by the reference authors. Intensities are given relative to H β = 100.

Reference number	He I λ 3614 [H β =100]	He I λ 3965 [H β =100]	He I λ 5016 [H β =100]	He I λ 5876 [H β =100]	He I λ 6678 [H β =100]	He I λ 7281 [H β =100]
PNe-1	-	0.83 ± 0.03	-	16.2 ± 0.6	4.3 ± 0.2	1.02 ± 0.05
PNe-2	-	0.61 ± 0.03	-	11.6 ± 0.3	3.0 ± 0.1	0.64 ± 0.03
PNe-3	-	0.42 ± 0.02	-	13.1 ± 0.4	3.4 ± 0.1	0.72 ± 0.03
PNe-4	-	0.43 ± 0.02	1.22 ± 0.06	11.4 ± 0.3	2.94 ± 0.09	0.65 ± 0.03
PNe-5	-	-	-	14 ± 2	-	0.7 ± 0.1
PNe-6	-	-	-	11 ± 1	3.0 ± 0.3	0.60 ± 0.06
PNe-7	0.53 ± 0.07	1.01 ± 0.08	2.9 ± 0.3	22 ± 1	5.7 ± 0.3	0.90 ± 0.06
PNe-8	0.22 ± 0.02	-	-	18.2 ± 0.9	4.7 ± 0.2	0.71 ± 0.04
PNe-9	-	-	-	15 ± 2	4.0 ± 0.4	0.90 ± 0.09
PNe-10	0.42 ± 0.04	-	3.4 ± 0.2	17.8 ± 0.9	4.4 ± 0.2	0.85 ± 0.04
PNe-11	-	-	2.6 ± 0.3	20 ± 1	5.2 ± 0.3	0.86 ± 0.07
PNe-12	-	-	-	13.4 ± 0.7	3.7 ± 0.2	0.40 ± 0.02
PNe-13	-	-	-	17.0 ± 0.9	4.6 ± 0.2	0.74 ± 0.04
PNe-14	-	0.74 ± 0.07	1.9 ± 0.1	15.6 ± 0.8	4.1 ± 0.2	0.73 ± 0.04
PNe-15	-	-	-	14.7 ± 0.7	3.5 ± 0.2	0.54 ± 0.03
PNe-16	-	0.66 ± 0.03	1.91 ± 0.04	14.9 ± 0.3	3.4 ± 0.1	0.54 ± 0.06
PNe-17	-	-	-	18 ± 2	3.7 ± 0.4	0.90 ± 0.09
PNe-18	-	-	-	21 ± 3	6.1 ± 0.9	0.9 ± 0.2
PNe-19	-	-	-	17 ± 2	4.0 ± 0.4	0.60 ± 0.06
PNe-20	0.32 ± 0.02	-	-	15.2 ± 0.8	3.6 ± 0.2	0.69 ± 0.03
PNe-21	-	-	-	6.2 ± 0.6	1.6 ± 0.2	0.20 ± 0.02
PNe-22	-	1.1 ± 0.1	2.9 ± 0.2	15.6 ± 0.8	5.0 ± 0.3	0.98 ± 0.08
PNe-23	-	-	-	13 ± 1	3.5 ± 0.3	0.60 ± 0.06
PNe-24	-	0.9 ± 0.1	2.0 ± 0.1	15.4 ± 0.8	4.1 ± 0.2	0.80 ± 0.04
PNe-25	-	1.10 ± 0.09	2.9 ± 0.1	20 ± 1	5.1 ± 0.5	1.0 ± 0.1
PNe-26	-	1.3 ± 0.2	2.7 ± 0.2	18.5 ± 0.9	5.0 ± 0.2	0.92 ± 0.05
PNe-27	-	-	-	15 ± 2	3.7 ± 0.4	0.80 ± 0.08
PNe-28	-	-	-	14 ± 1	4.1 ± 0.4	0.60 ± 0.06
PNe-29	-	-	-	15 ± 2	3.9 ± 0.6	0.6 ± 0.1
PNe-30	-	-	-	15 ± 2	3.9 ± 0.6	0.8 ± 0.1
PNe-31	-	-	-	8.7 ± 0.9	0.10 ± 0.01	0.60 ± 0.06
PNe-32	-	-	-	10 ± 1	3.2 ± 0.3	0.40 ± 0.04
PNe-33	0.43 ± 0.01	0.91 ± 0.03	2.50 ± 0.07	17.0 ± 0.5	4.4 ± 0.1	0.78 ± 0.02
PNe-34	-	-	-	13 ± 1	3.4 ± 0.3	0.60 ± 0.06
PNe-35	0.30 ± 0.01	0.92 ± 0.05	-	13.8 ± 0.7	3.7 ± 0.2	0.75 ± 0.04
PNe-36	0.56 ± 0.02	1.03 ± 0.03	2.39 ± 0.07	13.7 ± 0.4	3.9 ± 0.1	0.79 ± 0.02

Table A14 *continued*

Table A14 (*continued*)

Reference number	He I λ 3614 [H β =100]	He I λ 3965 [H β =100]	He I λ 5016 [H β =100]	He I λ 5876 [H β =100]	He I λ 6678 [H β =100]	He I λ 7281 [H β =100]
PNe-37	0.270 \pm 0.008	0.73 \pm 0.02	2.00 \pm 0.06	11.0 \pm 0.3	2.30 \pm 0.07	0.70 \pm 0.02
PNe-38	-	-	-	14.0 \pm 0.7	3.7 \pm 0.2	0.52 \pm 0.03
PNe-39	-	-	-	12.1 \pm 0.6	3.4 \pm 0.2	0.34 \pm 0.02
PNe-40	0.37 \pm 0.02	0.97 \pm 0.03	2.49 \pm 0.07	15.2 \pm 0.5	4.3 \pm 0.2	0.78 \pm 0.03
PNe-41	-	1.5 \pm 0.3	2.2 \pm 0.4	15 \pm 1	3.8 \pm 0.6	0.8 \pm 0.2
PNe-42	-	-	-	9.2 \pm 0.9	2.7 \pm 0.3	0.50 \pm 0.05
PNe-43	-	-	-	13 \pm 2	3.2 \pm 0.5	0.7 \pm 0.1
PNe-44	-	-	-	16 \pm 2	3.5 \pm 0.5	0.8 \pm 0.1
PNe-45	-	-	-	16 \pm 2	3.9 \pm 0.6	0.8 \pm 0.1
PNe-46	-	0.60 \pm 0.02	0.99 \pm 0.01	6.16 \pm 0.06	1.60 \pm 0.03	0.32 \pm 0.01
PNe-47	-	-	-	16 \pm 2	4.7 \pm 0.7	0.6 \pm 0.1
PNe-48	-	-	-	16 \pm 2	-	0.9 \pm 0.2
PNe-49	0.28 \pm 0.02	-	-	16.3 \pm 0.8	4.1 \pm 0.2	0.67 \pm 0.03
PNe-50	0.57 \pm 0.09	1.1 \pm 0.1	3.4 \pm 0.2	20 \pm 1	5.2 \pm 0.5	0.92 \pm 0.09
PNe-51	-	1.4 \pm 0.1	3.2 \pm 0.2	21 \pm 1	5.6 \pm 0.4	0.88 \pm 0.08
PNe-52	-	1.7 \pm 0.3	3.2 \pm 0.2	22 \pm 1	6.0 \pm 0.3	0.90 \pm 0.05
PNe-53	-	0.67 \pm 0.09	2.7 \pm 0.2	19 \pm 2	5.4 \pm 0.6	1.1 \pm 0.1
PNe-54	-	1.4 \pm 0.1	2.7 \pm 0.2	20 \pm 1	5.4 \pm 0.3	0.78 \pm 0.05
PNe-55	-	-	-	16 \pm 2	3.8 \pm 0.6	0.6 \pm 0.1
PNe-56	-	-	-	18 \pm 2	3.7 \pm 0.6	0.7 \pm 0.1
PNe-57	-	-	-	14 \pm 1	3.7 \pm 0.4	0.70 \pm 0.07
PNe-58	-	-	-	19 \pm 2	4.9 \pm 0.5	0.60 \pm 0.06
PNe-59	-	-	-	12 \pm 1	2.9 \pm 0.3	0.30 \pm 0.03
PNe-60	-	-	-	16 \pm 2	4.1 \pm 0.4	1.0 \pm 0.1
PNe-61	0.50 \pm 0.07	1.07 \pm 0.09	2.7 \pm 0.1	18 \pm 1	4.6 \pm 0.4	1.0 \pm 0.1
PNe-62	-	-	-	-	2.7 \pm 0.4	0.6 \pm 0.1
PNe-63	-	-	-	15 \pm 2	4.0 \pm 0.6	0.7 \pm 0.1
PNe-64	-	-	-	15 \pm 2	3.9 \pm 0.6	0.9 \pm 0.1
PNe-65	-	-	-	18.7 \pm 0.9	4.5 \pm 0.2	0.84 \pm 0.04
PNe-66	-	-	-	22 \pm 1	5.7 \pm 0.3	0.61 \pm 0.03
PNe-67	-	-	-	15 \pm 2	3.6 \pm 0.5	0.7 \pm 0.1
PNe-68	-	-	-	15.9 \pm 0.8	4.3 \pm 0.2	0.56 \pm 0.03
PNe-69	0.37 \pm 0.07	1.12 \pm 0.08	2.7 \pm 0.1	18.6 \pm 0.4	5.8 \pm 0.1	0.86 \pm 0.03
PNe-70	-	-	3.3 \pm 0.2	17.3 \pm 0.9	4.9 \pm 0.2	0.81 \pm 0.04
PNe-71	-	-	-	16.9 \pm 0.8	4.7 \pm 0.2	0.55 \pm 0.03
PNe-72	0.33 \pm 0.03	1.01 \pm 0.05	4.1 \pm 0.2	17.8 \pm 0.9	5.1 \pm 0.3	0.88 \pm 0.04
PNe-73	-	-	-	16.8 \pm 0.8	4.6 \pm 0.2	0.76 \pm 0.04
PNe-74	-	-	2.7 \pm 0.2	18 \pm 1	4.6 \pm 0.5	0.9 \pm 0.1
PNe-75	0.35 \pm 0.02	1.06 \pm 0.05	3.5 \pm 0.2	18.3 \pm 0.9	5.0 \pm 0.2	0.76 \pm 0.04
PNe-76	-	-	-	18.3 \pm 0.9	5.1 \pm 0.3	0.45 \pm 0.02

Table A14 *continued*

Table A14 (*continued*)

Reference number	He I λ 3614 [H β =100]	He I λ 3965 [H β =100]	He I λ 5016 [H β =100]	He I λ 5876 [H β =100]	He I λ 6678 [H β =100]	He I λ 7281 [H β =100]
PNe-77	-	-	-	13.9 ± 0.7	3.8 ± 0.2	0.52 ± 0.03
PNe-78	-	-	-	14 ± 2	3.5 ± 0.5	0.6 ± 0.1
PNe-79	-	-	-	17 ± 2	4.6 ± 0.5	0.60 ± 0.06
PNe-80	-	-	-	19 ± 1	4.7 ± 0.2	0.47 ± 0.02
PNe-81	-	-	-	25 ± 3	5.8 ± 0.9	0.9 ± 0.2
PNe-82	-	-	-	15.3 ± 0.8	3.8 ± 0.2	0.51 ± 0.03
PNe-83	-	-	-	10 ± 1	2.4 ± 0.4	0.29 ± 0.05
PNe-84	1.1 ± 0.1	-	-	11.4 ± 0.6	3.2 ± 0.2	0.55 ± 0.04
PNe-85	-	-	-	13 ± 2	-	0.49 ± 0.07
PNe-86	0.220 ± 0.007	0.53 ± 0.02	1.50 ± 0.04	12.0 ± 0.4	3.2 ± 0.1	0.60 ± 0.02
PNe-87	0.26 ± 0.03	0.56 ± 0.04	1.42 ± 0.07	10.9 ± 0.5	3.1 ± 0.2	0.61 ± 0.04
PNe-88	0.32 ± 0.04	-	1.74 ± 0.09	13.1 ± 0.7	3.6 ± 0.2	0.67 ± 0.05
PNe-89	-	-	-	16.3 ± 0.8	4.5 ± 0.2	0.85 ± 0.04
PNe-90	-	-	-	4.4 ± 0.4	1.8 ± 0.2	0.10 ± 0.01
PNe-91	-	-	-	12 ± 1	3.5 ± 0.3	0.40 ± 0.04
PNe-92	-	-	-	13 ± 1	3.5 ± 0.3	0.60 ± 0.06
PNe-93	-	-	-	11.6 ± 0.6	3.2 ± 0.2	0.42 ± 0.02
PNe-94	0.20 ± 0.02	0.46 ± 0.03	-	9.7 ± 0.6	2.6 ± 0.2	0.53 ± 0.04
PNe-95	0.66 ± 0.03	0.95 ± 0.05	-	9.2 ± 0.5	2.5 ± 0.1	0.58 ± 0.03
PNe-96	0.19 ± 0.03	0.70 ± 0.06	1.7 ± 0.1	12.0 ± 0.7	3.2 ± 0.3	0.64 ± 0.06
PNe-97	-	0.56 ± 0.06	1.49 ± 0.09	13.7 ± 0.3	3.8 ± 0.2	0.63 ± 0.05
PNe-98	0.52 ± 0.06	0.97 ± 0.08	3.0 ± 0.2	20 ± 1	5.2 ± 0.4	0.84 ± 0.08
PNe-99	-	-	-	16.0 ± 0.8	4.3 ± 0.2	0.61 ± 0.03
PNe-100	0.16 ± 0.01	-	-	13.7 ± 0.7	3.9 ± 0.2	0.67 ± 0.03
PNe-101	0.30 ± 0.03	-	-	17.5 ± 0.9	1.02 ± 0.05	0.89 ± 0.04
PNe-102	-	-	-	6.7 ± 0.7	3.1 ± 0.3	0.30 ± 0.03
PNe-103	-	0.83 ± 0.08	2.3 ± 0.1	16 ± 1	4.3 ± 0.3	0.90 ± 0.07
PNe-104	-	-	-	17 ± 2	4.3 ± 0.4	0.60 ± 0.06
PNe-105	-	-	-	17.6 ± 0.9	5.0 ± 0.3	0.70 ± 0.03
PNe-106	-	-	-	7.2 ± 0.7	2.2 ± 0.2	0.50 ± 0.05
PNe-107	-	-	-	11 ± 1	3.1 ± 0.3	0.40 ± 0.04
PNe-108	-	-	-	18 ± 2	4.2 ± 0.6	0.8 ± 0.1
PNe-109	-	1.5 ± 0.1	-	17.4 ± 0.9	4.7 ± 0.2	0.72 ± 0.07
PNe-110	-	-	-	14 ± 1	3.7 ± 0.4	1.1 ± 0.1
PNe-111	-	-	-	15 ± 1	4.0 ± 0.4	0.50 ± 0.05
PNe-112	0.36 ± 0.02	-	-	16.2 ± 0.8	4.0 ± 0.2	0.76 ± 0.04
PNe-113	-	1.1 ± 0.1	2.9 ± 0.3	16 ± 2	4.2 ± 0.4	0.90 ± 0.09
PNe-114	0.31 ± 0.02	-	-	16.9 ± 0.8	4.8 ± 0.2	0.59 ± 0.03
PNe-115	-	-	-	15 ± 2	4.1 ± 0.4	0.80 ± 0.08
PNe-116	0.28 ± 0.01	-	-	13.4 ± 0.7	3.7 ± 0.2	0.68 ± 0.03

Table A14 *continued*

Table A14 (*continued*)

Reference number	He I λ 3614 [H β =100]	He I λ 3965 [H β =100]	He I λ 5016 [H β =100]	He I λ 5876 [H β =100]	He I λ 6678 [H β =100]	He I λ 7281 [H β =100]
PNe-117	-	0.9 ± 0.2	1.76 ± 0.09	12.1 ± 0.7	3.1 ± 0.2	0.65 ± 0.02
PNe-118	-	-	-	20 ± 2	4.6 ± 0.5	1.2 ± 0.1
PNe-119	-	-	-	20 ± 2	4.6 ± 0.7	0.8 ± 0.1
PNe-120	-	-	-	7.5 ± 0.4	2.2 ± 0.1	0.25 ± 0.01
PNe-121	0.61 ± 0.03	1.14 ± 0.06	-	14.3 ± 0.7	4.1 ± 0.2	0.81 ± 0.04
PNe-122	-	-	-	14 ± 2	3.4 ± 0.5	0.9 ± 0.1
PNe-123	-	-	-	13 ± 2	3.1 ± 0.5	0.6 ± 0.1
PNe-124	-	-	-	15 ± 2	3.7 ± 0.4	0.70 ± 0.07
PNe-125	0.29 ± 0.01	1.2 ± 0.1	-	14.4 ± 0.1	3.7 ± 0.3	0.51 ± 0.02
PNe-126	-	-	-	12 ± 2	3.1 ± 0.5	0.47 ± 0.08
PNe-127	-	-	-	11 ± 1	3.2 ± 0.5	0.45 ± 0.08
PNe-128	0.66 ± 0.05	1.42 ± 0.09	2.7 ± 0.1	17 ± 1	5.2 ± 0.3	0.81 ± 0.07
PNe-129	0.34 ± 0.05	0.87 ± 0.07	2.1 ± 0.1	15.6 ± 0.9	4.1 ± 0.3	0.72 ± 0.06
PNe-130	-	-	-	9.8 ± 0.5	2.6 ± 0.3	0.45 ± 0.08
PNe-131	-	-	-	13.5 ± 0.7	3.3 ± 0.2	0.62 ± 0.06
PNe-132	-	-	2.7 ± 0.1	11.9 ± 0.6	3.8 ± 0.3	0.43 ± 0.03
PNe-133	-	-	3.1 ± 0.2	19.2 ± 0.8	6.3 ± 0.4	0.54 ± 0.04
PNe-134	-	-	3.1 ± 0.3	22 ± 1	6.5 ± 0.5	0.67 ± 0.06
PNe-135	-	0.80 ± 0.09	2.7 ± 0.3	17.2 ± 0.7	5.3 ± 0.6	0.61 ± 0.05
PNe-136	-	0.8 ± 0.2	2.7 ± 0.5	23 ± 1	7.8 ± 0.6	0.61 ± 0.05
PNe-137	-	-	2.05 ± 0.08	16.6 ± 0.8	4.8 ± 0.3	0.42 ± 0.05
PNe-138	-	-	-	9.5 ± 0.5	3.0 ± 0.3	0.44 ± 0.04
PNe-139	-	-	2.5 ± 0.3	16 ± 1	5.0 ± 0.4	0.37 ± 0.06
PNe-140	-	-	-	17 ± 2	4.6 ± 0.7	0.52 ± 0.09
PNe-141	-	-	2.7 ± 0.2	18 ± 1	5.5 ± 0.4	0.50 ± 0.05
PNe-142	-	-	2.8 ± 0.1	14.1 ± 0.6	3.8 ± 0.5	0.53 ± 0.04
PNe-143	-	-	2.5 ± 0.2	15.9 ± 0.8	4.2 ± 0.2	0.70 ± 0.05
PNe-144	-	-	3.4 ± 0.7	15.3 ± 0.9	4.4 ± 0.4	0.64 ± 0.09
PNe-145	-	-	-	7.6 ± 0.3	2.0 ± 0.1	0.38 ± 0.03
PNe-146	-	-	3.6 ± 0.5	13.9 ± 0.4	4.4 ± 0.7	0.68 ± 0.04
PNe-147	-	-	2.9 ± 0.6	13.5 ± 0.7	3.9 ± 0.4	0.62 ± 0.06
PNe-148	-	-	2.9 ± 0.2	12.6 ± 0.5	3.5 ± 0.3	0.62 ± 0.04
PNe-149	-	-	4.3 ± 0.7	18.6 ± 0.7	5.1 ± 0.3	0.94 ± 0.09
PNe-150	-	-	3.1 ± 0.2	21.9 ± 0.9	6.9 ± 0.4	0.55 ± 0.04
PNe-151	-	-	-	7.9 ± 0.3	2.4 ± 0.2	0.30 ± 0.02
PNe-152	-	-	3.0 ± 0.5	20 ± 1	5.8 ± 0.5	0.82 ± 0.09
PNe-153	-	-	2.1 ± 0.2	18.7 ± 0.7	5.2 ± 0.3	0.62 ± 0.05
PNe-154	-	-	-	9.7 ± 0.3	3.2 ± 0.3	0.38 ± 0.03
PNe-155	-	0.9 ± 0.2	-	19.6 ± 0.8	7.2 ± 0.7	0.81 ± 0.06
PNe-156	-	-	-	4.0 ± 0.1	1.08 ± 0.06	0.17 ± 0.03

Table A14 *continued*

Table A14 (*continued*)

Reference number	He I λ 3614 [H β =100]	He I λ 3965 [H β =100]	He I λ 5016 [H β =100]	He I λ 5876 [H β =100]	He I λ 6678 [H β =100]	He I λ 7281 [H β =100]
PNe-157	-	-	3.1 ± 0.3	15.1 ± 0.8	4.4 ± 0.4	0.59 ± 0.05
PNe-158	-	-	-	15 ± 1	3.9 ± 0.4	0.53 ± 0.07
PNe-159	-	-	-	14 ± 1	3.9 ± 0.5	0.43 ± 0.06
PNe-160	-	-	-	15.1 ± 0.6	6.2 ± 0.2	0.88 ± 0.05
PNe-161	-	-	2.0 ± 0.1	12.0 ± 0.4	3.2 ± 0.2	0.53 ± 0.05
PNe-162	-	-	2.9 ± 0.5	18.0 ± 0.5	5.9 ± 0.5	0.63 ± 0.04
PNe-163	-	-	-	15.3 ± 0.6	4.1 ± 0.2	0.65 ± 0.05
PNe-164	-	-	3.7 ± 0.6	16.6 ± 0.7	4.5 ± 0.4	0.92 ± 0.09
PNe-165	-	-	4.5 ± 0.9	20 ± 1	5.5 ± 0.4	0.73 ± 0.09
PNe-166	-	-	-	9.3 ± 0.5	2.4 ± 0.2	0.42 ± 0.04
PNe-167	-	-	-	11.9 ± 0.2	3.68 ± 0.07	0.64 ± 0.01
PNe-168	-	-	-	15.1 ± 0.9	4.6 ± 0.6	0.62 ± 0.06
PNe-169	-	-	4.2 ± 0.5	20 ± 1	6.1 ± 0.4	0.87 ± 0.09
PNe-170	-	-	2.8 ± 0.3	16.9 ± 0.7	5.3 ± 0.4	0.52 ± 0.04
PNe-171	-	-	2.5 ± 0.4	14.8 ± 0.6	4.7 ± 0.4	0.46 ± 0.02
PNe-172	-	-	3.0 ± 0.4	16.6 ± 0.8	5.1 ± 0.4	0.40 ± 0.04
PNe-173	-	-	0.46 ± 0.09	2.4 ± 0.1	0.53 ± 0.02	0.09 ± 0.01
PNe-174	-	-	2.9 ± 0.3	14.5 ± 0.6	3.5 ± 0.2	0.68 ± 0.05
PNe-175	-	-	3.0 ± 0.5	15.9 ± 0.8	4.7 ± 0.5	0.48 ± 0.07
PNe-176	-	-	-	7.3 ± 0.2	2.2 ± 0.1	0.14 ± 0.02
PNe-177	-	-	3.8 ± 0.4	17 ± 1	4.3 ± 0.5	0.68 ± 0.05
PNe-178	-	-	2.5 ± 0.1	13.1 ± 0.5	4.3 ± 0.2	0.52 ± 0.03
PNe-179	-	-	-	10.3 ± 0.3	3.0 ± 0.2	0.33 ± 0.02
PNe-180	-	-	2.9 ± 0.2	18.1 ± 0.4	4.4 ± 0.2	0.67 ± 0.03
PNe-181	-	-	3.7 ± 0.7	16.7 ± 0.7	5.6 ± 0.8	0.72 ± 0.07
PNe-182	-	-	3.0 ± 0.6	15.3 ± 0.2	4.7 ± 0.4	0.58 ± 0.02
PNe-183	-	-	3.7 ± 0.3	22.4 ± 0.9	6.6 ± 0.5	0.84 ± 0.06
PNe-184	-	-	3.4 ± 0.5	14.3 ± 0.7	3.8 ± 0.3	0.78 ± 0.05
PNe-185	-	1.4 ± 0.3	2.9 ± 0.1	15.8 ± 0.6	5.3 ± 0.4	0.55 ± 0.04
PNe-186	-	-	3.0 ± 0.4	11.8 ± 0.8	4.8 ± 0.4	0.74 ± 0.06
PNe-187	-	-	3.1 ± 0.4	17.2 ± 0.7	5.4 ± 0.5	0.67 ± 0.05
PNe-188	-	-	2.11 ± 0.08	7.7 ± 0.3	2.5 ± 0.3	0.55 ± 0.07
PNe-189	-	-	3.7 ± 0.2	22 ± 2	5.8 ± 0.5	0.8 ± 0.1
PNe-190	-	-	2.7 ± 0.1	18.0 ± 0.9	5.6 ± 0.3	0.59 ± 0.04
PNe-191	-	21 ± 1	2.4 ± 0.2	16.1 ± 0.8	5.0 ± 0.3	0.28 ± 0.03
PNe-192	-	16 ± 1	1.5 ± 0.1	14.7 ± 0.9	3.9 ± 0.4	0.34 ± 0.04
PNe-193	-	22 ± 1	2.2 ± 0.2	15.3 ± 0.6	4.4 ± 0.2	0.29 ± 0.03
PNe-194	-	-	-	14.0 ± 0.4	3.9 ± 0.2	0.34 ± 0.02
PNe-195	-	-	2.4 ± 0.1	14.9 ± 0.6	3.8 ± 0.3	0.56 ± 0.05
PNe-196	-	-	2.5 ± 0.4	11.2 ± 0.4	3.8 ± 0.2	0.44 ± 0.04

Table A14 *continued*

Table A14 (*continued*)

Reference number	He I $\lambda 3614$ [H β =100]	He I $\lambda 3965$ [H β =100]	He I $\lambda 5016$ [H β =100]	He I $\lambda 5876$ [H β =100]	He I $\lambda 6678$ [H β =100]	He I $\lambda 7281$ [H β =100]
PNe-197	-	-	-	16.1 ± 0.6	4.8 ± 0.2	0.54 ± 0.03
PNe-198	-	-	2.8 ± 0.3	13.8 ± 0.6	4.0 ± 0.3	0.43 ± 0.03
PNe-199	-	-	2.1 ± 0.3	17 ± 1	4.5 ± 0.4	0.37 ± 0.04
PNe-200	-	-	-	14.7 ± 0.9	4.0 ± 0.6	0.59 ± 0.06
PNe-201	-	-	3.1 ± 0.6	17.8 ± 0.7	5.2 ± 0.6	0.69 ± 0.05
PNe-202	-	-	1.6 ± 0.1	14.0 ± 0.7	3.7 ± 0.2	0.63 ± 0.04
PNe-203	-	-	3.9 ± 0.6	13 ± 1	3.7 ± 0.4	0.64 ± 0.07
PNe-204	-	1.06 ± 0.06	3.1 ± 0.5	15.5 ± 0.6	4.6 ± 0.2	0.67 ± 0.04
PNe-205	-	-	1.69 ± 0.08	17.7 ± 0.9	5.2 ± 0.3	0.38 ± 0.06
PNe-206	-	-	-	9.8 ± 0.4	3.2 ± 0.2	0.23 ± 0.02
PNe-207	-	-	3.5 ± 0.3	19.0 ± 0.8	5.6 ± 0.4	0.79 ± 0.06
PNe-208	-	-	2.5 ± 0.2	18.4 ± 0.7	4.9 ± 0.4	0.69 ± 0.06
PNe-209	-	15 ± 2	-	9.6 ± 0.7	2.0 ± 0.3	0.39 ± 0.05
PNe-210	-	-	2.7 ± 0.2	13.3 ± 0.7	4.3 ± 0.5	0.68 ± 0.07
PNe-211	-	-	2.2 ± 0.1	13.1 ± 0.7	3.8 ± 0.3	0.42 ± 0.03
PNe-212	-	-	-	11.9 ± 0.7	3.5 ± 0.6	0.52 ± 0.05
PNe-213	-	-	-	23 ± 1	5.8 ± 0.5	0.70 ± 0.06
PNe-214	-	-	-	22 ± 2	5.3 ± 0.5	0.80 ± 0.08
PNe-215	-	0.83 ± 0.09	2.5 ± 0.1	17 ± 1	4.3 ± 0.4	1.0 ± 0.1
PNe-216	-	-	-	16 ± 2	3.7 ± 0.6	0.7 ± 0.1
PNe-217	-	-	-	19 ± 1	5.4 ± 0.3	0.73 ± 0.04
PNe-218	-	-	-	13.1 ± 0.4	3.9 ± 0.1	0.92 ± 0.08

Table A15. Predicted He I fluxes for the sample of H II regions considering $T_{\text{e}}(\text{[O III]})$ and the adopted average n_{e} using the atomic data of [Del Zanna & Storey \(2022\)](#) under the “Case B” of recombination. The fluxes are normalized relative to He I $\lambda 5876=100$.

Reference number	He I $\lambda 3614$ [He I $\lambda 5876=100$]	He I $\lambda 3965$ [He I $\lambda 5876=100$]	He I $\lambda 5016$ [He I $\lambda 5876=100$]	He I $\lambda 6678$ [He I $\lambda 5876=100$]	He I $\lambda 7281$ [He I $\lambda 5876=100$]
HII-1	4.06	8.28	20.85	28.16	5.45
HII-2	3.96	8.10	20.39	28.36	5.16
HII-3	3.97	8.11	20.41	28.34	5.18
HII-4	4.27	8.70	21.78	28.19	5.74
HII-5	4.01	8.19	20.64	28.23	5.33
HII-6	3.74	7.65	19.35	28.54	4.69
HII-7	3.70	7.57	19.17	28.55	4.62
HII-8	3.75	7.68	19.42	28.50	4.75
HII-9	3.96	8.09	20.35	28.44	5.08

Table A15 *continued*

Table A15 (*continued*)

Reference number	He I λ 3614 [He I λ 5876=100]	He I λ 3965 [He I λ 5876=100]	He I λ 5016 [He I λ 5876=100]	He I λ 6678 [He I λ 5876=100]	He I λ 7281 [He I λ 5876=100]
HII-10	4.19	8.55	21.42	28.31	5.52
HII-11	4.18	8.52	21.35	28.32	5.49
HII-12	4.07	8.31	20.87	28.39	5.28
HII-13	4.47	9.12	22.72	28.10	6.12
HII-14	4.28	8.73	21.83	28.25	5.71
HII-15	4.07	8.31	20.87	28.39	5.28
HII-16	4.00	8.16	20.52	28.42	5.15
HII-17	4.04	8.25	20.73	28.39	5.24
HII-18	4.07	8.30	20.84	28.39	5.27
HII-19	4.01	8.18	20.59	28.30	5.26
HII-20	4.03	8.24	20.71	28.33	5.28
HII-21	3.89	7.94	20.02	28.47	4.95
HII-22	3.99	8.14	20.47	28.43	5.12
HII-23	3.91	7.98	20.12	28.40	5.04
HII-24	3.87	7.91	19.96	28.43	4.97
HII-25	4.03	8.24	20.70	28.41	5.21
HII-26	4.39	8.96	22.41	27.79	6.17
HII-27	4.49	9.15	22.84	27.61	6.39
HII-28	3.86	7.88	19.88	28.48	4.90
HII-29	3.85	7.86	19.84	28.47	4.90
HII-30	3.90	7.97	20.07	28.47	4.97
HII-31	4.20	8.57	21.46	28.31	5.54
HII-32	3.82	7.80	19.69	28.51	4.82
HII-33	3.79	7.75	19.60	28.43	4.87
HII-34	3.75	7.67	19.40	28.49	4.75
HII-35	3.73	7.64	19.55	27.59	5.53
HII-36	3.77	7.72	19.57	28.29	5.00
HII-37	3.73	7.63	19.53	27.61	5.52
HII-38	3.78	7.73	19.62	28.21	5.07
HII-39	3.72	7.63	19.55	27.51	5.60
HII-40	3.73	7.64	19.56	27.52	5.59
HII-41	3.73	7.64	19.54	27.63	5.50
HII-42	3.72	7.63	19.52	27.67	5.47
HII-43	3.74	7.65	19.54	27.74	5.42
HII-44	3.72	7.62	19.51	27.59	5.54
HII-45	3.76	7.70	19.57	28.13	5.14
HII-46	3.77	7.72	19.59	28.23	5.06
HII-47	3.93	8.03	20.33	27.96	5.44
HII-48	3.81	7.80	19.79	28.10	5.21
HII-49	3.83	7.83	19.96	27.65	5.58

Table A15 *continued*

Table A15 (*continued*)

Reference number	He I λ 3614 [He I λ 5876=100]	He I λ 3965 [He I λ 5876=100]	He I λ 5016 [He I λ 5876=100]	He I λ 6678 [He I λ 5876=100]	He I λ 7281 [He I λ 5876=100]
HII-50	3.83	7.83	19.78	28.41	4.94
HII-51	4.06	8.29	20.87	28.08	5.51
HII-52	3.90	7.98	20.18	28.10	5.29
HII-53	4.12	8.42	21.15	28.20	5.51
HII-54	3.95	8.08	20.37	28.27	5.23
HII-55	3.93	8.03	20.25	28.36	5.11
HII-56	4.77	9.70	24.07	27.73	6.80
HII-57	4.66	9.48	23.62	27.08	6.92
HII-58	3.82	7.81	19.71	28.50	4.82
HII-59	3.90	7.97	20.08	28.47	4.97
HII-60	3.84	7.85	19.79	28.50	4.86
HII-61	3.76	7.69	19.42	28.53	4.71
HII-62	4.13	8.42	21.13	28.33	5.41
HII-63	4.00	8.17	20.54	28.42	5.15
HII-64	4.02	8.21	20.64	28.41	5.19
HII-65	3.86	7.88	19.88	28.49	4.89
HII-66	4.11	8.39	21.05	28.37	5.35
HII-67	3.92	8.01	20.18	28.46	5.01
HII-68	4.13	8.42	21.13	28.36	5.39
HII-69	4.18	8.53	21.38	28.32	5.50
HII-70	3.87	7.92	19.96	28.48	4.92
HII-71	4.31	8.79	21.98	28.18	5.81
HII-72	4.32	8.80	21.99	28.23	5.78
HII-73	4.34	8.85	22.11	28.21	5.83
HII-74	4.37	8.90	22.22	28.19	5.88
HII-75	4.38	8.93	22.30	28.18	5.92
HII-76	4.30	8.78	21.95	28.17	5.81
HII-77	4.28	8.72	21.82	28.25	5.71
HII-78	4.34	8.85	22.10	28.21	5.83
HII-79	4.48	9.13	22.81	27.38	6.49
HII-80	4.40	8.96	22.40	27.90	6.11
HII-81	4.35	8.86	22.23	27.46	6.28
HII-82	4.33	8.83	22.11	27.94	5.98
HII-83	4.43	9.04	22.54	28.14	6.03
HII-84	4.33	8.84	22.11	27.96	5.97
HII-85	4.40	8.97	22.37	28.17	5.95

Table A16. Predicted He I fluxes for the sample of Star Forming Galaxies considering $T_e(\text{[O III]})$ and the adopted average n_e using the atomic data of [Del Zanna & Storey \(2022\)](#) under the “Case B” of recombination. The fluxes are normalized relative to He I $\lambda 5876=100$.

Reference number	He I $\lambda 3614$	He I $\lambda 3965$	He I $\lambda 5016$	He I $\lambda 6678$	He I $\lambda 7281$
	[He I $\lambda 5876=100$]				
SFG-1	4.75	9.66	23.98	27.78	6.74
SFG-2	4.86	9.90	24.57	26.17	7.61
SFG-3	4.72	9.61	23.86	27.80	6.69
SFG-4	4.56	9.28	23.10	28.00	6.31
SFG-5	4.49	9.14	22.77	28.09	6.14
SFG-6	4.71	9.59	23.84	27.31	6.90
SFG-7	4.59	9.35	23.26	27.96	6.39
SFG-8	4.78	9.73	24.13	27.73	6.82
SFG-9	4.71	9.59	23.84	27.42	6.85
SFG-10	4.64	9.45	23.49	27.90	6.50
SFG-11	4.95	10.06	24.89	27.44	7.27
SFG-12	4.40	8.97	22.39	28.17	5.96
SFG-13	4.78	9.73	24.14	27.55	6.91
SFG-14	5.02	10.21	25.22	27.32	7.46
SFG-15	4.63	9.42	23.44	27.79	6.53
SFG-16	4.51	9.19	22.88	28.06	6.20
SFG-17	4.46	9.10	22.82	26.07	7.01
SFG-18	3.67	7.50	19.05	28.44	4.69
SFG-19	4.49	9.16	22.81	28.08	6.16
SFG-20	4.37	8.91	22.35	27.24	6.43
SFG-21	4.09	8.36	21.16	22.04	7.54
SFG-22	4.81	9.80	24.31	27.33	7.08
SFG-23	4.52	9.20	22.92	28.05	6.21
SFG-24	4.19	8.56	21.43	28.31	5.53
SFG-25	4.11	8.39	21.06	28.29	5.41
SFG-26	4.76	9.70	24.06	27.75	6.78
SFG-27	4.30	8.78	21.95	28.20	5.79
SFG-28	4.62	9.41	23.39	27.93	6.45
SFG-29	4.52	9.21	22.93	28.05	6.22
SFG-30	4.13	8.43	21.15	28.30	5.44
SFG-31	4.22	8.61	21.57	28.18	5.67
SFG-32	3.99	8.14	20.47	28.43	5.13
SFG-33	3.95	8.08	20.34	28.41	5.10
SFG-34	4.01	8.19	20.60	28.35	5.23
SFG-35	4.06	8.28	20.80	28.35	5.29
SFG-36	4.46	9.09	22.67	28.12	6.09
SFG-37	4.12	8.40	21.10	28.26	5.45
SFG-38	4.19	8.55	21.45	28.14	5.65

Table A16 *continued*

Table A16 (*continued*)

Reference number	He I λ 3614 [He I λ 5876=100]	He I λ 3965 [He I λ 5876=100]	He I λ 5016 [He I λ 5876=100]	He I λ 6678 [He I λ 5876=100]	He I λ 7281 [He I λ 5876=100]
SFG-39	4.58	9.34	23.31	27.04	6.81
SFG-40	4.62	9.42	23.47	27.26	6.77
SFG-41	4.54	9.25	23.03	28.02	6.27
SFG-42	4.55	9.27	23.09	27.79	6.40
SFG-43	4.31	8.79	21.98	28.23	5.77
SFG-44	4.58	9.32	23.19	27.98	6.35
SFG-45	4.82	9.82	24.34	27.65	6.94
SFG-46	4.49	9.16	22.81	28.08	6.16
SFG-47	4.46	9.08	22.66	27.96	6.16
SFG-48	4.77	9.71	24.15	25.26	7.73
SFG-49	4.43	9.04	22.68	23.98	7.56
SFG-50	5.10	10.38	25.62	27.15	7.70
SFG-51	4.87	9.92	24.60	25.71	7.76
SFG-52	4.93	10.02	24.83	26.91	7.47
SFG-53	4.84	9.86	24.43	27.62	7.00
SFG-54	4.88	9.93	24.59	27.56	7.09
SFG-55	4.33	8.85	22.24	23.41	7.56
SFG-56	4.63	9.43	23.45	27.91	6.48
SFG-57	4.69	9.54	23.69	27.85	6.60
SFG-58	4.52	9.22	22.97	27.80	6.34
SFG-59	4.55	9.28	23.15	27.31	6.63
SFG-60	4.36	8.89	22.36	24.25	7.39
SFG-61	4.36	8.90	22.37	24.26	7.39
SFG-62	4.44	9.05	22.71	26.01	7.01
SFG-63	4.18	8.54	21.62	26.30	6.63
SFG-64	4.78	9.73	24.19	26.11	7.48
SFG-65	4.75	9.67	24.05	27.06	7.10
SFG-66	5.08	10.34	25.52	27.20	7.64
SFG-67	3.95	8.08	20.45	20.37	7.59
SFG-68	4.60	9.38	23.32	27.95	6.42
SFG-69	4.48	9.13	22.88	26.42	6.93
SFG-70	4.69	9.56	23.73	27.84	6.62
SFG-71	5.03	10.24	25.30	27.19	7.56
SFG-72	4.13	8.44	21.44	25.79	6.79
SFG-73	4.18	8.52	21.35	28.32	5.49
SFG-74	4.28	8.73	21.84	28.25	5.71
SFG-75	4.50	9.17	22.87	27.83	6.29
SFG-76	4.75	9.66	24.05	25.74	7.55
SFG-77	4.82	9.82	24.39	26.02	7.59
SFG-78	4.78	9.73	24.16	27.16	7.10

Table A16 *continued*

Table A16 (*continued*)

Reference number	He I $\lambda 3614$ [He I $\lambda 5876=100$]	He I $\lambda 3965$ [He I $\lambda 5876=100$]	He I $\lambda 5016$ [He I $\lambda 5876=100$]	He I $\lambda 6678$ [He I $\lambda 5876=100$]	He I $\lambda 7281$ [He I $\lambda 5876=100$]
SFG-79	4.87	9.92	24.56	27.57	7.08
SFG-80	4.62	9.40	23.39	27.68	6.56
SFG-81	4.58	9.33	23.24	27.55	6.56
SFG-82	5.07	10.32	25.48	27.22	7.62
SFG-83	4.34	8.85	22.10	28.21	5.83
SFG-84	4.42	9.00	22.46	28.15	5.99
SFG-85	4.37	8.92	22.28	28.08	5.97
SFG-86	4.75	9.67	24.00	27.77	6.75
SFG-87	4.75	9.67	24.00	27.77	6.75
SFG-88	4.90	9.97	24.69	27.52	7.15
SFG-89	4.72	9.61	23.86	27.80	6.69
SFG-90	4.66	9.49	23.66	26.68	7.09

Table A17. Predicted He I fluxes for the sample of Planetary Nebulae considering T_e ([O III]) and the adopted average n_e using the atomic data of [Del Zanna & Storey \(2022\)](#) under the “Case B” of recombination. The fluxes are normalized relative to He I $\lambda 5876=100$.

Reference number	He I $\lambda 3614$ [He I $\lambda 5876=100$]	He I $\lambda 3965$ [He I $\lambda 5876=100$]	He I $\lambda 5016$ [He I $\lambda 5876=100$]	He I $\lambda 6678$ [He I $\lambda 5876=100$]	He I $\lambda 7281$ [He I $\lambda 5876=100$]
PNe-1	3.70	7.59	19.75	25.37	6.80
PNe-2	3.78	7.76	20.08	24.35	7.04
PNe-3	3.68	7.55	19.70	24.30	7.15
PNe-4	3.65	7.51	19.59	23.70	7.24
PNe-5	4.24	8.65	21.71	27.90	5.87
PNe-6	4.49	9.16	22.82	28.08	6.16
PNe-7	3.77	7.71	19.72	27.50	5.62
PNe-8	3.77	7.73	19.96	26.39	6.40
PNe-9	3.83	7.84	20.24	25.34	6.82
PNe-10	3.85	7.87	20.08	27.49	5.71
PNe-11	3.79	7.77	20.03	26.48	6.35
PNe-12	3.98	8.12	20.56	27.86	5.58
PNe-13	3.80	7.79	20.05	26.56	6.31
PNe-14	3.73	7.65	19.84	25.41	6.75
PNe-15	3.78	7.74	19.89	26.89	6.06
PNe-16	4.24	8.66	21.85	26.67	6.55
PNe-17	3.62	7.42	19.17	20.51	7.44
PNe-18	4.35	8.87	22.35	25.59	7.05

Table A17 *continued*

Table A17 (*continued*)

Reference number	He I λ 3614 [He I λ 5876=100]	He I λ 3965 [He I λ 5876=100]	He I λ 5016 [He I λ 5876=100]	He I λ 6678 [He I λ 5876=100]	He I λ 7281 [He I λ 5876=100]
PNe-19	3.71	7.61	19.63	26.90	6.05
PNe-20	3.63	7.47	19.55	23.96	7.26
PNe-21	4.16	8.51	21.54	26.53	6.53
PNe-22	3.83	7.83	20.00	27.42	5.74
PNe-23	3.79	7.78	20.13	24.64	7.04
PNe-24	3.71	7.61	19.80	24.72	7.00
PNe-25	3.68	7.55	19.43	27.35	5.75
PNe-26	3.72	7.63	19.64	27.04	5.94
PNe-27	3.73	7.65	19.71	26.87	6.07
PNe-28	3.93	8.04	20.47	27.32	5.91
PNe-29	3.92	8.02	20.49	26.61	6.26
PNe-30	3.87	7.92	20.25	27.15	5.98
PNe-31	3.87	7.93	20.42	24.55	7.02
PNe-32	4.30	8.78	22.07	27.14	6.40
PNe-33	3.74	7.67	19.77	26.81	6.10
PNe-34	3.63	7.46	19.52	23.76	7.27
PNe-35	4.10	8.38	21.18	27.38	6.00
PNe-36	3.71	7.61	19.58	27.19	5.84
PNe-37	3.75	7.68	19.84	26.56	6.28
PNe-38	4.02	8.21	20.74	27.90	5.60
PNe-39	4.06	8.30	21.06	26.83	6.25
PNe-40	3.70	7.60	19.74	26.11	6.55
PNe-41	3.82	7.83	20.15	26.35	6.40
PNe-42	3.90	8.00	20.52	25.85	6.62
PNe-43	3.82	7.83	20.07	26.99	6.04
PNe-44	3.79	7.77	20.09	23.76	7.16
PNe-45	3.68	7.55	19.69	24.82	6.99
PNe-46	3.68	7.55	19.51	26.96	6.00
PNe-47	4.05	8.28	20.93	27.69	5.76
PNe-48	3.85	7.89	20.36	25.13	6.91
PNe-49	3.75	7.70	19.87	26.54	6.30
PNe-50	3.66	7.50	19.22	27.82	5.35
PNe-51	3.53	7.24	18.49	28.38	4.65
PNe-52	3.69	7.57	19.44	27.53	5.60
PNe-53	3.74	7.66	19.76	26.76	6.15
PNe-54	3.76	7.69	19.71	27.34	5.72
PNe-55	3.86	7.92	20.33	26.20	6.46
PNe-56	3.90	7.99	20.50	25.81	6.64
PNe-57	3.82	7.82	20.14	26.32	6.42
PNe-58	3.96	8.09	20.57	27.34	5.89

Table A17 *continued*

Table A17 (*continued*)

Reference number	He I λ 3614 [He I λ 5876=100]	He I λ 3965 [He I λ 5876=100]	He I λ 5016 [He I λ 5876=100]	He I λ 6678 [He I λ 5876=100]	He I λ 7281 [He I λ 5876=100]
PNe-59	3.76	7.71	19.98	24.18	7.08
PNe-60	3.77	7.73	19.96	26.41	6.39
PNe-61	3.71	7.60	19.63	26.82	6.10
PNe-62	3.71	7.60	19.41	27.91	5.31
PNe-63	4.07	8.31	20.99	27.61	5.82
PNe-64	3.75	7.69	19.89	26.13	6.49
PNe-65	3.65	7.51	19.61	24.45	7.10
PNe-66	3.69	7.57	19.41	27.60	5.55
PNe-67	4.07	8.33	21.18	26.25	6.58
PNe-68	3.77	7.70	19.54	28.29	4.99
PNe-69	3.77	7.71	19.66	27.86	5.36
PNe-70	3.31	6.78	17.37	16.89	7.05
PNe-71	3.76	7.71	19.65	27.81	5.40
PNe-72	3.72	7.62	19.54	27.46	5.63
PNe-73	3.79	7.77	20.02	26.57	6.30
PNe-74	3.71	7.60	19.49	27.54	5.58
PNe-75	3.74	7.67	19.83	26.40	6.38
PNe-76	3.86	7.89	20.01	28.00	5.34
PNe-77	4.05	8.26	20.89	27.71	5.75
PNe-78	4.28	8.73	22.00	26.77	6.56
PNe-79	3.76	7.70	19.59	28.05	5.22
PNe-80	3.68	7.53	19.20	28.16	5.03
PNe-81	3.85	7.88	20.21	26.78	6.19
PNe-82	3.62	7.41	18.95	28.09	5.03
PNe-83	3.81	7.80	20.14	25.75	6.66
PNe-84	4.08	8.35	21.10	27.37	5.99
PNe-85	4.04	8.26	20.99	26.71	6.29
PNe-86	3.73	7.66	19.84	23.25	7.24
PNe-87	3.87	7.94	20.43	25.55	6.77
PNe-88	3.91	8.00	20.50	26.08	6.51
PNe-89	3.99	8.15	20.56	28.20	5.34
PNe-90	4.13	8.44	21.43	25.73	6.82
PNe-91	3.98	8.14	20.76	26.34	6.41
PNe-92	4.00	8.18	20.82	26.52	6.33
PNe-93	4.00	8.18	20.85	26.43	6.39
PNe-94	3.74	7.68	19.95	24.35	7.11
PNe-95	3.98	8.14	20.67	27.29	5.91
PNe-96	4.07	8.31	21.09	26.90	6.23
PNe-97	3.93	8.04	20.58	26.05	6.52
PNe-98	3.71	7.60	19.57	27.13	5.89

Table A17 *continued*

Table A17 (*continued*)

Reference number	He I λ 3614 [He I λ 5876=100]	He I λ 3965 [He I λ 5876=100]	He I λ 5016 [He I λ 5876=100]	He I λ 6678 [He I λ 5876=100]	He I λ 7281 [He I λ 5876=100]
PNe-99	3.82	7.82	19.99	27.31	5.81
PNe-100	3.82	7.82	20.02	27.16	5.92
PNe-101	3.12	6.44	17.10	18.61	7.43
PNe-102	3.91	8.01	20.55	25.69	6.69
PNe-103	3.86	7.91	20.29	26.48	6.33
PNe-104	3.84	7.87	20.16	26.96	6.08
PNe-105	3.83	7.84	20.16	26.57	6.29
PNe-106	4.25	8.67	21.72	28.11	5.76
PNe-107	4.27	8.72	21.83	28.03	5.84
PNe-108	3.42	7.04	18.60	21.60	7.50
PNe-109	3.70	7.57	19.32	28.04	5.17
PNe-110	4.19	8.55	21.43	28.23	5.58
PNe-111	3.95	8.09	20.58	27.11	6.00
PNe-112	3.78	7.74	20.00	26.10	6.51
PNe-113	3.70	7.59	19.73	25.66	6.72
PNe-114	3.87	7.92	20.19	27.47	5.75
PNe-115	3.87	7.91	20.01	28.21	5.17
PNe-116	4.09	8.35	21.04	27.85	5.68
PNe-117	3.75	7.70	19.98	24.52	7.10
PNe-118	3.65	7.51	19.62	23.97	7.25
PNe-119	3.73	7.64	19.69	26.94	6.02
PNe-120	4.02	8.23	21.01	25.51	6.85
PNe-121	3.89	7.96	20.20	27.83	5.51
PNe-122	4.19	8.54	21.43	28.12	5.65
PNe-123	3.65	7.49	19.59	24.05	7.23
PNe-124	3.80	7.78	20.08	26.08	6.53
PNe-125	4.09	8.35	20.96	28.38	5.32
PNe-126	3.88	7.96	20.39	26.42	6.35
PNe-127	4.38	8.92	22.27	28.19	5.90
PNe-128	3.58	7.33	18.68	28.37	4.67
PNe-129	3.81	7.80	19.94	27.35	5.77
PNe-130	3.99	8.14	20.56	28.05	5.43
PNe-131	3.68	7.56	19.70	24.72	7.02
PNe-132	3.54	7.26	18.48	28.52	4.46
PNe-133	3.88	7.93	20.02	28.34	5.07
PNe-134	3.92	8.02	20.33	27.88	5.51
PNe-135	3.61	7.39	18.87	28.22	4.89
PNe-136	3.80	7.76	19.69	28.26	5.05
PNe-137	3.82	7.82	19.94	27.57	5.63
PNe-138	4.38	8.93	22.36	27.65	6.22

Table A17 *continued*

Table A17 (*continued*)

Reference number	He I λ 3614 [He I λ 5876=100]	He I λ 3965 [He I λ 5876=100]	He I λ 5016 [He I λ 5876=100]	He I λ 6678 [He I λ 5876=100]	He I λ 7281 [He I λ 5876=100]
PNe-139	3.97	8.11	20.42	28.31	5.20
PNe-140	3.83	7.85	20.02	27.52	5.68
PNe-141	3.82	7.81	19.78	28.31	5.03
PNe-142	3.82	7.82	19.83	28.16	5.16
PNe-143	3.75	7.67	19.49	28.19	5.07
PNe-144	3.78	7.75	19.84	27.27	5.80
PNe-145	4.28	8.73	22.06	25.38	7.05
PNe-146	3.75	7.68	19.53	28.13	5.13
PNe-147	3.83	7.84	20.17	26.36	6.39
PNe-148	3.71	7.62	19.78	25.90	6.62
PNe-149	3.78	7.74	19.78	27.54	5.60
PNe-150	3.95	8.07	20.40	28.07	5.37
PNe-151	4.07	8.33	21.22	25.77	6.78
PNe-152	3.77	7.72	19.72	27.56	5.57
PNe-153	3.94	8.05	20.36	28.03	5.39
PNe-154	3.98	8.13	20.67	27.08	6.02
PNe-155	3.73	7.65	19.55	27.67	5.47
PNe-156	4.08	8.35	21.27	25.70	6.81
PNe-157	4.03	8.24	20.91	27.11	6.06
PNe-158	4.10	8.38	21.20	27.25	6.08
PNe-159	3.92	8.01	20.36	27.59	5.71
PNe-160	3.54	7.25	18.49	28.43	4.57
PNe-161	3.71	7.61	19.45	27.80	5.38
PNe-162	3.86	7.89	20.01	28.03	5.31
PNe-163	3.85	7.88	20.11	27.45	5.74
PNe-164	3.73	7.66	19.84	26.04	6.54
PNe-165	3.65	7.47	19.14	27.91	5.25
PNe-166	3.90	8.00	20.55	24.32	7.09
PNe-167	3.85	7.90	20.36	25.38	6.82
PNe-168	3.65	7.47	19.05	28.22	4.91
PNe-169	3.75	7.67	19.54	27.98	5.25
PNe-170	4.02	8.21	20.72	28.06	5.48
PNe-171	4.05	8.27	20.91	27.57	5.83
PNe-172	3.98	8.14	20.53	28.12	5.38
PNe-173	3.21	6.61	17.39	18.54	7.40
PNe-174	3.92	8.02	20.49	26.64	6.24
PNe-175	3.86	7.90	20.08	27.84	5.48
PNe-176	4.03	8.23	20.88	27.15	6.04
PNe-177	3.65	7.48	19.10	28.09	5.07
PNe-178	3.56	7.30	18.61	28.41	4.61

Table A17 *continued*

Table A17 (*continued*)

Reference number	He I λ 3614 [He I λ 5876=100]	He I λ 3965 [He I λ 5876=100]	He I λ 5016 [He I λ 5876=100]	He I λ 6678 [He I λ 5876=100]	He I λ 7281 [He I λ 5876=100]
PNe-179	4.00	8.18	20.75	27.23	5.96
PNe-180	3.80	7.78	19.96	27.01	6.00
PNe-181	3.80	7.78	19.95	27.12	5.92
PNe-182	3.80	7.79	19.92	27.37	5.75
PNe-183	3.68	7.54	19.32	27.79	5.40
PNe-184	3.81	7.80	20.04	26.78	6.18
PNe-185	3.61	7.39	18.79	28.49	4.57
PNe-186	3.74	7.67	19.85	25.87	6.59
PNe-187	3.72	7.62	19.54	27.50	5.60
PNe-188	3.72	7.63	19.80	25.83	6.62
PNe-189	3.51	7.19	18.38	28.42	4.57
PNe-190	3.98	8.13	20.47	28.34	5.19
PNe-191	4.02	8.20	20.63	28.35	5.24
PNe-192	3.81	7.81	19.95	27.44	5.71
PNe-193	3.98	8.13	20.47	28.32	5.21
PNe-194	3.97	8.11	20.41	28.38	5.15
PNe-195	3.61	7.40	18.87	28.30	4.80
PNe-196	3.94	8.05	20.49	27.39	5.88
PNe-197	3.77	7.71	19.61	28.06	5.21
PNe-198	3.95	8.08	20.41	28.12	5.34
PNe-199	4.13	8.42	21.18	28.02	5.62
PNe-200	3.80	7.78	20.09	25.88	6.60
PNe-201	3.73	7.63	19.44	28.07	5.17
PNe-202	3.99	8.16	20.81	26.35	6.42
PNe-203	3.74	7.67	19.79	26.70	6.19
PNe-204	3.81	7.79	19.79	28.09	5.22
PNe-205	4.08	8.32	20.94	28.18	5.46
PNe-206	3.97	8.11	20.60	27.31	5.91
PNe-207	3.56	7.30	18.71	28.16	4.92
PNe-208	3.92	8.02	20.27	28.12	5.30
PNe-209	4.27	8.71	21.94	27.15	6.35
PNe-210	3.77	7.72	19.73	27.59	5.56
PNe-211	3.97	8.12	20.53	27.94	5.51
PNe-212	3.90	7.98	20.48	25.91	6.59
PNe-213	3.70	7.58	19.47	27.45	5.66
PNe-214	3.77	7.73	19.95	26.49	6.34
PNe-215	3.73	7.64	19.81	26.07	6.54
PNe-216	4.11	8.39	21.04	28.37	5.35
PNe-217	3.71	7.59	19.34	28.10	5.12
PNe-218	4.57	9.30	23.15	27.99	6.33

Table A18. Predicted He I fluxes for the sample of H II regions considering $T_e(\text{He I})$ and the adopted average n_e using the atomic data of [Del Zanna & Storey \(2022\)](#) under the “Case B” of recombination. The fluxes are normalized relative to He I $\lambda 5876=100$.

Reference number	He I $\lambda 3614$	He I $\lambda 3965$	He I $\lambda 5016$	He I $\lambda 6678$	He I $\lambda 7281$
	[He I $\lambda 5876=100$]				
HII-1	3.16	6.50	16.71	28.71	3.78
HII-2	3.18	6.53	16.78	28.70	3.80
HII-3	3.59	7.34	18.65	28.57	4.45
HII-4	4.34	8.84	22.11	28.10	5.90
HII-5	3.56	7.28	18.52	28.56	4.43
HII-6	3.47	7.12	18.12	28.63	4.24
HII-7	3.37	6.92	17.67	28.66	4.09
HII-8	3.20	6.58	16.89	28.70	3.84
HII-9	4.32	8.80	22.00	28.23	5.78
HII-10	3.62	7.41	18.78	28.58	4.48
HII-11	4.32	8.81	22.01	28.22	5.79
HII-12	3.80	7.77	19.61	28.51	4.78
HII-13	4.20	8.57	21.46	28.31	5.54
HII-14	4.43	9.02	22.50	28.15	6.01
HII-15	3.80	7.77	19.61	28.51	4.78
HII-16	3.65	7.46	18.91	28.57	4.53
HII-17	3.43	7.04	17.93	28.64	4.18
HII-18	5.13	10.43	25.73	27.08	7.78
HII-19	3.77	7.71	19.50	28.48	4.79
HII-20	2.96	6.10	15.78	28.76	3.49
HII-21	3.41	6.98	17.81	28.65	4.14
HII-22	4.52	9.22	22.95	28.04	6.23
HII-23	3.49	7.16	18.21	28.62	4.28
HII-24	3.27	6.72	17.22	28.68	3.95
HII-25	3.75	7.67	19.38	28.53	4.70
HII-26	3.36	6.90	17.62	28.66	4.08
HII-27	3.49	7.15	18.20	28.62	4.27
HII-28	4.08	8.32	20.89	28.36	5.31
HII-29	3.33	6.84	17.48	28.67	4.03
HII-30	2.71	5.60	14.61	28.81	3.15
HII-31	4.17	8.51	21.33	28.33	5.48
HII-32	2.36	4.91	12.99	28.90	2.71
HII-33	3.51	7.19	18.30	28.59	4.33
HII-34	3.89	7.95	20.06	28.40	5.02
HII-35	3.73	7.64	19.57	27.53	5.57
HII-36	3.88	7.93	20.09	28.04	5.32

Table A18 *continued*

Table A18 (*continued*)

Reference number	He I λ 3614 [He I λ 5876=100]	He I λ 3965 [He I λ 5876=100]	He I λ 5016 [He I λ 5876=100]	He I λ 6678 [He I λ 5876=100]	He I λ 7281 [He I λ 5876=100]
HII-37	3.71	7.59	19.41	27.90	5.31
HII-38	3.97	8.13	20.62	27.53	5.80
HII-39	3.63	7.44	19.02	28.10	5.04
HII-40	3.68	7.54	19.27	27.98	5.21
HII-41	3.60	7.38	18.83	28.26	4.85
HII-42	3.66	7.49	19.14	28.09	5.08
HII-43	3.68	7.53	19.21	28.12	5.07
HII-44	3.51	7.20	18.41	28.41	4.60
HII-45	3.58	7.34	18.71	28.37	4.68
HII-46	3.59	7.36	18.74	28.41	4.64
HII-47	3.78	7.73	19.60	28.30	4.99
HII-48	3.90	7.98	20.25	27.83	5.53
HII-49	3.78	7.75	19.72	27.90	5.35
HII-50	3.11	6.39	16.46	28.73	3.70
HII-51	3.47	7.12	18.14	28.61	4.27
HII-52	3.91	8.00	20.24	28.08	5.32
HII-53	3.24	6.66	17.08	28.69	3.90
HII-54	3.50	7.18	18.28	28.60	4.32
HII-55	3.91	8.00	20.17	28.37	5.08
HII-56	3.83	7.84	19.77	28.50	4.85
HII-57	3.86	7.89	19.91	28.45	4.94
HII-58	2.76	5.69	14.83	28.80	3.22
HII-59	2.08	4.36	11.69	28.94	2.39
HII-60	3.68	7.53	19.05	28.56	4.58
HII-61	3.33	6.84	17.47	28.67	4.03
HII-62	3.86	7.89	19.89	28.48	4.90
HII-63	4.31	8.78	21.96	28.23	5.76
HII-64	3.92	8.00	20.16	28.46	5.00
HII-65	4.00	8.17	20.53	28.42	5.15
HII-66	3.23	6.63	17.00	28.69	3.87
HII-67	4.01	8.20	20.60	28.41	5.18
HII-68	4.34	8.84	22.09	28.21	5.83
HII-69	4.25	8.67	21.70	28.27	5.65
HII-70	3.99	8.15	20.48	28.43	5.13
HII-71	3.84	7.86	19.82	28.48	4.88
HII-72	4.17	8.51	21.34	28.33	5.48
HII-73	4.20	8.58	21.48	28.30	5.55
HII-74	4.46	9.08	22.64	28.12	6.08
HII-75	4.28	8.72	21.81	28.25	5.70
HII-76	4.15	8.48	21.26	28.28	5.49

Table A18 *continued*

Table A18 (*continued*)

Reference number	He I $\lambda 3614$ [He I $\lambda 5876=100$]	He I $\lambda 3965$ [He I $\lambda 5876=100$]	He I $\lambda 5016$ [He I $\lambda 5876=100$]	He I $\lambda 6678$ [He I $\lambda 5876=100$]	He I $\lambda 7281$ [He I $\lambda 5876=100$]
HII-77	4.07	8.31	20.88	28.38	5.29
HII-78	4.34	8.85	22.10	28.21	5.83
HII-79	4.72	9.62	23.95	26.15	7.37
HII-80	4.99	10.15	25.10	25.23	8.11
HII-81	4.18	8.53	21.44	27.82	5.82
HII-82	5.00	10.17	25.15	24.50	8.40
HII-83	4.25	8.66	21.68	28.27	5.64
HII-84	4.16	8.49	21.30	28.22	5.55
HII-85	5.51	11.21	27.48	25.80	9.09

Table A19. Predicted HeI fluxes for the sample of Star Forming Galaxies considering $T_e(\text{HeI})$ and the adopted average n_e using the atomic data of [Del Zanna & Storey \(2022\)](#) under the “Case B” of recombination. The fluxes are normalized relative to HeI $\lambda 5876=100$.

Reference number	He I $\lambda 3614$ [He I $\lambda 5876=100$]	He I $\lambda 3965$ [He I $\lambda 5876=100$]	He I $\lambda 5016$ [He I $\lambda 5876=100$]	He I $\lambda 6678$ [He I $\lambda 5876=100$]	He I $\lambda 7281$ [He I $\lambda 5876=100$]
SFG-1	4.30	8.77	21.92	28.24	5.75
SFG-2	4.43	9.02	22.54	27.76	6.22
SFG-3	4.84	9.85	24.41	27.63	6.98
SFG-4	3.73	7.64	19.31	28.54	4.67
SFG-5	3.79	7.76	19.58	28.52	4.77
SFG-6	4.24	8.65	21.65	28.19	5.69
SFG-7	4.46	9.10	22.67	28.11	6.09
SFG-8	3.86	7.88	19.87	28.49	4.89
SFG-9	5.25	10.69	26.28	24.30	9.00
SFG-10	4.25	8.68	21.71	28.27	5.65
SFG-11	4.44	9.05	22.57	28.14	6.04
SFG-12	4.22	8.60	21.53	28.30	5.57
SFG-13	3.95	8.07	20.32	28.44	5.07
SFG-14	3.63	7.42	18.82	28.58	4.49
SFG-15	3.68	7.53	19.06	28.55	4.59
SFG-16	3.97	8.10	20.39	28.44	5.09
SFG-17	4.20	8.58	21.57	27.60	5.98
SFG-18	3.30	6.78	17.36	28.67	4.00
SFG-19	3.76	7.69	19.42	28.53	4.71
SFG-20	3.76	7.69	19.46	28.45	4.81
SFG-21	4.23	8.63	21.83	25.78	6.85

Table A19 *continued*

Table A19 (*continued*)

Reference number	He I λ 3614 [He I λ 5876=100]	He I λ 3965 [He I λ 5876=100]	He I λ 5016 [He I λ 5876=100]	He I λ 6678 [He I λ 5876=100]	He I λ 7281 [He I λ 5876=100]
SFG-22	4.36	8.90	22.23	28.11	5.94
SFG-23	4.26	8.68	21.72	28.27	5.66
SFG-24	3.68	7.54	19.09	28.56	4.59
SFG-25	3.79	7.76	19.59	28.49	4.80
SFG-26	4.42	9.01	22.46	28.16	5.99
SFG-27	3.90	7.97	20.07	28.46	4.98
SFG-28	5.09	10.34	25.54	27.19	7.65
SFG-29	3.55	7.27	18.47	28.60	4.36
SFG-30	3.74	7.66	19.36	28.52	4.71
SFG-31	3.63	7.44	18.87	28.55	4.54
SFG-32	3.77	7.72	19.49	28.52	4.74
SFG-33	3.87	7.91	19.96	28.46	4.95
SFG-34	3.79	7.75	19.58	28.49	4.80
SFG-35	4.06	8.30	20.84	28.34	5.31
SFG-36	3.56	7.30	18.54	28.60	4.39
SFG-37	3.80	7.77	19.63	28.49	4.82
SFG-38	3.42	7.01	17.89	28.64	4.17
SFG-39	4.00	8.17	20.57	28.30	5.25
SFG-40	4.25	8.68	21.73	28.10	5.77
SFG-41	4.30	8.76	21.90	28.24	5.74
SFG-42	4.44	9.06	22.60	27.98	6.13
SFG-43	3.73	7.63	19.30	28.54	4.67
SFG-44	4.92	10.00	24.75	27.50	7.19
SFG-45	4.47	9.11	22.70	28.11	6.11
SFG-46	3.71	7.60	19.22	28.55	4.64
SFG-47	3.77	7.72	19.50	28.51	4.75
SFG-48	4.31	8.79	22.03	27.81	6.03
SFG-49	4.23	8.63	21.73	27.40	6.15
SFG-50	4.98	10.13	25.05	27.38	7.37
SFG-51	4.40	8.98	22.45	27.80	6.18
SFG-52	5.07	10.31	25.46	26.01	8.02
SFG-53	4.45	9.07	22.62	28.13	6.06
SFG-54	4.26	8.68	21.71	28.27	5.65
SFG-55	4.29	8.75	22.03	27.00	6.46
SFG-56	5.40	10.98	26.96	26.28	8.64
SFG-57	3.82	7.81	19.71	28.50	4.82
SFG-58	3.42	7.02	17.89	28.64	4.16
SFG-59	3.89	7.96	20.06	28.43	5.00
SFG-60	4.36	8.90	22.38	24.16	7.43
SFG-61	4.37	8.91	22.41	24.09	7.46

Table A19 *continued*

Table A19 (*continued*)

Reference number	He I $\lambda 3614$ [He I $\lambda 5876=100$]	He I $\lambda 3965$ [He I $\lambda 5876=100$]	He I $\lambda 5016$ [He I $\lambda 5876=100$]	He I $\lambda 6678$ [He I $\lambda 5876=100$]	He I $\lambda 7281$ [He I $\lambda 5876=100$]
SFG-62	3.80	7.77	19.65	28.40	4.91
SFG-63	3.69	7.56	19.19	28.39	4.79
SFG-64	3.37	6.92	17.66	28.65	4.09
SFG-65	4.23	8.64	21.64	28.16	5.71
SFG-66	5.11	10.40	25.66	27.12	7.73
SFG-67	4.12	8.42	21.30	27.14	6.17
SFG-68	4.32	8.81	22.01	28.22	5.79
SFG-69	4.19	8.56	21.53	27.67	5.93
SFG-70	3.37	6.92	17.66	28.66	4.09
SFG-71	4.19	8.54	21.40	28.30	5.52
SFG-72	3.94	8.06	20.43	27.84	5.56
SFG-73	3.79	7.76	19.59	28.52	4.78
SFG-74	4.52	9.21	22.94	28.04	6.23
SFG-75	4.23	8.62	21.59	28.24	5.63
SFG-76	4.12	8.42	21.15	28.15	5.54
SFG-77	4.13	8.43	21.16	28.22	5.50
SFG-78	4.57	9.31	23.20	27.54	6.55
SFG-79	3.93	8.02	20.20	28.45	5.02
SFG-80	3.54	7.24	18.41	28.60	4.35
SFG-81	5.19	10.56	26.01	24.70	8.76
SFG-82	4.72	9.61	23.86	27.81	6.68
SFG-83	3.78	7.74	19.54	28.52	4.76
SFG-84	3.51	7.20	18.30	28.62	4.30
SFG-85	3.73	7.64	19.32	28.52	4.69
SFG-86	4.06	8.28	20.80	28.39	5.26
SFG-87	4.82	9.80	24.30	27.67	6.92
SFG-88	5.06	10.29	25.42	27.25	7.58
SFG-89	4.14	8.44	21.16	28.35	5.40
SFG-90	4.86	9.90	24.52	23.91	8.28

Table A20. Predicted HeI fluxes for the sample of Planetary Nebulae considering $T_e(\text{HeI})$ and the adopted average n_e using the atomic data of Del Zanna & Storey (2022) under the “Case B” of recombination. The fluxes are normalized relative to HeI $\lambda 5876=100$.

Reference number	He I $\lambda 3614$ [He I $\lambda 5876=100$]	He I $\lambda 3965$ [He I $\lambda 5876=100$]	He I $\lambda 5016$ [He I $\lambda 5876=100$]	He I $\lambda 6678$ [He I $\lambda 5876=100$]	He I $\lambda 7281$ [He I $\lambda 5876=100$]
PNe-1	3.22	6.65	17.63	19.61	7.51

Table A20 *continued*

Table A20 (*continued*)

Reference number	He I λ 3614 [He I λ 5876=100]	He I λ 3965 [He I λ 5876=100]	He I λ 5016 [He I λ 5876=100]	He I λ 6678 [He I λ 5876=100]	He I λ 7281 [He I λ 5876=100]
PNe-2	3.76	7.70	19.71	27.47	5.63
PNe-3	3.70	7.58	19.46	27.48	5.63
PNe-4	3.72	7.63	19.61	27.22	5.81
PNe-5	4.15	8.47	21.27	28.07	5.62
PNe-6	4.15	8.47	21.24	28.34	5.44
PNe-7	3.40	6.98	17.85	28.55	4.29
PNe-8	3.32	6.82	17.48	28.60	4.15
PNe-9	3.79	7.77	19.93	27.10	5.93
PNe-10	3.71	7.60	19.36	28.12	5.10
PNe-11	3.48	7.12	18.22	28.45	4.51
PNe-12	2.61	5.40	14.16	28.85	3.01
PNe-13	3.46	7.09	18.14	28.47	4.47
PNe-14	3.55	7.28	18.64	28.22	4.84
PNe-15	3.28	6.74	17.29	28.64	4.04
PNe-16	3.32	6.81	17.42	28.66	4.03
PNe-17	3.89	7.96	20.29	27.38	5.83
PNe-18	3.51	7.19	18.30	28.58	4.35
PNe-19	3.20	6.57	16.89	28.69	3.88
PNe-20	3.55	7.28	18.65	28.19	4.88
PNe-21	2.90	5.99	15.52	28.78	3.41
PNe-22	3.86	7.90	20.20	27.20	5.93
PNe-23	3.57	7.31	18.67	28.32	4.74
PNe-24	3.67	7.51	19.24	27.87	5.31
PNe-25	3.57	7.31	18.75	28.08	5.01
PNe-26	3.60	7.39	18.92	28.03	5.09
PNe-27	3.69	7.57	19.44	27.50	5.62
PNe-28	3.42	7.01	17.92	28.58	4.26
PNe-29	3.51	7.20	18.37	28.48	4.48
PNe-30	3.73	7.64	19.48	28.01	5.22
PNe-31	3.31	6.81	17.67	18.19	7.26
PNe-32	3.22	6.61	16.96	28.69	3.86
PNe-33	3.54	7.26	18.57	28.27	4.78
PNe-34	3.52	7.21	18.46	28.32	4.72
PNe-35	3.98	8.12	20.54	27.96	5.49
PNe-36	3.70	7.59	19.50	27.37	5.71
PNe-37	3.05	6.29	16.70	17.78	7.38
PNe-38	3.23	6.63	17.01	28.69	3.88
PNe-39	2.45	5.09	13.43	28.89	2.82
PNe-40	3.59	7.35	18.88	27.96	5.15
PNe-41	3.73	7.65	19.60	27.45	5.63

Table A20 *continued*

Table A20 (*continued*)

Reference number	He I λ 3614 [He I λ 5876=100]	He I λ 3965 [He I λ 5876=100]	He I λ 5016 [He I λ 5876=100]	He I λ 6678 [He I λ 5876=100]	He I λ 7281 [He I λ 5876=100]
PNe-42	3.77	7.71	19.65	27.88	5.35
PNe-43	3.73	7.65	19.55	27.66	5.48
PNe-44	3.79	7.76	19.82	27.56	5.60
PNe-45	3.63	7.44	19.07	27.91	5.24
PNe-46	3.62	7.42	19.06	27.81	5.33
PNe-47	3.19	6.56	16.85	28.70	3.83
PNe-48	3.84	7.85	20.11	27.07	6.00
PNe-49	3.41	7.00	17.94	28.50	4.39
PNe-50	3.52	7.21	18.47	28.31	4.72
PNe-51	3.39	6.96	17.83	28.53	4.32
PNe-52	3.33	6.84	17.54	28.58	4.18
PNe-53	3.68	7.55	19.36	27.71	5.47
PNe-54	3.29	6.75	17.30	28.63	4.05
PNe-55	3.45	7.07	18.06	28.52	4.38
PNe-56	3.48	7.13	18.20	28.52	4.41
PNe-57	3.66	7.51	19.18	28.03	5.14
PNe-58	2.89	5.96	15.46	28.78	3.39
PNe-59	2.46	5.10	13.47	28.90	2.82
PNe-60	3.76	7.71	19.88	26.58	6.27
PNe-61	3.67	7.53	19.34	27.63	5.55
PNe-62	3.82	7.83	20.11	26.77	6.20
PNe-63	3.59	7.36	18.72	28.50	4.55
PNe-64	3.72	7.62	19.60	27.16	5.85
PNe-65	3.54	7.27	18.62	28.21	4.86
PNe-66	2.58	5.34	14.04	28.87	2.96
PNe-67	3.70	7.58	19.26	28.29	4.91
PNe-68	3.08	6.33	16.32	28.73	3.66
PNe-69	3.48	7.14	18.24	28.51	4.43
PNe-70	3.59	7.35	18.74	28.37	4.68
PNe-71	2.82	5.82	15.14	28.81	3.29
PNe-72	3.58	7.33	18.74	28.23	4.86
PNe-73	3.52	7.21	18.43	28.39	4.63
PNe-74	3.67	7.52	19.25	27.89	5.29
PNe-75	3.36	6.89	17.66	28.54	4.26
PNe-76	2.18	4.56	12.18	28.96	2.50
PNe-77	3.19	6.56	16.85	28.70	3.83
PNe-78	3.82	7.82	19.79	28.33	5.02
PNe-79	3.08	6.33	16.32	28.73	3.66
PNe-80	2.37	4.94	13.09	28.92	2.72
PNe-81	3.37	6.92	17.72	28.57	4.24

Table A20 *continued*

Table A20 (*continued*)

Reference number	He I λ 3614 [He I λ 5876=100]	He I λ 3965 [He I λ 5876=100]	He I λ 5016 [He I λ 5876=100]	He I λ 6678 [He I λ 5876=100]	He I λ 7281 [He I λ 5876=100]
PNe-82	3.03	6.23	16.10	28.76	3.58
PNe-83	2.84	5.87	15.26	28.80	3.32
PNe-84	3.72	7.62	19.32	28.38	4.84
PNe-85	3.22	6.62	16.99	28.69	3.88
PNe-86	3.70	7.57	19.30	28.08	5.12
PNe-87	3.76	7.70	19.68	27.62	5.53
PNe-88	3.71	7.60	19.36	28.11	5.11
PNe-89	3.97	8.11	20.46	28.24	5.28
PNe-90	2.02	4.25	11.46	28.99	2.32
PNe-91	2.90	5.98	15.52	28.78	3.40
PNe-92	3.64	7.45	18.96	28.33	4.78
PNe-93	3.12	6.41	16.51	28.72	3.73
PNe-94	3.72	7.61	19.49	27.64	5.50
PNe-95	4.03	8.25	20.95	26.81	6.23
PNe-96	3.92	8.02	20.31	27.93	5.47
PNe-97	3.57	7.32	18.67	28.37	4.67
PNe-98	3.43	7.03	18.01	28.46	4.45
PNe-99	3.24	6.65	17.08	28.68	3.93
PNe-100	3.62	7.42	18.92	28.24	4.88
PNe-101	3.61	7.39	18.95	28.01	5.12
PNe-102	3.07	6.31	16.28	28.74	3.65
PNe-103	3.77	7.73	19.76	27.49	5.63
PNe-104	3.16	6.49	16.69	28.71	3.79
PNe-105	3.25	6.68	17.14	28.67	3.96
PNe-106	4.57	9.30	23.20	27.37	6.62
PNe-107	3.12	6.41	16.49	28.72	3.71
PNe-108	3.55	7.29	18.67	28.18	4.90
PNe-109	3.39	6.95	17.79	28.56	4.26
PNe-110	4.96	10.09	24.98	26.20	7.75
PNe-111	2.97	6.12	15.82	28.76	3.49
PNe-112	3.59	7.36	18.84	28.14	4.96
PNe-113	3.68	7.54	19.38	27.51	5.64
PNe-114	2.95	6.08	15.75	28.77	3.47
PNe-115	3.93	8.04	20.33	28.07	5.36
PNe-116	3.92	8.01	20.22	28.28	5.18
PNe-117	3.72	7.62	19.53	27.53	5.58
PNe-118	3.75	7.70	19.90	26.39	6.40
PNe-119	3.47	7.11	18.21	28.44	4.53
PNe-120	2.90	5.98	15.51	28.78	3.40
PNe-121	3.90	7.97	20.25	27.78	5.56

Table A20 *continued*

Table A20 (*continued*)

Reference number	He I λ 3614 [He I λ 5876=100]	He I λ 3965 [He I λ 5876=100]	He I λ 5016 [He I λ 5876=100]	He I λ 6678 [He I λ 5876=100]	He I λ 7281 [He I λ 5876=100]
PNe-122	4.66	9.50	23.66	26.96	6.99
PNe-123	3.61	7.40	18.96	28.01	5.12
PNe-124	3.60	7.38	18.86	28.17	4.94
PNe-125	3.12	6.42	16.50	28.71	3.72
PNe-126	3.33	6.84	17.51	28.61	4.11
PNe-127	3.34	6.86	17.52	28.66	4.04
PNe-128	3.55	7.28	18.57	28.41	4.60
PNe-129	3.59	7.35	18.75	28.31	4.76
PNe-130	3.70	7.57	19.20	28.43	4.75
PNe-131	3.56	7.29	18.68	28.18	4.90
PNe-132	2.95	6.08	15.74	28.76	3.47
PNe-133	2.33	4.84	12.85	28.91	2.67
PNe-134	2.64	5.47	14.32	28.84	3.06
PNe-135	2.90	5.99	15.54	28.79	3.40
PNe-136	2.20	4.60	12.28	28.95	2.52
PNe-137	2.26	4.72	12.58	28.95	2.59
PNe-138	3.56	7.29	18.53	28.58	4.41
PNe-139	2.15	4.49	12.01	28.95	2.46
PNe-140	2.75	5.68	14.81	28.83	3.19
PNe-141	2.38	4.95	13.12	28.90	2.74
PNe-142	3.23	6.64	17.04	28.69	3.90
PNe-143	3.56	7.29	18.57	28.42	4.59
PNe-144	3.33	6.83	17.51	28.60	4.14
PNe-145	3.86	7.89	19.97	28.22	5.15
PNe-146	3.59	7.35	18.73	28.36	4.70
PNe-147	3.50	7.17	18.33	28.45	4.54
PNe-148	3.56	7.30	18.71	28.15	4.94
PNe-149	3.70	7.57	19.31	28.09	5.12
PNe-150	2.16	4.51	12.07	28.96	2.47
PNe-151	3.12	6.42	16.52	28.72	3.73
PNe-152	3.31	6.80	17.43	28.62	4.09
PNe-153	2.90	5.98	15.50	28.78	3.40
PNe-154	3.11	6.39	16.46	28.72	3.71
PNe-155	3.08	6.33	16.33	28.74	3.66
PNe-156	3.46	7.09	18.09	28.57	4.30
PNe-157	3.23	6.63	17.02	28.69	3.89
PNe-158	3.15	6.48	16.65	28.71	3.76
PNe-159	2.73	5.64	14.71	28.83	3.17
PNe-160	3.66	7.50	19.11	28.20	4.96
PNe-161	3.49	7.15	18.27	28.47	4.50

Table A20 *continued*

Table A20 (*continued*)

Reference number	He I λ 3614 [He I λ 5876=100]	He I λ 3965 [He I λ 5876=100]	He I λ 5016 [He I λ 5876=100]	He I λ 6678 [He I λ 5876=100]	He I λ 7281 [He I λ 5876=100]
PNe-162	2.82	5.82	15.13	28.80	3.29
PNe-163	3.47	7.12	18.17	28.53	4.39
PNe-164	3.68	7.55	19.38	27.62	5.54
PNe-165	3.11	6.39	16.47	28.72	3.72
PNe-166	3.61	7.39	18.84	28.31	4.77
PNe-167	3.70	7.58	19.32	28.05	5.16
PNe-168	3.26	6.70	17.19	28.67	3.96
PNe-169	3.38	6.93	17.74	28.58	4.21
PNe-170	2.55	5.29	13.91	28.86	2.95
PNe-171	2.56	5.30	13.92	28.86	2.95
PNe-172	2.12	4.45	11.92	28.96	2.44
PNe-173	3.34	6.86	17.58	28.58	4.19
PNe-174	3.72	7.62	19.38	28.14	5.08
PNe-175	2.61	5.40	14.16	28.85	3.01
PNe-176	1.91	4.03	10.94	29.01	2.21
PNe-177	3.37	6.91	17.70	28.55	4.25
PNe-178	3.13	6.43	16.54	28.71	3.74
PNe-179	2.76	5.70	14.86	28.82	3.21
PNe-180	3.27	6.72	17.24	28.65	4.01
PNe-181	3.26	6.70	17.20	28.66	3.99
PNe-182	3.09	6.35	16.36	28.73	3.67
PNe-183	3.08	6.34	16.35	28.73	3.68
PNe-184	3.72	7.63	19.52	27.60	5.53
PNe-185	2.80	5.79	15.06	28.80	3.27
PNe-186	3.67	7.53	19.67	24.12	7.21
PNe-187	3.11	6.40	16.50	28.72	3.72
PNe-188	3.40	7.01	18.51	21.32	7.53
PNe-189	3.19	6.55	16.85	28.70	3.85
PNe-190	2.70	5.58	14.57	28.82	3.14
PNe-191	1.89	3.98	10.80	29.00	2.19
PNe-192	2.21	4.62	12.34	28.96	2.53
PNe-193	1.89	3.99	10.83	29.00	2.19
PNe-194	2.18	4.54	12.14	28.94	2.49
PNe-195	3.31	6.79	17.39	28.65	4.04
PNe-196	3.04	6.25	16.13	28.74	3.59
PNe-197	2.81	5.81	15.11	28.81	3.28
PNe-198	2.68	5.54	14.48	28.83	3.11
PNe-199	2.17	4.54	12.14	28.95	2.49
PNe-200	3.31	6.79	17.42	28.61	4.11
PNe-201	3.18	6.54	16.80	28.70	3.83

Table A20 *continued*

Table A20 (*continued*)

Reference number	He I $\lambda 3614$ [He I $\lambda 5876=100$]	He I $\lambda 3965$ [He I $\lambda 5876=100$]	He I $\lambda 5016$ [He I $\lambda 5876=100$]	He I $\lambda 6678$ [He I $\lambda 5876=100$]	He I $\lambda 7281$ [He I $\lambda 5876=100$]
PNe-202	3.57	7.32	18.65	28.40	4.63
PNe-203	3.55	7.27	18.61	28.23	4.83
PNe-204	3.44	7.06	18.01	28.58	4.28
PNe-205	2.09	4.37	11.74	28.97	2.40
PNe-206	2.04	4.27	11.51	28.98	2.34
PNe-207	3.29	6.75	17.34	28.62	4.08
PNe-208	3.25	6.67	17.10	28.68	3.91
PNe-209	3.74	7.64	19.37	28.42	4.81
PNe-210	3.60	7.38	18.82	28.29	4.80
PNe-211	2.77	5.72	14.90	28.81	3.23
PNe-212	3.43	7.02	17.95	28.55	4.31
PNe-213	2.82	5.82	15.16	28.81	3.28
PNe-214	3.24	6.66	17.10	28.67	3.96
PNe-215	3.71	7.62	19.65	26.89	6.06
PNe-216	3.73	7.64	19.32	28.54	4.68
PNe-217	3.21	6.60	16.95	28.69	3.88
PNe-218	4.76	9.68	24.02	27.76	6.76

Table A21. Electron temperatures derived from the sample of H II regions, considering the toy model described in Sec. 4.3, which accounts for mixed Case A-Case B conditions.

Reference number	γ_{5016}	$T_e(\text{He I } \lambda 7281/\lambda 5876)_{TM}$	$T_e(\text{He I } \lambda 7281/\lambda 6678)_{TM}$	Average $T_e(\text{He I})_{TM}$
		[K]	[K]	[K]
HII-1	0.87	5390 ± 490	5670^{+550}_{-540}	5530^{+550}_{-540}
HII-2	0.95	5010^{+1160}_{-850}	5200^{+1050}_{-880}	5110^{+1090}_{-870}
HII-3	0.89	7640^{+710}_{-570}	7460^{+750}_{-620}	7570^{+720}_{-620}
HII-4	0.78	14550^{+1230}_{-1190}	-	14550^{+1230}_{-1190}
HII-5	0.93	7190^{+1300}_{-1130}	6860^{+1320}_{-1200}	7010^{+1310}_{-1160}
HII-7	0.93	6240^{+700}_{-720}	6230^{+840}_{-770}	6230^{+770}_{-750}
HII-8	0.97	4470^{+540}_{-550}	5640^{+760}_{-700}	4980^{+1030}_{-810}
HII-9	0.76	13560^{+4760}_{-3890}	14850^{+4670}_{-4100}	14200^{+4740}_{-4120}
HII-11	0.69	15200^{+4450}_{-4050}	15240^{+3770}_{-3900}	15230^{+4100}_{-3970}
HII-13	0.78	11220^{+4480}_{-4030}	14770^{+5380}_{-4870}	12740^{+5600}_{-4610}
HII-21	0.93	5600^{+1260}_{-1070}	6910^{+1410}_{-1390}	6210^{+1500}_{-1420}
HII-23	0.83	7190^{+950}_{-890}	7780^{+1150}_{-1030}	7460^{+1170}_{-1010}
HII-24	0.86	5960^{+1550}_{-1340}	6400^{+1690}_{-1510}	6190^{+1600}_{-1460}
HII-28	0.85	10970^{+3500}_{-2830}	11770^{+3570}_{-3080}	11400^{+3500}_{-2970}

Table A21 *continued*

Table A21 (*continued*)

Reference number	γ_{5016}	$T_e(\text{He I } \lambda 7281/\lambda 5876)_{TM}$	$T_e(\text{He I } \lambda 7281/\lambda 6678)_{TM}$	Average $T_e(\text{He I})_{TM}$
		[K]	[K]	[K]
HII-29	0.92	5770^{+990}_{-830}	6410^{+960}_{-980}	6090^{+990}_{-940}
HII-31	0.73	13460^{+4480}_{-3860}	13170^{+4580}_{-3540}	13290^{+4530}_{-3680}
HII-32	0.96	1960^{+430}_{-370}	2320^{+520}_{-450}	2130^{+550}_{-430}
HII-33	0.90	7250^{+800}_{-740}	6800^{+830}_{-710}	7060^{+810}_{-790}
HII-34	0.99	8880^{+1020}_{-970}	8520 ± 980	8700^{+1010}_{-1020}
HII-35	1.00	8980^{+670}_{-630}	8130^{+470}_{-520}	8480^{+800}_{-660}
HII-36	0.96	8490^{+520}_{-560}	9750^{+520}_{-540}	9110^{+880}_{-870}
HII-39	0.80	8200^{+550}_{-540}	8550 ± 430	8400^{+490}_{-540}
HII-41	0.81	7680^{+540}_{-520}	8260^{+460}_{-450}	8000^{+540}_{-590}
HII-42	0.95	7850^{+580}_{-560}	7630^{+430}_{-450}	7730^{+510}_{-500}
HII-43	0.90	7380^{+780}_{-810}	8910^{+930}_{-840}	8100^{+1290}_{-1120}
HII-44	0.84	7210^{+790}_{-880}	7280^{+840}_{-960}	7250^{+810}_{-930}
HII-45	0.93	7100^{+1300}_{-1080}	7760^{+1210}_{-1110}	7420^{+1320}_{-1120}
HII-46	0.94	7410^{+550}_{-490}	7120^{+540}_{-450}	7280^{+550}_{-510}
HII-47	0.77	8650^{+880}_{-790}	10530^{+850}_{-750}	9640^{+1290}_{-1380}
HII-49	0.75	9940^{+1170}_{-990}	10090^{+900}_{-870}	10010^{+1020}_{-940}
HII-50	0.75	5580^{+1420}_{-1290}	6510^{+1580}_{-1560}	6020^{+1640}_{-1470}
HII-51	0.88	6610^{+850}_{-910}	7310^{+1090}_{-870}	6960^{+1030}_{-970}
HII-52	0.98	8250^{+1000}_{-950}	10190^{+860}_{-930}	9260^{+1360}_{-1460}
HII-53	0.81	5220^{+1220}_{-1030}	7340^{+1450}_{-1380}	6170^{+1810}_{-1520}
HII-55	0.96	9260^{+1160}_{-1090}	9010^{+970}_{-960}	9110^{+1110}_{-990}
HII-57	0.72	9880^{+1370}_{-1210}	11710^{+1460}_{-1280}	10850^{+1690}_{-1680}
HII-58	0.91	3300^{+1220}_{-950}	3890^{+1270}_{-1140}	3580^{+1280}_{-1080}
HII-59	0.88	1570^{+1290}_{-600}	1760^{+720}_{-500}	1680^{+950}_{-630}
HII-60	0.89	7840^{+1530}_{-1450}	8300^{+1540}_{-1460}	8050^{+1600}_{-1450}
HII-61	0.94	5950^{+3120}_{-2400}	5450^{+2380}_{-2320}	5680^{+2860}_{-2370}
HII-62	0.83	9890^{+720}_{-670}	9800^{+660}_{-650}	9840^{+700}_{-650}
HII-63	0.82	-	13220^{+990}_{-930}	13220^{+990}_{-930}
HII-64	0.78	11210^{+3930}_{-3330}	10140^{+3080}_{-2940}	10720^{+3540}_{-3250}
HII-67	0.94	10780^{+3670}_{-3220}	8630^{+2780}_{-2590}	9570^{+3410}_{-2990}
HII-70	0.90	10240^{+3580}_{-3200}	10330 ± 3220	10280^{+3390}_{-3200}
HII-73	0.76	13240 ± 1320	13430^{+1300}_{-1310}	13350^{+1310}_{-1320}
HII-76	0.86	12420^{+2620}_{-2170}	11020^{+2160}_{-1750}	11750^{+2480}_{-2120}
HII-77	0.84	11610^{+460}_{-450}	10950^{+540}_{-530}	11300^{+600}_{-640}
HII-78	0.95	12140^{+3000}_{-2560}	12570^{+2760}_{-2600}	12360^{+2840}_{-2570}
HII-81	0.88	12430^{+1350}_{-1200}	12000^{+1210}_{-1130}	12210^{+1340}_{-1180}
HII-84	0.99	10900^{+1930}_{-1780}	10400^{+1810}_{-1630}	10670^{+1840}_{-1760}
HII-85	0.99	-	28860^{+9830}_{-8090}	28860^{+9830}_{-8090}

Table A22. Electron temperatures derived from the sample of Star Forming Galaxies, considering the toy model described in Sec. 4.3, which accounts for mixed Case A-Case B conditions.

Reference number	γ_{5016}	$T_e(\text{He I } \lambda 7281/\lambda 5876)_{TM}$	$T_e(\text{He I } \lambda 7281/\lambda 6678)_{TM}$	Average $T_e(\text{He I})_{TM}$
		[K]	[K]	[K]
SFG-14	0.98	7300 ± 860	7040^{+1330}_{-1060}	7200^{+1080}_{-990}
SFG-15	0.65	9870^{+1220}_{-1110}	10670^{+1310}_{-1120}	10300^{+1330}_{-1250}
SFG-17	0.72	14610^{+1380}_{-1240}	14820^{+760}_{-910}	14740^{+980}_{-1120}
SFG-18	0.52	8690^{+810}_{-970}	8910^{+770}_{-790}	8810^{+780}_{-920}
SFG-19	0.35	14900^{+1690}_{-1490}	14560^{+1520}_{-1290}	14760^{+1580}_{-1410}
SFG-21	0.64	-	19140^{+2250}_{-1990}	19140^{+2250}_{-1990}
SFG-22	0.73	11990^{+1630}_{-1280}	18100^{+1840}_{-1880}	14920^{+4070}_{-3520}
SFG-23	0.90	13820^{+770}_{-850}	10680^{+500}_{-540}	12070^{+2100}_{-1670}
SFG-30	0.87	8970^{+2020}_{-1840}	8370^{+1830}_{-1720}	8690^{+2020}_{-1850}
SFG-31	0.59	11730^{+560}_{-600}	9580^{+590}_{-550}	10650 ± 1350
SFG-34	0.93	9150^{+5500}_{-3390}	7890^{+3950}_{-2870}	8500^{+4490}_{-3200}
SFG-35	0.88	10750^{+3040}_{-2580}	10730^{+3470}_{-3000}	10740^{+3290}_{-2810}
SFG-36	0.77	8200^{+1270}_{-1030}	8780^{+1090}_{-1100}	8490^{+1230}_{-1100}
SFG-37	0.87	10510^{+590}_{-570}	7510 ± 390	9070^{+1740}_{-1750}
SFG-38	0.82	6700^{+1410}_{-1250}	7440^{+1640}_{-1290}	7080^{+1560}_{-1390}
SFG-39	0.82	10850 ± 440	11030^{+260}_{-250}	10960^{+330}_{-380}
SFG-40	0.73	15410^{+2220}_{-2050}	13270^{+1930}_{-1750}	14260^{+2500}_{-2040}
SFG-42	0.58	19490^{+3350}_{-2270}	17130^{+1770}_{-1800}	18200^{+2820}_{-2240}
SFG-43	0.68	10010^{+3000}_{-2780}	10810^{+2980}_{-2870}	10450^{+2940}_{-2860}
SFG-45	0.85	14720^{+6890}_{-4710}	13640^{+5280}_{-4370}	14260^{+5970}_{-4700}
SFG-46	0.80	8740^{+1710}_{-1530}	9740^{+2050}_{-1760}	9190^{+2090}_{-1710}
SFG-47	0.77	9940 ± 420	9710^{+510}_{-460}	9840^{+460}_{-470}
SFG-48	0.82	12870^{+1010}_{-790}	14940^{+840}_{-790}	14010^{+1320}_{-1560}
SFG-50	0.78	23460^{+1720}_{-1690}	20960^{+1350}_{-1300}	22060^{+2240}_{-1860}
SFG-51	0.74	16130^{+1870}_{-1590}	15510^{+1380}_{-1290}	15770^{+1730}_{-1440}
SFG-52	0.91	27620^{+13080}_{-11300}	22240^{+7520}_{-6790}	24420^{+11740}_{-8620}
SFG-54	0.33	20390^{+2920}_{-2350}	20120^{+2510}_{-2020}	20240^{+2760}_{-2180}
SFG-55	0.78	14700^{+3550}_{-2040}	16290^{+2090}_{-1570}	15640^{+2700}_{-2190}
SFG-56	0.85	27980^{+4660}_{-4540}	30630^{+4430}_{-4190}	29380^{+4740}_{-4830}
SFG-60	0.75	-	22660^{+2050}_{-1980}	22660^{+2050}_{-1980}
SFG-61	0.75	-	22790^{+1710}_{-1570}	22790^{+1710}_{-1570}
SFG-63	0.26	16050^{+9500}_{-3590}	-	16050^{+9500}_{-3590}
SFG-64	0.57	9150^{+1180}_{-1300}	8750^{+1280}_{-1180}	8940^{+1260}_{-1240}
SFG-65	0.67	11560^{+1130}_{-1160}	17840^{+1620}_{-1580}	14520^{+4050}_{-3540}
SFG-66	0.68	27050^{+2310}_{-2250}	26130^{+2040}_{-1890}	26550^{+2250}_{-2040}
SFG-68	0.39	21080^{+1490}_{-1400}	18790^{+980}_{-950}	19740^{+2060}_{-1460}
SFG-74	0.68	18510^{+3420}_{-3070}	16590^{+3120}_{-2460}	17580^{+3380}_{-2860}
SFG-75	0.82	13090^{+2560}_{-2200}	12460^{+2660}_{-2000}	12770^{+2560}_{-2120}
SFG-82	0.66	19860^{+1520}_{-1180}	20440^{+1240}_{-1220}	20170^{+1390}_{-1250}

Table A22 *continued*

Table A22 (*continued*)

Reference number	γ_{5016}	$T_e(\text{He I } \lambda 7281/\lambda 5876)_{TM}$	$T_e(\text{He I } \lambda 7281/\lambda 6678)_{TM}$	Average $T_e(\text{He I})_{TM}$
		[K]	[K]	[K]
SFG-83	0.77	8960^{+720}_{-760}	10770^{+880}_{-860}	9790^{+1390}_{-1150}
SFG-84	0.65	8860^{+620}_{-580}	9540^{+580}_{-590}	9210^{+710}_{-680}
SFG-85	0.68	10190^{+400}_{-420}	10640 ± 510	10390^{+540}_{-510}
SFG-86	0.93	6600^{+1260}_{-1210}	13640^{+2350}_{-2160}	9240^{+5530}_{-3190}
SFG-89	0.80	12160^{+2200}_{-1920}	12100^{+2220}_{-1700}	12130^{+2220}_{-1770}
SFG-90	0.82	-	29740^{+3100}_{-2990}	29740^{+3100}_{-2990}

Table A23. Electron temperatures derived from the sample of Planetary Nebulae, considering the toy model described in Sec. 4.3, which accounts for mixed Case A-Case B conditions.

Reference number	γ_{5016}	$T_e(\text{He I } \lambda 7281/\lambda 5876)_{TM}$	$T_e(\text{He I } \lambda 7281/\lambda 6678)_{TM}$	Average $T_e(\text{He I})_{TM}$
		[K]	[K]	[K]
PNe-4	0.54	12930^{+3990}_{-1190}	11800^{+590}_{-600}	12140^{+1970}_{-780}
PNe-7	0.66	7250^{+1000}_{-870}	7900^{+950}_{-820}	7620^{+1000}_{-980}
PNe-10	0.95	7410^{+870}_{-780}	8740^{+810}_{-790}	8090^{+1090}_{-1060}
PNe-11	0.65	7750^{+950}_{-880}	8240^{+880}_{-850}	8000^{+970}_{-890}
PNe-14	0.61	8730^{+940}_{-860}	8930^{+740}_{-690}	8850^{+820}_{-780}
PNe-16	0.58	6880^{+1470}_{-1360}	9570^{+1590}_{-1660}	8210^{+2200}_{-2020}
PNe-22	0.93	11300^{+2230}_{-1810}	9070^{+1130}_{-1140}	9850^{+2380}_{-1530}
PNe-24	0.64	9840^{+1330}_{-870}	9690^{+710}_{-700}	9760^{+1010}_{-780}
PNe-25	0.74	7790^{+1530}_{-1210}	8490^{+1350}_{-1080}	8240^{+1360}_{-1300}
PNe-26	0.74	8410^{+830}_{-690}	8610^{+720}_{-660}	8520^{+760}_{-690}
PNe-33	0.74	7700 ± 410	8280 ± 360	8010^{+470}_{-520}
PNe-36	0.89	9320^{+580}_{-530}	8800^{+420}_{-390}	9010^{+640}_{-480}
PNe-37	0.91	10660^{+850}_{-760}	13320^{+720}_{-680}	12250^{+1460}_{-1960}
PNe-40	0.83	8090^{+530}_{-500}	7880^{+460}_{-470}	7980^{+520}_{-480}
PNe-41	0.71	8700^{+3330}_{-5490}	10760^{+3290}_{-2810}	9830^{+3360}_{-3370}
PNe-46	0.82	8130^{+470}_{-450}	8550^{+390}_{-400}	8360^{+460}_{-490}
PNe-50	0.86	6800^{+1160}_{-1120}	7570^{+1180}_{-1110}	7180^{+1220}_{-1200}
PNe-51	0.83	6410^{+1030}_{-1090}	6990^{+1000}_{-1120}	6680^{+1080}_{-1110}
PNe-52	0.75	6460^{+740}_{-730}	6830^{+660}_{-620}	6660^{+730}_{-750}
PNe-53	0.71	10110^{+5920}_{-2050}	9340^{+1690}_{-1520}	9700^{+2400}_{-1790}
PNe-54	0.70	6760^{+740}_{-820}	6930^{+650}_{-660}	6850^{+700}_{-780}
PNe-61	0.77	8910^{+1660}_{-1390}	9400^{+1460}_{-1170}	9210^{+1540}_{-1310}
PNe-69	0.74	8320^{+460}_{-450}	7090 ± 340	7630^{+890}_{-690}
PNe-74	0.77	8640^{+2060}_{-1640}	9120^{+1850}_{-1410}	8970^{+1900}_{-1650}
PNe-75	0.96	5470^{+650}_{-520}	5900^{+620}_{-550}	5700^{+680}_{-610}

Table A23 *continued*

Table A23 (*continued*)

Reference number	γ_{5016}	$T_e(\text{He I } \lambda 7281/\lambda 5876)_{TM}$ [K]	$T_e(\text{He I } \lambda 7281/\lambda 6678)_{TM}$ [K]	Average $T_e(\text{He I})_{TM}$ [K]
PNe-86	0.62	10000^{+720}_{-590}	10050 ± 480	10030^{+590}_{-540}
PNe-87	0.63	11810^{+2370}_{-1740}	10580^{+1040}_{-1050}	11070^{+1710}_{-1380}
PNe-88	0.64	10360^{+1660}_{-1240}	9870^{+1120}_{-980}	10080^{+1410}_{-1110}
PNe-96	0.65	12120^{+3360}_{-2080}	12030^{+2190}_{-1680}	12080^{+2620}_{-1860}
PNe-97	0.52	10010^{+1350}_{-1130}	9860^{+910}_{-1060}	9920 ± 1100
PNe-98	0.77	6670^{+1150}_{-1180}	7200^{+1000}_{-950}	6970^{+1080}_{-1150}
PNe-103	0.68	10960^{+2060}_{-1730}	11030^{+1300}_{-1320}	11000^{+1510}_{-1490}
PNe-113	0.89	8580^{+1770}_{-1400}	8860^{+1390}_{-1220}	8740^{+1550}_{-1400}
PNe-117	0.72	9990^{+1240}_{-910}	10330^{+870}_{-890}	10160^{+1050}_{-910}
PNe-125	0.48	7710^{+480}_{-440}	9330^{+1500}_{-1310}	8150^{+1870}_{-740}
PNe-128	0.83	8130^{+1310}_{-1180}	7190^{+1240}_{-960}	7650^{+1360}_{-1120}
PNe-129	0.67	8520^{+1220}_{-1010}	8920^{+1130}_{-970}	8720^{+1180}_{-1020}
PNe-133	0.79	3050^{+720}_{-640}	2200^{+630}_{-500}	2630^{+840}_{-710}
PNe-134	0.69	4480 ± 950	4030^{+1080}_{-1020}	4270^{+1030}_{-1020}
PNe-135	0.82	4930^{+870}_{-1000}	4210^{+1280}_{-1200}	4640^{+1030}_{-1230}
PNe-136	0.57	3710^{+860}_{-740}	2530^{+730}_{-640}	3100^{+1040}_{-900}
PNe-137	0.61	3210^{+970}_{-840}	3080^{+1100}_{-860}	3160^{+1020}_{-850}
PNe-138	0.77	8970^{+1850}_{-1460}	7750^{+2110}_{-1810}	8430^{+2050}_{-1870}
PNe-139	0.74	2030^{+1140}_{-660}	1900^{+1090}_{-560}	1970^{+1130}_{-620}
PNe-141	0.74	3220^{+1080}_{-920}	2810^{+970}_{-810}	3000^{+1040}_{-870}
PNe-143	0.82	7270^{+1140}_{-850}	8200^{+1030}_{-1080}	7770^{+1200}_{-1090}
PNe-150	0.69	2800^{+670}_{-630}	2200^{+620}_{-550}	2500^{+700}_{-670}
PNe-152	0.77	6780^{+1220}_{-1310}	6440^{+1270}_{-1330}	6590^{+1300}_{-1350}
PNe-153	0.55	6250^{+1020}_{-1050}	6480^{+1110}_{-1120}	6370^{+1050}_{-1090}
PNe-157	0.97	5310^{+1090}_{-1080}	5000^{+1370}_{-1220}	5150^{+1230}_{-1160}
PNe-158	0.36	8740^{+2270}_{-1980}	9360^{+2410}_{-2300}	9030^{+2350}_{-2130}
PNe-159	0.68	4740^{+1470}_{-1530}	4740^{+1780}_{-1720}	4740^{+1640}_{-1630}
PNe-161	0.87	6770^{+900}_{-970}	7240^{+900}_{-910}	7020^{+900}_{-990}
PNe-162	0.80	4970^{+770}_{-640}	3760^{+880}_{-840}	4460^{+940}_{-1100}
PNe-168	0.27	10940^{+2240}_{-1790}	9180^{+1710}_{-1570}	10000^{+2170}_{-1760}
PNe-170	0.80	3780^{+780}_{-680}	3050^{+860}_{-760}	3450^{+890}_{-850}
PNe-171	0.82	3770^{+620}_{-560}	2890^{+740}_{-580}	3390^{+770}_{-810}
PNe-172	0.89	1760^{+540}_{-480}	1590^{+620}_{-520}	1680^{+580}_{-460}
PNe-174	0.96	7210^{+920}_{-890}	8880^{+980}_{-1030}	8010^{+1380}_{-1230}
PNe-175	0.95	2930^{+1170}_{-990}	2800^{+1400}_{-1060}	2880^{+1300}_{-1030}
PNe-176	0.67	1750^{+670}_{-530}	1670^{+1440}_{-600}	1710^{+930}_{-510}
PNe-179	0.95	3430^{+690}_{-600}	3310^{+770}_{-720}	3360^{+740}_{-650}
PNe-180	0.80	5350 ± 510	6930^{+570}_{-680}	6040^{+1170}_{-910}
PNe-182	1.00	4620^{+300}_{-290}	3980^{+890}_{-780}	4450^{+460}_{-870}
PNe-183	0.85	5180^{+680}_{-740}	4920^{+940}_{-920}	5070^{+790}_{-870}

Table A23 *continued*

Table A23 (*continued*)

Reference number	γ_{5016}	$T_e(\text{He I } \lambda 7281/\lambda 5876)_{TM}$	$T_e(\text{He I } \lambda 7281/\lambda 6678)_{TM}$	Average $T_e(\text{He I})_{TM}$
		[K]	[K]	[K]
PNe-185	0.97	4140^{+840}_{-890}	2800^{+780}_{-690}	3430^{+1150}_{-1020}
PNe-187	0.92	5300 ± 840	4310^{+1060}_{-1000}	4880^{+960}_{-1130}
PNe-189	0.90	4770^{+1610}_{-1620}	5580^{+1580}_{-1510}	5210^{+1600}_{-1670}
PNe-190	0.74	4790^{+850}_{-740}	3930^{+750}_{-690}	4380^{+880}_{-890}
PNe-191	0.71	1900^{+1950}_{-910}	3230^{+1720}_{-1660}	2610^{+1800}_{-1350}
PNe-192	0.48	3130^{+980}_{-910}	3590^{+1240}_{-1010}	3330^{+1130}_{-930}
PNe-193	0.70	1430^{+750}_{-510}	1460^{+700}_{-540}	1450^{+730}_{-520}
PNe-194	0.35	4680^{+760}_{-720}	4740^{+890}_{-740}	4700^{+840}_{-730}
PNe-195	0.84	5530^{+920}_{-990}	6740^{+1090}_{-1120}	6100^{+1200}_{-1170}
PNe-197	0.86	4160^{+610}_{-690}	3830^{+700}_{-680}	4000^{+670}_{-710}
PNe-199	0.59	2510^{+960}_{-860}	2920^{+1250}_{-1030}	2720^{+1110}_{-940}
PNe-200	0.83	6140^{+1120}_{-1180}	6560^{+1560}_{-1550}	6310^{+1380}_{-1310}
PNe-201	0.89	5450^{+840}_{-760}	5280^{+1200}_{-1180}	5370^{+980}_{-960}
PNe-202	0.52	9840^{+1450}_{-1050}	10030^{+1020}_{-960}	9960^{+1220}_{-1040}
PNe-204	1.00	6100^{+780}_{-810}	5920^{+720}_{-910}	6010^{+750}_{-890}
PNe-205	0.44	2900^{+1090}_{-1050}	2660^{+1090}_{-960}	2760^{+1110}_{-990}
PNe-207	0.99	5360^{+810}_{-650}	5130^{+970}_{-860}	5260^{+890}_{-770}
PNe-208	0.66	6840^{+1010}_{-1030}	7670^{+1630}_{-1370}	7180^{+1570}_{-1140}
PNe-211	0.84	4080^{+840}_{-790}	3960^{+930}_{-790}	4030^{+860}_{-810}
PNe-213	0.85	3340^{+840}_{-780}	4550^{+1090}_{-1060}	3880^{+1250}_{-1050}
PNe-215	0.73	10840^{+6040}_{-1790}	10750^{+1480}_{-1300}	10780^{+2250}_{-1600}

REFERENCES

- Aggarwal, K. M., & Keenan, F. P. 1999, ApJS, 123, 311, doi: [10.1086/313232](https://doi.org/10.1086/313232)
- Alpher, R. A., Bethe, H., & Gamow, G. 1948, Physical Review, 73, 803, doi: [10.1103/PhysRev.73.803](https://doi.org/10.1103/PhysRev.73.803)
- Annibali, F., Tosi, M., Romano, D., et al. 2017, ApJ, 843, 20, doi: [10.3847/1538-4357/aa7678](https://doi.org/10.3847/1538-4357/aa7678)
- Annibali, F., La Torre, V., Tosi, M., et al. 2019, MNRAS, 482, 3892, doi: [10.1093/mnras/sty2911](https://doi.org/10.1093/mnras/sty2911)
- Aver, E., Berg, D. A., Hirschauer, A. S., et al. 2022, MNRAS, 510, 373, doi: [10.1093/mnras/stab3226](https://doi.org/10.1093/mnras/stab3226)
- Aver, E., Olive, K. A., & Skillman, E. D. 2015, JCAP, 2015, 011, doi: [10.1088/1475-7516/2015/07/011](https://doi.org/10.1088/1475-7516/2015/07/011)
- Baker, J. G., & Menzel, D. H. 1938, ApJ, 88, 52, doi: [10.1086/143959](https://doi.org/10.1086/143959)
- Baldwin, J. A., Phillips, M. M., & Terlevich, R. 1981, PASP, 93, 5, doi: [10.1086/130766](https://doi.org/10.1086/130766)
- Belfiore, F., Santoro, F., Groves, B., et al. 2022, A&A, 659, A26, doi: [10.1051/0004-6361/202141859](https://doi.org/10.1051/0004-6361/202141859)
- Bell, K. L., & Kingston, A. E. 1967, Proceedings of the Physical Society, 90, 901, doi: [10.1088/0370-1328/90/4/303](https://doi.org/10.1088/0370-1328/90/4/303)
- Benjamin, R. A., Skillman, E. D., & Smits, D. P. 1999, ApJ, 514, 307, doi: [10.1086/306923](https://doi.org/10.1086/306923)
- Berg, D. A., Skillman, E. D., Croxall, K. V., et al. 2015, ApJ, 806, 16, doi: [10.1088/0004-637X/806/1/16](https://doi.org/10.1088/0004-637X/806/1/16)
- Berg, D. A., Skillman, E. D., Garnett, D. R., et al. 2013, ApJ, 775, 128, doi: [10.1088/0004-637X/775/2/128](https://doi.org/10.1088/0004-637X/775/2/128)
- Berg, D. A., Skillman, E. D., Chisholm, J., et al. 2024, ApJ, 971, 87, doi: [10.3847/1538-4357/ad5292](https://doi.org/10.3847/1538-4357/ad5292)
- Blagrave, K. P. M., Martin, P. G., Rubin, R. H., et al. 2007, ApJ, 655, 299, doi: [10.1086/510151](https://doi.org/10.1086/510151)
- Bowen, I. S., & Wyse, A. B. 1939, Lick Observatory Bulletin, 495, 1, doi: [10.5479/ADS/bib/1939LicOB.19.1B](https://doi.org/10.5479/ADS/bib/1939LicOB.19.1B)

- Bresolin, F. 2007, ApJ, 656, 186, doi: [10.1086/510380](https://doi.org/10.1086/510380)
- Brocklehurst, M. 1972, MNRAS, 157, 211, doi: [10.1093/mnras/157.2.211](https://doi.org/10.1093/mnras/157.2.211)
- Brown, R. L. 1971, ApJ, 164, 387, doi: [10.1086/150851](https://doi.org/10.1086/150851)
- Burgess, A., & Seaton, M. J. 1960, MNRAS, 121, 471, doi: [10.1093/mnras/121.5.471](https://doi.org/10.1093/mnras/121.5.471)
- Butler, K., & Zeippen, C. J. 1989, A&A, 208, 337
- Cameron, A. J., Katz, H., & Rey, M. P. 2023, MNRAS, 522, L89, doi: [10.1093/mnrasl/slad046](https://doi.org/10.1093/mnrasl/slad046)
- Chen, Y., Jones, T., Sanders, R., et al. 2023, Nature Astronomy, 7, 771, doi: [10.1038/s41550-023-01953-7](https://doi.org/10.1038/s41550-023-01953-7)
- Chen, Y., Jones, T., Sanders, R. L., et al. 2024, arXiv e-prints, arXiv:2405.18476, doi: [10.48550/arXiv.2405.18476](https://doi.org/10.48550/arXiv.2405.18476)
- Costero, R., & Peimbert, M. 1970, Boletin de los Observatorios Tonantzintla y Tacubaya, 5, 229
- Cota, S. A., & Ferland, G. J. 1988, ApJ, 326, 889, doi: [10.1086/166146](https://doi.org/10.1086/166146)
- Croxall, K. V., Pogge, R. W., Berg, D. A., Skillman, E. D., & Moustakas, J. 2016, ApJ, 830, 4, doi: [10.3847/0004-637X/830/1/4](https://doi.org/10.3847/0004-637X/830/1/4)
- Deb, N. C., & Hibbert, A. 2009, Atomic Data and Nuclear Data Tables, 95, 184, doi: [10.1016/j.adt.2008.12.001](https://doi.org/10.1016/j.adt.2008.12.001)
- Del Zanna, G., & Storey, P. J. 2022, MNRAS, 513, 1198, doi: [10.1093/mnras/stac800](https://doi.org/10.1093/mnras/stac800)
- Delgado-Ingla, G., Mesa-Delgado, A., García-Rojas, J., Rodríguez, M., & Esteban, C. 2016, MNRAS, 456, 3855, doi: [10.1093/mnras/stv2961](https://doi.org/10.1093/mnras/stv2961)
- Dinerstein, H. L. 1990, in Astrophysics and Space Science Library, Vol. 161, The Interstellar Medium in Galaxies, ed. J. Thronson, Harley A. & J. M. Shull, 257–285, doi: [10.1007/978-94-009-0595-5_10](https://doi.org/10.1007/978-94-009-0595-5_10)
- Domínguez-Guzmán, G., Rodríguez, M., García-Rojas, J., Esteban, C., & Toribio San Cipriano, L. 2022, MNRAS, 517, 4497, doi: [10.1093/mnras/stac2974](https://doi.org/10.1093/mnras/stac2974)
- Dors, O. L., Almeida, G. C., Oliveira, C. B., et al. 2024, MNRAS, 533, L1, doi: [10.1093/mnrasl/slae052](https://doi.org/10.1093/mnrasl/slae052)
- Ercolano, B., Wesson, R., Zhang, Y., et al. 2004, MNRAS, 354, 558, doi: [10.1111/j.1365-2966.2004.08218.x](https://doi.org/10.1111/j.1365-2966.2004.08218.x)
- Espíritu, J. N., & Peimbert, A. 2021, MNRAS, 508, 2668, doi: [10.1093/mnras/stab2746](https://doi.org/10.1093/mnras/stab2746)
- Esteban, C., Bresolin, F., García-Rojas, J., & Toribio San Cipriano, L. 2020, MNRAS, 491, 2137, doi: [10.1093/mnras/stz3134](https://doi.org/10.1093/mnras/stz3134)
- Esteban, C., Bresolin, F., Peimbert, M., et al. 2009, ApJ, 700, 654, doi: [10.1088/0004-637X/700/1/654](https://doi.org/10.1088/0004-637X/700/1/654)
- Esteban, C., Carigi, L., Copetti, M. V. F., et al. 2013, MNRAS, 433, 382, doi: [10.1093/mnras/stt730](https://doi.org/10.1093/mnras/stt730)
- Esteban, C., Fang, X., García-Rojas, J., & Toribio San Cipriano, L. 2017, MNRAS, 471, 987, doi: [10.1093/mnras/stx1624](https://doi.org/10.1093/mnras/stx1624)
- Esteban, C., García-Rojas, J., Carigi, L., et al. 2014, MNRAS, 443, 624, doi: [10.1093/mnras/stu1177](https://doi.org/10.1093/mnras/stu1177)
- Esteban, C., Peimbert, M., García-Rojas, J., et al. 2004, MNRAS, 355, 229, doi: [10.1111/j.1365-2966.2004.08313.x](https://doi.org/10.1111/j.1365-2966.2004.08313.x)
- Fang, X., & Liu, X. W. 2011, MNRAS, 415, 181, doi: [10.1111/j.1365-2966.2011.18681.x](https://doi.org/10.1111/j.1365-2966.2011.18681.x)
- Ferland, G. J. 1999, PASP, 111, 1524, doi: [10.1086/316466](https://doi.org/10.1086/316466)
- Ferland, G. J., Henney, W. J., O'Dell, C. R., & Peimbert, M. 2016, RMxAA, 52, 261, doi: [10.48550/arXiv.1605.03634](https://doi.org/10.48550/arXiv.1605.03634)
- Ferland, G. J., Chatzikos, M., Guzmán, F., et al. 2017, RMxAA, 53, 385, doi: [10.48550/arXiv.1705.10877](https://doi.org/10.48550/arXiv.1705.10877)
- Fernández, V., Amorín, R., Pérez-Montero, E., et al. 2022, MNRAS, 511, 2515, doi: [10.1093/mnras/stab3150](https://doi.org/10.1093/mnras/stab3150)
- Fernández, V., Terlevich, E., Díaz, A. I., Terlevich, R., & Rosales-Ortega, F. F. 2018, MNRAS, 478, 5301, doi: [10.1093/mnras/sty1206](https://doi.org/10.1093/mnras/sty1206)
- Fernández-Martín, A., Pérez-Montero, E., Vilchez, J. M., & Mampaso, A. 2017, A&A, 597, A84, doi: [10.1051/0004-6361/201628423](https://doi.org/10.1051/0004-6361/201628423)
- Fritzsche, S., Fricke, B., Geschke, D., Heitmann, A., & Sienkiewicz, J. E. 1999, ApJ, 518, 994, doi: [10.1086/307328](https://doi.org/10.1086/307328)
- Froese Fischer, C., & Tachiev, G. 2004, Atomic Data and Nuclear Data Tables, 87, 1, doi: [10.1016/j.adt.2004.02.001](https://doi.org/10.1016/j.adt.2004.02.001)
- García-Rojas, J., Delgado-Ingla, G., García-Hernández, D. A., et al. 2018, MNRAS, 473, 4476, doi: [10.1093/mnras/stx2519](https://doi.org/10.1093/mnras/stx2519)
- García-Rojas, J., & Esteban, C. 2007, ApJ, 670, 457, doi: [10.1086/521871](https://doi.org/10.1086/521871)
- García-Rojas, J., Esteban, C., Peimbert, A., et al. 2005, MNRAS, 362, 301, doi: [10.1111/j.1365-2966.2005.09302.x](https://doi.org/10.1111/j.1365-2966.2005.09302.x)
- . 2007, RMxAA, 43, 3, doi: [10.48550/arXiv.astro-ph/0610065](https://doi.org/10.48550/arXiv.astro-ph/0610065)
- García-Rojas, J., Esteban, C., Peimbert, M., et al. 2006, MNRAS, 368, 253, doi: [10.1111/j.1365-2966.2006.10105.x](https://doi.org/10.1111/j.1365-2966.2006.10105.x)
- . 2004, ApJS, 153, 501, doi: [10.1086/421909](https://doi.org/10.1086/421909)
- García-Rojas, J., Madonna, S., Luridiana, V., et al. 2015, MNRAS, 452, 2606, doi: [10.1093/mnras/stv1415](https://doi.org/10.1093/mnras/stv1415)
- García-Rojas, J., Morisset, C., Jones, D., et al. 2022, MNRAS, 510, 5444, doi: [10.1093/mnras/stab3523](https://doi.org/10.1093/mnras/stab3523)
- García-Rojas, J., Peña, M., Morisset, C., Mesa-Delgado, A., & Ruiz, M. T. 2012, A&A, 538, A54, doi: [10.1051/0004-6361/201118217](https://doi.org/10.1051/0004-6361/201118217)
- García-Rojas, J., Peña, M., & Peimbert, A. 2009, A&A, 496, 139, doi: [10.1051/0004-6361:200811185](https://doi.org/10.1051/0004-6361:200811185)

- Gómez-Llanos, V., García-Rojas, J., Morisset, C., et al. 2024, A&A, 689, A228, doi: [10.1051/0004-6361/202450822](https://doi.org/10.1051/0004-6361/202450822)
- Gómez-Llanos, V., Morisset, C., García-Rojas, J., et al. 2020, MNRAS, 498, L82, doi: [10.1093/mnrasl/slaa131](https://doi.org/10.1093/mnrasl/slaa131)
- Gonzalez-Delgado, R. M., Perez, E., Tenorio-Tagle, G., et al. 1994, ApJ, 437, 239, doi: [10.1086/174992](https://doi.org/10.1086/174992)
- González-Díaz, R., Rosales-Ortega, F. F., & Galbany, L. 2024a, arXiv e-prints, arXiv:2406.17123, doi: [10.48550/arXiv.2406.17123](https://doi.org/10.48550/arXiv.2406.17123)
- González-Díaz, R., Rosales-Ortega, F. F., Galbany, L., et al. 2024b, A&A, 687, A20, doi: [10.1051/0004-6361/202348453](https://doi.org/10.1051/0004-6361/202348453)
- Grotian, W., Born, M., & Franck, J. 1928, Graphische Darstellung der Spektren von Atomen und Ionen mit Ein, Zwei und Drei Valenzelektronen: Erster Teil, Struktur der Materie in Einzeldarstellungen (Springer Berlin Heidelberg). <https://books.google.de/books?id=ixfIoQEACAAJ>
- Guseva, N. G., Izotov, Y. I., Fricke, K. J., & Henkel, C. 2012, A&A, 541, A115, doi: [10.1051/0004-6361/201118742](https://doi.org/10.1051/0004-6361/201118742)
- Guseva, N. G., Izotov, Y. I., Papaderos, P., & Fricke, K. J. 2007, A&A, 464, 885, doi: [10.1051/0004-6361/20066067](https://doi.org/10.1051/0004-6361/20066067)
- Guseva, N. G., Izotov, Y. I., Stasińska, G., et al. 2011, A&A, 529, A149, doi: [10.1051/0004-6361/201016291](https://doi.org/10.1051/0004-6361/201016291)
- Guseva, N. G., Papaderos, P., Meyer, H. T., Izotov, Y. I., & Fricke, K. J. 2009, A&A, 505, 63, doi: [10.1051/0004-6361/200912414](https://doi.org/10.1051/0004-6361/200912414)
- Guseva, N. G., Thuan, T. X., & Izotov, Y. I. 2024, MNRAS, 527, 3932, doi: [10.1093/mnras/stad3485](https://doi.org/10.1093/mnras/stad3485)
- Haffner, L. M., Dettmar, R. J., Beckman, J. E., et al. 2009, Reviews of Modern Physics, 81, 969, doi: [10.1103/RevModPhys.81.969](https://doi.org/10.1103/RevModPhys.81.969)
- Heisenberg, W. 1926, Zeitschrift fur Physik, 39, 499, doi: [10.1007/BF01322090](https://doi.org/10.1007/BF01322090)
- Henry, R. B. C., Kwitter, K. B., Jaskot, A. E., et al. 2010, ApJ, 724, 748, doi: [10.1088/0004-637X/724/1/748](https://doi.org/10.1088/0004-637X/724/1/748)
- Hyung, S., & Aller, L. H. 1997, MNRAS, 292, 71, doi: [10.1093/mnras/292.1.71](https://doi.org/10.1093/mnras/292.1.71)
- Hyung, S., Aller, L. H., & Feibelman, W. A. 1994, MNRAS, 269, 975, doi: [10.1093/mnras/269.4.975](https://doi.org/10.1093/mnras/269.4.975)
- Hyung, S., Aller, L. H., & Lee, W.-b. 2001, PASP, 113, 1559, doi: [10.1086/324415](https://doi.org/10.1086/324415)
- Irimia, A., & Froese Fischer, C. 2005, PhyS, 71, 172, doi: [10.1238/Physica.Regular.071a00172](https://doi.org/10.1238/Physica.Regular.071a00172)
- Izotov, Y. I., Chaffee, F. H., & Green, R. F. 2001, ApJ, 562, 727, doi: [10.1086/323864](https://doi.org/10.1086/323864)
- Izotov, Y. I., Guseva, N. G., Fricke, K. J., & Henkel, C. 2011, A&A, 533, A25, doi: [10.1051/0004-6361/201016296](https://doi.org/10.1051/0004-6361/201016296)
- Izotov, Y. I., Guseva, N. G., Fricke, K. J., & Papaderos, P. 2009, A&A, 503, 61, doi: [10.1051/0004-6361/200911965](https://doi.org/10.1051/0004-6361/200911965)
- Izotov, Y. I., Papaderos, P., Guseva, N. G., Fricke, K. J., & Thuan, T. X. 2004, A&A, 421, 539, doi: [10.1051/0004-6361:20035847](https://doi.org/10.1051/0004-6361:20035847)
- Izotov, Y. I., Stasińska, G., & Guseva, N. G. 2013, A&A, 558, A57, doi: [10.1051/0004-6361/201220782](https://doi.org/10.1051/0004-6361/201220782)
- Izotov, Y. I., & Thuan, T. X. 1998a, ApJ, 500, 188, doi: [10.1086/305698](https://doi.org/10.1086/305698)
- . 1998b, ApJ, 500, 188, doi: [10.1086/305698](https://doi.org/10.1086/305698)
- . 2004, ApJ, 602, 200, doi: [10.1086/380830](https://doi.org/10.1086/380830)
- Izotov, Y. I., Thuan, T. X., & Guseva, N. G. 2014, MNRAS, 445, 778, doi: [10.1093/mnras/stu1771](https://doi.org/10.1093/mnras/stu1771)
- . 2017, MNRAS, 471, 548, doi: [10.1093/mnras/stx1629](https://doi.org/10.1093/mnras/stx1629)
- . 2021a, MNRAS, 508, 2556, doi: [10.1093/mnras/stab2798](https://doi.org/10.1093/mnras/stab2798)
- . 2021b, MNRAS, 504, 3996, doi: [10.1093/mnras/stab1099](https://doi.org/10.1093/mnras/stab1099)
- Izotov, Y. I., Thuan, T. X., & Lipovetsky, V. A. 1994, ApJ, 435, 647, doi: [10.1086/174843](https://doi.org/10.1086/174843)
- . 1997, ApJS, 108, 1, doi: [10.1086/312956](https://doi.org/10.1086/312956)
- Izotov, Y. I., Thuan, T. X., & Stasińska, G. 2007, ApJ, 662, 15, doi: [10.1086/513601](https://doi.org/10.1086/513601)
- Kauffmann, G., Heckman, T. M., Tremonti, C., et al. 2003, MNRAS, 346, 1055, doi: [10.1111/j.1365-2966.2003.07154.x](https://doi.org/10.1111/j.1365-2966.2003.07154.x)
- Khan, S., Rugel, M. R., Brunthaler, A., et al. 2024, A&A, 689, A81, doi: [10.1051/0004-6361/202449390](https://doi.org/10.1051/0004-6361/202449390)
- Kisielius, R., Storey, P. J., Ferland, G. J., & Keenan, F. P. 2009, MNRAS, 397, 903, doi: [10.1111/j.1365-2966.2009.14989.x](https://doi.org/10.1111/j.1365-2966.2009.14989.x)
- Kniazev, A. Y., Zijlstra, A. A., Grebel, E. K., et al. 2008, MNRAS, 388, 1667, doi: [10.1111/j.1365-2966.2008.13435.x](https://doi.org/10.1111/j.1365-2966.2008.13435.x)
- Kwitter, K. B., & Henry, R. B. C. 1998, ApJ, 493, 247, doi: [10.1086/305094](https://doi.org/10.1086/305094)
- . 2001, ApJ, 562, 804, doi: [10.1086/322505](https://doi.org/10.1086/322505)
- Kwitter, K. B., Henry, R. B. C., & Milingo, J. B. 2003, PASP, 115, 80, doi: [10.1086/345108](https://doi.org/10.1086/345108)
- Lee, H., Skillman, E. D., & Venn, K. A. 2006, ApJ, 642, 813, doi: [10.1086/500568](https://doi.org/10.1086/500568)
- Liu, X. W., Barlow, M. J., Zhang, Y., Bastin, R. J., & Storey, P. J. 2006, MNRAS, 368, 1959, doi: [10.1111/j.1365-2966.2006.10283.x](https://doi.org/10.1111/j.1365-2966.2006.10283.x)
- Liu, X. W., Luo, S. G., Barlow, M. J., Danziger, I. J., & Storey, P. J. 2001, MNRAS, 327, 141, doi: [10.1046/j.1365-8711.2001.04676.x](https://doi.org/10.1046/j.1365-8711.2001.04676.x)
- Liu, Y., Liu, X. W., Luo, S. G., & Barlow, M. J. 2004, MNRAS, 353, 1231, doi: [10.1111/j.1365-2966.2004.08155.x](https://doi.org/10.1111/j.1365-2966.2004.08155.x)

- López-Sánchez, Á. R., Esteban, C., García-Rojas, J., Peimbert, M., & Rodríguez, M. 2007, ApJ, 656, 168, doi: [10.1086/510112](https://doi.org/10.1086/510112)
- Luridiana, V., Morisset, C., & Shaw, R. A. 2015, A&A, 573, A42, doi: [10.1051/0004-6361/201323152](https://doi.org/10.1051/0004-6361/201323152)
- Luridiana, V., Simón-Díaz, S., Cerviño, M., et al. 2009, ApJ, 691, 1712, doi: [10.1088/0004-637X/691/2/1712](https://doi.org/10.1088/0004-637X/691/2/1712)
- Madonna, S., García-Rojas, J., Sterling, N. C., et al. 2017, MNRAS, 471, 1341, doi: [10.1093/mnras/stx1585](https://doi.org/10.1093/mnras/stx1585)
- McClymont, W., Tacchella, S., Smith, A., et al. 2024, MNRAS, 532, 2016, doi: [10.1093/mnras/stae1587](https://doi.org/10.1093/mnras/stae1587)
- Méndez-Delgado, J. E., Esteban, C., García-Rojas, J., & Henney, W. J. 2022, MNRAS, 514, 744, doi: [10.1093/mnras/stac1300](https://doi.org/10.1093/mnras/stac1300)
- Méndez-Delgado, J. E., Esteban, C., García-Rojas, J., et al. 2021a, MNRAS, 502, 1703, doi: [10.1093/mnras/stab068](https://doi.org/10.1093/mnras/stab068)
- Méndez-Delgado, J. E., Esteban, C., García-Rojas, J., Kreckel, K., & Peimbert, M. 2023a, Nature, 618, 249, doi: [10.1038/s41586-023-05956-2](https://doi.org/10.1038/s41586-023-05956-2)
- . 2024a, Nature Astronomy, 8, 275, doi: [10.1038/s41550-024-02198-8](https://doi.org/10.1038/s41550-024-02198-8)
- Méndez-Delgado, J. E., & García-Rojas, J. 2023, arXiv e-prints, arXiv:2311.10280, doi: [10.48550/arXiv.2311.10280](https://doi.org/10.48550/arXiv.2311.10280)
- Méndez-Delgado, J. E., Henney, W. J., Esteban, C., et al. 2021b, ApJ, 918, 27, doi: [10.3847/1538-4357/ac0cf5](https://doi.org/10.3847/1538-4357/ac0cf5)
- Méndez-Delgado, J. E., Esteban, C., García-Rojas, J., et al. 2023b, MNRAS, 523, 2952, doi: [10.1093/mnras/stad1569](https://doi.org/10.1093/mnras/stad1569)
- Méndez-Delgado, J. E., Kreckel, K., Esteban, C., et al. 2024b, A&A, 690, A248, doi: [10.1051/0004-6361/202450928](https://doi.org/10.1051/0004-6361/202450928)
- Mendoza, C., Méndez-Delgado, J. E., Bautista, M., García-Rojas, J., & Morisset, C. 2023, Atoms, 11, 63, doi: [10.3390/atoms11040063](https://doi.org/10.3390/atoms11040063)
- Mendoza, C., & Zeippen, C. J. 1982, MNRAS, 198, 127, doi: [10.1093/mnras/198.1.127](https://doi.org/10.1093/mnras/198.1.127)
- Mesa-Delgado, A., Esteban, C., García-Rojas, J., et al. 2009, MNRAS, 395, 855, doi: [10.1111/j.1365-2966.2009.14554.x](https://doi.org/10.1111/j.1365-2966.2009.14554.x)
- Milingo, J. B., Henry, R. B. C., & Kwitter, K. B. 2002, ApJS, 138, 285, doi: [10.1086/324292](https://doi.org/10.1086/324292)
- Milingo, J. B., Kwitter, K. B., Henry, R. B. C., & Souza, S. P. 2010, ApJ, 711, 619, doi: [10.1088/0004-637X/711/2/619](https://doi.org/10.1088/0004-637X/711/2/619)
- Morisset, C., Garcia-Rojas, J., Gomez-Llanos, V., & Monteiro, H. 2023, arXiv e-prints, arXiv:2311.14244, doi: [10.48550/arXiv.2311.14244](https://doi.org/10.48550/arXiv.2311.14244)
- Noeske, K. G., Guseva, N. G., Fricke, K. J., et al. 2000, A&A, 361, 33, doi: [10.48550/arXiv.astro-ph/0007130](https://doi.org/10.48550/arXiv.astro-ph/0007130)
- Olive, K. A., & Skillman, E. D. 2001, NewA, 6, 119, doi: [10.1016/S1384-1076\(01\)00051-3](https://doi.org/10.1016/S1384-1076(01)00051-3)
- Otsuka, M., & Tajitsu, A. 2013, ApJ, 778, 146, doi: [10.1088/0004-637X/778/2/146](https://doi.org/10.1088/0004-637X/778/2/146)
- Peña-Guerrero, M. A., Peimbert, A., Peimbert, M., & Ruiz, M. T. 2012, ApJ, 746, 115, doi: [10.1088/0004-637X/746/2/115](https://doi.org/10.1088/0004-637X/746/2/115)
- Peebles, P. J. 1966a, PhRvL, 16, 410, doi: [10.1103/PhysRevLett.16.410](https://doi.org/10.1103/PhysRevLett.16.410)
- Peebles, P. J. E. 1966b, ApJ, 146, 542, doi: [10.1086/148918](https://doi.org/10.1086/148918)
- Peimbert, A. 2003, ApJ, 584, 735, doi: [10.1086/345793](https://doi.org/10.1086/345793)
- Peimbert, A., Peña-Guerrero, M. A., & Peimbert, M. 2012, ApJ, 753, 39, doi: [10.1088/0004-637X/753/1/39](https://doi.org/10.1088/0004-637X/753/1/39)
- Peimbert, A., & Peimbert, M. 2013, ApJ, 778, 89, doi: [10.1088/0004-637X/778/2/89](https://doi.org/10.1088/0004-637X/778/2/89)
- Peimbert, A., Peimbert, M., & Luridiana, V. 2002, ApJ, 565, 668, doi: [10.1086/324601](https://doi.org/10.1086/324601)
- Peimbert, A., Peimbert, M., & Ruiz, M. T. 2005, ApJ, 634, 1056, doi: [10.1086/444557](https://doi.org/10.1086/444557)
- Peimbert, M. 1967, ApJ, 150, 825, doi: [10.1086/149385](https://doi.org/10.1086/149385)
- Peimbert, M., Luridiana, V., & Peimbert, A. 2007, ApJ, 666, 636, doi: [10.1086/520571](https://doi.org/10.1086/520571)
- Peimbert, M., Peimbert, A., & Delgado-Ingla, G. 2017, PASP, 129, 082001, doi: [10.1088/1538-3873/aa72c3](https://doi.org/10.1088/1538-3873/aa72c3)
- Peimbert, M., & Spinrad, H. 1970, ApJ, 159, 809, doi: [10.1086/150357](https://doi.org/10.1086/150357)
- Peimbert, M., & Torres-Peimbert, S. 1974, ApJ, 193, 327, doi: [10.1086/153166](https://doi.org/10.1086/153166)
- Porter, R. L., Bauman, R. P., Ferland, G. J., & MacAdam, K. B. 2005, ApJL, 622, L73, doi: [10.1086/429370](https://doi.org/10.1086/429370)
- Porter, R. L., Ferland, G. J., & MacAdam, K. B. 2007, ApJ, 657, 327, doi: [10.1086/510880](https://doi.org/10.1086/510880)
- Porter, R. L., Ferland, G. J., MacAdam, K. B., & Storey, P. J. 2009, MNRAS, 393, L36, doi: [10.1111/j.1745-3933.2008.00593.x](https://doi.org/10.1111/j.1745-3933.2008.00593.x)
- Porter, R. L., Ferland, G. J., Storey, P. J., & Detisch, M. J. 2012, MNRAS, 425, L28, doi: [10.1111/j.1745-3933.2012.01300.x](https://doi.org/10.1111/j.1745-3933.2012.01300.x)
- . 2013, MNRAS, 433, L89, doi: [10.1093/mnrasl/slt049](https://doi.org/10.1093/mnrasl/slt049)
- Ramsbottom, C. A., & Bell, K. L. 1997, Atomic Data and Nuclear Data Tables, 66, 65, doi: [10.1006/adnd.1997.0741](https://doi.org/10.1006/adnd.1997.0741)
- Reyes-Rodríguez, E., Méndez-Delgado, J. E., García-Rojas, J., et al. 2024, A&A, 687, A97, doi: [10.1051/0004-6361/202348820](https://doi.org/10.1051/0004-6361/202348820)
- Roman-Duval, J., Jenkins, E. B., Tchernyshov, K., et al. 2022a, ApJ, 935, 105, doi: [10.3847/1538-4357/ac7713](https://doi.org/10.3847/1538-4357/ac7713)
- . 2022b, ApJ, 928, 90, doi: [10.3847/1538-4357/ac5248](https://doi.org/10.3847/1538-4357/ac5248)
- Rubin, R. H. 1989, ApJS, 69, 897, doi: [10.1086/191330](https://doi.org/10.1086/191330)
- Ruiz, M. T., Peimbert, A., Peimbert, M., & Esteban, C. 2003, ApJ, 595, 247, doi: [10.1086/377255](https://doi.org/10.1086/377255)

- Scarlata, C., Hayes, M., Panagia, N., et al. 2024, arXiv e-prints, arXiv:2404.09015,
doi: [10.48550/arXiv.2404.09015](https://doi.org/10.48550/arXiv.2404.09015)
- Sharpee, B., Williams, R., Baldwin, J. A., & van Hoof, P. A. M. 2003, ApJS, 149, 157, doi: [10.1086/378321](https://doi.org/10.1086/378321)
- Sharpee, B., Zhang, Y., Williams, R., et al. 2007, ApJ, 659, 1265, doi: [10.1086/511665](https://doi.org/10.1086/511665)
- Skillman, E. D., Terlevich, E., & Terlevich, R. 1998, SSRv, 84, 105
- Smits, D. P. 1996, MNRAS, 278, 683,
doi: [10.1093/mnras/278.3.683](https://doi.org/10.1093/mnras/278.3.683)
- Sowicka, P., Jones, D., Corradi, R. L. M., et al. 2017, MNRAS, 471, 3529, doi: [10.1093/mnras/stx1697](https://doi.org/10.1093/mnras/stx1697)
- Stasińska, G. 2002, in Revista Mexicana de Astronomía y Astrofísica Conference Series, Vol. 12, Revista Mexicana de Astronomía y Astrofísica Conference Series, ed. W. J. Henney, J. Franco, & M. Martos, 62–69,
doi: [10.48550/arXiv.astro-ph/0102403](https://doi.org/10.48550/arXiv.astro-ph/0102403)
- Storey, P. J., & Hummer, D. G. 1995, MNRAS, 272, 41,
doi: [10.1093/mnras/272.1.41](https://doi.org/10.1093/mnras/272.1.41)
- Storey, P. J., Sochi, T., & Badnell, N. R. 2014, MNRAS, 441, 3028, doi: [10.1093/mnras/stu777](https://doi.org/10.1093/mnras/stu777)
- Storey, P. J., & Zeippen, C. J. 2000, MNRAS, 312, 813,
doi: [10.1046/j.1365-8711.2000.03184.x](https://doi.org/10.1046/j.1365-8711.2000.03184.x)
- Tan, S., Parker, Q. A., Zijlstra, A. A., & Rees, B. 2024, MNRAS, 527, 6363, doi: [10.1093/mnras/stad3496](https://doi.org/10.1093/mnras/stad3496)
- Tayal, S. S., & Zatsarinny, O. 2010, ApJS, 188, 32,
doi: [10.1088/0067-0049/188/1/32](https://doi.org/10.1088/0067-0049/188/1/32)
- Thuan, T. X., & Izotov, Y. I. 2005, ApJS, 161, 240,
doi: [10.1086/491657](https://doi.org/10.1086/491657)
- Thuan, T. X., Izotov, Y. I., & Lipovetsky, V. A. 1995, ApJ, 445, 108, doi: [10.1086/175676](https://doi.org/10.1086/175676)
- Toribio San Cipriano, L., García-Rojas, J., Esteban, C., Bresolin, F., & Peimbert, M. 2016, MNRAS, 458, 1866,
doi: [10.1093/mnras/stw397](https://doi.org/10.1093/mnras/stw397)
- Torres-Peimbert, S., Peimbert, M., & Daltabuit, E. 1980, ApJ, 238, 133, doi: [10.1086/157966](https://doi.org/10.1086/157966)
- Tsamis, Y. G., Barlow, M. J., Liu, X. W., Danziger, I. J., & Storey, P. J. 2003, MNRAS, 345, 186,
doi: [10.1046/j.1365-8711.2003.06972.x](https://doi.org/10.1046/j.1365-8711.2003.06972.x)
- Valerdi, M., Barrera-Ballesteros, J. K., Sánchez, S. F., et al. 2021a, MNRAS, 505, 5460, doi: [10.1093/mnras/stab1711](https://doi.org/10.1093/mnras/stab1711)
- Valerdi, M., Peimbert, A., & Peimbert, M. 2021b, MNRAS, 505, 3624, doi: [10.1093/mnras/stab1543](https://doi.org/10.1093/mnras/stab1543)
- Valerdi, M., Peimbert, A., Peimbert, M., & Sixtos, A. 2019, ApJ, 876, 98, doi: [10.3847/1538-4357/ab14e4](https://doi.org/10.3847/1538-4357/ab14e4)
- Virtanen, P., Gommers, R., Oliphant, T. E., et al. 2020, Nature Methods, 17, 261, doi: [10.1038/s41592-019-0686-2](https://doi.org/10.1038/s41592-019-0686-2)
- Wang, W., & Liu, X. W. 2007, MNRAS, 381, 669,
doi: [10.1111/j.1365-2966.2007.12198.x](https://doi.org/10.1111/j.1365-2966.2007.12198.x)
- Wesson, R., & Liu, X. W. 2004, MNRAS, 351, 1026,
doi: [10.1111/j.1365-2966.2004.07856.x](https://doi.org/10.1111/j.1365-2966.2004.07856.x)
- Wiese, W. L., Fuhr, J. R., & Deters, T. M. 1996, Journal of Physical and Chemical Reference Data, Monograph 7, 403
- Wood, K., & Mathis, J. S. 2004, MNRAS, 353, 1126,
doi: [10.1111/j.1365-2966.2004.07846.x](https://doi.org/10.1111/j.1365-2966.2004.07846.x)
- Wyse, A. B. 1942, ApJ, 95, 356, doi: [10.1086/144409](https://doi.org/10.1086/144409)
- Zamora, S., Díaz, Á. I., Terlevich, E., & Fernández, V. 2022, MNRAS, 516, 749, doi: [10.1093/mnras/stac2201](https://doi.org/10.1093/mnras/stac2201)
- Zhang, H. 1996, A&AS, 119, 523
- Zhang, Y., Liu, X. W., Liu, Y., & Rubin, R. H. 2005, MNRAS, 358, 457, doi: [10.1111/j.1365-2966.2005.08810.x](https://doi.org/10.1111/j.1365-2966.2005.08810.x)
- Zurita, A., & Bresolin, F. 2012, MNRAS, 427, 1463,
doi: [10.1111/j.1365-2966.2012.22075.x](https://doi.org/10.1111/j.1365-2966.2012.22075.x)